

# **A three-dimensional two-phase model for flow, transport and mass transfer processes in sewers**

vorgelegt von  
Master of Science  
Katharina Teuber

bei der Fakultät VI - Planen Bauen Umwelt  
der Technischen Universität Berlin  
zur Erlangung des akademischen Grades

Doktorin der Ingenieurwissenschaften  
- Dr.-Ing. -

genehmigte Dissertation

Promotionsausschuss:

Vorsitzender: Prof. Dr.-Ing. Matthias Barjenbruch  
Gutachter: Prof. Dr.-Ing. Reinhard Hinkelmann  
Gutachter: Prof. Dr. rer. nat. Gunnar Nützmann  
Gutachter: Prof. Dr.-Ing. Dirk Muschalla  
Gutachter: Prof. Dr.-Ing. Jann Strybny

Tag der wissenschaftlichen Aussprache: 01.10.2019

Berlin 2020



---

## Preface

I am very grateful for having had the possibility of conducting this doctoral thesis at the Chair of Water Resources Management and Modeling of Hydrosystems at TU Berlin within the DFG funded Research Training Group "Urban Water Interfaces" (UWI).

I would like to thank all current and former members of the Chair for creating such a great working environment and conducting high-level research at the same time: my supervisor Reinhard (Phillip) Hinkelmann, Ralf Duda for both his technical support and his kindness in every respect. My friends and colleagues Ilhan Özgen-Xian and Elena Matta who often took the part of being my mentors. And Tabea Broecker for being a good friend, sharing an office with me and being a peer in using OpenFOAM.

My thanks also go to the students who supported me during the course of the dissertation: Nicholas R. Bowsher, who was such a great support in the end of this thesis, as well as Waldemar Elsesser, Gerie Goitom and Shibashish D. Jaydev.

I am also very grateful for the members of the Research Training Group: Gunnar Nützmänn and Matthias Barjenbruch for valuable feedback and always offering a new perspective on my work; to Tosca Piotrowski and Gwendolin Porst for the great support in administrative and interdisciplinary work. My fellow doctoral students in UWI: Clara Romero, Mikael Gillefalk, Robert Ladwig and Daneish Despot, thanks for the support and so many nice social activities.

I am very thankful for the great support I received from my parents and brothers, not only during the time of my dissertation but also all the way along my education. Thank you for supporting me in every decision.

With all my love I am thankful to my partner Manuel and our son Leander for all the support and understanding. Thank you for showing me what is truly important in life.

Berlin, April 16, 2019

---

## Publications of cumulative doctoral thesis

### First author publications (in chronological order):

1. **Teuber, K.**, Broecker, T., Bayón, A., Nützmann, G. & Hinkelmann, R.: CFD-modelling of free-surface flows in closed conduits, *Progress in Computational Fluid Dynamics*, 19 (6), 368-380, 2019; doi:10.1504/PCFD.2019.103266. Postprint.
2. **Teuber, K.**, Broecker, T., Bentzen, T.R., Stephan, D., Nützmann, G. & Hinkelmann, R.: Using computational fluid dynamics to describe H<sub>2</sub>S mass transfer across the water-air interface in sewers, *Water Science and Technology*, 79 (10), 1934-1946, 2019; doi:10.2166/wst.2019.193. Postprint.
3. **Teuber, K.**, Broecker, T., Nützmann, G. & Hinkelmann, R.: CFD simulation of H<sub>2</sub>S mass transfer under turbulent conditions in a stirring tank. In preparation for submission to *Water Science and Technology* (IWA Publishing).

### Book chapter:

1. **Teuber, K.**, Broecker, T., Jaydev, S.D., Goitom, G.M., Sielaff (née Grüneberger), M., Despot, D., Stephan, D., Barjenbruch, M. & Hinkelmann, R.: Multiphase CFD-Simulation of Transport Phenomena in Sewer Systems, in: Mannina G. (ed) *New Trends in Urban Drainage Modelling*. UDM 2018. *Green Energy and Technology*, 584-853, Springer, Cham., 2019; 10.1007/978-3-319-99867-1\_146. Postprint.

### Conference papers (in chronological order):

1. **Teuber, K.**, Broecker, T., Barjenbruch, M. & Hinkelmann, R.: High-resolution numerical analysis of flow over a ground sill using OpenFOAM, *Proceedings of the 12th International Conference on Hydroscience & Engineering (ICHE)*, Tainan, Taiwan, 2016. Postprint.
2. **Teuber, K.**, Sielaff (née Grüneberger), M., Despot, D., Stephan, D., Barjenbruch, M. & Hinkelmann, R.: Modeling and Measuring of Interfaces in Sewer Systems, *Proceedings of the 37th IAHR (International Association for Hydro-Environment Engineering and Research) World Congress*, Kuala Lumpur, Malaysia, 2017. Postprint.

---

## Supplementary contributions

### Co-authored publication:

1. Broecker, T., Elsesser, W., **Teuber, K.**, Özgen, I., Nützmann, G. & Hinkelmann, R.: High-resolution simulation of free-surface flow and tracer transport over streambeds with ripples, *Limnologica*, 68: 46-58, 2018.

### Book chapter:

1. Broecker, T., **Teuber, K.**, Elsesser, W. & Hinkelmann, R.: Multiphase Modeling of Hydrosystems Using OpenFOAM, in: Gourbesville P., Cunge J., Caignaert G. (eds) *Advances in Hydroinformatics*, Springer Water, 1013-1029, Springer, Singapore, 2018.

### Conference poster:

1. Dixit, A., **Teuber, K.**, Barjenbruch, M., Stephan, D. & Hinkelmann, R.: Extension of a 3D two-phase flow model to multicomponent reactive transport for odour and corrosion control in sewer systems, *Workshop on Applications of Multi-scale Approaches in Environmental Chemistry (AMARE)*, Rennes, France, 2019.

### Presentation:

1. **Teuber, K.**, Broecker, T., Elsesser, W. & Hinkelmann, R.: Beyond shallow water flow: Navier-Stokes simulations with OpenFOAM, *BIMoS Day: Shallow Water Flow Simulations*, Berlin International Graduate School in Model and Simulation based Research, TU Berlin, Berlin, Germany, 2017.

An overview of all supplementary scientific work is given in Chapter 8.

This thesis was carried out as project T3 of the Research Training Group "Urban Water Interfaces (UWI)" (GRK 2032/1), which is funded by the German Research Foundation (DFG).

---

## Abstract

Sewer networks are one major pillar of modern cities' infrastructure. Their functionality ensures the transport of wastewater to the sewage treatment plant and the transport of rainwater from residential areas. Damages to sewers cause infiltration and exfiltration and at the same time high costs for rehabilitation. The formation of hydrogen sulphide ( $\text{H}_2\text{S}$ ) represents a risk factor for the conditions of concrete channels. Its emission cannot only cause the destruction of sewer walls by concrete corrosion, but can also represent a safety risk for sewer workers. Within the last decades, the characteristics of  $\text{H}_2\text{S}$  emissions were intensively investigated and various models for predicting odour and corrosion were developed. The current state of the art are one-dimensional model approaches. At the same time, some predominant processes, e.g. the flow velocities in the air phase, are three-dimensional, and  $\text{H}_2\text{S}$  emissions are very relevant on locations with high turbulence and complex flow fields (e.g. drops).

This work continues at this point. It investigates and extends a three-dimensional two-phase model with regard to different aspects. For this purpose the two-phase solver `interFoam` of the software `OpenFOAM` is used. Initially, the hydrodynamic properties for different models in closed conduits are investigated by analysing hydrodynamic properties for different models in closed cross sections. The analysis begins with the simulation of a simple single-phase water flow over a ground sill and is then extended to a highly complex sewer geometry. The complex sewer network geometry is compared with results of a 1:20 scale model and existing CFD simulations for an open geometry. The results show a good agreement. Extensions are based on the description of mass transfer using the Henry coefficient. Furthermore, adjustments are made to improve the specifics of  $\text{H}_2\text{S}$  emissions in sewers. These include the description of the temperature dependency of the Henry coefficient, the equilibrium between  $\text{H}_2\text{S}$  and the bisulphide ion ( $\text{HS}^-$ ) in the water phase and the influence of the pH value on this equilibrium. An additional extension describes the concentration of  $\text{H}_2\text{S}$  in the air phase as partial pressure. The extensions and adaptations are validated using different analytical examples and the advantages of using a three-dimensional model over a one-dimensional approach are demonstrated using the example of the complex sewer geometry. Finally, the extended solver is coupled with a solver for dynamic geometries to validate the simulated mass transfer under turbulent conditions. The comparison of simulation results for mass transfer in a stirring tank with different stirring rates leads to a good agreement with experimental results from laboratory experiments.

This work results in two new solvers, the difference of which lies in the geometry to be described. The first solver can be applied to static meshes, while the second solver can describe dynamic meshes, such as rotating geometries.

---

## Zusammenfassung

Kanalnetze stellen eine wichtige Säule in der Infrastruktur moderner Städte dar. Ihre Funktionsfähigkeit sichert den Transport von Abwasser zur Kläranlage und den Transport von Regenwasser aus Siedlungsgebieten. Schäden an Kanälen können zu In- und Exfiltrationen und gleichzeitig hohen Instandsetzungskosten führen. Einen Risikofaktor für den Zustand von Betonkanälen stellen Umwandlungsprozesse von Schwefelwasserstoff ( $\text{H}_2\text{S}$ ) dar. Ihre Emission kann nicht nur Kanalwände durch Betonkorrosion zerstören, sondern auch ein Sicherheitsrisiko für Kanalarbeiter\*innen darstellen. Innerhalb der letzten Dekaden wurden  $\text{H}_2\text{S}$  Emissionen intensiv erforscht und verschiedenste Modelle zur Vorhersage von Geruch und Korrosion entwickelt. Der aktuelle Stand der Technik sind eindimensionale Modellansätze. Gleichzeitig sind einige vorherrschende Prozesse, beispielsweise die Fließgeschwindigkeiten in der Luftphase, dreidimensional und  $\text{H}_2\text{S}$  Emissionen spielen eine besondere Rolle an Stellen mit hoher Turbulenz und komplexen Strömungsfeldern (z.B. Abstürze).

Diese Arbeit setzt an diesem Punkt an und untersucht und erweitert ein dreidimensionales Zweiphasenmodell hinsichtlich unterschiedlicher Aspekte. Hierfür wird der Zweiphasen-Löser interFoam der Software OpenFOAM verwendet. In einem ersten Schritt werden die hydrodynamischen Eigenschaften für unterschiedliche Modelle in geschlossenen Querschnitten untersucht. Die Testfälle beginnen bei der einfachen Simulation einer Einphasen-Wasserströmung über eine Schwelle und werden dann hin zu einer hochkomplexen Kanalnetzgeometrie erweitert. Die Ergebnisse der Simulationen werden mit experimentellen Ergebnissen und analytischen Lösungen verglichen. Die komplexe Kanalnetzgeometrie wird mit Ergebnissen eines im Verhältnis 1:20 gebauten Modellversuchs und mit existierenden CFD-Simulationen für eine offene Geometrie verglichen, und die Ergebnisse zeigen eine gute Übereinstimmung. Es werden Transport- und Massentransferprozesse anhand verschiedener Beispiele untersucht, wozu vorhandene Erweiterungen des Löser verwendet werden. Diese Erweiterungen basieren auf der Beschreibung von Massentransfer mittels des Henry-Koeffizienten. Es werden Anpassungen vorgenommen, um  $\text{H}_2\text{S}$  Emissionen im Kanal besser beschreiben zu können. Diese umfassen die Beschreibung der Temperaturabhängigkeit des Henry-Koeffizienten sowie das Gleichgewicht zwischen  $\text{H}_2\text{S}$  und dem Hydrogensulfid-Anion ( $\text{HS}^-$ ) in der Wasserphase und den Einfluss des pH Wertes auf dieses Gleichgewicht. Eine zusätzliche Erweiterung beschreibt die Konzentration von  $\text{H}_2\text{S}$  in der Luftphase als Partialdruck. Die Erweiterungen und Anpassungen werden anhand unterschiedlicher analytischer Beispiele validiert, und es werden die Vorteile der Anwendung eines dreidimensionalen Modells gegenüber eines eindimensionalen Ansatzes wird am Beispiel der komplexen Kanalgeometrie gezeigt. Zuletzt wird der erweiterte Löser mit einem Löser für dynamische Geometrien gekoppelt, um den simulierten Massentransfer unter turbulenten Bedingungen zu validieren. Der Vergleich von Simulationsergebnissen für Massentransfer in einem Rührbehälter mit unterschiedlichen Rührgeschwindigkeiten führt zu einer guten Übereinstimmung mit experimentellen Ergebnissen aus Laborversuchen.

Insgesamt resultieren aus der Arbeit zwei neue Löser, deren Unterschied in der zu beschreibenden Geometrie liegt. Der erste Löser kann im Bereich von statischen Netzen angewandt werden, während der zweite Löser dynamische Geometrien, wie zum Beispiel die Bewegung von Rotoren, beschreiben kann.

# Contents

<b>1</b>	<b>Introduction</b>	<b>1</b>
1.1	Odour and corrosion in sewers . . . . .	1
1.2	Scientific background . . . . .	5
1.2.1	Preliminary model developments for odour and corrosion . . . . .	5
1.2.2	Three-dimensional two-phase modelling using OpenFOAM . . . . .	8
1.2.3	Transport and mass transfer modelling . . . . .	12
1.2.3.1	Transport . . . . .	12
1.2.3.2	Mass transfer . . . . .	14
1.3	Scope of this thesis . . . . .	16
<b>2</b>	<b>Research on interfaces in sewer systems within the DFG Research Training Group "Urban Water Interfaces"</b>	<b>19</b>
2.1	Introduction . . . . .	20
2.2	Pilot plant investigations . . . . .	22
2.2.1	Sulfide formation in pressure or rising mains . . . . .	22
2.2.2	Elevated H <sub>2</sub> S emissions in gravity sewers due to flow interruptions caused by the accumulation of gross solids (debris / solid materials) . . . . .	23
2.2.3	Investigation of H <sub>2</sub> S emissions at drop structures of sewer systems . . . . .	23
2.2.4	Impact of countermeasures at hotspots . . . . .	24
2.3	Investigations of corrosion processes in sewer and laboratory tests . . . . .	25
2.3.1	Concrete and mortar types . . . . .	25
2.3.2	Pilot plant acid resistance tests . . . . .	26
2.3.3	Laboratory performance tests . . . . .	26
2.3.4	Analysis of concrete and mortar specimens . . . . .	26
2.4	Development of a three-phase CFD simulation model . . . . .	27
2.4.1	Numerical model . . . . .	27
2.4.2	Validation of the water phase behavior . . . . .	29
2.5	Conclusions . . . . .	31
<b>3</b>	<b>Validation of hydrodynamic two-phase simulations</b>	<b>33</b>
3.1	Introduction . . . . .	33
3.2	Methods and materials . . . . .	35
3.2.1	Geometry and mesh . . . . .	35
3.2.2	Numerical model . . . . .	35
3.2.3	Boundary conditions . . . . .	37
3.3	Applications . . . . .	38
3.3.1	Single phase water flow over a ground sill . . . . .	38
3.3.2	Free surface flow over a hill . . . . .	44
3.3.3	Complex free surface flow in a sewer model . . . . .	46

---

3.4	Conclusions . . . . .	51
<b>4</b>	<b>Parameter study on hydrodynamic two-phase simulations of flow over a ground sill</b>	<b>52</b>
4.1	Introduction . . . . .	52
4.2	Computational framework . . . . .	53
4.2.1	Numerical model . . . . .	53
4.2.2	Turbulence modelling . . . . .	54
4.2.3	Boundary conditions . . . . .	54
4.2.4	Geometry and mesh . . . . .	54
4.3	Single-phase flow . . . . .	55
4.4	Two-phase flow . . . . .	57
4.5	Conclusions . . . . .	60
<b>5</b>	<b>Single-phase transport simulations</b>	<b>61</b>
5.1	Introduction . . . . .	61
5.2	Material and methods . . . . .	62
5.2.1	Hydrodynamic simulations . . . . .	62
5.2.2	Transport simulations . . . . .	63
5.2.3	Mass transfer . . . . .	63
5.3	Results and discussion . . . . .	63
5.3.1	Spreading of hydrogen sulphide in headspace of sewer pilot plant (air phase) . . . . .	63
5.3.2	Tracer transport in sewer pipe (water phase) . . . . .	66
5.4	Conclusions . . . . .	68
<b>6</b>	<b>Mass transfer simulations under equilibrium conditions: Validation and solver extension</b>	<b>69</b>
6.1	Abstract . . . . .	69
6.2	Introduction . . . . .	70
6.3	Methods . . . . .	71
6.3.1	Numerical model . . . . .	71
6.3.2	Henry coefficient . . . . .	74
6.3.3	Extensions . . . . .	74
6.3.4	Case studies . . . . .	77
6.4	Results and discussion . . . . .	78
6.4.1	Saturation of H <sub>2</sub> S in a tank . . . . .	78
6.4.2	Mass transfer in a rectangular channel . . . . .	82
6.4.3	Complex sewer geometry . . . . .	84
6.5	Conclusions . . . . .	86
6.6	Acknowledgements . . . . .	86
<b>7</b>	<b>Mass transfer under turbulent conditions</b>	<b>87</b>
7.1	Abstract . . . . .	87
7.2	Introduction . . . . .	87
7.3	Methods . . . . .	89
7.3.1	Geometry and mesh . . . . .	89
7.3.2	Numerical model . . . . .	89
7.3.3	Turbulence . . . . .	92
7.3.4	Case study . . . . .	93

---

7.3.5	Initial and boundary conditions . . . . .	94
7.4	Results and discussion . . . . .	95
7.4.1	Graphic analysis . . . . .	95
7.4.2	Sensitivity analysis . . . . .	96
7.4.3	Quantitative analysis . . . . .	99
7.5	Conclusions . . . . .	103
<b>8</b>	<b>Supplementary contributions</b>	<b>104</b>
8.1	Advantages of three-dimensional flow simulations . . . . .	104
8.2	Possibilities extending the interH2SFoam solver to multicomponent reactive transport . . . . .	105
8.3	Research on further multiphase CFD applications carried out at the Chair of Water Resources Management and Modeling of Hydrosystems, TU Berlin . . .	106
8.4	Application of free-surface flow and transport simulations to natural river beds	107
<b>9</b>	<b>Synthesis</b>	<b>108</b>
9.1	Conclusions . . . . .	108
9.1.1	General outcomes . . . . .	108
9.1.2	Outcomes of hydrodynamic modelling . . . . .	109
9.1.3	Outcomes of single-phase transport modelling . . . . .	110
9.1.4	Outcomes of mass transfer modelling . . . . .	111
9.1.5	Final notes . . . . .	113
9.2	Outlook . . . . .	113
<b>Appendix A</b>	<b>Flow charts of solver extensions</b>	<b>116</b>
A.1	Integration into the solution procedure . . . . .	117
A.1.1	interH2SFoam solver . . . . .	117
A.1.2	interDyMH2SFoam solver . . . . .	119
A.2	Code extensions and integration into the object-oriented framework . . . . .	121
A.2.1	File structure . . . . .	121
A.2.2	Make/files . . . . .	126
A.2.3	createFields.H . . . . .	127
A.2.4	CEqn.H . . . . .	129
A.2.5	interH2SFoam.C . . . . .	130
A.2.6	Integration of interDyMH2SFoam . . . . .	133
A.2.7	Passive scalar transport . . . . .	134
A.3	Function objects and boundary conditions . . . . .	135
A.3.1	Equilibrium conditions . . . . .	135
A.3.2	Calculation of partial pressure in ppm . . . . .	136
<b>Appendix B</b>	<b>Test case overview</b>	<b>137</b>
B.1	Single-phase flow over a ground sill . . . . .	138
B.2	Two-phase flow over a two-dimensional hill . . . . .	140
B.3	Complex sewer geometry . . . . .	142
B.4	Single-phase transport in rectangular pipe . . . . .	144
B.5	Concrete probes in sewer pilot plant . . . . .	146
B.6	Quasi one-dimensional cubic tank . . . . .	148
B.7	Mass transfer in rectangular duct . . . . .	150
B.8	Stirring tank . . . . .	152
<b>Bibliography</b>		<b>154</b>

# List of Figures

1.1	Sewer processes (following Hvitved-Jacobsen et al. (2013)) . . . . .	3
1.2	Connection between rising and gravity main (Jiang et al., 2015) . . . . .	4
1.3	Previous model developments . . . . .	5
1.4	Three-dimensional air phase velocities [m/s] in circular sewer headspace (Edwini-Bonsu and Steffler, 2004) . . . . .	7
1.5	Transport processes, Schankat (2010) after Barlag et al. (1998) . . . . .	13
1.6	Overview over different chapters . . . . .	18
2.1	Interface processes in sewer systems. . . . .	21
2.2	Research pilot plant. . . . .	22
2.3	Schematic drawing of the research pilot plant. . . . .	22
2.4	Experiment 2 – Elevated H <sub>2</sub> S emissions due to gross solids in wastewater. . . . .	23
2.5	Experiment 3 – Pilot plant scale investigation of H <sub>2</sub> S emissions at drop structures. . . . .	24
2.6	Model domain of water surface validation case. . . . .	30
3.1	Domain of single-phase, two-dimensional hill flow including measurement locations, three selected indicator locations for grid convergence study and computational mesh (Davroux et al., 1995). . . . .	39
3.2	Mesh sensitivity analysis, (a) Comparison of simulated indicator values $\phi$ (flow velocities) for different grid sizes in three points within the domain; (b) RMSE between different refinement steps over all 15 indicator values . . . . .	41
3.3	Comparison of simulated velocities $U_x$ using different turbulence models with experimental data for flow over a two-dimensional hill, (a) $U_x$ velocities at $x_{-03} = -0.30$ m, (b) $U_x$ velocities at $x_{00} = 0.00$ m, (c) $U_x$ velocities at $x_{01} = 0.03$ m (d) $U_x$ velocities at $x_{02} = 0.05$ m . . . . .	42
3.4	Comparison of simulated velocities $U_y$ using different turbulence models with experimental data for flow over a two-dimensional hill, (a) $U_y$ velocities at $x_{00} = 0.00$ m, (b) $U_y$ velocities at $x_{03} = 0.03$ m . . . . .	43
3.5	Free surface flow over a hill - Model domain of case 1 . . . . .	45
3.6	Complex sewer geometry - Geometry of the sewer stretch (Bayón et al., 2015) . . . . .	48
3.7	Complex sewer geometry - Overview of monitoring points for water surface profiles . . . . .	49
3.8	Complex sewer geometry - Comparison of water surface profile at different locations (existing CFD model - results obtained by Bayón et al. (2015); new CFD model - results obtained in this paper) . . . . .	50
4.1	Model setup and measurement locations of single-phase case. . . . .	54
4.2	Velocity profiles at $x_{-03} = -0.30m$ (inlet profile). . . . .	56
4.3	Velocity profiles at $x_{01} = 0.03m$ (end of sill). . . . .	56

---

4.4	Filling of the domain, segment of the computational domain for different time steps. . . . .	59
4.5	Comparison of water level drawdown for different sill structures . . . . .	59
4.6	Comparison of water level drawdown for two- and three-dimensional model setup . . . . .	59
5.1	Tracer transport in water phase of rectangular pipe with non-physical spreading across water surface. . . . .	62
5.2	Top view of the model domain (pipeline containing the concrete probes). . . .	64
5.3	Resulting tracer distribution. . . . .	65
5.4	Movement and spreading of tracer along sewer. . . . .	66
5.5	Movement and spreading of tracer along sewer. . . . .	67
6.1	H <sub>2</sub> S saturation in a tank (left: phase fraction value, right: concentration profiles along the vertical axis over time). . . . .	79
6.2	H <sub>2</sub> S saturation in a tank for different temperatures (298.15K (cp. Figure 6.1, right) and 288.15K) (left: phase fraction value, right: concentration profiles along the vertical axis). . . . .	80
6.3	Application example for HS <sup>-</sup> and H <sub>2</sub> S equilibrium and partial pressure of air phase concentration (left: Phase fraction value profile over domain height, middle: concentration profile, right: partial pressure of gas-phase concentration). . . . .	81
6.4	Mass transfer in rectangular channel for test 7 (see Table 6.1) (left: phase fraction value, middle: velocity, right: concentration profiles). . . . .	82
6.5	Mass transfer in rectangular channel for test 21(see Table 6.1) (left: phase fraction value, middle: velocity, right: concentration profiles). . . . .	83
6.6	Mass transfer simulations in complex sewer geometry at t=10s (a) overview of the domain filled with water under steady-state conditions, b) flow velocities and water surface behaviour in hydraulic jump, c) tracer distribution in hydraulic jump, d) top view on tracer distribution). . . . .	85
7.1	System sketch of stirring tank including relevant variables (Wu (1995), modified). . . . .	88
7.2	Computational grid used for the simulations including boundaries (red: stirrer, grey: shaft, blue (outer cylinder): cylinder walls, blue (inner cylinder): AMI, blue (upper plane): top). . . . .	94
7.3	Vortex shapes for different stirring rates (left: $N=0.8333$ 1/s, middle: $N=1.667$ 1/s, right: $N=2.333$ 1/s). . . . .	95
7.4	Influence of different turbulence models on the resulting mass transfer coefficient (inundation ratio of $h/R = 0.7$ ). . . . .	97
7.5	Influence of stirrer inundation on the mass transfer coefficient. . . . .	98
7.6	Influence of stirring rate and inundation ratio on mass transfer (Wu, 1995). . .	100
7.7	Influence of stirring rate on mass transfer (Carrera et al., 2017). . . . .	101
7.8	Comparison of relation between Reynolds number and volumetric mass transfer coefficient (Wu, 1995, Carrera et al., 2017). . . . .	102
9.1	Sewer processes (following Hvitved-Jacobsen et al. (2013)) . . . . .	115
A.1	Flow chart of interFoam solver (following Devolder et al. (2015), Lopes et al. (2017)) . . . . .	117

---

A.2	Flow chart of interH2SFoam solver (following Devolder et al. (2015), Lopes et al. (2017)), solver extensions compared to interFoam solver in green . . . . .	118
A.3	Flow chart of interDyMFoam solver (following Devolder et al. (2015), Lopes et al. (2017)) . . . . .	119
A.4	Flow chart of interDyMH2SFoam solver (following Devolder et al. (2015), Lopes et al. (2017)), solver extensions compared to interFoam solver in green .	120
A.5	File structure of interFoam solver . . . . .	122
A.6	File structure of interH2SFoam solver . . . . .	123
A.7	File structure of interDyMH2SFoam solver . . . . .	124
A.8	File structure of passiveScalarInterFoam solver . . . . .	125

# List of Tables

2.1	Composition and assumed acid resistances of concrete types used for acid resistance tests. Cement types are classified after DIN EN 197-1:2011-11. MS: microsilica, FA: hard coal fly ash. . . . .	26
2.2	Testing parameters of the four laboratory performance tests. . . . .	28
3.1	Water phase validation - $RMSE/U_0$ [-] between experimental results and simulation . . . . .	40
3.2	Water-air-interface - Properties of the different test cases . . . . .	45
4.1	Overview over different sill structures. . . . .	57
4.2	Subcritical two-phase flow: Properties of different testcases. . . . .	58
6.1	Mass transfer in rectangular channel: flow properties of analysed test cases. . . . .	78
7.1	Fluid properties as defined in the CFD simulations. . . . .	93
7.2	Setup of stirring tank in CFD simulations and known metrics of experimental setup by Carrera et al. (2017) and Wu (1995). . . . .	99
B.1	Model setup of ERCOFTAC test case . . . . .	138
B.2	Boundary conditions for hydrodynamic simulations of single-phase flow over a ground sill . . . . .	139
B.3	Model setup, two-phase flow over a two-dimensional hill . . . . .	140
B.4	Boundary conditions for hydrodynamic simulations of two-phase flow over a hill . . . . .	141
B.5	Model setup of complex sewer geometry . . . . .	142
B.6	Boundary conditions for simulations of complex sewer geometry . . . . .	143
B.7	Model setup of single-phase transport in rectangular pipe test case . . . . .	144
B.8	Boundary conditions for simulations of single-phase transport in rectangular pipe . . . . .	145
B.9	Concrete probes in sewer pilot plant . . . . .	146
B.10	Boundary conditions for transport simulations around concrete probes . . . . .	147
B.11	Model setup of quasi one-dimensional cubic tank . . . . .	148
B.12	Boundary conditions for simulations of quasi one-dimensional cubic tank . . . . .	149
B.13	Model setup of mass transfer in rectangular duct . . . . .	150
B.14	Boundary conditions for mass transfer in rectangular duct . . . . .	151
B.15	Model setup of stirring tank . . . . .	152
B.16	Boundary conditions for stirring tank . . . . .	153

# Chapter 1

## Introduction

### 1.1 Odour and corrosion in sewers

Every year damages of sewers due to concrete corrosion caused by hydrogen sulphide ( $\text{H}_2\text{S}$ ) result in high costs for sewer maintenance. In 1998, the restoration costs for corroded sewers in Germany were estimated to be in a range of billions of US \$ (Kaempfer and Berndt, 1999). Barjenbruch et al. (2008) state that Veolia Eau Germany employs 800 t/a for the countermeasure Nutriox which is suppressing the production of  $\text{H}_2\text{S}$  for around 200,000 €/a. At the same time, high  $\text{H}_2\text{S}$  concentrations in the sewer atmosphere are a health risk for sewer workers. This is why three research projects within the DFG Research Training Group "Urban Water Interfaces" (UWI) focus on the enhanced understanding of odour and corrosion processes as well as on the development of new prediction models. A detailed explanation of the ongoing research will be given in the course of this thesis.

In general, odourous substances from sewers stem from multiple substances such as sulphides, nitrogen containing compounds, acids, aldehydes and ketones. Depending on the pH value in the wastewater, different compounds are emitted from the sewer due to different chemical states with varying pH values. Low pH value emissions are considered as more intense which is why  $\text{H}_2\text{S}$  is often considered as key parameter for odour nuisance (Matsché et al., 2005).

There are several factors, why odour and corrosion due to hydrogen sulphide have become more relevant in the last years and will strongly gain importance in future:

- Decreasing water consumption: Due to demographic change and an increased water efficiency the water consumption decreases (Barjenbruch et al., 2008);
- Higher detention times: More centralized sewer systems cause higher detention times of wastewater in the sewers (Barjenbruch et al., 2008). The current discussion on decentralized urban water systems could help decreasing the problem of long detention times in the future (Leigh and Lee, 2019);
- Climate change: Warmer climates reduce the concentration of dissolved oxygen (DO), which enhances more rapid depletion of oxygen in the sewers and stimulates the generation of  $\text{H}_2\text{S}$  by the sulfate reducing bacteria (SRB) (Rootsey and Yuan, 2010).

These aspects emphasize why it is important to better understand and to be able to estimate transformation processes in sewers. In the past 70 years several models have been developed in order to predict the occurrence of odour and corrosion. They will be outlined in Chapter

1.2.1 but it is important to note that the state-of-the-art models are one-dimensional models, neglecting three-dimensional effects of flow velocities, non-uniform flow and highly turbulent effects (e.g. most hydraulic structures). This is why in this thesis, a three-dimensional model was developed to better describe local effects of H<sub>2</sub>S emissions, to provide advice for the optimization of H<sub>2</sub>S hotspots and -as a long-term goal- to provide parametrizations for the improvement of existing model approaches. To be able to better understand the importance of model developments in the field of H<sub>2</sub>S emissions, first a general introduction regarding relevant processes, locations with high H<sub>2</sub>S emissions and mitigation strategies is given.

Figure 1.1 shows an overview of the relevant processes. For the work of this thesis and the different projects working on interfaces in sewer systems in UWI, three main interfaces are highly relevant and of main interest. These are namely:

- The biofilm - (waste)water interface;
- The (waste)water - (sewer) air interface;
- The (sewer) air - biofilm - (concrete) wall interface.

At the biofilm - (waste)water interface sulphate-reducing bacteria (SRB), which are located in the biofilm, can reduce sulphate in the wastewater. This process can take place under anaerobic conditions in the wastewater. In the water phase, an equilibrium between H<sub>2</sub>S and bisulphide ion (HS<sup>-</sup>) exist, together they are described as the total dissolved sulphide. The pH value and the temperature impact this equilibrium. At the (waste)water - (sewer) air interface, H<sub>2</sub>S can be emitted from the water phase into the air phase, depending on factors such as the pH value, temperature and the concentration of oxygen and nitrate. H<sub>2</sub>S is classified to be a volatile compound, which defines a compound that has a high vapor pressure at normal temperatures causing molecules to change phases, in this case considered as emission from the water into the air phase. For these compounds, the water-air equilibrium can be described by the Henry coefficient, which is a key parameter in this thesis. It describes the state at which the transfer rates between the two phases are equal and thus no net transfer between the phases occurs (Hvitved-Jacobsen et al., 2013). The Henry coefficient itself depends on the overall temperature in the domain. In the literature, many different ways to describe this equilibrium exist. An overview and a conversion table are given in Sander (2015). One way to describe the temperature dependency of the Henry coefficient is by using the van't Hoff equation (Hvitved-Jacobsen et al., 2013).

The mass transfer between the phases depends on factors, such as the concentration of H<sub>2</sub>S in the water. The concentration is influenced by the pH value and hydrodynamic parameters, which enhance the transport of H<sub>2</sub>S in the sewer. The transport is furthermore influenced by the turbulence of the phases. The higher the turbulence in a system, the higher the turbulent diffusion, the faster the mass transfer and therefore the faster equilibrium conditions develop. Due to the strong effect of turbulence on the local mass transfer, it is important to account for the effects properly.

At the (waste)water - (sewer) air interface, the transfer of oxygen, called reaeration, is another relevant process. Reaeration is the only way to aerate the water phase and thus influences the potential of aerobic and anaerobic processes in the wastewater (Hvitved-Jacobsen et al., 2013).

Moving on to the third interface, the (sewer) air - biofilm - (concrete) wall interface,  $H_2S$  can cause the corrosion of concrete or cement-bound materials depending on the humidity of the pipe walls. All processes described above highly depend on further factors, i.e. the activity of SRB strongly depends on factors such as the availability of oxygen, redox potentials, temperature, retention time etc., which cannot be addressed as a whole in the framework of this thesis. A complete overview can be found in Barjenbruch et al. (2008).

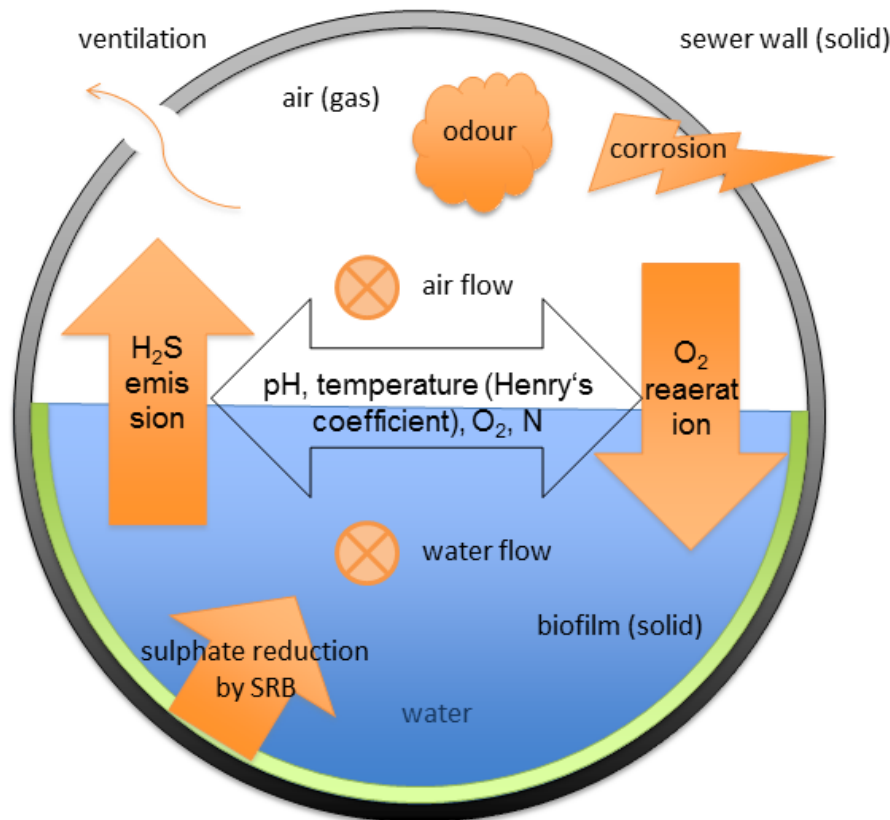


Figure 1.1: Sewer processes (following Hvitved-Jacobsen et al. (2013))

Apart from the underlying processes, it is important to fully understand the different designs of sewers and the influence of the design on  $H_2S$  formation and emission. The design and age of the city, as well as its topography, determine, which type of sewer is used. These sewer networks can be designed in very different ways. Hvitved-Jacobsen et al. (2013) propose three different ways to classify sewers:

1. Based on the type of sewage collected (sanitary sewers, storm sewers and combined sewers);
2. Based on the transport model applied (gravity sewers and pressure pipes);
3. Based on the size and function.

Wastewater is generally collected in sanitary and combined sewers. In a gravity sewer, the flow is driven by the slope of the pipe and has a free water surface whereas in a pressure sewer the flow is mainly driven by a pump and only water is present in the pipe. In a

gravity sewer, mass transfer processes across the wastewater-air interface ( $\text{H}_2\text{S}$  emissions, reaeration) are enabled due to the exposure to the sewer atmosphere. In pressure pipes, oxygen within the pipe can be consumed leading to anaerobic conditions which enable the reduction of sulphate.

All of these design classes influence the processes in the sewer and therefore the possible occurrence of odour and corrosion. Due to the variety of influence factors, odour and corrosion can develop in many different places in a sewer network, however, there are some areas which are more likely to suffer these problems. As reported in Barjenbruch (2003), one particularly problematic location are connection shafts between rising mains and gravity sewers with long detention times. These structures enable a direct contact between wastewater from anaerobic conditions and the surrounding air and are in general locations of higher turbulence. Figure 1.2 illustrates such a connection. Nevertheless, it should be pointed out that also pure gravity sewers could suffer from odour and corrosion when anaerobic conditions prevail due to long retention times, low slopes and therefore low flow velocities.

As this short overview shows, the design of a sewer is a major factor in the possible occurrence of odour and corrosion problems. One main aspect is the occurrence of anaerobic conditions, the other is the level of turbulence further downstream which enhances  $\text{H}_2\text{S}$  emissions.

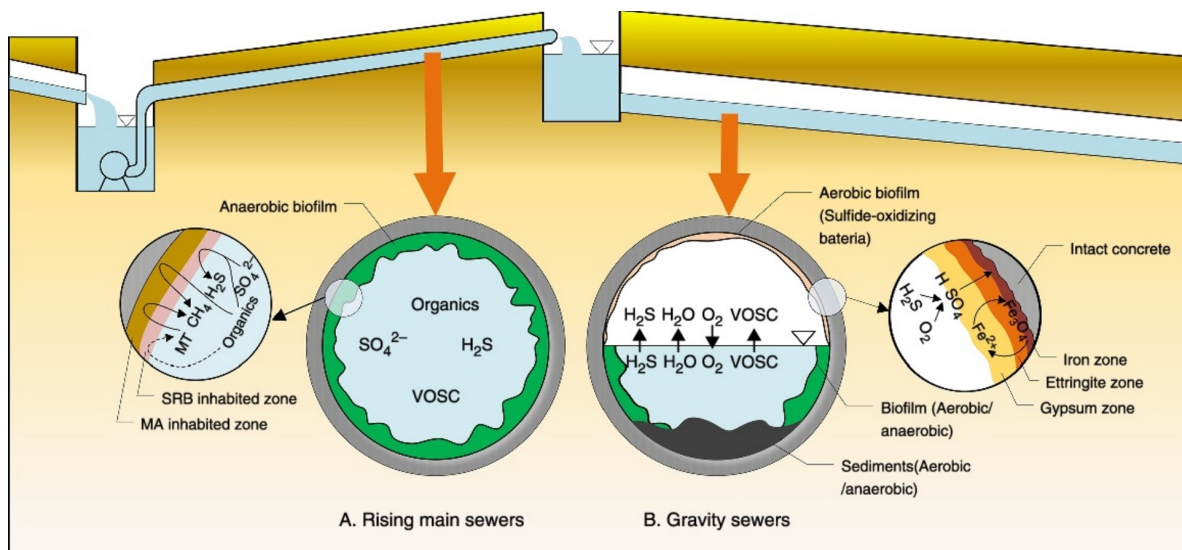


Figure 1.2: Connection between rising and gravity main (Jiang et al., 2015)

A number of countermeasures are available to mitigate the development of odour and corrosion. There are chemical solutions on the one hand, which include the enrichment with oxidants, precipitation of sulphide and pH-regulation techniques. On the other hand, physical measures, such as gas treatment with biofilters, covering systems and constructive solutions, exist (Barjenbruch et al., 2008). The range of these countermeasures shows that a model should be able to account for the countermeasures in order to become a good planning tool. The physical countermeasures, such as covering systems, could be accounted for by a purely physical model but chemical countermeasures would need to be modelled using reactive transport modelling. The long-term goal of the model developed in this thesis is to be able to model countermeasures such as ventilation, dosages and flushing.

## 1.2 Scientific background

### 1.2.1 Preliminary model developments for odour and corrosion

In this Chapter, a short overview over existing model approaches is given. Their strengths and weaknesses are outlined and the possible advantages of a new model are highlighted.

Within the last 50 years, odour and corrosion in sewer systems caused by  $H_2S$  has been intensively analysed by different researchers. The main milestones are illustrated in Figure 1.3. Vollertsen et al. (2005) give a short overview about the history of research on hydrogen sulphide:

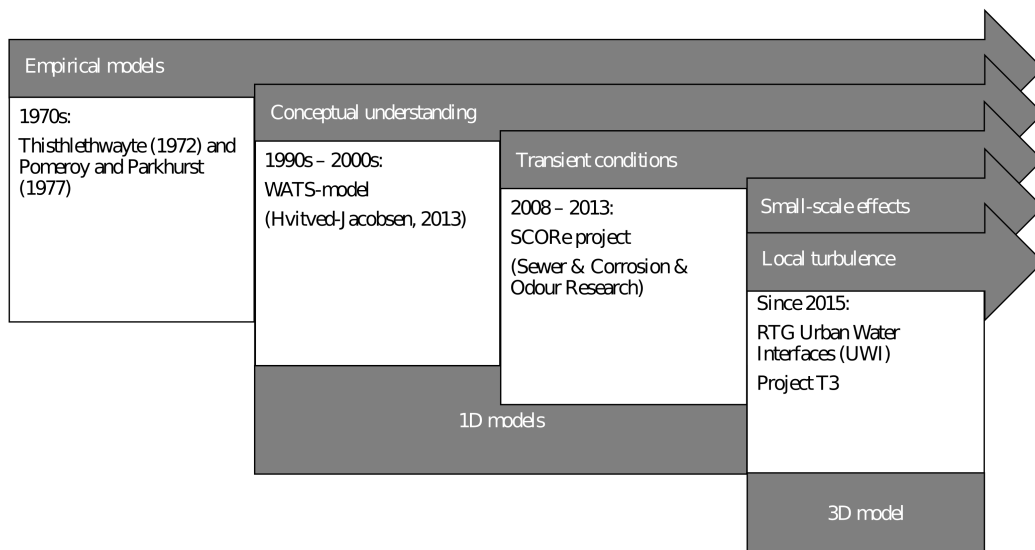


Figure 1.3: Previous model developments

In the 1970s, research on  $H_2S$  was intensified in the USA and Australia, and empirical models were developed by Pomeroy and Parkhurst (1978) as well as Thistlethwayte (1972).

From the beginning of the 1990s to the late 2000s, the Danish research group around Thorkhild Hvitved-Jacobsen has made major contributions to developing a conceptual understanding of major processes during  $H_2S$  transformations: In the 1990s, research focussed on an conceptual understanding of organic matter transformations in sewers. A conceptual model inspired by the Activated Sludge Model (ASM) called WATS (Wastewater Aerobic/Anaerobic Transformations in Sewers) has been developed by Bjerre et al. (1998). The ASM is a one-dimensional model to describe biochemical transformations solving transport-reaction or mass-balance equation for different components based on the description of different interacting processes. This model is mainly used for the description of processes in wastewater treatment plants. Due to several differences between a sewer and a wastewater treatment plant, the applicability of the model is limited (Barjenbruch et al., 2008). In the late 1990s, research on anaerobic transformations was performed with a focus on transformations in pressure mains and gravity sewers under alternating aerobic and anaerobic conditions. Especially  $H_2S$  and anaerobic transformations of organic matter were investigated. In the early 2000s, the release of  $H_2S$  from bulk water into the sewer gas phase, the

oxidation of hydrogen sulphide from the biofilm and bulk water and air injections into pressure pipes were investigated. The latest version of the WATS model includes the following functionalities (HV-Consult, 2019):

- Hydrodynamics: Description of gas and water flow along the sewer, ventilation of sewer gas to atmosphere;
- Water-air interface: Transfer of oxygen, H<sub>2</sub>S, carbon dioxide, mercaptanes, others;
- Air phase: Oxidation of H<sub>2</sub>S on moist concrete walls, concrete corrosion;
- Water phase: Transformation in bulk water, biofilms, sediments of organic matter, sulphurous compounds, specific organic compounds, oxygen, nitrate, nitrite; precipitation of H<sub>2</sub>S by iron; chemical oxidation of H<sub>2</sub>S by strong oxidizing agents; pH and buffer strength of wastewater;
- Focus on dry weather conditions.

The model's focus lies on the description of dry weather conditions: Furthermore, uniform flow is being considered under steady-state conditions. The gas phase velocity is estimated as a proportion of the water phase velocity (less than 35 to 50 %), dispersion of transported substances is not considered (Hvitved-Jacobsen et al., 2013). Carrera et al. (2016) give an overview over the capabilities of existing model approaches and discuss the ability of the WATS model to describe turbulent effects. Different simplified expressions have been used in different applications to link H<sub>2</sub>S emissions to O<sub>2</sub> emissions or to flow properties in the pipe. Furthermore, an empirical approach exists to quantify H<sub>2</sub>S emissions in drop structures (Matias et al., 2017).

In late 2008, a research project was launched in Australia. It was funded by the major water utilities in Australia in cooperation with the Australian Research Council. The so-called Sewer & Corrosion & Odour Research (SCORE) project ran for five years with a total budget around \$20 million. The project focussed on different research areas, which are namely corrosion processes, gas phase technologies, liquid phase control and knowledge management (Rootsey et al., 2012). A new model named SeweX has been developed. In this model the mathematical model of Hvitved-Jacobsen for predicting sulphide generation in sewers has been improved in order to predict spatial and temporal variations in sulphide concentrations as well as other parameters. The model has also been linked to sewer hydraulic models to predict dynamic changes in sulphur compounds within the sewer system due to changing sewer characteristics such as diurnal variations (Rootsey et al., 2012). In SeweX, anaerobic and aerobic carbon and sulphur transformation processes in a rising main are described using the model developed by Freudenthal et al. (2005): instead of the ASM, the Anaerobic Digestion Model No. 1 (ADM1) is used in order to account for anaerobic fermentation processes happening downstream of a sewer pipe (Sharma et al., 2008b). Regarding corrosion and odour control methods, the SeweX model can be used to predict the performance of different chemicals and various dosing locations (Rootsey et al., 2012, Sharma et al., 2008a). Ventilation is an important factor when analysing odour and corrosion processes in sewer systems. It can be used as a measure against unwanted processes in two different ways. The most common approach is to change the air sufficiently to maintain dry sewer structures at all times and to minimise hydrogen sulphide buildup in the sewer air. But it is also possible to maintain zero relative velocity between wastewater and ventilating air to minimise the rate of H<sub>2</sub>S emission and evaporation from the wastewater surface. However, it has to be emphasized that the second approach is not used as a practical measure against H<sub>2</sub>S

emissions. Within the SeweX project, a new algorithm has been developed to describe air movement (Rootsey et al., 2012). The algorithm describes ventilation from a viewpoint of conservation of momentum. A force balance is used to describe the influences bearing on ventilation. The influences accounted for are pressure differences, gravitational forces, drag forces at the air/water interface and friction forces at the air/pipe interface (Ward et al., 2011).

After analysing the two main models that have been developed in recent years, different deficits can be identified. One main disadvantage of the WATS model has been removed in the SeweX model: the fact that it only accounts for stationary flow conditions. Nevertheless, both models are one-dimensional models. Further deficits are the lack of possibilities to describe non-uniform flow, turbulent flow, and the simplifications when describing highly turbulent locations (e.g. drops), gas flow velocities and transport phenomena (Barjenbruch et al., 2008). Another deficit of the models is their availability. Both the WATS and the SeweX model are not public domain. These advantages and disadvantages show that the existing models are a suitable tool to analyse long sewer networks under the assumption of steady flow conditions. They can account for typical H<sub>2</sub>S hotspots such as drop structures by parametrizations but lack a detailed view on specific flow and emission characteristics on a local scale. A three-dimensional model accounting for non-uniform flow conditions, transient flows as well as highly turbulent flow characteristics can help improving the design of H<sub>2</sub>S hotspots such as connecting shafts between rising mains and gravity sewers.

Furthermore, different researchers concerned with sewer processes are describing three-dimensional effects in sewers. Vollertsen et al. (2008) mention, that corrosion processes start close to the water surface and develops further in direction of the sewer crown. Edwini-Bonsu and Steffler (2006) show secondary flows in the air phase that do not move in the main flow direction (Figure 1.4). These observations show that processes occurring in a circular sewer are three-dimensional. The error caused by simplifications due to one-dimensional models have not been analysed in publications yet. A three-dimensional model could furthermore analyse the effects of physical or chemical countermeasures in detail. To begin with, physical countermeasures could be analysed with an implementation without reactive transport. With reactive transport included, the model could analyse the effect of chemical countermeasures.

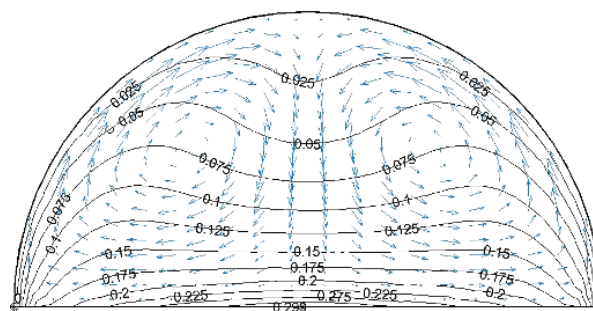


Figure 1.4: Three-dimensional air phase velocities [m/s] in circular sewer headspace (Edwini-Bonsu and Steffler, 2004)

## 1.2.2 Three-dimensional two-phase modelling using OpenFOAM

There are many different factors which influence H<sub>2</sub>S formations in a sewer, ranging from hydrodynamic conditions, such as the flow velocities and turbulence rate, to biochemical factors, such as the pH value. Numerical models and Computational Fluid Dynamics (CFD) software products offer the possibility of describing even complex hydrodynamics for single- or multiphase systems as well as transport processes under various conditions. Their application ranges from natural systems, such as reservoirs with a scale of kilometers, to technical systems, such as combined sewer overflows or even biofilters with a scale of millimeters. Numerical modelling can therefore be considered as the simulation of single- or multiphase systems in response to certain forcing conditions. They can help in identifying the influence of different factors and future needs (Matta, 2018). In the context of sewer processes, models can help estimate pollutant load as well as the influence of hydrodynamics on the transport and mass transfer of these loads. They can support deciding for correct countermeasures ranging from construction measures to dosing strategies. "The processes occurring in a water body are described by mathematical models, often a set of coupled, non-linear, partial differential equations, which are known as the Navier-Stokes equations for momentum and the continuity equation (Ji, 2008, Hinkelmann, 2005). In order to determine flow and transport in complex natural hydrosystems, time and space are discretized through various methods, leading to an approximated solution, which must be fairly close to the reality and should be reached sufficiently fast"(Matta, 2018). Depending on the "key hydrodynamic processes, the water quality concerns, as well as the proper scaling (time, space) and the most suitable simulation scenarios"(Matta, 2018) the right model for the application has to be chosen. In the case of sewer systems, the choice has to be made between a horizontal one-dimensional (1D) or a three-dimensional (3D) approach. A 1D approach is commonly used when the effects in two of the three dimensions can be neglected. This is common for sewer network modelling, when filling ratios of pipes and main flow velocities are of main importance. When specifics of the detailed built environment - as in this thesis - are of interest, i.e. the effects of a combined sewer overflow on the pollutant load, 3D modelling is preferred. This highlights one main advantage of the model developed in this thesis: Instead of simplified 1D simulations for long sewer networks, local small-scale effects can be analysed using a three-dimensional approach. The findings can lead to an improved design of H<sub>2</sub>S hotpots.

As a basis for a three-dimensional model for odour and corrosion, the open source software OpenFOAM is chosen. OpenFOAM offers the possibility of solving complex partial differential equations and contains multiple solvers and utilities addressing different numerical problems. It contains pre- and postprocessing environments and can describe two- and three-dimensional problems (Greenshields, 2015). The partial differential equations are discretized based on the Finite Volume Method in space and the Finite Differences Method in time (Schulze and Thorenz, 2014). Due to the nature of the problem addressed in this thesis, a two-phase flow model is needed in order to be able to account for water and air flow. In order to introduce the software, a short overview over the model setup in OpenFOAM is given and relevant solvers for multiphase problems are introduced. Setting up a model in OpenFOAM can be divided into three main steps:

1. Preprocessing: Mesh generation, definition of boundary and initial conditions;
2. Solving;
3. Postprocessing.

The preprocessing step consists of the generation of the computational mesh and the definition of boundary and initial conditions. A computational mesh is needed in order to solve the relevant equations. By generating the mesh, the computational domain is divided into a finite number of volumes where the solution is calculated. The number of volumes influences the calculation effort (Schulze and Thorenz, 2014). Structured meshes can be created with the built-in utility blockMesh. Several other mesh generators such as gmsh and snappyHexMesh exist and come with different advantages and disadvantages (Kortelainen, 2009). Importing meshes from other CFD programs is also possible. The development of a high-quality three-dimensional mesh is a complex and time consuming process, but the effect of the mesh's quality on the simulation results is substantial and should not be underestimated.

For the second part of preprocessing, boundary and initial conditions need to be defined for each variable that is being solved. Good initial conditions can lead to faster convergence. For boundary conditions, the user has the possibility to define Dirichlet and Neumann conditions but also variations combining both types exist.

For multiphase flow simulations, a number of different solvers are available in OpenFOAM. Multiphase flows can be classified in different ways and depending on their classification, a different kind of solver can be chosen (Schulze and Thorenz, 2015). A phase in this context is a defined material class with homogeneous features, which can also be different physical states of one fluid. Multiphase flows can then be classified by the physical state of the different fluids as well as the topology of the interface between phases. According to the physical state, one can therefore distinguish between gas-solid, gas-fluid, fluid-solid and fluid-fluid flows. Gaseous phases can additionally be considered as compressible or incompressible flows depending on the flow velocity and speed of sound. When considering the properties of the interface, one can differentiate between disperse and separated flows. Separated flows are not mixed and share a continuous interface at which the phases generally share the same velocity. Disperse flows consist of one continuous phase and a disperse phase. The phases penetrate each other and the interface between phases is not continuous (Schulze and Thorenz, 2015). For the free-surface flows considered in this thesis, incompressible water-air flows are of interest. The compressibility of air is only important for very high velocities or pressure differences (Schulze and Thorenz, 2015). The free-surface flows considered in this thesis are very closely related to the field of hydraulic engineering, where the Volume of Fluid (VOF) method is the most popular method used in CFD applications. This method is able to describe non-mixing fluids but exchange of mass and momentum are not accounted for in their original form. Disperse particles are only described correctly when their size is bigger than multiple mesh cells (Schulze and Thorenz, 2015). Since the incompressible, separated two-phase flows are best described by using the VOF method, this method will be used in this thesis.

In OpenFOAM, the VOF method is implemented in a solver called interFoam. The governing equations that have to be solved simultaneously are the continuity equation for compressible flow, the momentum equations and the  $\alpha$  transport equation together with the constitutive relations for the density and dynamic viscosity (Ubbink, 1997). The continuity equation is solved in the non-conservative form, since for two-fluid systems with high density differences it is much more suitable for numerical solution, because the velocity field  $\mathbf{U}$  is in contrast to the momentum  $\rho\mathbf{U}$  continuous at the interface (Ubbink, 1997). Additionally, incompressible flow is considered here, and therefore density changes are negligible. As a result, the non-conservative form for incompressible flow can be written

as:

$$\nabla \cdot \mathbf{U} = 0 \quad (1.1)$$

Here,  $\mathbf{U}$  is the velocity field [m/s].

As for the momentum equation, the basic form is:

$$\frac{\partial \rho \mathbf{U}}{\partial t} + \nabla \cdot (\rho \mathbf{U} \mathbf{U}) = -\nabla p + \nabla \cdot \mathbf{T} + \rho \mathbf{f}_b \quad (1.2)$$

Where  $\rho$  is the density [kg/m<sup>3</sup>];  $t$  is time [s];  $p$  is the pressure [Pa];  $\mathbf{T}$  is the deviatoric viscous stress tensor [N/m<sup>2</sup>] and  $\mathbf{f}_b$  are body forces per unit mass [m/s<sup>2</sup>].

Since both fluids are considered to be Newtonian and incompressible, the stress tensor can be decomposed into a more convenient form for discretization (Berberović et al., 2009):

$$\nabla \cdot \mathbf{T} = \mu[\nabla \mathbf{U} + (\nabla \mathbf{U})^T] = \nabla \cdot (\mu \nabla \mathbf{U}) + (\nabla \mathbf{U}) \cdot \nabla \mu \quad (1.3)$$

Where  $\mu$  is the dynamic viscosity [Ns/m<sup>2</sup>]. A detailed derivation and explanation can be found in Ubbink (1997).

The VOF method used in the interFoam solver considers a single pressure system.  $p_{rgh}$  is a modified pressure which is used to avoid the occurrence of steep pressure gradients caused by hydrostatic effects and in order to simplify the definition of boundary conditions, thus describing the static pressure minus hydrostatic pressure component:

$$p_{rgh} = p - \rho \cdot \mathbf{g} \cdot \mathbf{x} \quad (1.4)$$

Here,  $\mathbf{g}$  is the acceleration vector due to gravity [m/s<sup>2</sup>] and  $\mathbf{x}$  is a spatial position vector [m]. This simplification has been first defined by Rusche (2003).

Taking these assumptions into account, the resulting momentum equation is:

$$\begin{aligned} \frac{\partial \rho \mathbf{U}}{\partial t} + \nabla \cdot (\rho \mathbf{U} \mathbf{U}) = & -\nabla p_{rgh} + \nabla \cdot (\mu \nabla \mathbf{U}) \\ & + (\nabla \mathbf{U}) \cdot \nabla \mu - \mathbf{g} \cdot \mathbf{x} \nabla \rho \end{aligned} \quad (1.5)$$

Since the VOF method considers the two immiscible fluids liquid and gas as one fluid, the fluid properties density and viscosity in the domain are described by a function based on the volume fraction  $\alpha$ :

$$\rho = \alpha \rho_L + \rho_G (1 - \alpha) \quad (1.6)$$

$$\mu = \alpha \mu_L + \mu_G (1 - \alpha) \quad (1.7)$$

$$(1.8)$$

Here,  $\alpha$  is a volume fraction or indicator function [-] and the subscripts L and G denote the fluids water (L - liquid) and air (G - gas). The viscosity divides into the physical viscosity  $\mu_{phys}$  as well as the turbulent viscosity  $\mu_{turb}$ , where  $\mu_{turb}$  is calculated by a turbulence model:

$$\mu_i = \mu_{i,phys} + \mu_{i,turb} \quad (1.9)$$

Where  $i$  is the subscript for the respective phase L or G.

The  $\alpha$  transport equation - also known as VOF equation - is used with an advanced formulation. In general, it is implemented as an additional transport equation, which is used as a marker to describe the distribution of the phases through the domain and therefore the position of the free surface (Morgan, 2013). These marker variables are known as volume

fractions  $\alpha$ , that are strictly bounded:  $0 \leq \alpha \leq 1$  (Morgan, 2013). Both phases share an interface at which both phases have the same velocity (Schulze and Thorenz, 2015). "In this model an additional convective term originating from modelling the velocity in terms of a weighted average of the corresponding liquid and gas velocities is introduced into the transport equation for phase fraction, providing a sharper interface resolution. The model makes use of the two-fluid Eulerian model for two-phase flow, where phase fraction equations are solved separately for each individual phase" (Berberović et al., 2009):

$$\frac{\partial \alpha}{\partial t} + \nabla \cdot (\alpha \mathbf{U}_L) = 0 \quad (1.10)$$

$$\frac{\partial (1 - \alpha)}{\partial t} + \nabla \cdot ((1 - \alpha) \mathbf{U}_G) = 0 \quad (1.11)$$

"Assuming that the contributions of the liquid and gas velocities to the evolution of the free surface are proportional to the corresponding phase fraction, and defining the velocity of the effective fluid in a VOF model as a weighted average" (Berberović et al., 2009) leads to:

$$\mathbf{U} = \alpha \mathbf{U}_L + (1 - \alpha) \mathbf{U}_G \quad (1.12)$$

Equation 1.10 can be rearranged and used as an evolution equation for the phase fraction  $\alpha$ :

$$\frac{\partial \alpha}{\partial t} + \nabla \cdot (\alpha \mathbf{U}) + \nabla \cdot ((1 - \alpha) \mathbf{U}_r \alpha) = 0 \quad (1.13)$$

Where " $\mathbf{U}_r = \mathbf{U}_G - \mathbf{U}_L$  is the vector of relative velocity, designated as the "compression velocity" (Berberović et al., 2009). A detailed derivation of the equations can be found in Damián (2012).

The values of  $\alpha$  can be interpreted for a water-air flow as follows:

$$\alpha = \begin{cases} 1 & \text{fluid L - water} \\ 0 < \alpha < 1 & \text{transitional region} \\ 0 & \text{fluid G - air} \end{cases} \quad (1.14)$$

In the transitional region, the water surface is considered to be the area where  $\alpha=0.5$ .

In the range of high Reynolds numbers, turbulence models become relevant to correctly solve CFD problems. OpenFOAM enables the use of a wide number of turbulence models, ranging from Reynolds averaging to Direct Numerical Simulation (DNS).

DNS leads to the highest accuracy of the simulations, because the turbulence is discretized by using small enough cell sizes and time steps to display all vortices (Maric et al., 2014). This leads to a computational effort, which is in most cases still not practically applicable today.

Large Eddy Simulation (LES) offers a compromise between DNS and RANS models in terms of complexity. Small enough cell sizes enable the model to resolve large eddies spatially and small eddies are modelled using a subgrid scale model. The necessary grid resolution is therefore not as small as for DNS and the computational effort smaller (Maric et al., 2014). In this thesis, the majority of cases are simulated using Reynolds averaging. Here, turbulent flow is described by dividing the mean velocity into an average velocity component and a fluctuating velocity component, resulting in a Reynolds stress tensor in the Navier-Stokes equations (RANS). This tensor describes an additional eddy viscosity and leads to new unknowns in the equations, which can be either  $k$  (the turbulent kinetic energy) and  $\epsilon$  (the

turbulent dissipation) for  $k$ - $\epsilon$  turbulence models or  $k$  and  $\omega$  (the specific dissipation) for  $k$ - $\omega$  turbulence models. These unknowns can be solved by using a two-equation model, that adds two coupled transport equations in order to describe convection and diffusion of turbulent energy.

The partial differential equations that describe the flow need to be transformed to algebraic equations by integrating them over a certain time step and a control volume. The user has to define spatial and temporal discretization schemes for the above mentioned system of equations (Schulze and Thorenz, 2014). Therefore, every differential operator as well as the interpolation between fields have to be defined. OpenFOAM comes with the option of defining one default parameter or one parameter for every term in the solution procedure.

The discretized equations then result in a sparse matrix which can be solved using iterative solution techniques (Schulze and Thorenz, 2014). The parameters of the solution procedure also need to be defined by the user. For every variable, the procedure to solve the systems of equations and possible preconditioners and tolerances for the exact solution need to be defined.

For the VOF method, a special solution procedure is required for the four variables of the flow field, the velocities in three directions and the pressure. The velocities can be calculated with the Navier-Stokes equations but the mass conservation equation is not capable to solve for the pressure. This issue can be solved by a pressure linking equation. In the interFoam solver, this is done with an extended algorithm called PIMPLE (PISO-SIMPLE) (Greenshields, 2015) which is based on the PISO (Pressure-Implicit with Splitting of Operators) and the SIMPLE (Semi-Implicit Method for Pressure-Linked Equations) algorithm (Caretto et al., 1973).

Due to the high number of cells in the computational domains, the OpenFOAM simulations presented in this thesis were mostly computed on supercomputers of the Norddeutscher Verbund für Hoch- und Höchstleistungsrechnen (hlrn) in Berlin or on high performance computing (HPC) clusters of TU Berlin.

### 1.2.3 Transport and mass transfer modelling

#### 1.2.3.1 Transport

When developing a model to predict the occurrence of odour and corrosion, it becomes clear that the model needs to include transport processes in order to account for the movement of  $H_2S$  in the sewer. The previously outlined interFoam solver in OpenFOAM, which uses the VOF method, is able to describe two-phase hydrodynamics but the transport of substances need to be included separately. This is why in this Chapter, the basics of transport processes are outlined.

Transport processes can be divided in conservative and reactive transport, where reactive transport considers the formation of substances due to chemical reactions. In this thesis only conservative transport will be considered.

Conservative transport can generally be divided into three driving processes which are illustrated in Figure 1.5:

- Advection / Convection;

- Molecular Diffusion;
- Dispersion / Turbulent diffusion.

Advection is the linear transport of a particle along the flow direction without any spreading taking place (Hvitved-Jacobsen et al., 2013) (see Figure 1.5).

Diffusion can be divided into molecular and turbulent diffusion. Molecular diffusion describes Brown's molecular movement and is caused by temperature-induced impact of the molecules and is a disordered movement. On a macroscopic scale it can be expressed by Fick's first law of diffusion. The diffusivity of a substance depends on the substance itself and on the transport medium. It is also temperature dependent (Hvitved-Jacobsen et al., 2013).

Dispersion or turbulent diffusion is caused by flow velocity variations in space and time and is related to turbulent conditions. Depending on the dimensionality of the computational model (1D, 2D or 3D), dispersion is included in different ways. When using a 1D or 2D model, dispersion is accounted for by using a dispersion term. In 3D models, it can be accounted for by including a turbulent diffusion by employing a turbulent Schmidt number (Bates et al., 2005).

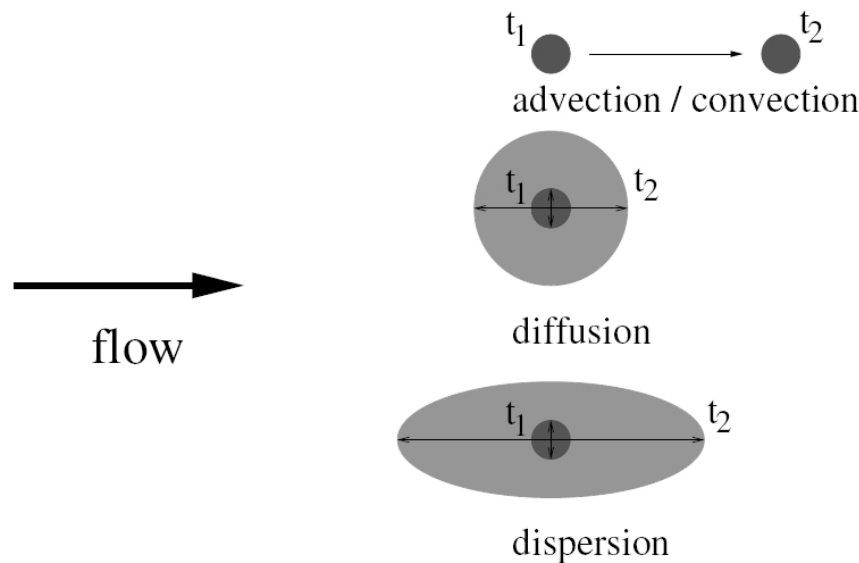


Figure 1.5: Transport processes, Schankat (2010) after Barlag et al. (1998)

OpenFOAM's interFoam solver does not have a built-in solver for transport equations but the relevant equations were implemented into the solver. An advection-diffusion equation to describe transport of a passive tracer with a concentration  $C$  is shown in Equation 1.15). Here, the diffusivity is divided into the physical diffusivity  $D_{phys}$  and the turbulent diffusivity  $D_{turb}$  which is calculated using Equation 1.16. The physical diffusivity  $D_{phys}$  and the turbulent Schmidt number  $Sc_{turb}$  have to be defined by the user.

Advection-diffusion equation:

$$\frac{\partial C}{\partial t} + \nabla \cdot (\mathbf{UC}) = \nabla \cdot ((D_{phys} + D_{turb})\nabla C) + W \quad (1.15)$$

with

$$D_{turb} = \frac{\mu_{turb}/\rho}{Sc_{turb}} \quad (1.16)$$

Where  $W$  can be a sink or source term or the production term related to chemical reaction.

### 1.2.3.2 Mass transfer

The description of relevant processes in Chapter 1.1 shows the relevance of accurately including  $H_2S$  mass transfer into a three-dimensional model for odour and corrosion. Mass transfer between liquid and gas phase depends on many influence factors. The exchange of mass itself is defined by mass transfer rates and equilibrium conditions. The mass flow between the phases is in general described by the mass transfer coefficient. The equilibrium between the two phases can be described by the Henry coefficient.

In general, three main approaches exist to describe mass transfer across the air-water interface in a model. These are namely:

1. Two-film theory,
2. Penetration theories, and
3. Surface renewal theory.

The two-film theory assumes that two static films exist at the interface between the two fluids. Through these films the volatile substance diffuses based on the molecular diffusion. During this process, Fick's first law is assumed to be consequently valid. This theory has been applied in the WATS model. The advantage of this theory is the fact that it leads to simple expressions for gas-liquid mass transfer that are useful for basic practical applications (Hvitved-Jacobsen et al., 2013). A formulation has been integrated into the WATS model to account for mass transfer in drop structures and its formulation has been further developed by the work by Matias et al. (2017). However, the simplicity comes with a price of certain assumptions:

1. The species concentrations in any location is constant over time.
2. The films at the interface of both phases are laminar.
3. Equilibrium conditions at the interface are achieved immediately.

Wang et al. (2018) give an overview over multiple criteria, why these assumptions are complicated to be applied to real-life applications. Local flow regimes could vary between laminar, transitional or turbulent. Furthermore, variations of fluid properties could occur. These variations cannot be accounted for when applying the two-film theory. Flow instabilities can occur and change the liquid film. Most importantly, the two-film theory is a one-dimensional approach.

Other approaches, such as the penetration theory and the surface renewal theory offer some improvements compared to the two-film theory. Both account for the variability of the flux over time. But still they do not account for local variations of fluid velocities, physical properties and different flow regimes (Wang et al., 2018).

This is why in recent years, more and more advanced CFD models have been developed to analyse mass transfer phenomena, many of them using the VOF method. A one-fluid formulation accounting for advection, diffusion and possibly chemical reactions can be used

to describe flow and chemical kinetics (Wang et al., 2018).

Using a CFD approach to describe mass transfer phenomena offers a number of advantages, such as the possibility to account for three-dimensional effects. As outlined above, H<sub>2</sub>S mass transfer processes in sewers can be influenced by high turbulent effects and three-dimensionalities, even in simple structures such as circular pipes. It is therefore necessary to apply a three-dimensional two-phase model which can account for mass transfer to the environment of a sewer system.

In OpenFOAM, mass transfer can be simulated with different solvers. But as mentioned above, the VOF method offers different advantages to describe the systems considered in this thesis. Therefore, mass transfer will be considered using the one-fluid approach for the VOF method as defined by Haroun et al. (2010a,b) as it has been implemented by Nieves-Remacha et al. (2015) and Severin (2017). The approach is based on the interFoam solver and considers one additional transport equation for both phases as outlined in Equations 1.15 and 1.16.

Haroun et al. (2010a) introduced a one-fluid formulation for transport and mass transfer using Henry's law as a constant coefficient. This approach has been implemented into the JADIM code and compared to the penetration theory and a good agreement has been observed. Nieves-Remacha et al. (2015) implemented the formulation into OpenFOAM. Note that the formulation by Haroun et al. (2010a) considers  $D$  as the molecular diffusivity and thus does not account for the turbulent diffusivity  $D_{turb}$ . This is due to the fact, that DNS simulations have been performed, and no turbulent viscosity  $\mu_{turb}$  has been computed by the solver. The work shown in Chapter 7 will highlight the importance of including  $D_{turb}$  into the mass transfer formulation presented in this thesis. The following equations contain the turbulent diffusivity  $D_{turb}$ :

$$\frac{\partial C}{\partial t} + \nabla \cdot (\mathbf{UC}) = \nabla \cdot ((D_{phys} + D_{turb})\nabla C + \phi) + W \quad (1.17)$$

With  $\phi$  being a concentration flux expression at the interface resulting in the following:

$$\phi = -(D_{phys} + D_{turb}) \left( \frac{C(1 - He)}{\alpha + He(1 - \alpha)} \right) \nabla \alpha \quad (1.18)$$

The production term will not be considered in this thesis. As shown in Hvitved-Jacobsen et al. (2013), the Henry coefficient is highly dependent on the temperature. The mass transfer rate depends on the Reynolds number and pH value (Yongsiri et al., 2004). These driving factors are not accounted for in the original form of the approach.

At the interface, Henry's law must be fulfilled and the molecular diffusive transport expressed by Fick's law is supposed to be the same in both phases:

$$He = \frac{C_L}{C_G} \quad (1.19)$$

$$(D_{phys,L} + D_{turb,L})\nabla C_L = (D_{phys,G} + D_{turb,G})\nabla C_G \quad (1.20)$$

Like density and viscosity, the concentrations and diffusion coefficients are considered as single-phase properties depending on the phase fraction value  $\alpha$ . While the concentrations

are calculated by linear averaging, the diffusion coefficient is calculated by using a harmonic average:

$$C = \alpha C_L + C_G(1 - \alpha) \quad (1.21)$$

$$D_{phys} = \left( \frac{D_{phys,L} \cdot D_{phys,G}}{\alpha D_{phys,L} + (1 - \alpha) D_{phys,G}} \right) \quad (1.22)$$

The diffusion coefficients for  $D_{phys,L}$  and  $D_{phys,G}$  are defined by the user. Note that these coefficients are also temperature dependent and that the temperature dependency of the coefficients has to be taken into account by the user when defining the values.

In order to validate mass transfer rates, the local mass transfer can be computed as follows:

$$K_{L,local} = - \frac{((D_{phys,L} + D_{phys,G}) \nabla C + \phi) \cdot n_L}{\Delta C_{L,local}} \quad (1.23)$$

with  $n_L$  being the normal to the interface pointing into the liquid which is obtained by  $n_L = \frac{\nabla \alpha}{|\nabla \alpha|}$ ,  $\Delta C_{L,local}$  is the difference between the free surface region and the bulk liquid concentration. The overall mass transfer across the interface can be obtained by integrating over the interface

$$K_L = \frac{1}{\lambda} \int_0^\lambda K_{L,local} d\zeta \quad (1.24)$$

where  $\lambda$  is the interface length and  $\zeta$  the curvilinear coordinate associated to the interface. Following Carrera et al. (2017), the mass transfer can also be obtained by fitting the decrease of concentration in the liquid phase to the following function:

$$C_{L,H2S} = C_{L,0} e^{-K_{L,H2S} a (t - t_0)} \quad (1.25)$$

The approach by Haroun et al. (2010a) offers another advantage when modelling transport processes using the interFoam solver. Because one set of Navier-Stokes equations is solved, a standard advection-diffusion equation cannot account for the interface between phases. If a tracer is modelled in the nearfield of the interface between two phases, an unphysical spreading can occur. Using the approach by Haroun et al. (2010a) with a small value for the Henry coefficient can avoid the unphysical spreading to a certain extent and therefore enable the user to simulate single-phase transport.

### 1.3 Scope of this thesis

In this thesis, a model for the correct description of processes occurring at the water-air interface was developed. The main focus lies in the use and extension of the three-dimensional two-phase solver interFoam, which is implemented in OpenFOAM, to describe water-air flow and H<sub>2</sub>S emissions across the air-water interface in closed conduits.

Therefore, existing approaches are applied and extended to describe three-dimensional water (single phase) and water-air flow (two phases) and conservative tracer transport of H<sub>2</sub>S. First, a validation of the hydrodynamics of the interFoam solver is performed. Then, an existing mass transfer solver (interHarounFoam) which accounts for mass transfer depending on the Henry coefficient as described by Haroun et al. (2010a) is extended to describe the specifics of H<sub>2</sub>S transfer in sewers. As a result, a three-dimensional implementation of parts of an in-sewer model exists and this solver is then applied and tested under turbulent

conditions in a stirring tank.

This thesis is structured into nine chapters consisting of the introduction (the current **Chapter 1**), three peer-reviewed journal articles (one in press, two submitted), one book chapter, two peer-reviewed conference contributions, further related work and a synthesis. An overview over the different topics covered in each Chapter is given in Figure 1.6.

The thesis has several connection points to the two other projects in UWI which are working on interfaces in sewer systems. The relevance of the collaboration and the mutual influence will be outlined in **Chapter 2**. The projects focus on two main aims: The enhanced understanding of odour and corrosion mechanisms and the development of a CFD simulation model. The research is carried out at the three different interfaces biofilm - (waste)water interface, the (waste)water - (sewer) air interface and the (sewer) air - biofilm - (concrete) wall interface. This Chapter aims to give an overview over the integration of the work into the Research Training Group.

After this overview, **Chapters 3 and 4** show results of a hydrodynamic study with the interFoam solver for two-phase flow in closed conduits. **Chapter 3** is a validation of the water phase described by the numerical model concerning different hydraulic conditions, the consideration especially focuses on flow in closed conduits. The validation is carried out by analysing the simulation results of three different test cases: single-phase flow over a hill under consideration of different turbulence models, free-surface flow over a ground sill and the analysis of a complex sewer geometry. The latter case has been analysed to investigate the stability of the simulations using the setup of a closed conduit and the overall accuracy in such a complex model domain. The results of the complex sewer are compared with results of an existing CFD model as well as measured results from a 1:20 scale model. **Chapter 4** deals with a further parameter study of a test case analysed in **Chapter 3**. A two-phase free-surface flow over a ground sill has been simulated and different parameters such as the structure of the ground sill, discharge, water level and flow regime have been evaluated concerning their influence on the water level drawdown.

**Chapter 5** introduces two different ways to analyse single-phase transport in a multiphase system. The implementation of a standard advection-diffusion equation into the interFoam solver can lead to an unphysical spreading across the water-air interface. In a first example, tracer transport around concrete probes in the headspace of the sewer pilot plant of the Berliner Wasserbetriebe (BWB) is simulated. The model setup considers the two-phase system of the sewer as a single-phase system by describing the water surface as a boundary condition. Then, a standard advection-diffusion tracer transport equation is applied. In a second case, tracer transport in the complex sewer stretch described in **Chapter 3** is simulated. Instead of a passive tracer, the interHarounFoam solver by Haroun et al. (2010a) is used to achieve phase-constrained transport.

**Chapter 6** explores the capabilities of the interHarounFoam solver for mass transfer which is based on the two-phase flow approach used in **Chapters 3 and 4** and extends the solver for specifics of  $H_2S$  mass transfer in sewers, namely the temperature dependency of the Henry coefficient, a conversion from pH value and total dissolved sulphide to the equilibrium between  $H_2S$  and bisulphide ion ( $HS^-$ ) and a conversion of the gas phase concentration  $H_2S_G$  to its respective partial pressure. The latter two are especially important when considering the experimental work carried out at the sewer pilot plant of the BWB as outlined in **Chapter 2**: Being able to insert the measured pH value and the total dis-

solved sulphide, enables the user to directly feed measurements into the model. The partial pressure of  $H_2S_G$  is another parameter that is measured in the pilot plant and supports the user in the direct interpretation of modelling results in the close future. The advantages of three-dimensional mass transfer simulations in complex geometries are highlighted by performing mass transfer simulations in the complex sewer geometry presented in **Chapter 3**.

**Chapter 7** uses the functionalities of the solver introduced in **Chapter 6** to analyse and validate the effect of turbulence on the  $H_2S$  mass transfer coefficient in a stirring tank. Therefore, the interH2SFoam solver is connected to a dynamic meshing functionality and extended to compute the occurring mass transfer coefficient. Being able to describe the mass transfer in a three-dimensional model can help to improve existing model concepts as well as to better examine hotspots of  $H_2S$  emissions in order to give recommendations for design improvement. The analysis of turbulence effects of drop structures on  $H_2S$  mass transfer, as it is introduced in **Chapter 2**, is one example of the importance of the correct description of turbulent effects.

**Chapter 8** gives an overview of supplementary scientific work and **Chapter 9** synthesizes the outcomes of this thesis and gives an outlook for future research.

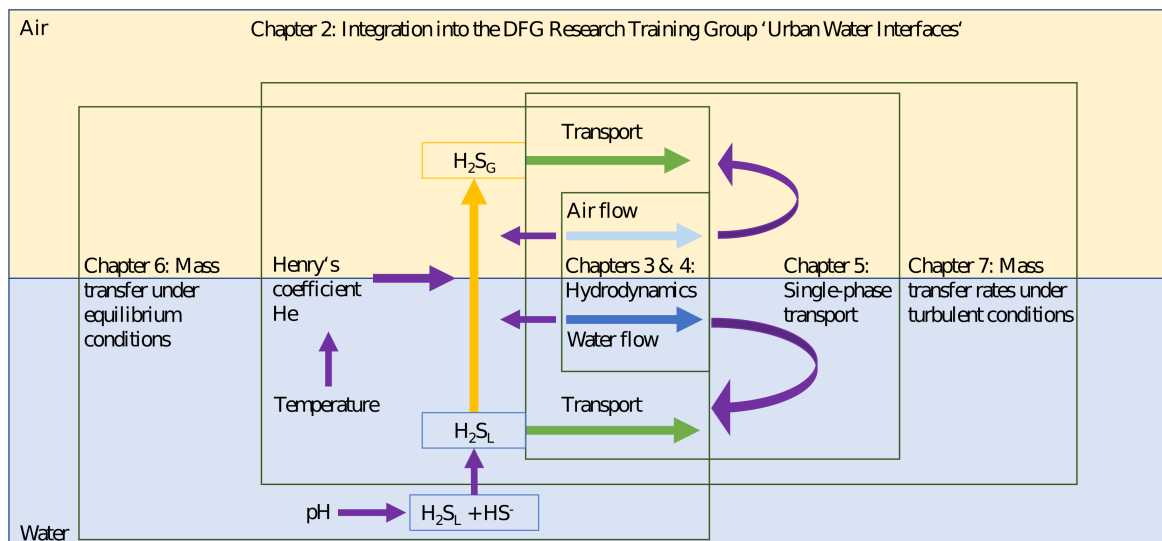


Figure 1.6: Overview over different chapters

## Chapter 2

# Research on interfaces in sewer systems within the DFG Research Training Group "Urban Water Interfaces"

This study was published as:

---

Teuber, K., Sielaff (née Grüneberger), M., Despot, D., Stephan, D., Barjenbruch, M. & Hinkelmann, R.: Modeling and Measuring of Interfaces in Sewer Systems, Proceedings of the 37th IAHR (International Association for Hydro-Environment Engineering and Research) World Congress, Kuala Lumpur, Malaysia, 2017.

---

This is the postprint version of the article.

The test cases' setups are listed in Appendix B (single-phase flow over ground sill: B.1, free-surface flow over ground hill B.2, complex sewer: B.3).

### Abstract

This paper presents the research focusing on interfaces in sewer systems as it is carried out within the DFG Research Training Group Urban Water Interfaces. During its transportation, wastewater in sewer systems undergoes a number of physical, biological and chemical processes and transformations. Under certain conditions such as high detention times, the formation of hydrogen sulfide ( $H_2S$ ) in sewer systems leads to odor in the sewer atmosphere, and after a biogenic oxidation to sulfuric acid ( $H_2SO_4$ ) to corrosion at sewer walls. In 1998, the restoration costs for corroded sewers in Germany were estimated to be in a range of billions of US \$ (Kaempfer and Berndt, 1999). High concentrations of odorous substances in the atmosphere can even lead to death of sewer workers. Within the research training group, three dissertation projects focus on two driving aspects: The enhanced understanding of odor and corrosion mechanisms and the development of a CFD simulation model. In order to gain a deeper understanding, a research pilot plant owned by the Berliner Wasserbetriebe (BWB) is operated. The work of this group enables a deeper in-detail understanding of  $H_2S$  formation in sewer systems and can therefore lead to an improvement of existing models as well as to developments that enable a detailed analysis of odor and corrosion problems in sewers.

## 2.1 Introduction

Every year damages of sewers due to corrosion cause high costs for sewer maintenance. At the same time, high hydrogen sulfide ( $\text{H}_2\text{S}$ ) concentrations in the sewer atmosphere are a health risk for sewer workers. The processes leading to odor and corrosion as well as the empirical and conceptual description of these processes have been investigated since more than 70 years (e.g. Parker (1945), Gilchrist (1953), Thistlethwayte (1972)). However, within the last 20 years a deeper understanding has been gained thanks to the efforts of research groups in Denmark and Australia (Rootsey and Yuan (2010), Rootsey et al. (2012), Hvitved-Jacobsen et al. (2013)). Conceptual model approaches have been developed in order to estimate corrosion risks. The aim of our research is to gain a deeper insight into the influence of small-scale structures such as obstacles and drop structures in sewers, to evaluate the comparability of different laboratory tests for sewer corrosion and to develop a Computational Fluid Dynamics (CFD) simulation model that is able to account for three-dimensional effects.

In order to better understand the processes investigated, the main processes leading to odor and corrosion shall be outlined in the following (see Figure 2.1). Under anaerobic conditions in sewage, sulfate present in the wastewater can be reduced to sulfide by sulfate-reducing bacteria (SRB) residing in the biofilms on the walls of sewer pipes (Sharma et al., 2008a). Sulfide is diffused from the biofilm into the water phase as  $\text{H}_2\text{S}$ . Influenced by the pH value and the temperature, different amounts of sulfide as  $\text{H}_2\text{S}$  and bisulfide ion ( $\text{HS}^-$ ) are present in the water phase. Described by the air-water equilibrium, emission of  $\text{H}_2\text{S}$  from the water into the air phase can occur. This process depends on factors such as the air and water phase velocities, pH value, temperature and the concentration of oxygen and nitrate. The air-water equilibrium for a volatile compound such as  $\text{H}_2\text{S}$  can be described by Henry's law which describes the relative amount of a volatile compound in the gas phase as a function of its relative occurrence in the water phase under equilibrium conditions and at constant temperature. The temperature dependency of Henry's law can be described by different equations for example, the van't Hoff equation. The concentration of  $\text{H}_2\text{S}$  in the air phase defines the intensity of odor. Another process taking place at the air - water interface is reaeration which is the transfer of oxygen across the air - water interface. This process is the only way to supply oxygen to the water phase and therefore influences the potential of aerobic and anaerobic processes in the wastewater (Hvitved-Jacobsen et al., 2013).

At moist concrete pipe walls,  $\text{H}_2\text{S}$  can be oxidized to sulfuric acid ( $\text{H}_2\text{SO}_4$ ) by aerobic microbial reactions (Hvitved-Jacobsen et al., 2013). Sulfuric acid can lead to the corrosion of the building material of the sewer system, especially of concrete and other cement-bound materials. A combined attack of the cement stone mineral's chemical dissolution and of expansive mineral formation (e.g. gypsum) can result in corrosion rates up to  $1 \text{ cm yr}^{-1}$  or higher, even for concretes developed for such conditions (Grenng et al., 2015).

The research is carried out in three different sub-projects focusing on different interfaces in sewer systems as well as applying different principles. The projects collaborate in diverse states and exchange results of their investigations. Measurements of  $\text{H}_2\text{S}$  emissions as well as corrosion rates are performed in a research pilot plant. The findings of this research pilot plant are used in order to validate a CFD model describing  $\text{H}_2\text{S}$  emissions across the air - water interface. Corrosion rates are measured on a laboratory scale, a pilot plant scale and on a sewer scale. Different concrete samples are compared and different laboratory tests are compared among each other in order to generalize the test procedure for corrosion at the

sewer atmosphere - biofilm - sewer wall (concrete) interface.

In the following, the respective projects will be presented. In Section 2.2, the experiments planned in the research pilot plant will be outlined. Section 2.3 presents the different tests that will be performed in order to investigate corrosion rates. An overview of the development of the CFD model will be given in Section 2.4.

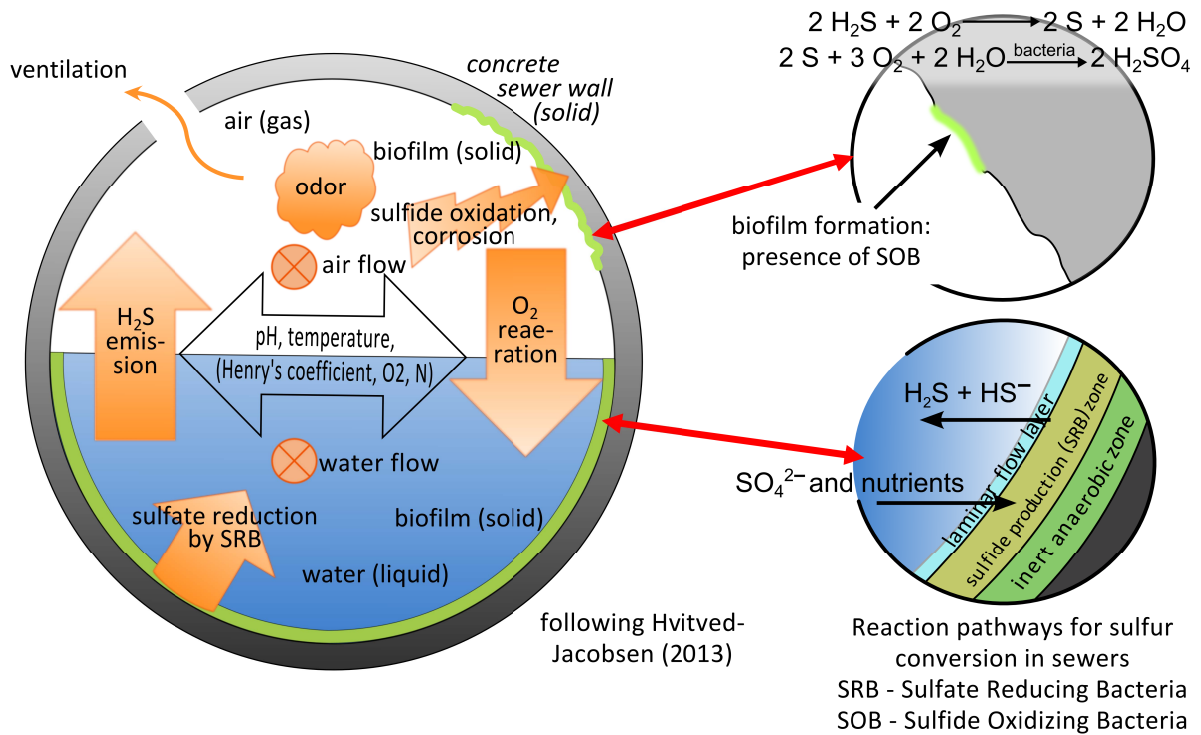


Figure 2.1: Interface processes in sewer systems.

## 2.2 Pilot plant investigations

The research pilot plant provided by Berliner Wasserbetriebe (BWB) facilitates a unique opportunity for performing experiments under realistic but controlled conditions (Figure 2.2). Here, wastewater from a wastewater pumping station in Berlin is directly fed into the experimental sewer pipes of the research pilot plant. The facility comprises of two pressure sewers with diameters of 100 mm that act as a fermenter, providing anaerobic conditions for the wastewater to reach the required levels of septicity and thus adequate  $H_2S$  formation (Figure 2.3). The wastewater is then conveyed into two corresponding gravity sewers having a length of 25 m each and a diameter of 400mm. The experimental sewer lines are duplicated so that one is used for experiments dealing with containment strategies and the other is used as a reference line for comparison. The concrete samples outlined in Section 2.3.2 will be placed in both the experimental line and the reference line. Sensor probes are used for continuous measurements in both the liquid and gas phases which can be accessed digitally by storage on a database. Measurement of pH values, temperature, dissolved oxygen (DO), equivalent chemical oxygen demand ( $COD_{eq}$ ) and equivalent suspended solids ( $TS_{eq}$ ) in the water phase can be made at various sampling points of the pilot plant setup. The s::can spectro:lyser™ UV-VIS spectrometer probes (s::can Messtechnik GmbH, Austria) are used for continuous measurement of total dissolved sulfides and nitrate concentration in the liquid phase. As for the gas phase, it is possible to measure the  $H_2S$ , temperature and relative humidity. The  $H_2S$  concentration in the gas phase is measured using the Kemira H2S-Guard™.

The experimental devices are used to further understand the key physicochemical and biochemical processes responsible for odor and corrosion in four different experiments. The experiments will be outlined in the following.

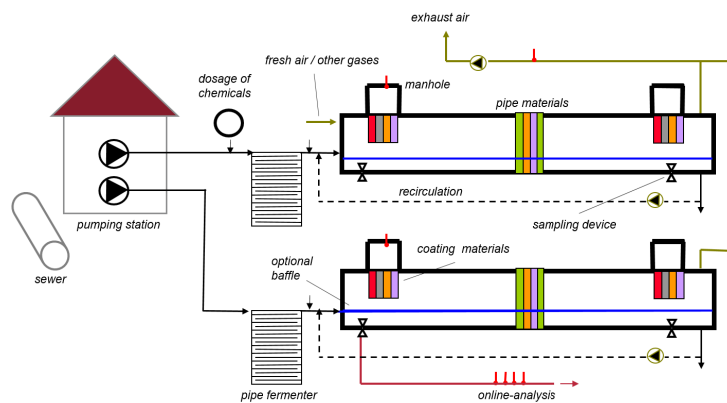


Figure 2.2: Research pilot plant.

Figure 2.3: Schematic drawing of the research pilot plant.

### 2.2.1 Sulfide formation in pressure or rising mains

Severe problems are associated with the microbial reduction of sulfate to sulfides in sewer systems, especially in pressurized flows (Hvitved-Jacobsen et al., 1995). Previous studies on sulfide production in pressure mains have resulted in a number of empirical formulas

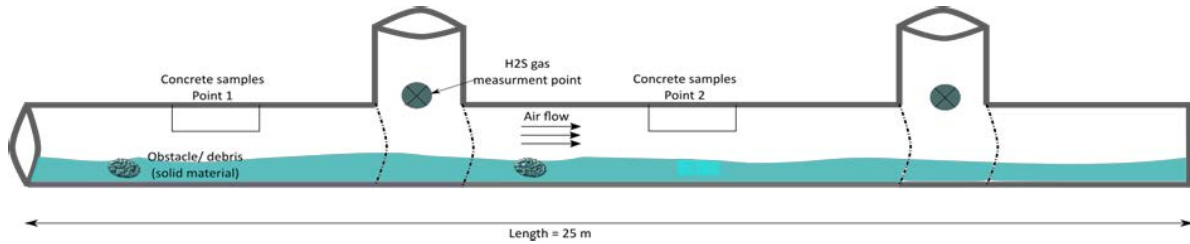


Figure 2.4: Experiment 2 – Elevated H<sub>2</sub>S emissions due to gross solids in wastewater.

which are still used in praxis and are based on parameters such as biochemical oxygen demand (BOD), chemical oxygen demand (COD), sulfate concentration and temperature etc. (Thistlethwayte (1972), Boon and Lister (1975), Pomeroy and Parkhurst (1978), Hvitved-Jacobsen et al. (1988), Nielsen et al. (1998)). In this investigation, the mostly used empirical formulas are to be evaluated using statistical analysis to determine the relationships of the key parameters promoting sulfide formation in pressure sewers, especially sulfide production at the biofilm - wastewater interface. The main goal of the experiments carried out in the first stage is to gain an improved understanding of the conversion processes within the sewer sulfur cycle under anaerobic conditions.

### 2.2.2 Elevated H<sub>2</sub>S emissions in gravity sewers due to flow interruptions caused by the accumulation of gross solids (debris / solid materials)

Gross solids are of particular concern for sewer systems since they can cause maintenance problems such as blockages and their sedimentation can increase the formation of toxic gases (e.g. sulfide and methane) (Rutz, 2016). The sewer blockage formation process is attributed by materials such as plastics, wet-wipes etc. that enter into gravity sewers. The accumulation of gross solids in gravity sewers can contribute to the emission of H<sub>2</sub>S in two ways: Due to a disruption of the flow regime, turbulence effects can occur at the surrounding regions of the obstacle and a higher amount of pollutants develops due to the accumulation of sediments (Ashley, 2004).

Until now, the influence of these small-scale structures in the water phase on the emissions has not been quantified. Investigating this relation can lead to better predictions in simulation models as well as better recommendations for countermeasures. The aim of this experiment is to quantify the levels of H<sub>2</sub>S emitted into the sewer atmosphere at these hotspots with respect to different hydraulic conditions (Figure 2.4). The highlighted interface for this experiment is the wastewater - sewer atmosphere interface in gravity sewers.

### 2.2.3 Investigation of H<sub>2</sub>S emissions at drop structures of sewer systems

The release or emission of H<sub>2</sub>S to the sewer atmosphere is known to be related to turbulence, pH, temperature and wastewater constituents (Matias et al., 2016). Drop structures found at manholes and transfer zones of sewer networks in sewers lead - similar to small-scale obstacles - to changed flow conditions and therefore facilitate increased H<sub>2</sub>S emissions. Previous efforts in understanding the H<sub>2</sub>S emission processes at drop structures of sewer systems have been only elaborated in laboratory experiments (i.e. with artificial wastewater) (Matias

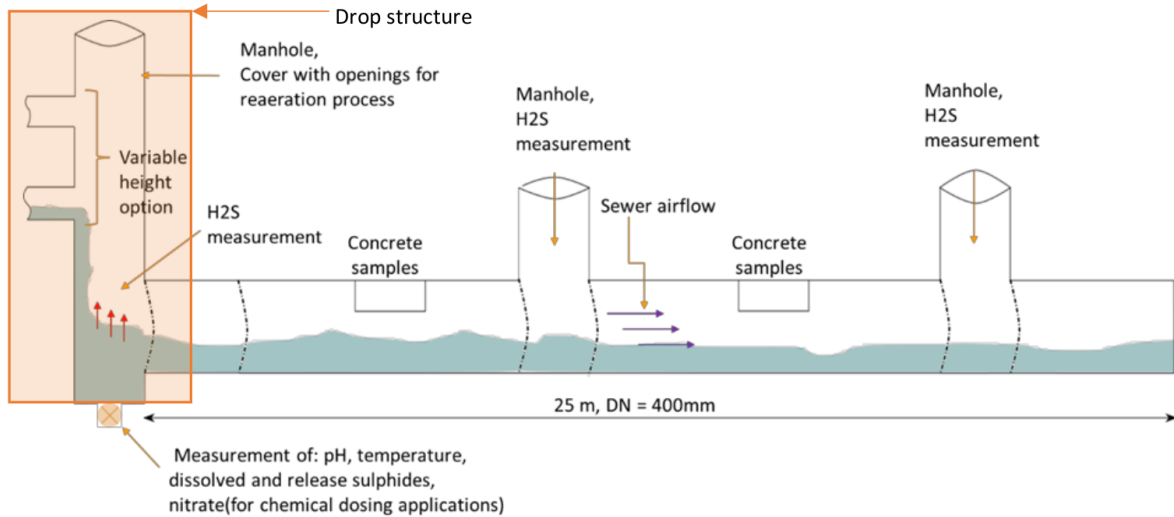


Figure 2.5: Experiment 3 – Pilot plant scale investigation of H<sub>2</sub>S emissions at drop structures.

et al., 2016). Extending these investigations to a pilot scale study can help to verify the laboratory experiments to more realistic conditions (sewer geometry and real wastewater). The knowledge obtained from this investigation provides essential information to predict the effects of sulfides in wastewater infrastructures, and has the potential to substantially improve the design and management approach of sewer systems (Matias et al., 2016).

A drop structure as displayed in Figure 2.5 will be added to the pilot plant and different parameters will be varied. Again, the H<sub>2</sub>S emissions into the sewer atmosphere will be measured. As in the previous experiment, the wastewater - sewer atmosphere interface is the main focus. The tailwater depth will be calculated by using the validated CFD model which will be described in Section 2.4.

#### 2.2.4 Impact of countermeasures at hotspots

In a fourth experiment, the impact of different countermeasures at hotspots is being tested. Problems of odor and corrosion in sewers are solved by several methods which have been intensively investigated. Today, most water companies and operators of sewer networks rely on several chemicals which have been proven to be effective in controlling sulfides in sewers. Chemical dosing of oxygen, nitrate, iron salts caustic, free nitrous acids and magnesium hydroxide (Mg(OH)<sub>2</sub>) are all examples of effective chemicals that are most widely used (Ganigué et al., 2016). Recent research on the application of countermeasures for controlling and reducing sulfides has been carried out on the optimization of the dosage strategies. Two optimization techniques that can be used are: (1) to consider the dosage location and response time for the chemicals to take effect, (2) online dosing control strategies.

The countermeasures to be used in this research project were selected with respect to the optimization techniques mentioned above. The first countermeasure application is based on a new method proposed by Auguet et al. (2015) which studied the effectiveness of downstream nitrite dosage. This study was conducted using a lab-scale sewer system and until now there is no report on its application to field studies. Evaluation of this method under

more realistic sewer network conditions can be studied in the pilot plant setup. A further step in this investigation will consider an online dosing control strategy.

The second countermeasure application will be based on the online control of  $\text{Mg}(\text{OH})_2$  dosing. This investigation follows Ganigué et al. (2016) which developed an online control algorithm for the optimized dosing of  $\text{Mg}(\text{OH})_2$  for sulfide mitigation in sewers. The use of  $\text{Mg}(\text{OH})_2$  for sulfide control in sewer systems in Germany is undocumented. Therefore, an assessment of this chemical dosing usage will also be made during this investigation.

## 2.3 Investigations of corrosion processes in sewer and laboratory tests

In the second research topic, corrosion processes in sewers at the interfaces of sewer atmosphere, biofilm and concrete sewer is being investigated. The use of concrete with a higher resistance against biogenic sulfuric acid corrosion (BSC) can increase the lifetime of sewer system components and reduce rehabilitation and replacement costs. In the past much research on the development and testing of high resistance concrete has been done and a large variety of laboratory performance tests for acid resistance of concrete has been developed (e.g. De Belie et al. (2002), Belgium; Petersen and Lohaus (2006), Germany; Fourie and Alexander (2008), South Africa; OENORM B 4710 APPENDIX K, Austria; Hüttl (2008), Germany). Those performance tests have not been experimentally compared. Also, most laboratory performance tests have not been directly compared to BSC in sewer systems by using the same concrete mixtures. Therefore, concrete samples in a sewer pilot plant will be compared with the same concrete mixtures tested in four laboratory performance tests developed in Germany and Belgium. The test developed by the Materialprüfungsanstalt (MPA) Berlin- Brandenburg (hereafter MPA Berlin-Brandenburg test) is performed in the original facility of MPA-Berlin- Brandenburg (now Kiwa Berlin) at TU Berlin. The facilities according to the LPI test and the E DIN 19573 appendix B test have been installed at TU Berlin for this project. The TAP test will be performed in the original facility at the Magne Laboratory for Concrete Research at Ghent University (Belgium). A special focus lies on the time laps effect of the laboratory performance tests and the corrosion mechanisms and sulfate containing components on the interface between sewer atmosphere, biofilm and concrete.

### 2.3.1 Concrete and mortar types

Five concrete types with different binders and water/binder value (w/b) are being produced to be tested in the pilot plant and in three laboratory performance tests. The different compositions result in varying acid resistances. The use of concrete with low, medium and high acid resistance will allow a comprehensive comparison of the pilot plant processes and the laboratory performance tests. Table 2.1 presents the composition of the five concrete types and their assumed acid resistances. A maximum grain size of 16 mm and the grading curve between A16 and B16 according to DIN 1045-2:2008-08 appendix L for all concrete types were chosen.

The laboratory performance test after E DIN 19573 appendix B (E DIN 19573:2013-06) requires mortar samples. The binder composition and w/b values of the five mortar types

Table 2.1: Composition and assumed acid resistances of concrete types used for acid resistance tests. Cement types are classified after DIN EN 197-1:2011-11. MS: microsilica, FA: hard coal fly ash.

Concrete type	1	2	3	4	5
Type of binder	white CEM I 42.5 R (dw)	CEM I 42.5 R	CEM III B 42.5 N-NA	CEM III B 42.5 N-NA	CEM I 42.5 R - MS - FA
$m_{\text{binder}}/V_{\text{concrete}}$ [kg/m <sup>3</sup> ]	360	360	360	373	350*
w/b value	0.45	0.45	0.45	0.35	0.42
assumed acid resistance	very low	low	medium	high	high

\*cement 270 kg/m<sup>3</sup>; microsilica 27 kg/m<sup>3</sup>; hard coal fly ash 53 kg/m<sup>3</sup>.

are equivalent to the concrete types. For each mortar type 450 g binder and 1350 g CEN-Reference-Sand DIN EN 196-1:2005-05 are being used.

### 2.3.2 Pilot plant acid resistance tests

The concrete samples are positioned in the concrete sample point 1 (see Figure 2.4) of both gravity pipes in the pilot plant. Six cuboids per concrete type are stored in each gravity pipe. The cuboids' edge lengths are 150 mm x 100 mm x 40 mm. As a reference sample, another six cuboids per concrete type are stored over water in a closed container at 20°C. One cuboid per concrete type is being taken from each gravity pipe of the pilot plant every six months. Also one cuboid per concrete mixture of the reference samples is being taken for analysis every six months. Results will be evaluated using the parameters monitored in the pilot plant, such as H<sub>2</sub>S concentration in the sewer gas phase.

### 2.3.3 Laboratory performance tests

All concrete types are analyzed using the MPA Berlin-Brandenburg (Hüttl, 2008), the LPI (Petersen and Lohaus, 2006) and the TAP test (De Belie et al., 2002). All mortar types are examined according to E DIN 19573:2013-06. An overview of the four tests is given in Table 2.2.

### 2.3.4 Analysis of concrete and mortar specimens

Concrete and mortar specimens from the pilot plant and the laboratory performance tests are being analyzed with reflected-light microscopy of polished samples and polarizing light microscopy of thin sections to measure the damage depth. In addition scanning electron microscopy with energy-dispersive X-ray spectroscopy will be performed. Powder X-ray diffraction will be done to characterize minerals formed during the experiments. Micro X-ray fluorescence spectroscopy will be performed to produce element maps of polished samples and to measure the damage depth. The proton consumption is calculated using the titrated acid in E DIN 19573 appendix B test. The concrete degradation and surface roughness is measured by laser measurements during the TAP test (see De Belie et al. (2002)).

Because for all tests the same concrete types are being used, the corrosion in the pilot plant and in the laboratory performance tests can be directly compared. New information

is being gained on the applicability of laboratory acid resistance tests concerning sewer systems. The time laps effect of the laboratory performance test will be estimated. Thereby more detailed insights are being gained concerning corrosion mechanisms caused by BSC.

## 2.4 Development of a three-phase CFD simulation model

In the third project, a CFD simulation model is being developed in order to numerically describe formations across the wastewater - sewer atmosphere interface. So far, existing model approaches (Sharma et al. (2008a); Hvitved-Jacobsen et al. (2013)) are one-dimensional approaches, neglecting three-dimensional flow effects in sewage and air. The three-dimensional model approach will be able to verify these assumptions and can be an extension of these models in respect to a more detailed analysis of hydraulic aspects.

The work carried out in this research divides in three different parts. The first step is a validation of the water phase described by the numerical model concerning different hydraulic conditions. Results obtained within this working package will be presented in Section 2.4.2. Because of the fact that sewer systems are focused on in the work of this group of researchers, the consideration especially focuses on flow in closed conduits. After the first validation step is completed, the model can be used to support the experimental work in the pilot plant in hydraulic questions. Possible applications are the estimation of the tailwater depth in the experiment outlined in Section 2.2.3. The two remaining working steps are the validation of the air phase behavior in closed systems as well as the implementation of transport as well as mass transfer processes depending on factors such as Henry's law in order to describe H<sub>2</sub>S formations. At a later stage, the model could even be extended to describe corrosion effects at the atmosphere - biofilm - sewer wall (concrete) interface and interact with the research project outlined in Section 2.3.

### 2.4.1 Numerical model

Surface water flow is calculated by using the two-phase flow solver interFoam based on a volume of fluid (VOF) approach for one- and two-phase flows as it is implemented in the open source model OpenFOAM. Both phases are considered as one fluid with rapidly changing fluid properties, therefore one set of Navier-Stokes equations is solved. The phases are distinguished by an additional transport equation for the volume fraction which is used as a marker to describe the distribution of the phases throughout the domain. The equations can be formulated as follows Rusche (2003):

Mass conservation equation:

$$\nabla \cdot \vec{\mathbf{U}} = 0 \quad (2.1)$$

Momentum conservation equation:

$$\frac{\partial \rho \vec{\mathbf{U}}}{\partial t} + \nabla \cdot (\rho \vec{\mathbf{U}} \vec{\mathbf{U}}) = -\nabla p_{rgh} + \nabla \cdot (\mu \Delta \vec{\mathbf{U}}) + (\nabla \vec{\mathbf{U}}) \nabla \mu - \vec{\mathbf{g}} \cdot \vec{\mathbf{x}} \nabla \rho \quad (2.2)$$

Where  $p_{rgh}$  is the static pressure minus hydrostatic pressure:

$$p_{rgh} = p - \rho \cdot \mathbf{g} \cdot \mathbf{h} \quad (2.3)$$

Table 2.2: Testing parameters of the four laboratory performance tests.

Testing parameter	MPA Berlin- Brandenburg test	LPI-test	E DIN 19537 appendix B test (bath test)	TAP test
<i>Test specimen:</i>				
Type	concrete	concrete or mortar	mortar	concrete
Geometry	4x15 cuboids: 150 mm x 100mm x 40 mm	2x4 concrete cuboids: 70 mm x 35 mm x 150 mm 2x6 mortar cuboids: 40 mm x 20 mm x 160 mm	5 cuboids: 40 mm x 40 mm x 80 mm	cylinder: d = 270 mm, h= 70 mm
Testing age	28 days*	28 days*	28 days*	28 days*
<i>Testing medium:</i>				
Type	sulfuric acid	sulfuric acid*	sulfuric acid	sulfuric acid or acetic/lactic acid mix
Concentration	pH 3.5	pH 3.0*	pH 4.0	sulfuric acid: pH 0.8 - 1.0 acetic/lactic acid mix: pH 2.0 - 2.2
<i>Performance:</i>				
Test duration	12 weeks	12 weeks*	4,000 h	dependent on testing procedure
Testing facility	5 tanks (45 l), 1 reservoir tank (80 l)	tank (13 l)	tank (4 l)	tank (2 l)
Acid renewal	every 2 weeks	every week*	every 1,000 h	after every attack cy- cle
Constant pH	yes (automatic titration)	yes (automatic titration)	yes (automatic titration)	no
Mixing of medium	circulation of medium	rotation of sample in acid tank (150 s per revolution)	magnetic stirrer	rotation of sample in acid tank (1.04 revolutions per h)
Abrasion	manual brushing of a part of the samples once per week	automatic brushing of a part of the samples every 150 s	none	automatic brushing after every attack cycle
<i>Evaluation:</i>				
Analysis	thin-section polariz- ing light microscopy and mass loss	thin-section polariz- ing light microscopy	proton consumption during the test	laser measurements
Assessment criterion	measured damage depth in comparison with reference concrete	measured damage depth	calculated damage depth	concrete degradation, surface roughness

\*Parameters can be changed according to the behavior and application of the building material.

Volume of Fluid equation:

$$\frac{\partial \alpha}{\partial t} + \nabla \cdot (\alpha \vec{U}) + \nabla \cdot ((1 - \alpha) \mathbf{U}_r \alpha) = 0 \quad (2.4)$$

with the following parameters:

$$\rho = \alpha \rho_w + \rho_a (1 - \alpha) \quad (2.5)$$

$$\mu = \alpha \mu_w + \mu_a (1 - \alpha) \quad (2.6)$$

$$\mu = \mu_w + \mu_a \quad (2.7)$$

where  $\vec{U}$  is the velocity field [m/s];  $\rho$  is the density [kg/m<sup>3</sup>];  $t$  is time [s];  $p$  is pressure [Pa];  $\mu$  is dynamic viscosity [Ns/m<sup>2</sup>];  $g$  is acceleration vector due to gravity [m/s<sup>2</sup>];  $x$  is a spatial position vector [m];  $\alpha$  is volume fraction or indicator function [-];  $\mathbf{U}_r$  is the relative velocity between the phases [m/s]; the subscripts  $a$  and  $w$  denote different fluids air and water.

The indicator function  $\alpha$  is defined as:

$$\alpha = \begin{cases} 1 & \text{fluid water} \\ 0 < \alpha < 1 & \text{transitional region} \\ 0 & \text{fluid air} \end{cases}$$

The water surface is considered as the area described by a volume fraction  $\alpha = 0.5$ . For single-phase test cases the volume fraction  $\alpha$  is 1 and constant over the whole domain and during the simulation time. A special definition of boundary conditions for two-phase flows is necessary in order to obtain stability of simulations in closed ducts. The upper and lower walls are defined as no-slip conditions. Depending on the fact whether the simulations are two- or three-dimensional, the sidewalls are defined as no-slip conditions for three-dimensional cases and as empty boundary conditions for two-dimensional cases. The empty boundary condition in OpenFOAM is a special boundary condition for two-dimensional model setups. The definition of inlet and outlet is displayed in Figure 2.6. The inlet is divided in two parts, an inlet for the air phase, where a total pressure is defined. The second part is the inlet for the water phase, defined by a fixed discharge or flow velocity. At the outlet, a constant pressure is defined leading to a free outflow of the water without definition of a certain upstream water level. This upstream water level is achieved by adding a weir structure in the proximity of the outlet to the model geometry. This type of outlet boundary condition has originally been outlined for open systems with top atmospheric boundaries by Bayón and Lopez-Jimenez (2015). For a more detailed description of further properties, such as the chosen boundary conditions for each test case and the turbulence models, the reader is referred to Teuber et al. (2019a).

## 2.4.2 Validation of the water phase behavior

In order to secure the applicability of the chosen numerical model, flow properties such as the water flow velocity and the water surface behavior described by the VOF approach have been validated (Teuber et al., 2016, 2019a).

First, a validation of the water velocity has been performed by using experimental results of single-phase water flow over a ground sill in a closed duct by (Almeida et al., 1993). Different Reynolds averaged (RANS) turbulence models and Large Eddy Simulations (LES)

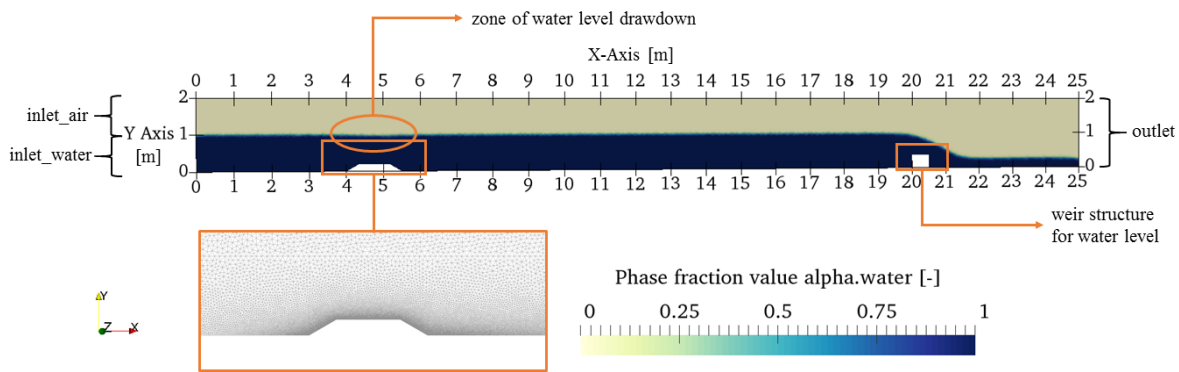


Figure 2.6: Model domain of water surface validation case.

were compared as well. The RANS models investigated were the Standard  $k-\epsilon$  (Launder and Sharma, 1974),  $k-\omega$  (Wilcox, 1988) and  $k-\omega$  Shear Stress Transport (SST) model (Menter, 1993, 1994). As the subgrid-scale model for the LES simulations, the Smagorinsky model (Smagorinsky, 1963) was chosen. The results led to the conclusion that the chosen RANS models as well as the LES simulations lead to a good approximation of the experimental results. Due to the nature of the different turbulence models, the LES simulations were able to capture fluctuations in the flow velocity which can be of interest for some application areas. With this advantage of LES comes the disadvantage of a higher necessary mesh resolution which leads to significantly increased computation times.

In order to validate the behavior of the water surface, two-phase flow over a ground sill was simulated. The basic setup of the model domain is displayed in Figure 2.6. Simulations were performed for different two- and three-dimensional model setups with variations concerning the structure of the sill, discharge, water level and the flow regime. Since fluctuations of the flow velocity were of minor interest, the  $k-\epsilon$  turbulence model was used. The water level drawdown was compared to analytical solutions obtained by using continuity and Bernoulli's equation. A detailed discussion of the results can be found in Teuber et al. (2016). Overall, the results showed a good agreement of the simulations with measured water velocities and a reasonable behavior of the water - air interface. However, the numerically computed water level drawdown was smaller than the analytically calculated drawdown. Explanation can be found in the treatment of single losses. The three-dimensional CFD model is able to account for single losses caused by the structure of the sill whereas the analytical solution is a one-dimensional solution that neglects single losses.

In a last step, simulations have been performed in a complex sewer geometry described in Bayón et al. (2015), proving the applicability of the simulations under demanding hydraulic conditions. This geometry contains different hydraulic structures such as weirs, different flow regimes and a hydraulic jump. The simulation results were compared to experimental measurements carried out on a 1:20 scale model as well as to CFD simulations previously performed by Bayón et al. (2015) by using a different model setup (open system, without upper wall). A detailed analysis will be published in Teuber et al. (2019a). The results showed a good agreement between both the existing simulation model as well as the experimental results and lead to the conclusion, that the solver is applicable to complex hydraulic cases in closed conduits such as sewer systems.

Overall, the simulations performed show that the solver is able to simulate different hydraulic cases. The chosen turbulence models were comparable in their accuracy, however, the LES simulations were able to account for fluctuations in the velocity under increased computational effort. A second validation step will be to analyze the accuracy of the air-phase behavior.

## 2.5 Conclusions

In this paper we presented the research as it is carried out in the sewer interfaces group within the DFG Research Training Group Urban Water Interfaces. Different sub-projects focus on a deeper understanding of H<sub>2</sub>S formations at and across the wastewater - biofilm, the wastewater - sewer atmosphere and the sewer atmosphere - biofilm - sewer wall (concrete) interface.

The first project conducts experimental investigations on a pilot plant in order to gain an enhanced understanding of sulfide formations in pressure mains as well as on investigating the influence of flow interruptions caused by gross solids and drop structures. Further, the effects of different countermeasures at hotspots are being analyzed. In another project, this research pilot plant is used in order to investigate BSC in sewers. The main goal is to investigate different laboratory performance tests and to compare them among each other as well as to concrete probes installed in the pilot plant. In the third project, a CFD simulation model is being developed in order to describe H<sub>2</sub>S emissions across the wastewater - sewer atmosphere interface. First results show, that the model is able to accurately describe the behavior of the water phase. Therefore, the model can be used in order to estimate different hydraulic properties within the sewer pilot plant. On the other hand, results concerning H<sub>2</sub>S formations obtained by the sewer pilot plant can be used to validate the extended CFD model.

The added value of the work carried out by this group lies in the detailed insight into H<sub>2</sub>S formation processes and sensitivity analyses that can be carried out. The influence of gross solids or drop structures on the H<sub>2</sub>S release can be investigated on a pilot plant scale. The validated CFD model can be used to investigate the effect of measures such as i.e. changed discharges or ventilation measures on H<sub>2</sub>S emissions. These findings can be integrated into existing model approaches in order to improve predictions. The development of a CFD model can generalize the findings of the investigations in the pilot plant to different conditions. The detailed analysis of different laboratory performance tests helps to generalize the development of acid-resistant concrete.

## Acknowledgements

The funding provided by the German Research Foundation (DFG) within the Research Training Group Urban Water Interfaces is gratefully acknowledged.

Parts of the simulations were computed on the supercomputers of Norddeutscher Verbund für Hoch- und Höchstleistungsrechnen in Berlin.

The sewer pilot plant is provided by the Berliner Wasserbetriebe (BWB). We also thank the

Kompetenzzentrum Wasser Berlin for providing s::can probes, the Kiwa (Berlin) for providing the apparatus for the MPA Berlin-Brandenburg test, and the Magnel Laboratory of the University Ghent for providing the TAP apparatus.

## Chapter 3

# Validation of hydrodynamic two-phase simulations

This study was published in *Progress in Computational Fluid Dynamics* (Inderscience) as:

---

Teuber, K., Broecker, T., Bayón, A., Nützmann, G. & Hinkelmann, R.: CFD-modelling of free-surface flows in closed conduits, *Progress in Computational Fluid Dynamics*, 19 (6), 368-380, 2019; doi:10.1504/PCFD.2019.103266.

©Inderscience 2019. The definitive peer-reviewed and edited version of this article is published in doi:10.1504/PCFD.2019.103266 and available at [www.inderscienceonline.com](http://www.inderscienceonline.com).

---

Reproduced from Teuber et al. 2019 *Progress in Computational Fluid Dynamics* 19(6) 368-380, with permission from the copyright holders, Inderscience.

The test cases' setups are listed in Appendix B (single-phase flow over ground sill: B.1, free-surface flow over ground hill B.2, complex sewer: B.3).

### Abstract

Computational Fluid Dynamics (CFD) is gaining an increasing importance in the field of hydraulic engineering. This publication presents different application examples of a two-phase approach as implemented in the open source software OpenFOAM. The chosen approach is based on the volume of fluid method focusing on the simulation of flow in closed conduits. Three examples are presented: single-phase flow over a ground sill and free surface flow over a hill as well as complex free surface flow in a sewer model. The first example compares the results of different RANS turbulence models with experimental results. The results of the second example are compared with an analytical solution. In the last example the behaviour of the free surface flow is compared with the results of a model test and existing simulations using a simplified, open channel geometry for the closed conduit. For the examples analysed, the two-phase approach provides stable and reliable results.

### 3.1 Introduction

Numerical multiphase solvers have gained an increasing importance in the field of hydraulic research. In this paper, the open field operation and manipulation (OpenFOAM) solver interFoam (Rusche, 2003) which is based on a VOF interface capturing approach (Section 3.2.2) will be analysed.

In a number of recent publications, such as Bayón et al. (2015), Bayón and Lopez-Jimenez (2015), Schulze and Thorenz (2014) and Thorenz and Strybny (2012) the interFoam solver was used to analyse complex hydraulic cases in open channels. Possible application areas are inland waters (Thorenz and Strybny, 2012), coastal areas (Higuera et al., 2013) as well as sewer systems (Bayón et al., 2015). The previously mentioned publications simulated the water phase behaviour and used the two-phase approach in order to display the movement of the free water surface.

Bayón and Lopez-Jimenez (2015) used the interFoam solver to analyse a hydraulic jump in a rectangular channel with smooth walls. A comparison of different variables with experimental results led to the conclusion that the model can be applied to real-life cases of designing hydraulic structures. In Bayón et al. (2015), the test case of the hydraulic jump was extended to a more complicated surrounding consisting of an existing sewer stretch with different hydraulic structures such as weirs, quickly-varying shapes, macro-roughness elements, fast and slow flow regimes as well as hydraulic jumps. The results were compared with experimental results from a 1:20 scale model and also showed a good agreement. In our last example we will use this sewer geometry. Due to stability problems, the sewer has been simulated as an open channel with an atmospheric top boundary.

The novelty applied to the existing setup is the closed system setup by defining a closed (wall) top boundary instead of an open atmospheric top boundary as it has been used in Bayón et al. (2015) and a different definition of the outlet boundary condition.

The importance of the correct choice of a turbulence model was shown in Bayón et al. (2015) and Bayón and Lopez-Jimenez (2015). A sensitivity analysis in Bayón and Lopez-Jimenez (2015) showed a good performance of the Standard  $k-\epsilon$  turbulence model.

A number of pipe flow simulations have already been performed applying the VOF approach in closed ducts. A few of them shall be outlined in the following and their certain characteristics shall be pointed out.

Shuard et al. (2016) compared simulations of two-phase flow in a circular pipe using the interFoam solver with results of a mechanistic model. Similar simulations have been carried out by Thaker and Banerjee (2013) analysing the transition between different flow regimes as well as the development of flow regimes. The results were compared to experimental measurements using similar boundary conditions. The boundary conditions that have been used by Shuard et al. (2016) have been used for a different area of application by Kinyua et al. (2016). Here, tubular anaerobic digesters have been modelled by including tracer simulations. The simulations carried out by Shuard et al. (2016), Thaker and Banerjee (2013) and Kinyua et al. (2016) analysed flow behaviour in closed ducts. By applying a constant value as an outlet pressure boundary condition, a free outflow out of the domain was achieved, assuming that the water level is not impounded by any downstream water level.

This short literature review shows that CFD models are an upcoming topic in hydraulic engineering but the simulation results strongly depend on factors such as boundary conditions, mesh quality and turbulence models. Existing validation shows a good accuracy of the interFoam solver with experimental data for open systems with atmospheric top boundaries and for closed ducts with free outflows, however, there is a lack of research on the behaviour of free surface flows in closed ducts with a defined water level.

In this paper we want to investigate simulations that describe free surface flow in closed

pipes where at the same time a certain outlet water level is desired (see also Bayón et al. (2015)). This problem occurs in cases where the area of interest comprises a large system, i.e. a complete sewer system. Due to limitations of computational resources it is usually not feasible to simulate the whole system, however, it is possible that the water level at the end of the stretch that is being considered in the simulation influences the water level within the model domain. Therefore it is not possible to use a free outflow as it has been used in previous studies. The literature analysis shows that these systems have not been addressed in previous publications.

The simulation of closed systems is interesting for different areas of application, i.e. for the modelling of in-sewer processes (Edwini-Bonsu and Steffler, 2004, Gessner et al., 2014, Hvitved-Jacobsen et al., 2013, Rootsey et al., 2012). A detailed analysis of the air phase behaviour will be subject to future research. To ensure a correct behaviour of the water phase, a thorough validation of flow simulations in closed conduits using the solver *interFoam* is performed in three steps. First, the behaviour of the water phase is analysed by comparing the numerical data of flow over a hill for single-phase flow with experimental results by Almeida et al. (1993). The results of the first test case show us which turbulence model is most suitable for the problems analysed. Then, the different outlet boundary conditions are compared using a simple two-phase simulation. The interface behaviour is analysed by comparing the simulated results of water level drawdown due to a ground sill with analytical results based on continuity and Bernoulli's equation. In a last step, the stability and the accuracy in describing a practical test case is checked by simulating a complex sewer geometry (Bayón et al., 2015).

The paper is organized as follows: Section 3.2 gives an overview over the methods and materials. The computational test cases are presented in Section 3.3. The validation of the different parts is done as follows: single phase water flow over a ground sill, free surface flow over a hill, complex free surface flow in a sewer model. In Section 3.4, the results of the validation are summarized.

## **3.2 Methods and materials**

### **3.2.1 Geometry and mesh**

Unstructured meshes created in the open source mesh generation tool *gmsh* were used for the single phase validation case (see Section 3.3.1) and for the free surface flow over a hill (see Section 3.3.2). The complex sewer case of Section 3.3.3 was discretized with a structured grid using the *OpenFOAM* utility *snappyHexMesh*. The detailed geometry of the different test cases will be outlined in the subsequent sections.

### **3.2.2 Numerical model**

The Open Source CFD software *OpenFOAM* (Open Field Operation and Manipulation) version 2.4.0 was used to simulate different test cases. Single and two-phase flow is calculated by using the solver *interFoam* based on a VOF approach. *interFoam* is a multiphase solver for immiscible and isothermal fluids that solves the three-dimensional Navier-Stokes equations using the finite-volume-method in space and the finite-differences-method in time. *OpenFOAM* allows parallel computations on a theoretically unlimited number of processor cores (Keough, 2014).

The conservation of mass (Equation 3.1) and momentum (Equation 3.2) for incompressible flow can be written as:

$$\nabla \cdot \mathbf{U} = 0 \quad (3.1)$$

$$\frac{\partial \rho \mathbf{U}}{\partial t} + \mathbf{U} \cdot \nabla \rho \mathbf{U} = -\nabla p + \mu \Delta \mathbf{U} + \rho \mathbf{g} \quad (3.2)$$

The viscosity term  $\mu$  referred to in Equation 3.2 contains the physical viscosity  $\mu_{phys}$  as well as the turbulent viscosity  $\mu_{turb}$  which will be obtained by a turbulence model:

$$\mu = \mu_{phys} + \mu_{turb} \quad (3.3)$$

The VOF method used in the interFoam solver uses a specific pressure formulation where  $p_{rgh}$  is a modified pressure which is used in order to avoid the occurrence of steep pressure gradients caused by hydrostatic effects. In the following,  $p_{rgh}$  will be referred to as:

$$p_{rgh} = p - \rho \cdot \mathbf{g} \cdot \mathbf{h} \quad (3.4)$$

The two immiscible fluids liquid and gas “are considered as one effective fluid throughout the domain, the physical properties of which are calculated as weighted averages based on the distribution of the liquid volume fraction, thus being equal to the properties of each fluid in their corresponding occupied regions and varying only across the interface”(Berberović et al., 2009), leading to a definition of  $\rho$  and  $\mu$  as follows:

$$\rho = \alpha \rho_{water} + \rho_{air} (1 - \alpha) \quad (3.5)$$

$$\mu = \alpha \mu_{water} + \mu_{air} (1 - \alpha) \quad (3.6)$$

The  $\alpha$  transport equation - also known as VOF equation - is used with an advanced formulation which can be considered as an evolution equation for the phase fraction  $\alpha$  (Berberović et al., 2009):

$$\frac{\partial \alpha}{\partial t} + \nabla \cdot (\alpha \mathbf{U}) + \nabla \cdot ((1 - \alpha) \mathbf{U}_r \alpha) = 0 \quad (3.7)$$

“where  $\mathbf{U}_r = \mathbf{U}_g - \mathbf{U}_l$  is the vector of relative velocity, designated as the “compression velocity””(Berberović et al., 2009). A detailed derivation of the equations can be found in Damián (2012).

In the equations above,  $\mathbf{U}$  represents the ensemble averaged velocity field shared by the two fluids throughout the flow domain [m/s];  $\rho$  is the density [ $kg/m^3$ ];  $t$  is time [s];  $p$  is pressure [Pa];  $\mu_{phys}$  and  $\mu_{turb}$  are the physical and turbulent viscosity [ $Ns/m^2$ ];  $\mathbf{g}$  is the acceleration vector due to gravity [ $m/s^2$ ];  $\mathbf{h}$  is a spatial position vector [m];  $\alpha$  is the volume fraction or indicator function [-];  $\mathbf{U}_r$  is the relative velocity between the phases [m/s]; the subscripts  $l$  and  $g$  denote different fluids liquid (water) and gas (air). The indicator function  $\alpha$  is defined as:

$$\alpha = \begin{cases} 1 & \text{for a point inside fluid } water \\ 0 < \alpha < 1 & \text{for a point in the transitional region} \\ 0 & \text{for a point inside fluid } air \end{cases}$$

The water surface is defined as the transition area where  $\alpha = 0.5$ . The solver can be used as well for single-phase flow simulations. The volume fraction  $\alpha$  is then 1 and constant over the whole domain.

Since the relative velocity cannot be computed directly from the one-fluid formulation in OpenFOAM, the numerical implementation of the relative velocity is as follows (Cifani et al., 2016):

$$U_r = n_\alpha \min\left[C_\alpha \frac{|\phi|}{|S_\alpha|}, \max\left(\frac{|\phi|}{|S_\alpha|}\right)\right] \quad (3.8)$$

where  $n_\alpha$  is the normal vector of the cell surface,  $\phi$  is the mass flux,  $S_\alpha$  is the cell surface area,  $C_\alpha$  is an adjustable coefficient on which the level of compression depends. The maximum of  $U_r$  is bounded to the maximum face velocity in the flow field and the direction is aligned with  $n_\alpha$  (Cifani et al., 2016, Hoang et al., 2013).

Equations 3.1 and 3.2 are solved by using the PIMPLE algorithm. As outlined in Bayón et al. (2015), pressure-velocity coupling is done by combining the inner corrector loops of the PISO (Pressure Implicit with Splitting of Operators) algorithm (Issa, 1986) with outer corrector loops of the SIMPLE (Semi-Implicit Method for Pressure-Linked Equations) algorithm (Patankar and Spalding, 1983). Detailed information on the algorithms can be found in Jasak (1996). As advection schemes, a total variation diminishing scheme (interGamma) (Jasak, 1996) combined with a flux corrected transport approach MULES (Multidimensional Limiter for Explicit Solutions) (Damián, 2013) is used.

Simulations were carried out until a quasi-steady state was reached. This quasi-steady state has been determined by sampling variables of interest such as the pressure and the velocity at different points in the water and air phase.

In the first example, different RANS turbulence models, namely the Standard  $k-\varepsilon$  (Lauder and Sharma, 1974),  $k-\omega$  (Wilcox, 1988) and  $k-\omega$  Shear Stress Transport (SST) (Menter, 1993, 1994) are compared. Wall functions have been used to describe the near-wall turbulent flow. It was ensured that the  $y^+$ -values for each simulation were in a range between 30 and 300 to guarantee the applicability of the wall functions.

### 3.2.3 Boundary conditions

Different boundary conditions were defined for single and two-phase simulations. The definition of sidewalls was similar for single and two-phase simulations but varied depending on the fact whether two or three-dimensional model setups were used. For two-dimensional test cases, so-called empty boundary conditions, which are implemented in OpenFOAM to describe sidewalls of two-dimensional geometries, were used. They declare that the sidewalls do not constitute solution directions within the defined domain. The sidewalls of three-dimensional testcases were defined by no-slip conditions. The detailed set of boundary conditions is explained in the chapters containing the respective test cases. However, a short description about the definition of outlet boundary conditions in free surface CFD models shall be given in the following.

In general, the definition of the outlet boundary condition in OpenFOAM using the interFoam solver differs from the definition in shallow-water models. In these models, often a water level is fixed at the outlet of the domain. In OpenFOAM, such a definition of a constant water level is not possible, therefore alternatives have to be looked for. Possibilities described in recent publications are to fix the pressure and the phase fraction value at the outlet (Thorenz and Strybny, 2012) or to specify a velocity profile at the outlet. A third option which circumvents the direct definition of a boundary condition in order to ensure a certain water level is to set an atmospheric pressure condition at the outlet and integrate a

weir in the geometry close to the outlet (Bayón and Lopez-Jimenez, 2015).

In this paper, a certain water level  $h$  at the outlet has been obtained in two different ways which will be referred to in the respective sections:

- Pressure boundary condition:  $p_{rgh}$  is defined as a stepwise function at the outlet. The built-in function *setFields* is used to overwrite uniform values at the outlet which is initially defined using a *calculated* boundary condition:

$$p_{rgh} = \begin{cases} 0 & \text{if } z < h \\ \max(\rho gh) & \text{if } z \geq h \end{cases}$$

After the writing process, the type of boundary condition is changed to *fixedValue*. The velocity at the outlet is defined as *inletOutlet* condition which applies a null Neumann boundary condition in case of positive flux out of the domain and a user-specified fixed velocity in case of negative flux into the domain. In case of negative flux, the velocity is set to  $U = (0 \ 0 \ 0)$ . The phase fraction value  $\alpha$  is defined as null Neumann boundary condition.

- Integration of weir: a weir structure in close proximity to the outlet is used as a means to maintain the water level in the domain. At the outlet, a constant pressure is defined using a Dirichlet boundary condition, the velocity is defined using the *inletOutlet* condition. The phase fraction value  $\alpha$  is specified using a null Neumann boundary condition.

In order to avoid stability problems, pressure boundary conditions need an accurate definition of initial conditions, i.e. the initial water level, flow velocity and pressure. Therefore, for simulations using this set of boundary conditions, suitable initial conditions have to be specified. They will be further outlined in the subsequent sections. Depending on the RANS turbulence model, an additional definition of boundary conditions for turbulent properties such as the turbulent kinetic energy  $k$  and the turbulent dissipation  $\varepsilon$  for  $k$ - $\varepsilon$  or the turbulent kinetic energy  $k$  and the specific dissipation  $\omega$  for  $k$ - $\omega$  models is needed depending on the chosen model. For the boundary condition, an initial guess of the turbulent properties has to be defined. During the simulation, these values are rewritten according to the simulation results.

## 3.3 Applications

### 3.3.1 Single phase water flow over a ground sill

In the first example, single-phase water flow over a two-dimensional model hill in a duct has been simulated and compared with experimental results obtained by Almeida et al. (1993).

Experiments were conducted in a two-dimensional duct with a height of  $h_{max} = 0.17m$  bounded by an upper and lower wall with a polynomial-shaped obstacle on its bottom (see Figure 3.1). The mean centreline velocity at the inlet amounted to  $U_0 = 2.147m/s$  causing pressurized flow throughout the domain. Velocity profiles of the simulations in  $x$  and  $y$ -direction at four (velocities in  $x$ -direction) respectively two (velocities in  $y$ -direction) different locations were compared to the measurements:  $x_{-03} = -0.30 \ m$  (in front of the hill),  $x_{00} = 0.00 \ m$  (top of the hill),  $x_{01} = 0.03 \ m$  (end of the hill) and  $x_{02} = 0.05 \ m$  (middle of recirculation zone). Figure 3.1 shows the model domain including the mesh that has been used

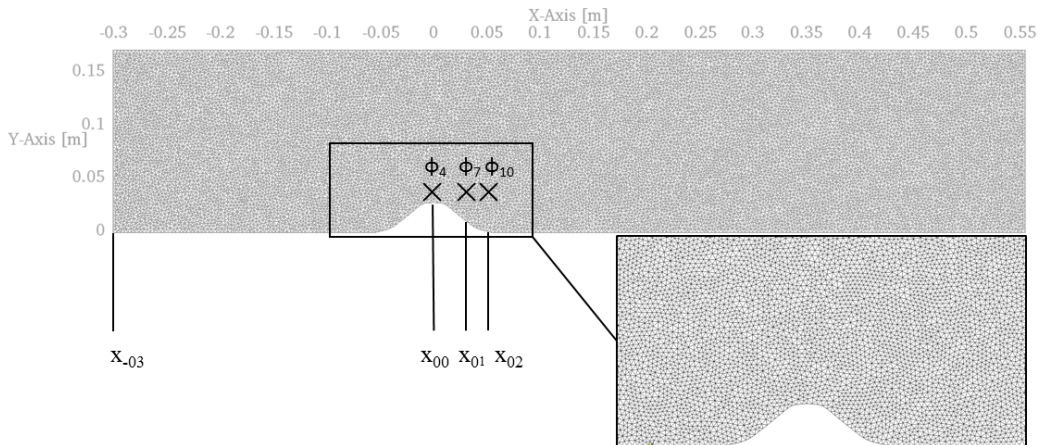


Figure 3.1: Domain of single-phase, two-dimensional hill flow including measurement locations, three selected indicator locations for grid convergence study and computational mesh (Davroux et al., 1995).

and the different measurement stations. Simulations have been carried out using different RANS turbulence models (Standard  $k-\varepsilon$ ,  $k-\omega$ , and  $k-\omega$  SST).

A grid convergence study following Celik et al. (2008) has been conducted in order to ensure mesh independence. Five different meshes with different cell sizes were tested using the flow velocity in  $x$ -direction  $U_x$  in 15 locations in the nearfield of the hill structure. The cell sizes and total number of cells of the analysed meshes were 0.0293 m (69,326 cells), 0.0346 m (31,102 cells), 0.0416 m (15,319 cells), 0.0495 m (7,338 cells), and 0.0581 m (3,855 cells), leading to a global refinement ratio between meshes of 2, which is above the minimum recommended value of 1.3 (Celik et al., 2008). Figure 3.2 a) shows the resulting velocities of three indicator locations  $\phi_4$ ,  $\phi_7$  and  $\phi_{10}$ . The position of these three points is displayed in Figure 3.1. Convergence was reached between the second finest and finest mesh. The computed RMSE for the different refinement steps (i.e. step 1: between coarsest and second coarsest mesh) is displayed in Figure 3.2 b). It shows a significant decline between the third and fourth refinement step to  $5.5e-5$  m/s. These results lead to the conclusion that the second finest mesh analysed has reached grid independence, so all subsequent analysis is conducted on the mesh of 0.0346 m element size and a total number of 31,102 cells. For the selected mesh, the average apparent order as defined by Celik et al. (2008) is 1.9, very close to the model formal order. A variable time step in dependence of the Courant number has been used, which converged to approximately  $\Delta t = 0.0007$  s. The model convergence to a quasi-steady state can be observed after a few seconds. All simulations have been carried out with a simulation time of 10 seconds. For all simulations, Intel Xeon IvyBridge E5-2695v2 cores have been selected. Using parallel computations on 16 cores led to computation times of approximately 34 minutes. In order to reach a good agreement with the experimental setup, a velocity profile using the experimental data has been imposed as an

inlet boundary condition. The upper and lower walls were specified with no-slip conditions. At the sidewalls, empty boundary conditions have been applied. At the outlet, the water level was defined using a constant  $p_{rgh}$ -value defined by the maximum hydrostatic pressure:  $p_{rgh} = \max(\rho gh)$ . As the initial condition, the domain is filled with water but no velocities are predefined. The velocity profile therefore develops during the simulation.

Simulated and measured velocity profiles are compared in Figures 3.3 ( $U_x$ ) and 3.4 ( $U_y$ ). On the horizontal axis, the velocities are displayed in relation to the average flow velocity  $U_0$ . The height on the vertical axis is displayed in relation to the channel height  $h_{max}$ . The imposed velocity profile at the inlet of the domain differs slightly from the experimental results of the freestream profile (Figure 3.3(a)). Figures 3.3(b) to 3.3(d) show the resulting velocity profiles in the reach of the hill structure and enable a qualitative analysis of the accuracy of the different turbulence models. Small deviations can be found between simulations and experimental results. The resulting root mean square error (RMSE) normalized by  $U_0$  for the different locations is listed in Table 3.1. The error has been calculated using linear interpolation between the cell values of the simulation results. Overall, the Standard k- $\epsilon$  turbulence model leads to slightly better results in all locations than the other RANS models analysed. The velocities in y-direction ( $U_y$ ) show similar results (Figure 3.4). Table 3.1 shows that the error between the experimental results and the simulated cases is smaller than the error of the  $U_x$ -velocities. In comparison to the velocities in x-direction, the velocities in y-direction are very small, being more challenging for numerical simulations and measuring.

It can be concluded, that the chosen model set-up is able to describe a relatively complex hydraulic test case for a single-phase flow problem appropriately and all turbulence models show a good accuracy. Due to the good performance in this case as well as in the cases referred to in Section 3.1, the Standard k- $\epsilon$  turbulence model will be used in the following cases.

Table 3.1: Water phase validation -  $RMSE/U_0$  [-] between experimental results and simulation

Observation point	k- $\epsilon$	k- $\omega$	k- $\omega$ SST
$U_x$			
$x_{-03}$	0.0515	0.0515	0.0515
$x_{00}$	0.0232	0.0307	0.0237
$x_{01}$	0.0595	0.1077	0.0681
$x_{02}$	0.0361	0.0637	0.0361
$U_y$			
$x_{00}$	0.0116	0.0131	0.0130
$x_{01}$	0.0156	0.0309	0.0193

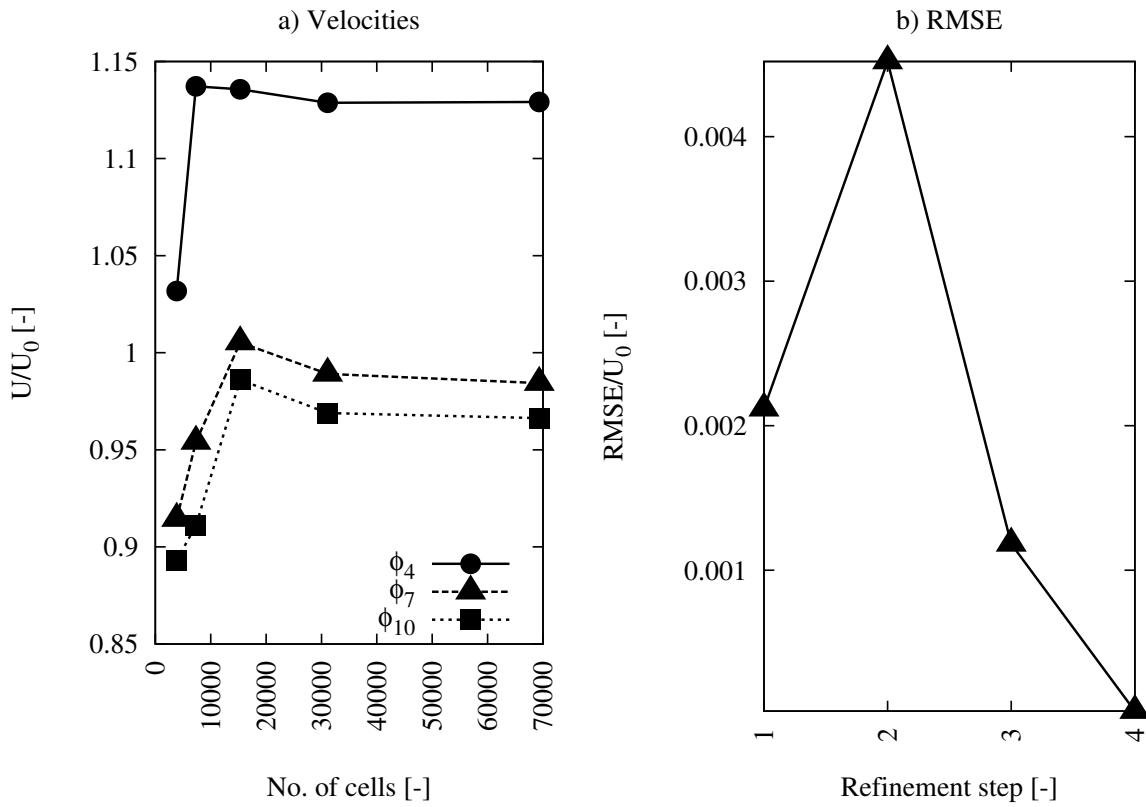


Figure 3.2: Mesh sensitivity analysis, (a) Comparison of simulated indicator values  $\phi$  (flow velocities) for different grid sizes in three points within the domain; (b) RMSE between different refinement steps over all 15 indicator values

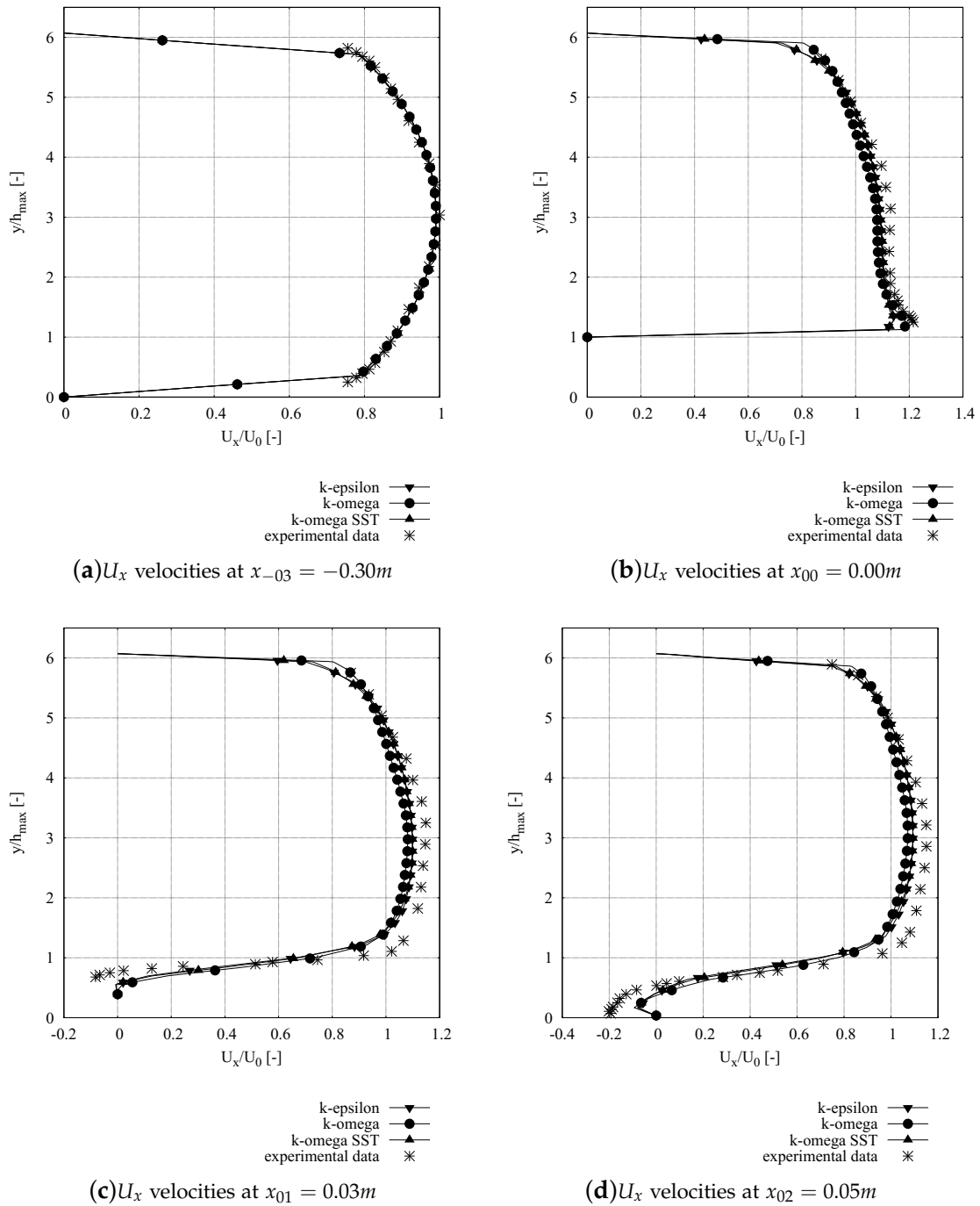


Figure 3.3: Comparison of simulated velocities  $U_x$  using different turbulence models with experimental data for flow over a two-dimensional hill, (a)  $U_x$  velocities at  $x_{-03} = -0.30$  m, (b)  $U_x$  velocities at  $x_{00} = 0.00$  m, (c)  $U_x$  velocities at  $x_{01} = 0.03$  m (d)  $U_x$  velocities at  $x_{02} = 0.05$  m

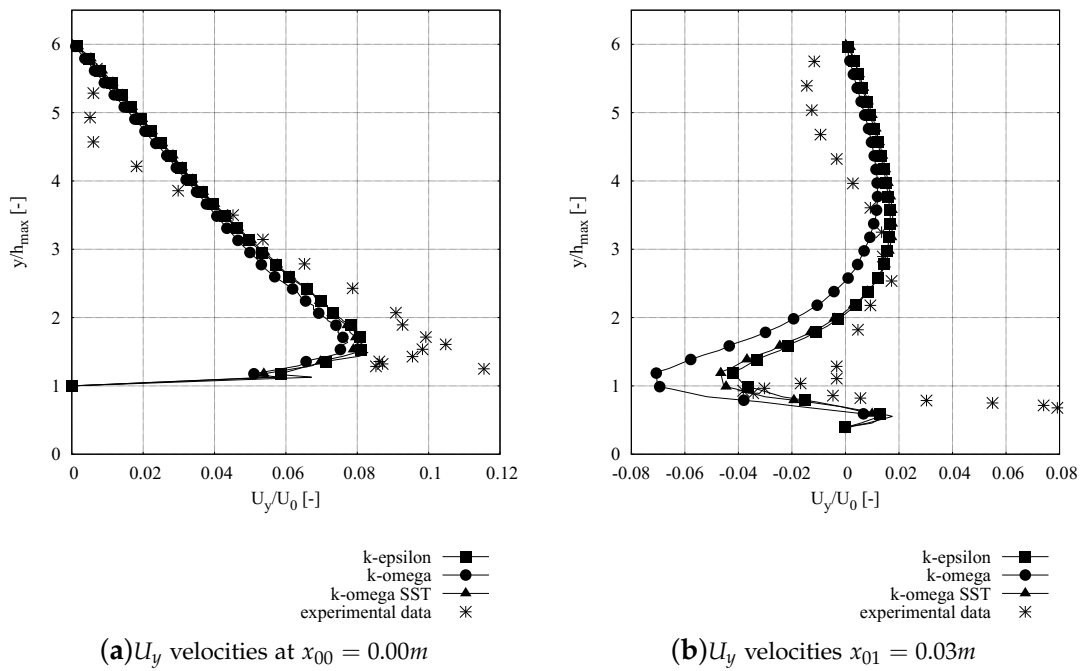


Figure 3.4: Comparison of simulated velocities  $U_y$  using different turbulence models with experimental data for flow over a two-dimensional hill, (a)  $U_y$  velocities at  $x_{00} = 0.00 m$ , (b)  $U_y$  velocities at  $x_{03} = 0.03 m$

### 3.3.2 Free surface flow over a hill

After having analysed the water phase behaviour, a two-phase flow has been simulated in order to investigate the water surface behaviour. The model setup was slightly changed. A free surface flow was modelled in a two-dimensional model domain. Again, the system was bounded by upper and lower walls. Under subcritical flow conditions the water level drawdown was analysed and compared to the analytically computed water level deviation by using continuity and Bernoulli's equation. The computation time was approximately 1 h for parallel computation on 16 cores. In the following, three cases are investigated (Table 3.2). The two-dimensional model domains of cases 1 and 2 consisted of 68,542 cells with a minimum cell length of 0.0024 m and a maximum cell length of 0.15 m. The domain of case 3 was discretized into 175,762 cells. The cell length ranged between 0.0035 m and 0.144 m. A time step of  $\Delta t=0.001$  s was chosen.

The boundary conditions were defined as follows: The inlet was divided in two parts, containing an inlet for the air phase and an inlet for the water phase. The air-inlet was specified with a fixed total pressure, the water-inlet was specified with a fixed discharge. Since the analysed test cases are two-dimensional, sidewalls were defined as empty boundaries. The upper and lower walls were specified using no-slip conditions. The outlet was defined using the pressure boundary condition mentioned in Section 3.2.3. As initial conditions for the pressure and velocity, the freestream velocities ( $v_1$ ) and water levels ( $h_1$ ) as listed in Table 3.2 have been defined.

In the following, the results of different two-phase flow simulations for three different model setups are presented. Variations were made concerning the discharge and water level. A deeper analysis of factors such as the structure of the sill and the flow regime can be found in Teuber et al. (2016).

In the three cases presented here, the water depth and flow velocity have been varied using the two-dimensional test case with a  $30^\circ$  angular structure of the ground sill (Figure 3.5), the flow regime was kept subcritical. Information about the setup including the analytically calculated water level drawdown and the numerically simulated water level drawdown are listed in Table 3.2, where  $v_1$  is the approaching velocity and  $h_1$  the water depth in front of the sill. The domain of case 1 is displayed in Figure 3.5. The results show a similar trend between the simulated results and the analytical solution. The reason for the higher drawdown obtained by the numerical solution are additional energy losses due to the structure of the sill that can be accounted for by the CFD simulation whereas the analytical solution using continuity and Bernoulli's equation leads to a one-dimensional solution that neglects single energy losses caused by the structure of the sill. In addition, Teuber et al. (2016) simulated a strictly supercritical setup leading to a rise of the water level above the sill. In agreement with the previous observations, the water level deviation coincided with the analytical solution.

It can be concluded that all the cases investigated show that the numerically calculated deviation of the water level reasonably coincides with the analytical solution.

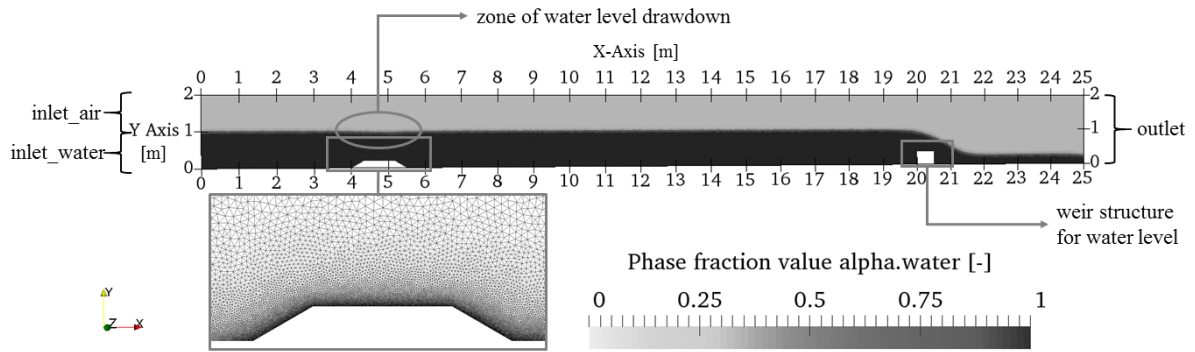


Figure 3.5: Free surface flow over a hill - Model domain of case 1

Table 3.2: Water-air-interface - Properties of the different test cases

Class	Case 1	Case 2	Case 3
Length of domain	25 m	25m	35 m
Height of domain	2 m	2m	6 m
$h_1$	1.0 m	1.0 m	3.0 m
$v_1$	1.0 m/s	1.25 m/s	3.0 m/s
$\Delta z$	0.2 m	0.2 m	0.2 m
$\Delta h$ , analytical	0.036 m	0.070 m	0.110 m
$\Delta h$ , numerical	0.042 m	0.090 m	0.140 m

### 3.3.3 Complex free surface flow in a sewer model

As a third step, the overall performance of the chosen model setup was tested using the complex sewer geometry of Bayón et al. (2015). Data from an existing CFD model as well as measured data gained from a 1:20 scale model has been compared to simulations using a model setup describing a closed duct bounded by upper and lower walls as well as side-walls. The simulation results reported in Bayón et al. (2015) were obtained using a similar configuration as presented in this paper, also implemented in OpenFOAM with the difference in the definition of a simplified top and outlet boundary condition. The Standard  $k-\epsilon$  model was used as closure to the turbulent stresses in both models.

The model domain describes a planned sewer stretch which has been developed due to a necessary diversion of an existing sewer stretch in València, Spain (Figure 3.6). The chosen stretch has a length of approx. 95 m and consists of an initial stretch, which was modelled in order to achieve fully developed flow conditions. After the initial stretch, a  $45^\circ$  constant radius curve and a straight stabilisation stretch with a length of 10 m follow. Having passed the curve, the water then reaches a spillway followed by a stilling basin which is designed in order to control the occurrence of critical flow conditions, obtain a smooth change of slope between the existing and new sewer stretch and to expand the channel width from 6.0 m to 7.5 m. An adjacent transition zone leads the flow into the ovoid channel with a length of 20 m which is the last part of the section. In order to force the flow back to a subcritical state before reentering into the ovoid section, macro-roughness elements are placed in the stilling basin and a hydraulic jump is forced. Due to its different features as well as the different flow regimes, the chosen geometry leads to a model domain that is highly complex in terms of hydraulic behaviour.

The innovation of the simulations presented in this paper compared to the existing CFD simulations carried out by Bayón et al. (2015) is that here the whole domain was considered as a closed duct leading to a realistic top boundary condition and another outflow boundary condition to ensure stability. As mentioned before, the same case has been previously simulated by Bayón et al. (2015) with a simplification for the closed conduit, i.e. an atmospheric top boundary in order to avoid stability problems. In this paper, the top boundary was not described with an atmospheric condition but as a wall with no-slip condition. The lower walls as well as the sidewalls were defined using no-slip conditions in both cases. The remaining boundary conditions were defined as follows by Bayón et al. (2015): The outlet water level was set to 5.01 m and the discharge was defined as  $100 \text{ m}^3/\text{s}$ . Accordingly, the pressure and velocity outlet boundary condition were defined. At the outlet, the velocity was defined to a constant value which forced the water level to a certain height. Within the domain, an initial water level and flow velocity were defined according to these values.

In this paper, a weir structure has been added in close proximity to the outlet in order to obtain the desired water level. This setup is very robust concerning initial conditions and does not necessarily need a correct initialisation of water level and flow velocity. Stable simulations can even be obtained under dry initial conditions. In the following, the simulation results using the weir outlet boundary condition will be compared to experimental measurements as well as to existing CFD simulations as they have been carried out by Bayón et al. (2015).

In Bayón et al. (2015) the accuracy of different mesh sizes ranging from 0.0861 m to 0.1236 m were compared. Mesh convergence has been reached for a mesh size of 0.103 m. In this paper, simulations were performed on a grid with the same resolution, leading to an overall number of 3,029,223 cells. The simulations demanded a computation time of 336 h on 96

cores. Simulations were performed with an adjustable time step in relation to the Courant number which converged against  $\Delta t = 0.0002$  s. The simulations run stable on different grid sizes, even if the domain is dry in the beginning of the simulations.

In order to compare the accuracy of the results for this complex test case, the water level distribution at four different cross sections has been compared. Figure 3.7 shows the location of the different monitoring points (1 - beginning of curve, 2 - end of the curve, 3 - stabilisation stretch, 4 - spillway crest). The resulting water surface profiles in the different cross sections of the two CFD models and the physical model are displayed in Figure 3.8. The results obtained in this paper are called "new CFD model" in the following, while the results of Bayón et al. (2015) are called "existing CFD model". A qualitative comparison shows an overall good agreement of the new CFD model with the existing model. In the beginning of the curve, the water level is closer to the physical model than the existing CFD model. In the remaining monitoring points, the results of the new CFD model are similar to the results of the existing model. This leads to the conclusion that the new CFD model with a realistic top boundary condition is as accurate as the existing model using a simplified boundary condition (atmospheric top boundary).

The results show that the closed model setup consisting of a weir structure as outlet boundary condition, a high-resolution mesh and the Standard k- $\epsilon$  turbulence model is stable concerning initially dry conditions, flow transitions from super to subcritical flow as well as high filling ratios and leads to reliable results.

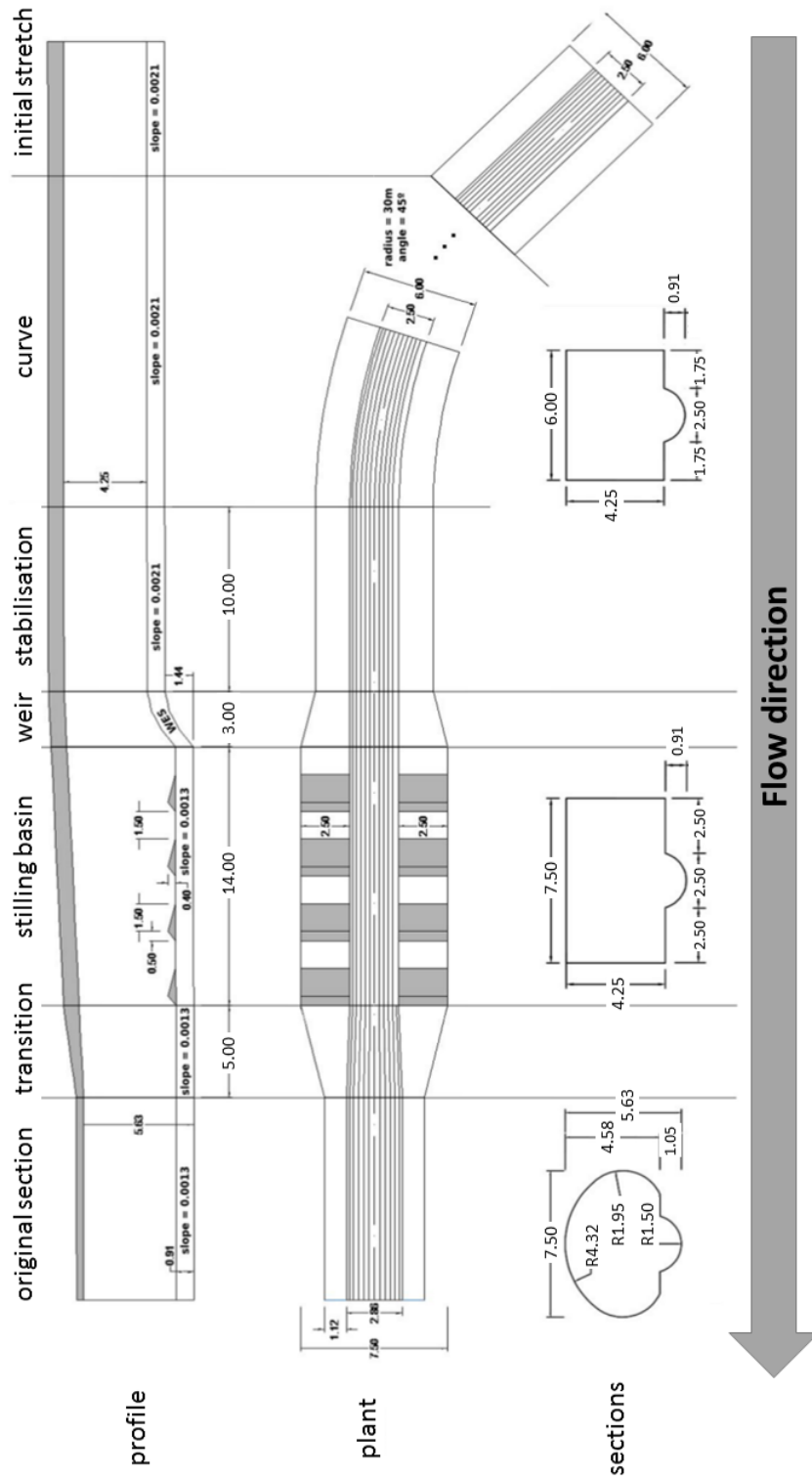


Figure 3.6: Complex sewer geometry - Geometry of the sewer stretch (Bayón et al., 2015)

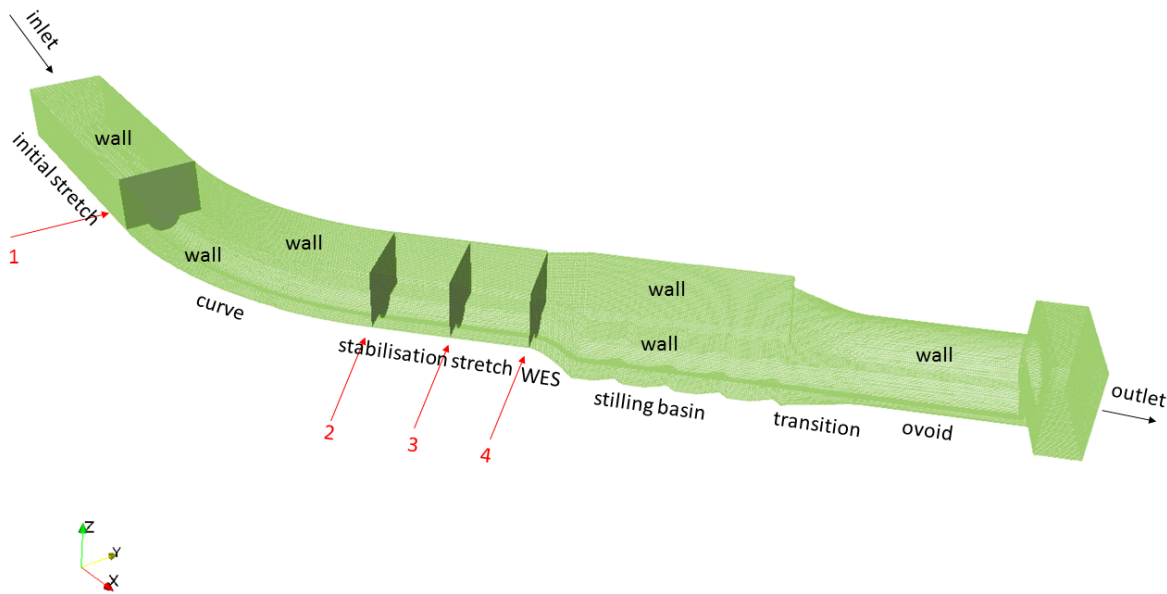


Figure 3.7: Complex sewer geometry - Overview of monitoring points for water surface profiles

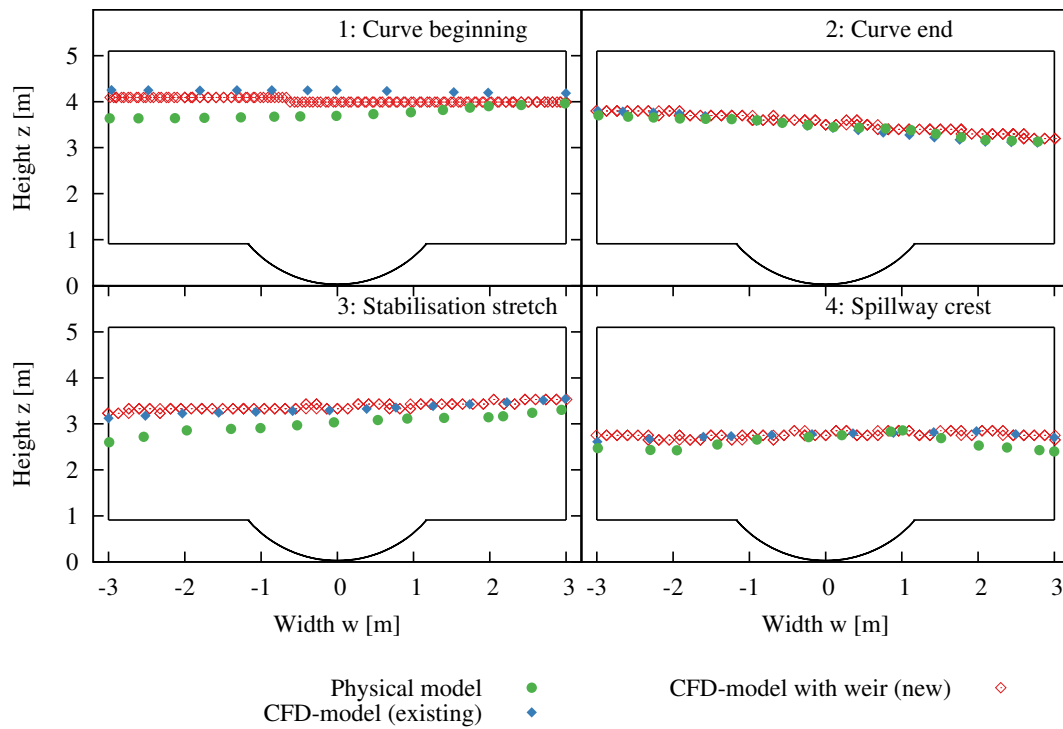


Figure 3.8: Complex sewer geometry - Comparison of water surface profile at different locations (existing CFD model - results obtained by Bayón et al. (2015); new CFD model - results obtained in this paper)

### 3.4 Conclusions

The aim of this study was to investigate OpenFOAM's two-phase solver `interFoam` concerning its ability to accurately describe complex hydraulic test cases in closed ducts when a certain outlet water level is given. This paper presents three different application cases where the `interFoam` solver has been used. Another aim was to evaluate the accuracy and suitability of different RANS turbulence models.

In a first step, a single-phase water flow over a hill has been simulated and different RANS turbulence models have been validated concerning their accuracy in describing the eddy structure behind the hill. The flow velocities measured experimentally were successfully reproduced by the different models. In the following, the Standard  $k-\epsilon$  turbulence model has been used for test cases describing the water surface behaviour under quasi-steady state conditions.

As second test case, free surface flow over a hill has been simulated. Different parameters such as the discharge and the water level have been varied and the numerically computed results were compared to an analytical solution obtained by using continuity and Bernoulli's equation. The simulations were able to predict a similar trend of the water level drawdown compared to the analytical solution. Due to additional energy losses caused by the specific structure of the sill, the analytically calculated drawdown is smaller than the CFD simulations but reasonably coincides for different simulations. These results can be seen to support the adequacy of the applied numerical modelling.

In a third step, complex free surface flow in a sewer model has been analysed in order to investigate the stability of the simulations using the setup of a complex geometry. A comparison with results of an existing CFD model, which used a simplified top boundary condition (atmospheric instead of closed) and another outflow boundary condition, as well as measured results from a 1:20 scale model showed a good agreement of this setup with the existing results.

Summing up, the VOF approach implemented in OpenFOAM is capable of describing complex two-phase flows in closed ducts. Small differences in the accuracy have been observed depending on the chosen turbulence models. The possibility of simulating even complex closed systems opens up the chance to describe complex phenomena such as odour and corrosion caused by hydrogen sulphide in concrete sewers. Future research will focus on the detailed behaviour of the air phase.

### Acknowledgement

Parts of the simulations were computed on the supercomputers of Norddeutscher Verbund für Hoch- und Höchstleistungsrechnen in Berlin.

### Funding

The funding provided by the German Research Foundation (DFG) within the Research Training Group "Urban Water Interfaces" (GRK 2032) is gratefully acknowledged.

## Chapter 4

# Parameter study on hydrodynamic two-phase simulations of flow over a ground sill

This study was published as:

---

Teuber, K., Broecker, T., Barjenbruch, M. & Hinkelmann, R.: High-resolution numerical analysis of flow over a ground sill using OpenFOAM, Proceedings of the 12th International Conference on Hydrosience & Engineering (ICHE), Tainan, Taiwan, 2016.

---

This is the postprint version of the article.

The test cases' setups are listed in Appendix B (single-phase flow over ground sill: B.1, free-surface flow over ground hill B.2).

### Abstract

In the field of hydraulic engineering, attention towards Computational Fluid Dynamics (CFD) has increased within the last years. In this study, flow over a two-dimensional ground sill is simulated and analyzed using the open source model OpenFOAM. Single-phase flow simulations are compared to experimental results obtained by Almeida et al. (1993) and two-phase flow simulations are compared to analytical solutions by using Bernoulli's and continuity equation. The results show that the model is capable of simulating such hydraulic testcases. Different RANS and LES simulations were found to reproduce the analyzed flow behavior well.

### 4.1 Introduction

Within the last years, Computational Fluid Dynamics (CFD) has gained importance in the field of hydraulic engineering. Several publications, such as Bayón et al. (2015), Bayón and Lopez-Jimenez (2015), Schulze and Thorenz (2014), Thorenz and Strybny (2012) have investigated complex hydraulic testcases such as hydraulic jumps, and filling and emptying of locks using the open source model OpenFOAM. In these publications the Volume of Fluid (VoF) approach for two-phase flows has been used in order to describe free surface flows. But the model also offers the possibility to simulate cases where two phases are of importance. One application is the simulation of in-sewer processes (Edwini-Bonsu and

Steffler, 2004, Gessner et al., 2014, Hvitved-Jacobsen et al., 2013). In this work, a first step of the validation process regarding two-phase flows in closed ducts such as sewer pipes is made. The model is used to simulate flow over a two-dimensional ground sill. Validation is first performed by comparing the results of single-phase flow with measurements by Almeida et al. (1993). Two-phase flow simulations are performed for different two- and three-dimensional model setups, variations are made concerning the structure of the sill, discharge, water level and the flow regime.

## 4.2 Computational framework

### 4.2.1 Numerical model

Surface water flow is calculated by using the two-phase flow solver interFoam based on a volume of fluid (VoF) approach for one- and two-phase flows. Both phases are considered as one fluid with rapidly changing fluid properties, therefore one set of Navier-Stokes equations is solved. The phases are distinguished by an additional transport equation for the volume fraction which is used as a marker to describe the distribution of the phases throughout the domain. The equations can be formulated as follows (Rusche, 2003):

Mass conservation equation:

$$\nabla \cdot \vec{\mathbf{U}} = 0 \quad (4.1)$$

Momentum conservation equation:

$$\frac{\partial \rho \vec{\mathbf{U}}}{\partial t} + \nabla \cdot (\rho \vec{\mathbf{U}} \vec{\mathbf{U}}) = -\nabla p_{rgh} + \nabla \cdot (\mu \Delta \vec{\mathbf{U}}) + (\nabla \vec{\mathbf{U}}) \nabla \mu - \vec{\mathbf{g}} \cdot \vec{\mathbf{x}} \nabla \rho \quad (4.2)$$

Where  $p_{rgh}$  is the static pressure minus hydrostatic pressure:

$$p_{rgh} = p - \rho \cdot \mathbf{g} \cdot \mathbf{h} \quad (4.3)$$

Volume of Fluid equation:

$$\frac{\partial \alpha}{\partial t} + \nabla \cdot (\alpha \vec{\mathbf{U}}) + \nabla \cdot ((1 - \alpha) \mathbf{U}_r \alpha) = 0 \quad (4.4)$$

with the following parameters:

$$\rho = \alpha \rho_w + \rho_a (1 - \alpha) \quad (4.5)$$

$$\mu = \alpha \mu_w + \mu_a (1 - \alpha) \quad (4.6)$$

$$(4.7)$$

where  $\vec{\mathbf{U}}$  is the velocity field [m/s];  $\rho$  is the density [kg/m<sup>3</sup>];  $t$  is time [s];  $p$  is pressure [Pa];  $\mu$  is dynamic viscosity [Ns/m<sup>2</sup>];  $\vec{\mathbf{g}}$  is acceleration vector due to gravity [m/s<sup>2</sup>];  $\vec{\mathbf{x}}$  is a spatial position vector [m];  $\alpha$  is a volume fraction or indicator function [-];  $\mathbf{U}_f$  is the relative velocity between the phases [m/s]; the subscripts a and w denote the fluids air and water.

The indicator function  $\alpha$  is defined as:

$$\alpha = \begin{cases} 1 & \text{fluid w} \\ 0 < \alpha < 1 & \text{transitional region} \\ 0 & \text{fluid a} \end{cases}$$

For single-phase simulations the volume fraction  $\alpha$  is 1 and constant over the whole domain and during the simulation time.

### 4.2.2 Turbulence modelling

Turbulence effects and their impact on the flow have been simulated using different Reynolds averaged (RANS) turbulence models and Large Eddy Simulations (LES). From the wide range of RANS models the Standard  $k-\epsilon$  (Launder and Sharma, 1974),  $k-\omega$  (Wilcox, 1988) and  $k-\omega$  Shear Stress Transport (SST) model (Menter, 1993, 1994) were used. As subgrid scale model for the LES simulations the Smagorinsky model (Smagorinsky, 1963) was chosen.

### 4.2.3 Boundary conditions

For all cases presented in this paper, a similar set of boundary conditions has been used. The inlet of the domain has been subdivided in two components, an inlet for the air phase and an inlet for the water phase. The height of the water inlet depends on the desired water level and the flow is prescribed by using a fixed flow velocity or a discharge. The air inlet is specified by using a total pressure boundary condition. The upper and lower walls of the domain are defined using a no-slip condition. The outlet of the domain is specified by using a pressure boundary condition. The water level in the domain is fixed by defining a weir in close proximity to the outlet as outlined in Bayón et al. (2015). For three-dimensional testcases, the sidewalls are determined using a no-slip condition. Two-dimensional testcases are simulated with so-called empty boundary conditions which are implemented in OpenFOAM to describe sidewalls of a two-dimensional geometry.

### 4.2.4 Geometry and mesh

Unstructured meshes with local refinements at the walls were set up using the open source mesh generation tool gms. The single-phase flow cases (Figure 4.1) consist of 12,106 cells for the RANS turbulence models and 89,284 cells for the LES simulations, leading to a cell length between 0.0042 m and 0.056 m for the RANS simulations and between 0.00035 m and 0.041 m for the LES simulations. The two-dimensional model domains of cases 1 and 2 consist of 68,542 cells with a minimum cell length of 0.0024 m and a maximum cell length of 0.15 m. The three-dimensional setup is based on the two-dimensional domain but extended in z-direction by ten layers. The model consequently consists of 685,420 cells. The domain of case 3 consists of 175,762 cells. The cell length ranges between 0.0035 m and 0.144 m.

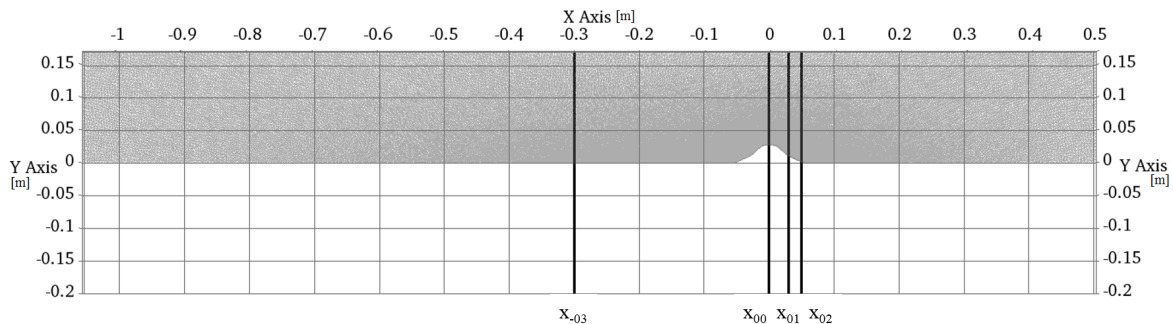


Figure 4.1: Model setup and measurement locations of single-phase case.

### 4.3 Single-phase flow

In order to analyze the accuracy of the interFoam solver regarding flow behavior behind a two-dimensional ground sill, a single-phase testcase has been implemented using different turbulence models. Experimental data for this case has been obtained by Almeida et al. (1993) and is available in the database of the European Research Community on Flow, Turbulence and Combustion (ERCOFTAC) (Davroux et al., 1995). The domain consists of a two-dimensional duct bounded by an upper and lower wall with a polynomial shaped obstacle on its bottom. The mean centerline velocity at the inlet amounts to 2.147 m/s. At four, respectively two different locations the velocities in x- and y-direction were compared to the experimental results:  $x_{-03} = -0.30$  m (in front of the sill, inlet profile),  $x_{00} = 0.00$  m (top of the sill),  $x_{01} = 0.03$  m (end of the sill),  $x_{02} = 0.05$  m (recirculation zone). Turbulence models used were the RANS and LES models previously outlined.

The results show that the chosen RANS models as well as the LES simulations lead to a good approximation of the experimental results (Figure 4.2 and Figure 4.3), however, the LES simulations are able to capture fluctuations as well which can be of interest when analyzing eddy structures behind ground sills. One disadvantage of LES is the higher resolution of the mesh that is needed in order to display large scale eddies which lead to much higher computation times.

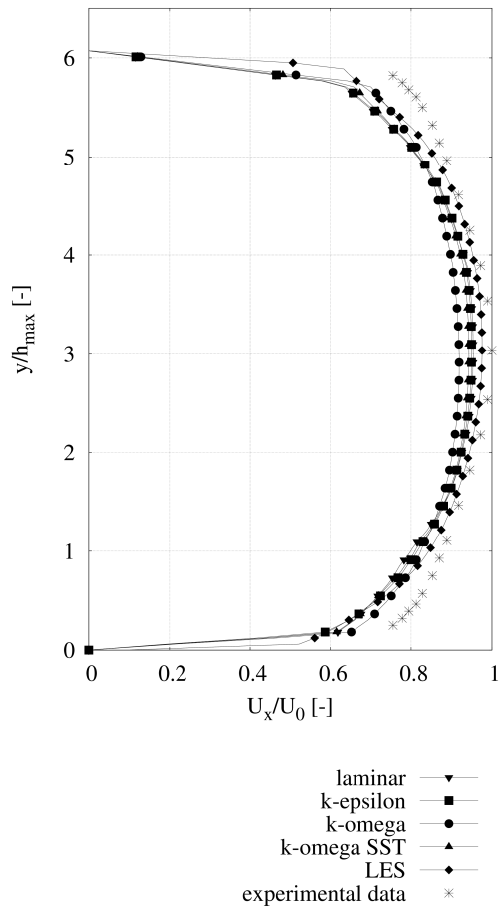


Figure 4.2: Velocity profiles at  $x_{-03} = -0.30m$  (inlet profile).

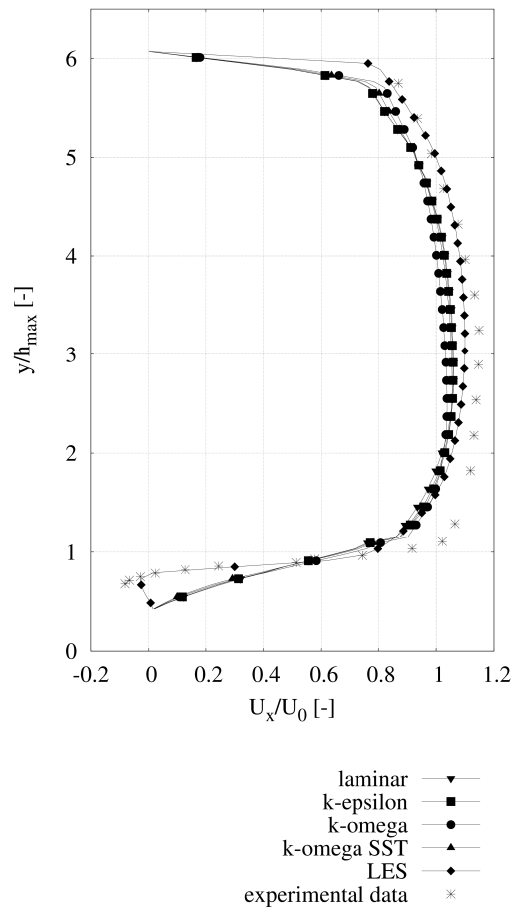


Figure 4.3: Velocity profiles at  $x_{01} = 0.03m$  (end of sill).

## 4.4 Two-phase flow

When analyzing two-phase flow over a two-dimensional ground sill, two main aspects are of interest: eddy structures behind the sill and the water level drawdown. Since the accuracy concerning eddy structures has already been analyzed in the previous case, the focus of the two-phase flow cases will lie on the water level drawdown. Since the water level drawdown is constant as soon as a quasi steady-state is reached, LES simulations are not necessary. Therefore, the Standard  $k-\epsilon$ -turbulence model has been chosen in this part in order to save computation time (approximately 1 h instead of 4 h for parallel computation on 16 processors).

As a first step, the effect of the sill structure on the water level drawdown has been analyzed. A two-dimensional model setup similar to case 1 as listed in Table 4.2 has been used. Angular shaped structures with three different angles for the ground sill as well as a round structure have been investigated (see Table 4.1). The maximum height of the sill is  $\Delta z = 0.20\text{m}$  and similar for all cases.

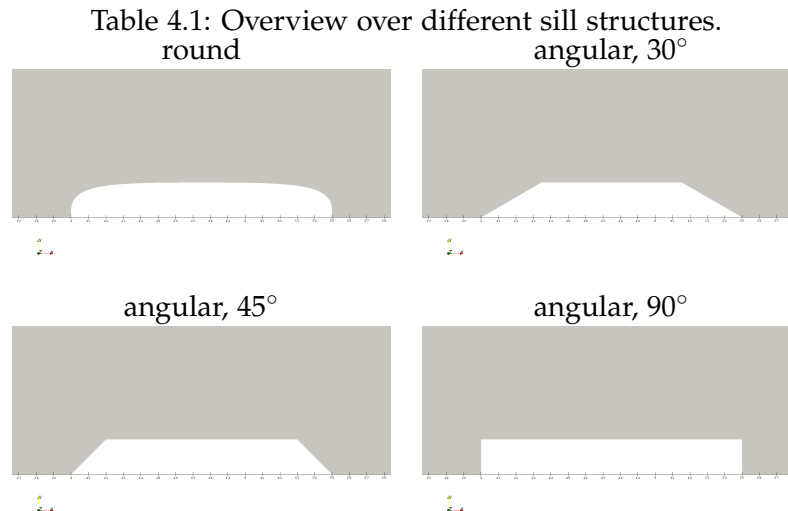


Figure 4.5 shows the resulting water level drawdowns for the different structures. The maximum water level drawdown is the smallest ( $\Delta h = 0.03\text{m}$ ) for the round structure. The drawdown for the 30° and 45° angular structure are in a comparable order of magnitude ( $\Delta h = 0.04\text{m}$ ). A significantly higher drawdown is caused by the ground sill with an angle of 90° ( $\Delta h = 0.09\text{m}$ ). With an analytically calculated drawdown of  $\Delta h = 0.036\text{m}$  (Table 4.2), the sill structures with small angles or round structures show the highest accuracy. The effect of the ground sill is higher for steeper hill structures which can be explained by higher single losses for steeper structures.

In a next step, changes have been made concerning the water depth and the flow velocity using the 30° angular structure of the ground sill. All cases have subcritical flow conditions and do not show a flow transition over the ground sill.

The setups including the analytically calculated water level drawdown and the simulated water level drawdown are listed in Table 4.2 (case 1 to 3), where  $v_1$  is the approaching velocity and  $h_1$  the water depth in front of the sill. The results show a good agreement of the

Table 4.2: Subcritical two-phase flow: Properties of different testcases.

	Case 1	Case 2	Case 3	Case 4
Length of domain	25 m	25 m	35 m	25 m
Height of domain	2 m	2 m	6 m	2 m
$h_1$	1.0 m	1.0 m	3.0 m	0.3 m
$v_1$	1.00 m/s	1.25 m/s	3.00 m/s	3.00 m/s
$\Delta z$	0.2 m	0.2 m	0.2 m	0.1 m
$\Delta h$ , analytical	0.036 m	0.070 m	0.110 m	0.100 m
$\Delta h$ , numerical	0.042 m	0.090 m	0.140 m	0.055 m

simulated results with the analytical solution obtained by using Bernoulli's and continuity equation. A reason for the slightly higher drawdown obtained by the numerical solution are additional energy losses which have already been shown when analyzing the influence of the structure due to the structure of the sill.

Case 1 has also been extended to a three-dimensional geometry with a width of 1 m and sidewalls with no-slip condition.

The resulting water level drawdown is compared to the drawdown resulting from the two-dimensional simulation in Figure 4.6. The Figure shows that the three-dimensionality of the testcase causes a smaller drawdown and a shorter length of the water level drawdown. The reason for this is the influence of the sidewalls. The no-slip condition at the sidewalls causes additional continuous energy losses that were neglected in the two-dimensional geometry.

As a next step, a strictly supercritical setup (case 4) has been analyzed. The supercritical flow case has been simulated with a height of the ground sill of  $\Delta z = 0.10$  m and an approaching flow velocity  $v_1 = 3$  m/s (see Table 4.2). Compared to the analytical rise of the water level ( $\Delta h = 0.10$  m), the maximum increase achieved in the simulations ( $\Delta h = 0.055$  m) is considerably smaller. The high difference between analytical and numerical solution can be considered reasonable since the high flow velocity of this testcase leads to higher single losses at the sill structure and therefore a higher deviation between analytical and numerical solution.

In the last case, the stability of the simulations has been analyzed under initially dry conditions. A water level of  $h_1 = 1$  m and a flow velocity of  $v_1 = 1$  m/s has been chosen at the inlet (similar to case 1) and at the outlet a free outflow without weir. Figure 4.4 shows the behavior of the two phases in the domain at different time steps. After a simulation time of 20 seconds a quasi-steady state is reached and subcritical conditions in the upstream part of the domain and supercritical conditions in the downstream part of the domain are reached. A flow transition occurs over the ground sill. Close to the inlet, a disturbance of the water surface can be found. This disturbance develops due to an eddy in the air phase that is caused by the increase of the water level from the ground sill upstream to the inlet. Due to the inlet boundary patch the eddy is trapped in this point. This effect could be moved further upstream by choosing an inlet in a higher distance to the ground sill.

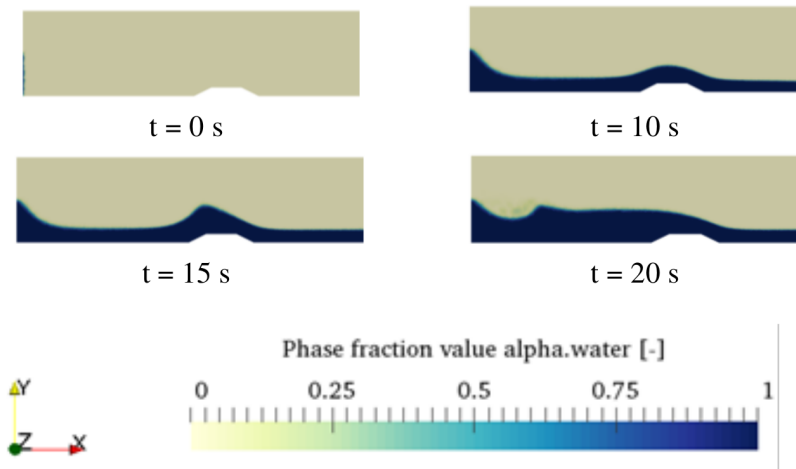


Figure 4.4: Filling of the domain, segment of the computational domain for different time steps.

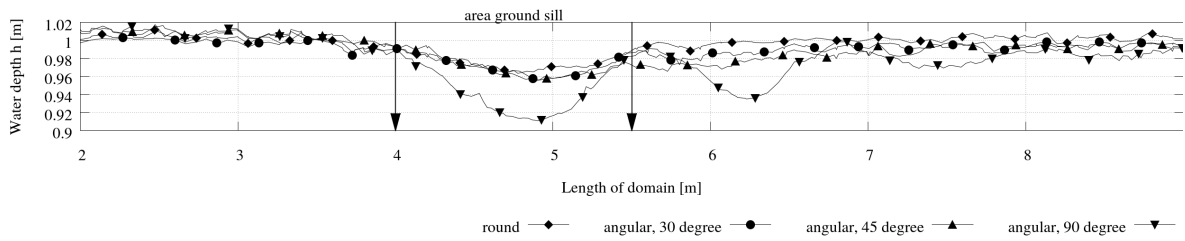


Figure 4.5: Comparison of water level drawdown for different sill structures

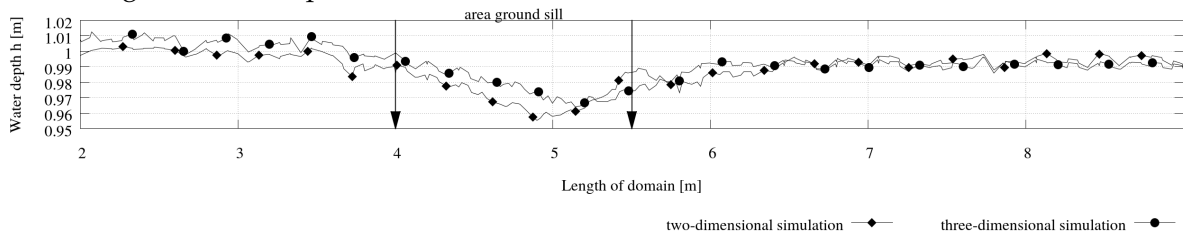


Figure 4.6: Comparison of water level drawdown for two- and three-dimensional model setup

## 4.5 Conclusions

In this study, flow over a two-dimensional ground sill has been analyzed using OpenFOAM. First, a single-phase flow has been simulated and different turbulence models have been validated concerning their accuracy in describing the eddy structure behind the sill. All models analyzed led to a good accuracy, however, the LES turbulence model was capable to account for fluctuations as well. One disadvantage of the model is the smaller necessary grid size which leads to much higher computation times.

In a second step, two-phase flow has been simulated using the  $k-\epsilon$  turbulence model and different parameters such as the structure of the ground sill, discharge, water level and flow regime have been evaluated concerning their influence on the water level drawdown.

Due to additional energy losses caused by the angular structure of the sill as well as losses due to sidewalls when a three-dimensional model is chosen, the analytically calculated drawdown is smaller than the two-dimensional simulations but reasonably coincides for different simulations. Changes of the water level drawdown due to the structure of the ground sill and sidewalls when three-dimensional testcases are computed are plausible. The simulations are also stable for a filling case with initially dry conditions.

Summing up, the VoF approach implemented in OpenFOAM is capable of describing flow over a ground sill and similar hydraulic cases. Future research aims to closer look at the behavior of the air phase.

## Acknowledgements

This work is carried out within the DFG Research Training Group Urban Water Interfaces which is a joint initiative of TU Berlin and Leibniz-Institute of Freshwater Ecology and Inland Fisheries (IGB) Berlin. The authors acknowledge the funding.

Parts of the simulations were computed on the supercomputers of Norddeutscher Verbund für Hoch- und Höchstleistungsrechnen in Berlin.

## Chapter 5

# Single-phase transport simulations

This study was published as:

---

Teuber, K., Broecker, T., Jaydev, S.D., Goitom, G.M., Sielaff (née Grüneberger), M., Despot, D., Stephan, D., Barjenbruch, M. & Hinkelmann, R.: Multiphase CFD-Simulation of Transport Phenomena in Sewer Systems, in: Mannina G. (eds) *New Trends in Urban Drainage Modelling*. UDM 2018. Green Energy and Technology, 584-853, Springer, Cham., 2019; 10.1007/978-3-319-99867-1\_146.

---

This is the postprint version of the article.

The test cases' setups are listed in Appendix B (transport in rectangular pipe: B.4, transport around concrete probes B.5, complex sewer: B.3).

### Abstract

This paper presents different computational fluid dynamics applications using the multiphase solver *interFoam* which is implemented in the open source software *OpenFOAM*. The solver uses the volume of fluid approach. When modelling tracer transport in the proximity of the interface between two phases, the problem of non-physical tracer spreading across the interface has to be overcome. In this paper, two ways are presented to model such systems successfully. First, tracer transport around concrete probes in the headspace of a sewer pilot plant is considered. In this case a two-phase (water-air) system is assumed by describing an idealized water surface as a boundary condition and a passive tracer is applied. Second, flow in a complex sewer stretch containing a hydraulic jump is simulated and a tracer is applied in the water phase. A multiphase transport approach based on the Henry coefficient is used in this case and plausible results are obtained.

### 5.1 Introduction

In the field of hydraulic engineering, shallow water flow models using the depth-averaged Navier-Stokes equations are often suitable to analyse flow phenomena. However, in certain application areas where a hydrostatic pressure distribution within the flow field is not given, these models reach their limits and alternatives have to be looked for. In the field of urban drainage such structures can occur in complex sewer systems containing hydraulic jumps due to changes of the flow regime. A thorough description of transport in the different phases and mass transfer across the phase interface can be used to describe complex species transport and biochemical processes, for example the development of odour and corrosion

due to hydrogen sulphide in sewer systems. Therefore, this study focuses on transport phenomena in multiphase (water-air) systems.

When a passive advection-diffusion tracer is applied in the nearfield of the interface, a non-physical spreading across the interface between two phases can occur. Figure 5.1 illustrates the problem using the example of a rectangular pipe which is partially filled with water. After a few seconds the tracer spreads across the water surface into the air due to diffusion. Since the interFoam solver only distinguishes between phases by using an additional transport equation that modifies phase specific variables, a passive tracer can spread into the air phase. This paper presents two ways to overcome this issue by using different approaches.

## Standard transport equation

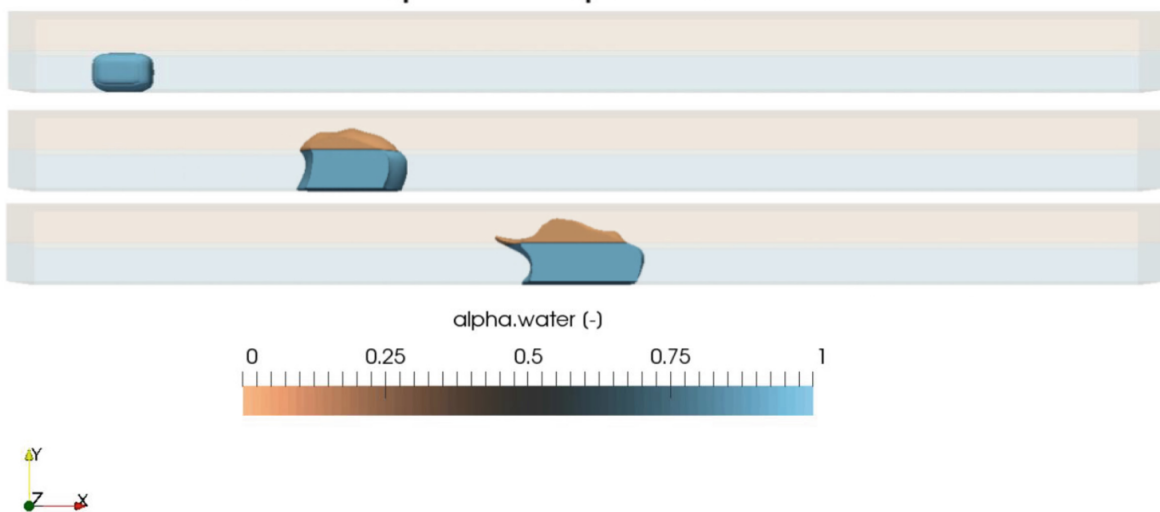


Figure 5.1: Tracer transport in water phase of rectangular pipe with non-physical spreading across water surface.

In the first part the headspace of a sewer pilot plant is being investigated with a simplified single-phase approach, assuming an idealized water surface. The second study presents tracer transport in a sewer stretch containing complex hydraulic flow phenomena. In this case the tracer is present in the water phase. A special formulation that regards the mass transfer depending on the Henry coefficient has been introduced by Haroun et al. (2010a) and has been applied in this study.

## 5.2 Material and methods

### 5.2.1 Hydrodynamic simulations

Surface water and air flow is calculated by using the two-phase flow solver interFoam based on a volume of fluid approach for one- and two-phase flows as it is implemented in the open source model OpenFOAM. Both phases are considered as one fluid with rapidly changing fluid properties, therefore one set of Navier-Stokes equations is solved. The phases are distinguished by an additional transport equation for the volume fraction which is used as

a marker to describe the distribution of the phases throughout the domain. The governing equations can be found in Rusche (2003).

## 5.2.2 Transport simulations

For the first study, the transport of a passive tracer with a concentration  $C$  is examined with an advection-diffusion equation that was implemented into the interFoam solver (see Equation 5.1). The physical diffusivity  $D_{phys}$  as well as the turbulent Schmidt number  $Sc_{turb}$ , which defines the turbulent diffusivity coefficient  $D_{turb}$ , have to be defined by the user (Equation 5.2):

$$\frac{\partial C}{\partial t} + \nabla \cdot (uC) = (D_{phys} + D_{turb}) \frac{\partial^2 C}{\partial x^2} \quad (5.1)$$

with

$$D_{turb} = \frac{\mu_{turb}/\rho}{Sc_{turb}} \quad (5.2)$$

## 5.2.3 Mass transfer

For the second study, the approach introduced by Haroun et al. (2010a) as it has been implemented by Nieves-Remacha et al. (2015) has been used. The approach is based on the interFoam solver and adds a transport equation as outlined in Equations 5.1 and 5.2. At the interface the following boundary conditions have to be satisfied:

$$He = \frac{C_L}{C_G} \quad (5.3)$$

$$D_i^L \nabla C_i^L = D_i^G \nabla C_i^G \quad (5.4)$$

Where  $D_i$  is the diffusivity and  $C_i$  is the concentration in the respective phase.  $He$  denotes the dimensionless Henry coefficient and superscripts L and G denote the liquid and gas phase. To avoid spreading of the tracer across the water surface in the case presented in section 5.3.2, the Henry coefficient has been set to  $10^{-6}$  which prevents mass exchange across the water-air interface.

## 5.3 Results and discussion

### 5.3.1 Spreading of hydrogen sulphide in headspace of sewer pilot plant (air phase)

In the first part the headspace of a sewer pilot plant is being investigated. In the pilot plant, probes made of various types of concrete are installed to investigate their resistance against sulphuric acid corrosion. The diameter of the pipe is 400mm. The original setup of the pipe has a length of 25m, for the computational domain a length of 2m has been chosen.

Simulations are performed to detect whether the concentration around the concrete probes is distributed homogeneously or whether peaks occur that might influence the corrosion rate locally. The simulations are being performed with a simplified single-phase approach, assuming an idealized water surface. Since the water surface is being described using a slip boundary condition, only the upper half of the pipe has to be discretized with

the computational mesh. The computational domain is shown in Figure 5.2 and the resulting tracer concentration is illustrated in Figure 5.3. The results show an accumulation of the tracer around the probes in the rear part of the pipe.

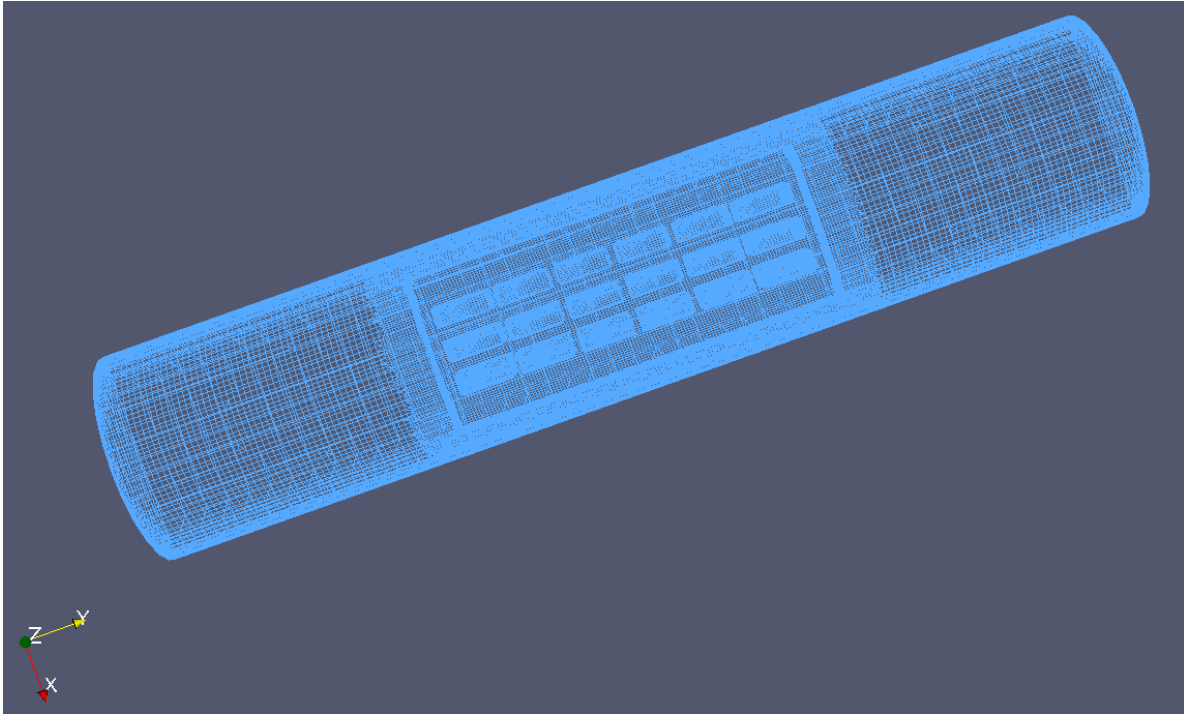


Figure 5.2: Top view of the model domain (pipeline containing the concrete probes).

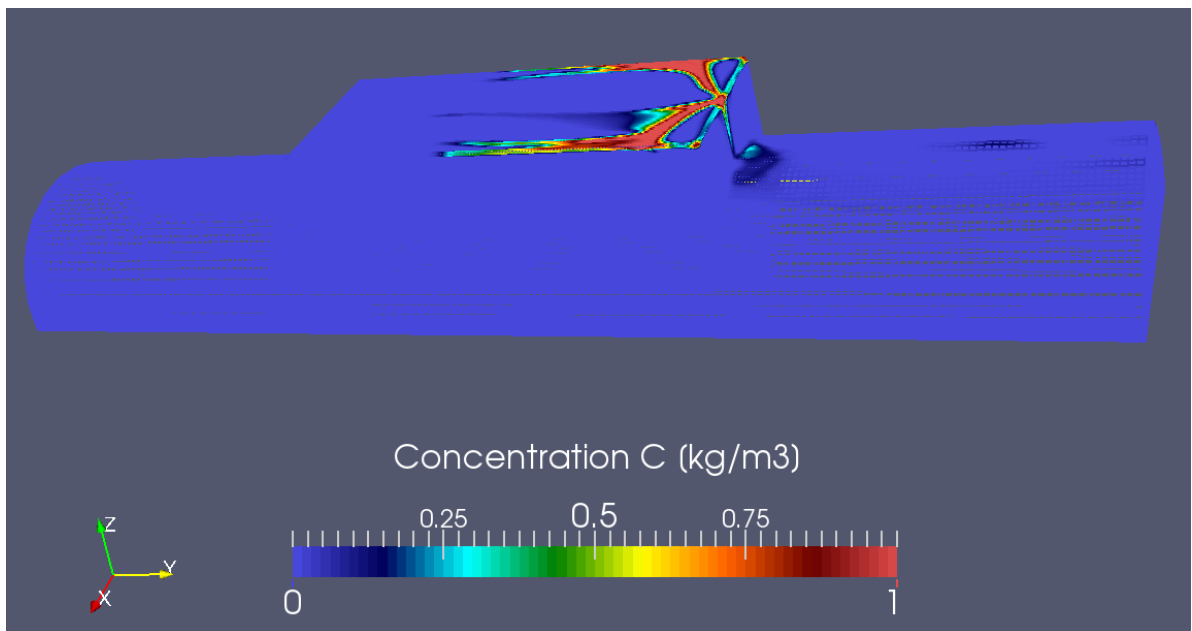


Figure 5.3: Resulting tracer distribution.

### 5.3.2 Tracer transport in sewer pipe (water phase)

In the second case, a complex sewer stretch containing a hydraulic jump has been analysed. The overall geometry has a length of roughly 90m and the sewer pipe consists of different cross sections with widths up to 7.50m and a maximum height of 5.63m. The detailed geometry has been outlined in Bayón et al. (2015). In this case the mass transfer formulation by Haroun et al. (2010a) has been applied to keep the tracer in the water phase. Figure 5.4 shows that the tracer does not cross the water surface in the case of the simple rectangular geometry introduced in Section 5.3.1. Figure 5.5 illustrates the movement of the tracer along the complex sewer stretch and through the hydraulic jump. The results confirm that also in cases with high turbulence the tracer remains in the water phase.

#### Mass transfer equation (Haroun, 2010)

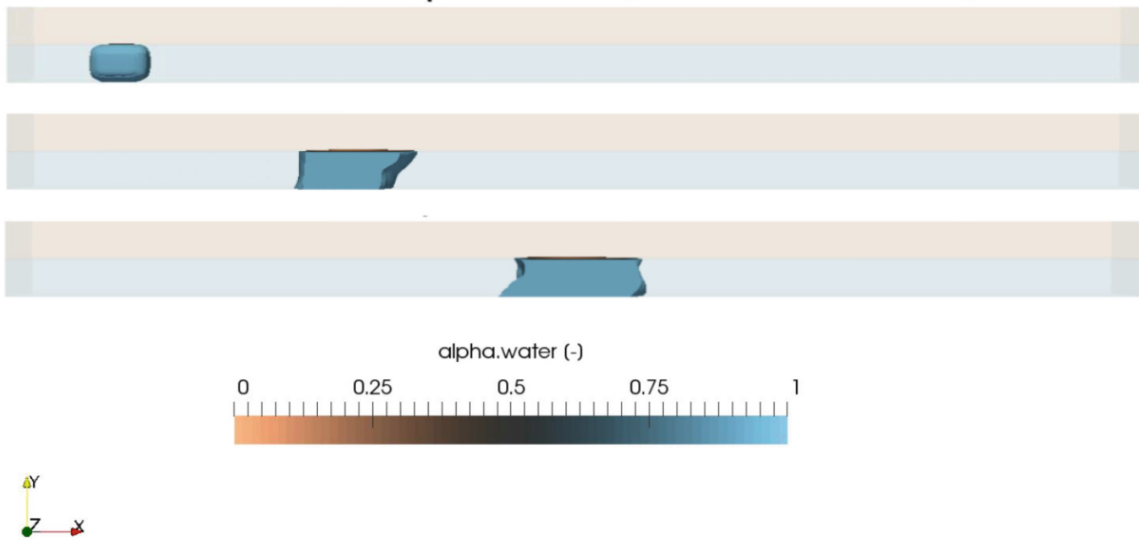


Figure 5.4: Movement and spreading of tracer along sewer.

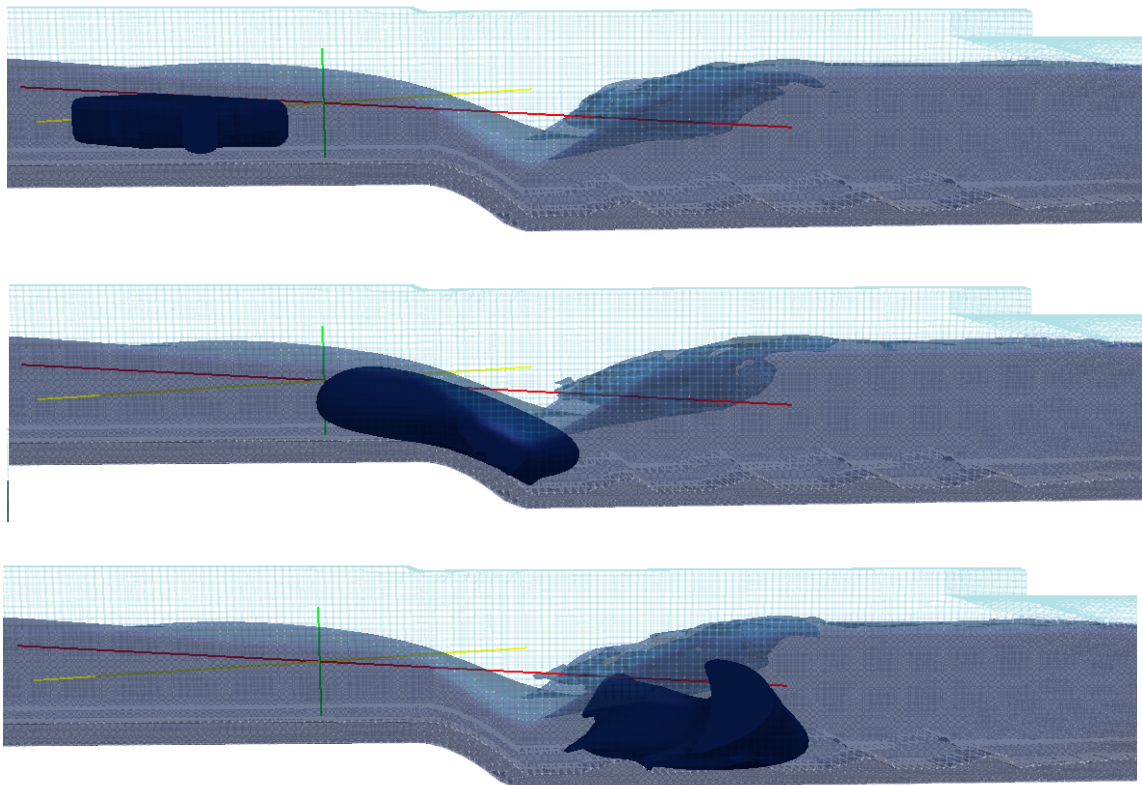


Figure 5.5: Movement and spreading of tracer along sewer.

## 5.4 Conclusions

Within this study three-dimensional two-phase (water-air) flow and transport simulations have been carried out in two different examples. These systems are difficult to model in a way that a passive advection-diffusion tracer can cross the barrier of the water surface without any physical constraints due to the formulation of the interFoam solver. In this paper, two ways are presented to overcome this obstacle. First, to model the air phase as a single phase system which can be valid for stratified flows in sewers and second, to use a mass transfer approach based on the Henry coefficient and modify the Henry coefficient in order to avoid mass transfer across the water surface.

## Chapter 6

# Mass transfer simulations under equilibrium conditions: Validation and solver extension

This study was published in Water Science and Technology (IWA Publishing) as:

---

Teuber, K., Broecker, T., Bentzen, T.R., Stephan, D., Nützmann, G. & Hinkelmann, R.: Using computational fluid dynamics to describe H<sub>2</sub>S mass transfer across the water-air interface in sewers, *Water Science and Technology*, 79 (10), 1934-1946, 2019; doi:10.2166/wst.2019.193. ©IWA Publishing 2019. The definitive peer-reviewed and edited version of this article is published in doi:10.2166/wst.2019.193 and available at [www.iwapublishing.com](http://www.iwapublishing.com).

---

Reproduced from Teuber et al. 2019 *Water Science & Technology* 79(10) 1934-1946, with permission from the copyright holders, IWA Publishing.

A detailed explanation of the solver extensions addressed in this paper is given in Appendix A. The test cases' setups are listed in Appendix B (quasi one-dimensional tank: B.6, rectangular pipe B.7, complex sewer: B.3).

### 6.1 Abstract

For the past 70 years, researchers have dealt with the investigation of odour in sewer systems caused by hydrogen sulphide formations and the development of approaches to describe it. The state-of-the-art models are one-dimensional. At the same time, flow and transport phenomena in sewers can be three-dimensional, for example the air flow velocities in circular pipes or flow velocities of water and air in the reach of drop structures. Within the past years, increasing computational capabilities enabled the development of more complex models. This paper uses a three-dimensional two-phase Computational Fluid Dynamics model to describe mass transfer phenomena between the two phases: water and air. The solver has been extended to be capable to account for temperature dependency, the influence of pH value and a conversion to describe simulated air phase concentrations as partial pressure. Its capabilities are being explored in different application examples and its advantages compared to existing models are demonstrated in a highly complex three-dimensional test case. The resulting interH<sub>2</sub>SFoam solver is a significant step in the direction of describing and analysing H<sub>2</sub>S emissions in sewers.

## 6.2 Introduction

Wastewater in sewers undergoes a lot of physical and biochemical processes. One important factor is the formation of hydrogen sulphide ( $\text{H}_2\text{S}$ ), which can cause health risks for sewer workers. The tendency of more complex and longer sewer networks can lead to longer retention times, which enhance the emission of  $\text{H}_2\text{S}$ . Climate change at the same time causes higher temperatures in the wastewater, which increases emission rates.

In the past 70 years extensive research has been performed to increase the knowledge on  $\text{H}_2\text{S}$  formations and to develop approaches, which describe the development of odour in sewers (e.g. Gilchrist (1953), Thistlethwayte (1972)). The state-of-the-art models, which have been developed within the last 20 years, are horizontal one-dimensional. These are the SeweX model from Australia (Rootsey and Yuan, 2010, Rootsey et al., 2012) and the WATS model from Denmark (Hvitved-Jacobsen et al., 2013). Both are not public domain.

An overview of existing model approaches has been given in Carrera et al. (2016) and the need for further research has been highlighted.

To begin with, the mass transfer approach of the existing models is based on the so-called two-film theory, which uses different assumptions. The WATS model additionally uses different approaches to account for turbulent  $\text{H}_2\text{S}$  transfer rates across the water surface in various applications. These different approaches are empirical or theoretical connections between oxygen and  $\text{H}_2\text{S}$  transfer on the one hand and empirical models linking  $\text{H}_2\text{S}$  emissions to flow properties in the pipe on the other hand (Carrera et al., 2016).

Wang et al. (2018) highlight the shortcomings of the two-film theory. It cannot account for local changes of the flow regime or variations of fluid properties. Furthermore, the theory is based on a constant liquid film that can change in real-life conditions due to flow instabilities. The most limiting factor however is assumed to be the one-dimensionality of the approach. More advanced approaches, the penetration theory and the surface renewal theory, can account for the variability of the flux over time but do not account for local variations, the change of fluid properties or flow regimes (Wang et al., 2018). This has already led to wide applications of CFD models for mass transfer applications in the chemical industry (Wang et al., 2018).

Carrera et al. (2016) identified the models' lack to describe mass transfer processes across the water surface, the current approaches of which were considered to be simplified, especially when considering hydraulic structures such as gravity sewers, junctions and water falls. Recent research on water falls or drop structures in sewer systems led to improved formulations to account for the effect of local turbulence (Matias et al., 2017), but these approaches are still empirical equations which are fed into the model.

This short overview leads to the question whether a three-dimensional simulation model could help in increasing the process understanding, especially when analysing complex and turbulent flows in a sewer. Another benefit could be the in-depth analysis and design optimization in hotspots of  $\text{H}_2\text{S}$  emissions.

In order to address this question, a volume of fluid (VOF) approach as it is implemented in OpenFOAM's solver `interFoam` has been chosen to describe the two-phase flow of water and air. This solver has already been used for a number of demanding hydraulic applica-

tions (e.g. Thorenz and Strybny (2012), Bayón et al. (2015)) and enables a stable, robust and accurate description of complex flow phenomena.

The VOF method is often used to describe mass transfer processes in CFD applications (Wang et al., 2018). Therefore, Haroun et al. (2010a,b) have developed an approach to describe mass transfer processes across the interface between two fluids using the Henry coefficient for the VOF method. This approach has been implemented in OpenFOAM's solver `interFoam` by Nieves-Remacha et al. (2015), Yang et al. (2017) and Severin (2017), resulting in a solver which will be called `interHarounFoam` in the following.

A short outline of the driving processes leading to  $\text{H}_2\text{S}$  formation shall be given to highlight important factors. When anaerobic conditions occur in the wastewater, sulphate-reducing bacteria, which reside in the biofilms of sewer walls can reduce sulphate to sulphide (Sharma et al., 2008a). From the biofilm, sulphide is then diffused into the wastewater as  $\text{H}_2\text{S}$ . In the water, equilibrium conditions depending on the pH value and temperature determine which amounts of sulphide are present as  $\text{H}_2\text{S}$  and as bisulphide ion ( $\text{HS}^-$ ). The air-water equilibrium, which can be described by the Henry coefficient for a volatile compound such as  $\text{H}_2\text{S}$ , can cause emissions of  $\text{H}_2\text{S}$  from the water into the air phase. The rate of the transfer process is influenced by factors such as the flow velocities within the different phases, the pH value, temperature and the concentration of oxygen and nitrate. The Henry coefficient describes the relative amount of a volatile compound in the gas phase as a function of its relative occurrence in the water phase under equilibrium conditions and at constant temperature. The temperature dependency of Henry's law can be described by different equations for example, the van't Hoff equation. The concentration of  $\text{H}_2\text{S}$  in the air phase defines the intensity of odour (Hvitved-Jacobsen et al., 2013).

As this overview of the relevant processes shows, a sole consideration of the Henry coefficient when describing  $\text{H}_2\text{S}$  emissions is not sufficient. Therefore, relevant extensions have been made to the solver, resulting in a new, specialized solver, `interH2SFoam`. This solver is able to account for the temperature dependency of the Henry coefficient. Further extensions enable the user to describe the equilibrium between  $\text{HS}^-$  and pH value in the water phase and to compute the partial pressure of  $\text{H}_2\text{S}_g$  in the air phase in ppm in order to gain a better comparability between simulations and measured values. The assessment of turbulent flow effects on mass transfer will be subject to future research.

In the following, after an introduction on the methods used, the capabilities of the `interH2SFoam` solver are explored in three simple application examples of vertical one-dimensional flow. Then, mass transfer in a rectangular pipe is simulated. In a final example, the new solver is applied to a highly complex sewer geometry.

## 6.3 Methods

### 6.3.1 Numerical model

OpenFOAM version 2.4.0 has been used for the work presented in this paper. Additionally, a supplementary library called `swak4Foam` has been used to generate customized function objects to calculate the equilibrium conditions between  $\text{H}_2\text{S}$  and  $\text{HS}^-$  as well as the partial pressure in the air phase. This approach makes the use of this function optional for the user. Depending on the framework of the model, the user can then decide whether these

functions are needed or not. The temperature dependency on the Henry coefficient of H<sub>2</sub>S has been directly implemented in the solver and makes a definition of the temperature as an input parameter mandatory.

### Hydrodynamic simulations

The mass transfer solvers are based on the two-phase flow solver interFoam which is based on a VOF approach that considers both phases as one fluid with changing fluid properties. One set of Navier-Stokes equations is solved. The volume fraction of a phase is stored as an additional variable and the phases are distinguished by an additional transport equation. The equations are defined as follows Rusche (2003):

Mass conservation equation:

$$\nabla \cdot \vec{\mathbf{U}} = 0 \quad (6.1)$$

Momentum conservation equation:

$$\frac{\partial \rho \vec{\mathbf{U}}}{\partial t} + \nabla \cdot (\rho \vec{\mathbf{U}} \vec{\mathbf{U}}) = -\nabla p_{rgh} + \nabla \cdot (\mu \Delta \vec{\mathbf{U}}) + (\nabla \vec{\mathbf{U}}) \nabla \mu - \vec{\mathbf{g}} \cdot \vec{\mathbf{x}} \nabla \rho \quad (6.2)$$

Where  $p_{rgh}$  is the static pressure minus hydrostatic pressure:

$$p_{rgh} = p - \rho \cdot \mathbf{g} \cdot \mathbf{h} \quad (6.3)$$

Volume of Fluid equation:

$$\frac{\partial \alpha}{\partial t} + \nabla \cdot (\alpha \vec{\mathbf{U}}) + \nabla \cdot ((1 - \alpha) \mathbf{U}_r \alpha) = 0 \quad (6.4)$$

with the following parameters:

$$\rho = \alpha \rho_{aq} + \rho_g (1 - \alpha) \quad (6.5)$$

$$\mu = \alpha \mu_{aq} + \mu_g (1 - \alpha) \quad (6.6)$$

$$\mu_i = \mu_{i,phys} + \mu_{i,turb} \text{ with } i=aq,g \quad (6.7)$$

where  $\vec{\mathbf{U}}$  is the velocity field [m/s];  $\rho$  is the density [kg/m<sup>3</sup>];  $t$  is time [s];  $p$  is the pressure [Pa];  $\mu$  is the dynamic viscosity [Ns/m<sup>2</sup>];  $\vec{\mathbf{q}}$  is the acceleration vector due to gravity [m/s<sup>2</sup>];  $\vec{\mathbf{x}}$  is a spatial position vector [m];  $\alpha$  is a volume fraction or indicator function [-];  $\mathbf{U}_f$  is the relative velocity between the phases [m/s]; the subscripts aq and g denote the fluids water (aq - aqueous) and air (g - gas). For the dynamic viscosity  $\mu$ , the physical viscosity and the turbulent viscosity are considered (see Equation 6.7).

The indicator function  $\alpha$  is defined as:

$$\alpha = \begin{cases} 1 & \text{fluid aq} \\ 0 < \alpha < 1 & \text{transitional region} \\ 0 & \text{fluid g} \end{cases} \quad (6.8)$$

The water surface is defined as the area where  $\alpha=0.5$ .

A turbulence model based on the Reynolds averaged Navier-Stokes equations (Standard  $k-\epsilon$ ) is applied to consider the turbulent part and the near-wall turbulence is modelled by so-called wall functions. More advanced turbulence models, such as Large Eddy Simulations (LES) or Direct Numerical Simulations (DNS), would offer the opportunity of resolving small-scale velocity variations but would come with the price of a highly increased

computation time. As we expect that the application of more advanced turbulence effects would not change the insights on the equilibrium conditions of the mass transfer simulations addressed in this publication, a RANS turbulence model has been considered to be sufficient as well as the best way to save computational resources. Even with the Standard  $k-\epsilon$  turbulence model, the computation time of 10 seconds simulation for the complex sewer geometry amounted to 12 hours on 80 parallel processors using the high performance computing (HPC) clusters of TU Berlin.

The accuracy of the hydrodynamic simulations has been assessed in Teuber et al. (2019a).

### Transport simulations

In general, the transport of a passive tracer with a concentration  $c$  is examined with an advection-diffusion equation that can be implemented into the interFoam solver (see Equation 6.9). The physical diffusivity  $D_{phys}$  as well as the turbulent Schmidt number  $Sc_{turb}$ , which defines the turbulent diffusivity coefficient  $D_{turb}$ , then have to be defined by the user (Equation 6.10).

Advection-diffusion equation:

$$\frac{\partial c}{\partial t} + \nabla \cdot (\vec{\mathbf{U}}c) = (D_{phys} + D_{turb})\nabla c \quad (6.9)$$

with

$$D_{turb} = \frac{\mu_{turb}/\rho}{Sc_{turb}} \quad (6.10)$$

### Mass transfer

Mass transfer has been simulated using the approach defined by Haroun et al. (2010a,b) as it has been implemented by Nieves-Remacha et al. (2015) and Severin (2017). The approach is based on the interFoam solver and considers one additional transport equation for both phases as outlined in Equations 6.9 and 6.10.

$$\frac{\partial c}{\partial t} + \nabla \cdot (\vec{\mathbf{U}}c) = ((D_{phys} + D_{turb})\nabla c + \phi) \quad (6.11)$$

A concentration flux expression at the interface results in the following:

$$\phi = -(D_{phys} + D_{turb}) \left( \frac{c(1 - He)}{\alpha + He(1 - \alpha)} \right) \nabla \alpha \quad (6.12)$$

In order to distinguish the species transport between the two phases, Henry's law must be fulfilled and the concentration flux must be consistent:

$$He = \frac{c_{aq}}{c_g} \quad (6.13)$$

$$(D_{phys,aq} + D_{turb,aq})\nabla c_{aq} = (D_{phys,g} + D_{turb,g})\nabla c_g \quad (6.14)$$

The concentrations and diffusion coefficients are considered as single-phase properties depending on the phase fraction value  $\alpha$ :

$$c = \alpha c_{aq} + c_g(1 - \alpha) \quad (6.15)$$

$$D_{phys} = \left( \frac{D_{phys,aq} \cdot D_{phys,g}}{\alpha D_{phys,aq} + (1 - \alpha) D_{phys,g}} \right) \quad (6.16)$$

The diffusion coefficients for  $D_{phys,aq}$  and  $D_{phys,g}$  are defined by the user. Note that these coefficients are temperature dependent which has to be taken into account when defining the values.

### 6.3.2 Henry coefficient

The Henry coefficient, also known as Henry constant, is a temperature dependent variable which is reported in many different forms in literature and is often presented in different units.

In this paper, three different definitions of the Henry coefficient are relevant for derivation and comparison with analytical solutions. Sander (2015) lists values of Henry coefficients in the unit [mol/(m<sup>3</sup>Pa)] and defines this Henry coefficient as  $H^{cp}$ . For the implementation in the interHarounFoam solver, the dimensionless Henry coefficient  $H^{cc}$  is relevant (see Equation 6.13):

$$H^{cc} = H^e = \frac{c_{aq}}{c_g} \quad (6.17)$$

Where the Henry coefficient is expressed as the ratio between the concentration in the aqueous phase  $c_{aq}$  and the concentration in the gas phase  $c_g$ .

$H^{cp}$  can be converted to  $H^{cc}$  using the ideal gas law:

$$H^{cc} = H^{cp} \cdot R \cdot T \quad (6.18)$$

Where R is the universal gas constant  $8.314 \frac{kgm^2}{s^2molK}$  and T is the temperature [K].

For H<sub>2</sub>S, the Henry coefficient at standard temperature (25°C) results in:

$$H_{H_2S}^{cc} = 10^{-3} \frac{mols^2}{m^2kg} \cdot 8.314 \frac{kgm^2}{s^2molK} \cdot 298.15K = 2.479 \quad (6.19)$$

### 6.3.3 Extensions

#### Temperature dependency of Henry coefficient

The Henry coefficient depends on the overall temperature in the domain. Therefore, the temperature dependency has been added in a way that the solver takes one global temperature value as an input parameter.

The temperature dependent Henry coefficient is computed using the van't Hoff equation following Sander (2015):

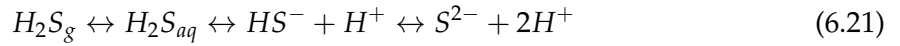
$$H^{cp}(T) = H^{cp} \exp \left( C \left( \frac{1}{T} - \frac{1}{T\Phi} \right) \right) \quad (6.20)$$

Where  $C$  is a temperature coefficient which is depending on the enthalpy of dissolution and defined as 2100 K (Sander, 2015),  $T^\Phi$  is the standard temperature 298.15 K corresponding to 25°C.

### Equilibrium conditions

The equilibrium conditions are implemented following Hvitved-Jacobsen et al. (2013). The aim is to describe the water-phase concentration of  $H_2S$  depending on the amount of total dissolved sulphide and the pH value since those values are usually measured in field investigations.

The dissociation of  $H_2S$  is generally expressed by the following equilibrium:



The equilibrium between  $H_2S$  in the gas phase ( $H_2S_g$ ) and  $H_2S$  in the water phase ( $H_2S_{aq}$ ) is described by the Henry coefficient. In the water phase, an equilibrium between hydrogen sulphide  $H_2S_{aq}$  and bisulphide ion ( $HS^-$ ) exists, where the total amount of both is described as total dissolved sulphide.

Only  $H_2S_{aq}$  can be transferred across the air-water interface, not the ionized form  $HS^-$ , however, usually the concentration of total dissolved sulphide and the pH value are measured. Therefore it is useful to derive a way to calculate the concentration of  $c_{H_2S_{aq}}$  when  $c_S$  and pH are given.

The equilibrium depends on the equilibrium constant  $K_{a1}$  (also known as acid dissociation constant):

$$K_{a1} = \frac{c_{H^+} c_{HS^-}}{c_{H_2S_{aq}}} \quad (6.22)$$

The dissociation can also be described using the negative logarithm of  $K_{a1}$ ,  $pK_{a1}$  ( $pK_{a1} = -\log K_{a1}$ ), resulting in the Henderson-Hasselbalch equation:

$$\log_{10} \frac{c_{H_2S_{aq}}}{c_{HS^-}} = pK_{a1} - pH \quad (6.23)$$

For a temperature of 20°C the equilibrium constant is  $pK_{a1} = 7.0$ . Between the ionized form  $HS^-$  and the sulphide ion another equilibrium exists in the water phase:



$$K_{a2} = \frac{c_{H^+} c_{S^{2-}}}{c_{HS^-}} \quad (6.25)$$

The value of  $pK_{a2} = 14.0$  indicates that measurable amounts of the sulphide ion  $S^{2-}$  only exist at a value above a pH of about 12. Therefore, only the equilibrium value of  $K_{a1}$  is important for wastewater and has been implemented for the interHarounFoam solver in OpenFOAM using the utilities `funkySetFields` (for initial conditions) and `funkySetBoundaryFields` (as boundary conditions) from `swak4Foam`.

The step-by-step reformulation based on Hvitved-Jacobsen et al. (2013) of the equations which results in the equation implemented in OpenFOAM is shown in the following, beginning with the Henderson-Hasselbalch equation:

$$\log_{10} \frac{c_{H_2S_{aq}}}{c_{HS^-}} = pK_{a1} - pH \quad (6.26)$$

Solving the log-function and using the expression  $c_S = c_{HS^-} + c_{H_2S_{aq}}$  for the total dissolved sulphide:

$$10^{pK_{a1}-pH} = \frac{c_{H_2S_{aq}}}{c_{HS^-}} = \frac{c_{H_2S_{aq}}}{c_S - c_{H_2S_{aq}}} \quad (6.27)$$

Rearranging leads to the mass concentration  $\gamma_{H_2S_{aq}}$  in  $[\text{kg}/\text{m}^3]$ :

$$\gamma_{H_2S_{aq}} = \frac{c_S \cdot 10^{pK_{a1}-pH}}{1 + 10^{pK_{a1}-pH}} \quad (6.28)$$

This can be converted into a molar concentration  $[\text{mol}/\text{m}^3]$  by dividing through the atomic weight  $M_S$  (0.032 kg/mol) of sulphur (S):

$$c_{H_2S_{aq}} = \frac{\gamma_{H_2S_{aq}}}{M_S} = \frac{\gamma_{H_2S_{aq}}}{0.032 \text{ kg/mol}} \quad (6.29)$$

Thus, the resulting equation implemented in OpenFOAM is:

$$c_{H_2S_{aq}} = \frac{c_S \cdot 10^{pK_{a1}-pH}}{1 + 10^{pK_{a1}-pH}} \quad (6.30)$$

Note that the equilibrium constants  $K_{a1}$  and  $K_{a2}$  are temperature dependent (Yongsiri et al., 2004), which is not considered in the current version of the code. The value of  $K_{a1}$  is a user-defined variable and the temperature dependency of the equilibrium constant has to be accounted for by defining the corresponding  $K_{a1}$  value for the temperature analysed.

### Calculation of partial pressure of $H_2S_g$ in ppm

The partial pressure of  $H_2S_g$  is being computed using a function object in swak4Foam.

The input value in OpenFOAM is a tracer  $c_{H_2S_{aq}}$  in  $[\text{mol}/\text{m}^3]$ , requiring a unit conversion:

$$c \left[ \frac{\text{mol}}{\text{l}} \right] = 1 \frac{\text{mol}}{\text{l}} = \frac{c_{H_2S_{aq}}}{1000} = \frac{1000 \text{ mol}/\text{m}^3}{1000} \quad (6.31)$$

The conversion from ppm to atm is:

$$10^{-6} \text{ atm} = 1 \text{ ppm} \quad (6.32)$$

According to Hvitved-Jacobsen et al. (2013), the partial pressure of a trace quantity in the air phase can be expressed by multiplying the molar concentration with the molar volume:

$$p_{H_2S_g} [\text{atm}] = c_{H_2S_{aq}} [\text{mol}/\text{l}] \cdot 22.4 \text{ l/mol} \quad (6.33)$$

Together, this leads to the following equation for conversion:

$$p_{H_2S_g} [\text{ppm}] = 10^6 \cdot \frac{c_{H_2S_{aq}} [\text{mol}/\text{l}]}{1000} \cdot 22.4 \text{ l/mol} \quad (6.34)$$

This conversion is only valid for the gas phase concentration, therefore the expression is multiplied with  $(1-\alpha)$  in order to keep the values constrained to the air phase.

### 6.3.4 Case studies

In the following, three different cases will be used to explore the possibilities of the existing solver, to validate the new features added to the solver and to show the importance of the model compared to the existing model approaches. For all simulations, at a temperature of 25°C, physical diffusivities for H<sub>2</sub>S in water of  $2.2 \cdot 10^{-9} m^2/s$  and in air of  $1.74 \cdot 10^{-5} m^2/s$  are chosen.

The first setup is a quasi-one-dimensional cubic tank with the measures 1m x 1m x 1m bounded by upper, lower and sidewalls with no-slip conditions. The tank is partially filled with water (water depth  $d = 0.5$  m). Both fluids water and air are at rest. As an initial condition, an H<sub>2</sub>S concentration of  $c_{H_2S_{aq}} = 1 mol/m^3$  in the water phase is given, the concentration in the air phase is  $c_{H_2S_g} = 0 mol/m^3$ . The domain is discretized with 100 cells in y-direction, which is the vertical dimension of the domain, and 10 cells in x- and z-direction. At the bottom wall, a concentration source is assumed, using a fixed value boundary condition of  $1 mol/m^3$ . The top wall as well as the sidewalls are defined with zeroGradient conditions. This setup is used to illustrate the solver's capabilities in a simple setup. In a first example, mass transfer, as it can be described with the existing interHarounFoam solver, is shown in a vertical one-dimensional case. Then, the extensions leading to the interH2SFoam solver are demonstrated in different examples using this first setup.

In a second setup, mass transfer in a rectangular duct is analysed using two well-documented examples of water-air pipe flow as they have been described by Bentzen et al. (2016) (test cases no. 7 and 21). The investigated pipe has a length of 15.0m, a height of 0.26m and a width of 0.3m with two different water depths and slopes. The air phase is only accelerated by the movement of the water surface. Bentzen et al. (2016) measured resulting velocity profiles in detail using Laser Doppler Anemometry (LDA) velocity measurements. The flow characteristics of the two test cases analysed are listed in Table 6.1. The setup is a relatively simple three-dimensional setup of a pipe. It illustrates the applicability of the model to regular pipes. The computational domain consists of 307,970 cells. The inlet has been divided in two parts: one for the water phase and one for the air phase. For the water phase, a fixed discharge has been defined, and the phase fraction value  $\alpha$  has been defined to be  $\alpha = 1$ . The pressure boundary condition has been defined as null Neumann condition. For the air phase, a fixed pressure has been defined and the phase fraction value has been set to  $\alpha = 0$ . The velocity has been defined using a null Neumann condition. At the outlet, a free outflow has been assumed. A fixed pressure has been defined and the remaining boundary conditions were defined as null Neumann conditions. At the walls, no-slip conditions were applied. Hydrodynamic simulations (without mass transfer) were run for 200s, until quasi steady state conditions were reached, afterwards a concentration  $c_{H_2S_{aq}} = 1 mol/m^3$  has been defined for the water at the inlet, assuming contaminated water flowing into the domain. The upper fluid then has a concentration of  $c_{H_2S_g} = 0 mol/m^3$  at the inlet, all remaining boundaries were defined with null Neumann conditions.

The third setup describes a complex sewer geometry with an overall length of 93.3m, a width ranging from 6.0m to 7.5m and a sewer height between 4.3m and 5.3m. The setup is shown in Figure 6.6. This geometry has been simulated in OpenFOAM and compared to experimental results from a 1:20 scale model by Bayón et al. (2015) and Teuber et al. (2019a). The setup describes a highly three-dimensional pipe diversion, including bends and geometry changes as well as a hydraulic jump. The computational mesh consists of 3,029,223 cells. The setup of boundary conditions is similar to the rectangular pipe of Bentzen et al. (2016).

Table 6.1: Mass transfer in rectangular channel: flow properties of analysed test cases.

Test no.	Duct slope [%]	Water depth [cm]	$U_{aq}$ [m/s]	$U_g$ [m/s]	Reynolds number $Re_{aq}$	Reynolds number $Re_g$
7	0.57	3.15	0.77	0.226	72,300	5,400
21	1.34	4.00	1.37	0.336	175,300	7,900

The hydrodynamic model has been simulated for 200s, until steady-state conditions were reached. Then, a concentration  $c_{H_2S_{aq}} = 1 \text{ mol/m}^3$  has been defined for the water phase and the simulations using the interH2SFoam solver have been carried out for a simulation time of 10s. A temperature of 25°C is assumed.

The results of the numerical simulations are presented in the following Section.

## 6.4 Results and discussion

### 6.4.1 Saturation of H<sub>2</sub>S in a tank

#### Mass transfer modelling

In our first test case, we present the application of the model to a vertical one-dimensional problem. It illustrates the advantage of the new model in describing vertical concentration profiles in contrast to the existing horizontal one-dimensional approaches. The simplicity of the test case enables a first illustration of the model's capabilities. The simulation has been carried out assuming normal temperature (25°C).

Figure 6.1 shows the presence of the two phases within the domain ( $\alpha = 1$ : water,  $\alpha = 0$ : air) and the development of the concentration profile within the domain over time. After  $t = 50$ s, a decrease of the overall concentration in the water phase can be observed. This is due to the concentration jump at the interface, which has to be fulfilled by the solver. This concentration jump occurs in the first second due to a direct flux of concentration across the interface. After several seconds, the concentration in the water phase is re-established by the source term at the bottom and after  $t = 1000$ s, a steady-state has developed and a constant concentration profile is achieved. The concentration in the water phase is then equal to the source term concentration and the air phase concentration is defined by the Henry coefficient. A detailed validation of the flux under transient conditions has been performed by Haroun et al. (2010a).

The concentration profile illustrates that the resulting air phase concentration is  $c_{H_2S_g} = 0.4034 \text{ mol/m}^3$ , which is the expected concentration in the air phase when applying Henry's law for H<sub>2</sub>S:

$$c_{H_2S_g} = \frac{c_{H_2S_{aq}}}{H_{H_2S}^{cc}} = \frac{1 \frac{\text{mol}}{\text{m}^3}}{2.479} = 0.4034 \frac{\text{mol}}{\text{m}^3} \quad (6.35)$$

#### Temperature dependency

In this test case, we will analytically analyse the temperature dependency of the Henry coefficient, which has been implemented. The application example is based on example 4.2 in Hvitved-Jacobsen et al. (2013). The Henry coefficient at a temperature of 15°C is being

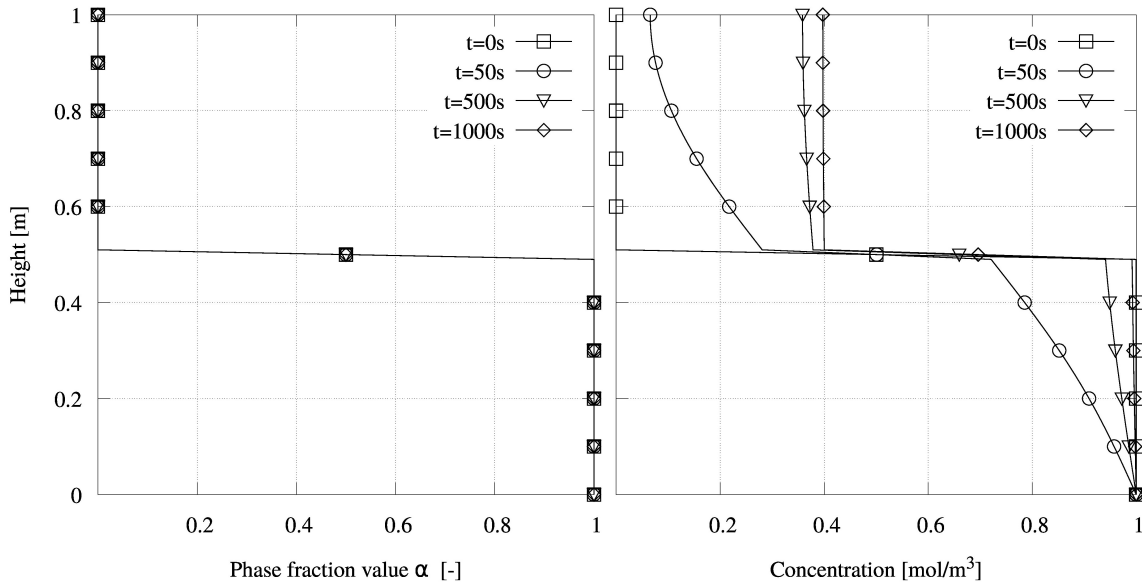


Figure 6.1: H<sub>2</sub>S saturation in a tank (left: phase fraction value, right: concentration profiles along the vertical axis over time).

calculated.

In this case, a temperature of 288.15 K has been chosen. The resulting Henry coefficient can be determined as follows (following Equations 6.18 - 6.20):

$$H^{cc}(T) = H^{cp} \exp \left( C \left( \frac{1}{T} - \frac{1}{T\Phi} \right) \right) RT \quad (6.36)$$

$$H^{cc}(288.15) = 0.001 \cdot \exp \left( 2,200 \left( \frac{1}{288.15} - \frac{1}{298.15} \right) \right) \cdot 8.314 \cdot 288.15 \quad (6.37)$$

$$H^{288.15} = 3.083 \quad (6.38)$$

Resulting in the following expected gas-phase concentration  $c_{H_2S_g} = 0.324 \text{ mol/m}^3$ :

$$c_{H_2S_g}(288.15) = \frac{1}{3.083} = 0.324 \text{ mol/m}^3 \quad (6.39)$$

Figure 6.2 shows the resulting concentration in the domain after  $t = 1000\text{s}$ . The result agrees well with the expected concentration. The implemented temperature dependency can therefore be considered as accurate.

### Equilibrium conditions and unit conversion

In order to validate the solver extensions regarding the equilibrium conditions and the partial pressure in the air phase, example 4.3 by Hvitved-Jacobsen et al. (2013) is simulated. The resulting H<sub>2</sub>S<sub>aq</sub> and H<sub>2</sub>S<sub>g</sub> concentrations for a measured concentration of dissolved sulphide  $c_S$  and pH value have been simulated. Again, the basic setup of the case is the same as for the first application example. A temperature of 15°C,  $pK_{a1} = 7.0$ ,  $pH = 7.0$  and a

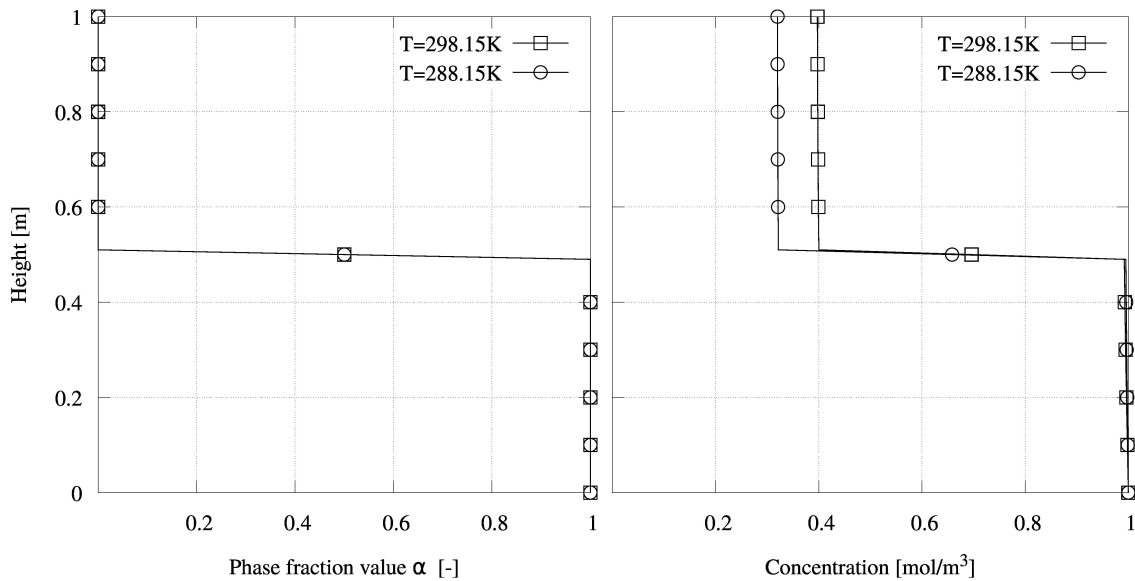


Figure 6.2: H<sub>2</sub>S saturation in a tank for different temperatures (298.15K (cp. Figure 6.1, right) and 288.15K) (left: phase fraction value, right: concentration profiles along the vertical axis).

dissolved sulphide concentration of 0.001 kg/m<sup>3</sup> are given.

In Hvitved-Jacobsen et al. (2013), the Henry coefficient for the given temperature of 15°C is assumed to be the same as the Henry coefficient from a previous calculation for a temperature of 20°C, i.e. 433 atm. For comparing the analytical solution with the simulated values, the exact Henry coefficient for 15°C has been calculated. Using this value and performing the same calculation steps with the corrected Henry coefficient, the analytical solution leads to a water phase H<sub>2</sub>S concentration of  $c_{H_2S_{aq}} = 0.0075 \text{ mol/m}^3$ , a gas phase concentration of  $c_{H_2S_g} = 0.0027 \text{ mol/m}^3$  and a corresponding partial pressure of  $p_{H_2S_g} = 66 \text{ ppm}$ .

Figure 6.3 shows the results of the numerical simulations. In the water phase, the concentration of H<sub>2</sub>S is  $c_{H_2S_{aq}} = 0.0075 \text{ mol/m}^3$ , in the air phase the concentration reaches a value of  $c_{H_2S_g} = 0.0027 \text{ mol/m}^3$  and a corresponding partial pressure (in the gas phase) of  $p_{H_2S_g} = 66 \text{ ppm}$  and thus agrees well with the analytical solution. The implemented approach predicts the resulting concentrations accurately.

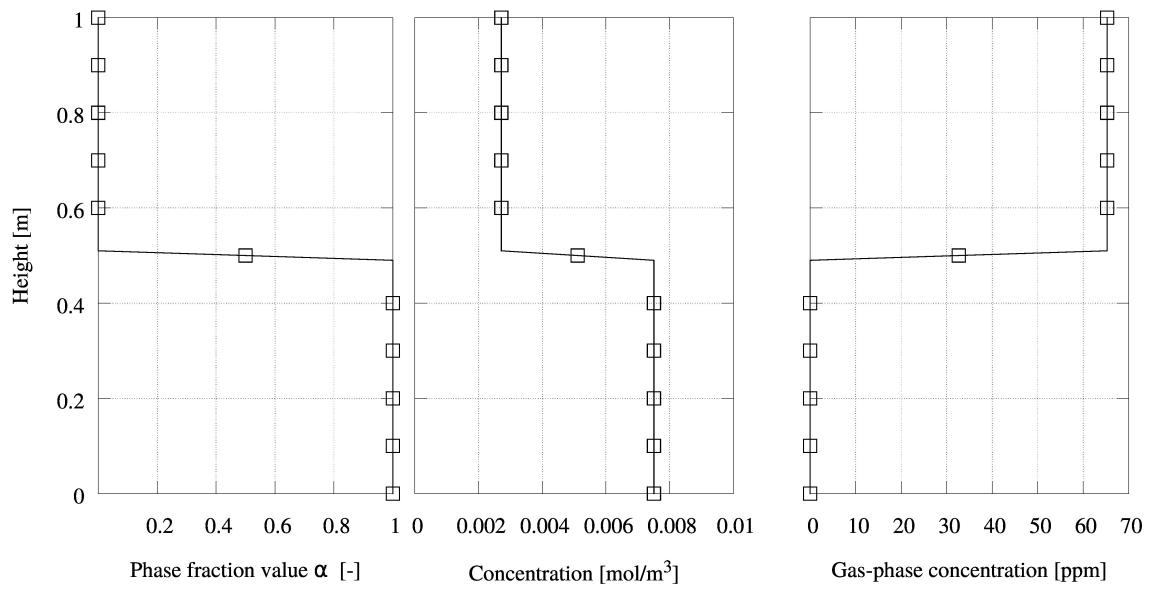


Figure 6.3: Application example for  $\text{HS}^-$  and  $\text{H}_2\text{S}$  equilibrium and partial pressure of air phase concentration (left: Phase fraction value profile over domain height, middle: concentration profile, right: partial pressure of gas-phase concentration).

### 6.4.2 Mass transfer in a rectangular channel

In this test case, we present mass transfer simulations in a rectangular pipe. Figures 6.4 and 6.5 present the resulting phase fraction, velocity and concentration profiles along the height of the domain in the middle of the pipe. The simulated velocity profiles indicate a good agreement with the measured values by Bentzen et al. (2016). For a pipe with a length of 15 m and the analysed flow velocities, the concentration profiles show that almost no mass transfer across the water surface into the air phase can be observed. This can be explained by small velocities in directions other than the main flow direction (i.e. in the  $yz$ -plane) which cause advective transport to occur mostly in the main flow direction ( $x$ -direction). Furthermore, the small diffusion coefficients cause mainly advective transport. This example opens the question how simulated mass transfer is influenced under highly turbulent conditions or in cases with higher velocities in the  $yz$ -plane, which will be analysed in the next example.

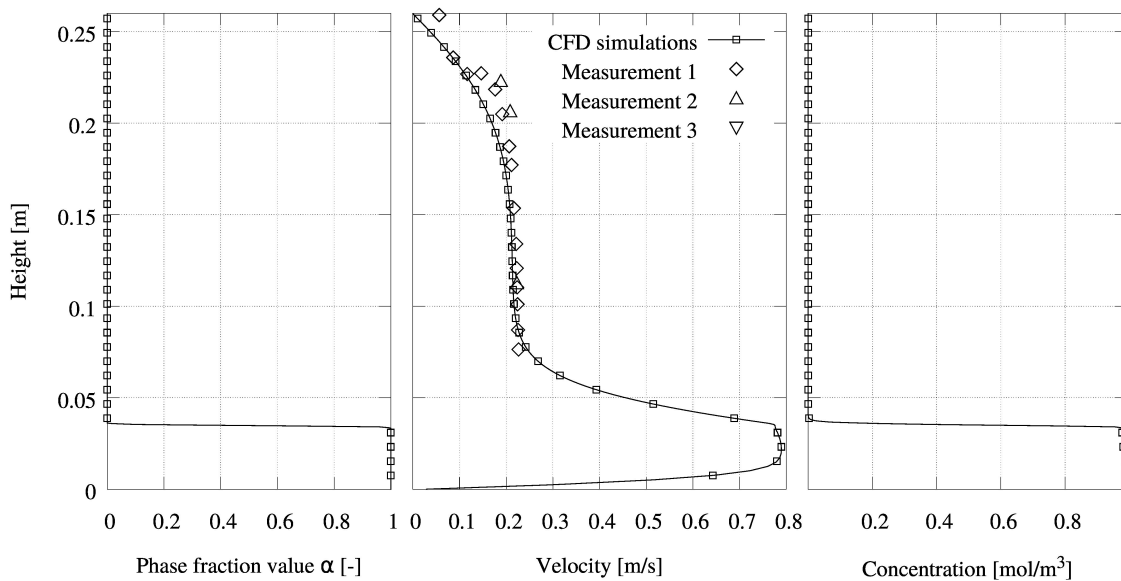


Figure 6.4: Mass transfer in rectangular channel for test 7 (see Table 6.1) (left: phase fraction value, middle: velocity, right: concentration profiles).

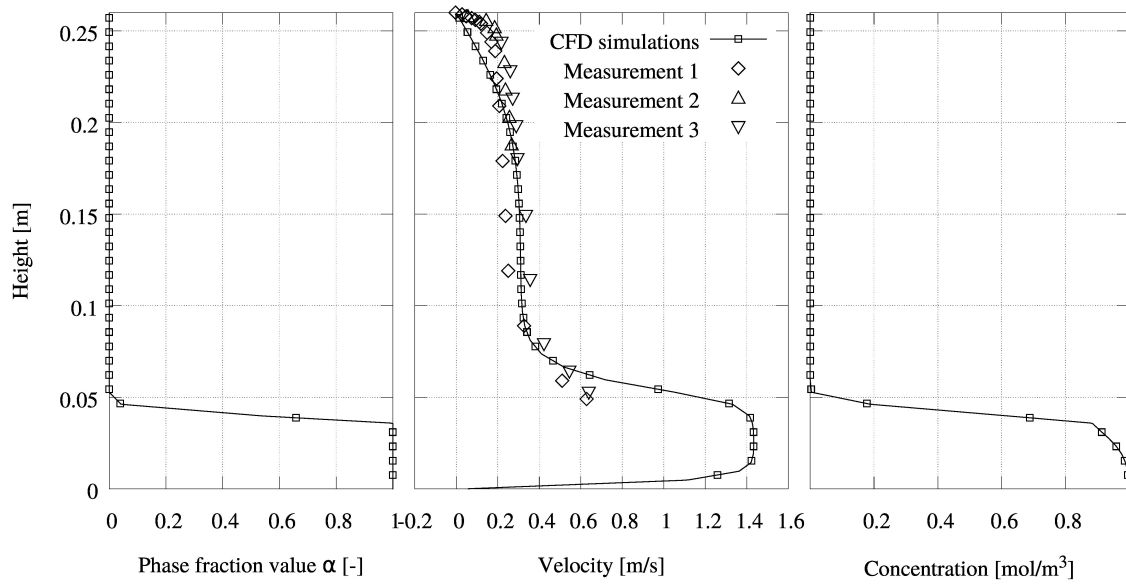


Figure 6.5: Mass transfer in rectangular channel for test 21(see Table 6.1) (left: phase fraction value, middle: velocity, right: concentration profiles).

### 6.4.3 Complex sewer geometry

In a final example, the advantage of the new model are demonstrated by applying the solver to a complex and highly three-dimensional sewer geometry. The existing models are not public domain, therefore a direct comparison to the one-dimensional models is not possible, but the results of the CFD model will be used to highlight the advantages compared to the concepts of the existing approaches.

The results of the simulations at  $t = 10\text{s}$  are displayed in Figure 6.6. Figure 6.6 a) gives an overview of the computational domain and the water phase behaviour. The location of highest turbulence occurs in the hydraulic jump, which is displayed in Figures 6.6 b) and 6.6 c). The velocity vectors in Figure 6.6 b) indicate the highly three-dimensional flow behaviour in this location and show the complex water surface movement. In Figures 6.6 c) and 6.6 d), the isosurfaces of the resulting  $\text{H}_2\text{S}$  concentration in the domain are displayed. The concentration range between  $0\text{ mol/m}^3$  and  $1\text{ mol/m}^3$  has been divided into 10 surfaces. The value range in between is not displayed, leaving white spaces for better illustration of the surfaces. The contour plots show, that a more diverse and highly three-dimensional concentration profile develops at the reach of the hydraulic jump. This indicates the increased mass transfer (i.e. higher distance of concentration isolines to the water surface) in the location of the hydraulic jump.

Because the existing model approaches are not public domain, a direct comparison to simulation results is not possible, however, the advantages of the new CFD based mass transfer approach are the following:

1. In respect to the hydrodynamic behaviour, the new model can describe the three-dimensional flow velocities in the air and water phase. The sewer geometry analysed consists of a bent pipe structure with varying shapes and a hydraulic jump. A hydrodynamic one-dimensional approach would describe this geometry as one connection pipe between beginning and end point. The flow velocity would be calculated as a uniform value without accounting for the complexity of the geometry. The existing model would not account for the highly complex interaction of water and air phase in the hydraulic jump.
2. Regarding the mass transfer, the model would then account for advection and molecular diffusion and for turbulence in the free-stream flow areas as well as in drop structures in a very simplified way. This would lead to a simplified assumption of the actual mass transfer occurring in the pipe, since the effect of turbulence on the mass transfer is substantial. A validation of the actual mass transfer rate due to turbulence effects is performed in Teuber et al. (in preparation).

Most sewer stretches in urban areas are not as complex as the previously shown example and wide networks without high levels of turbulence justify the use of one-dimensional models. However, locations of high turbulence can enhance  $\text{H}_2\text{S}$  emissions and the three-dimensional approach presented in this paper can help analyse the effect of local design aspects on the resulting  $\text{H}_2\text{S}$  emissions and improve the sewer network design.

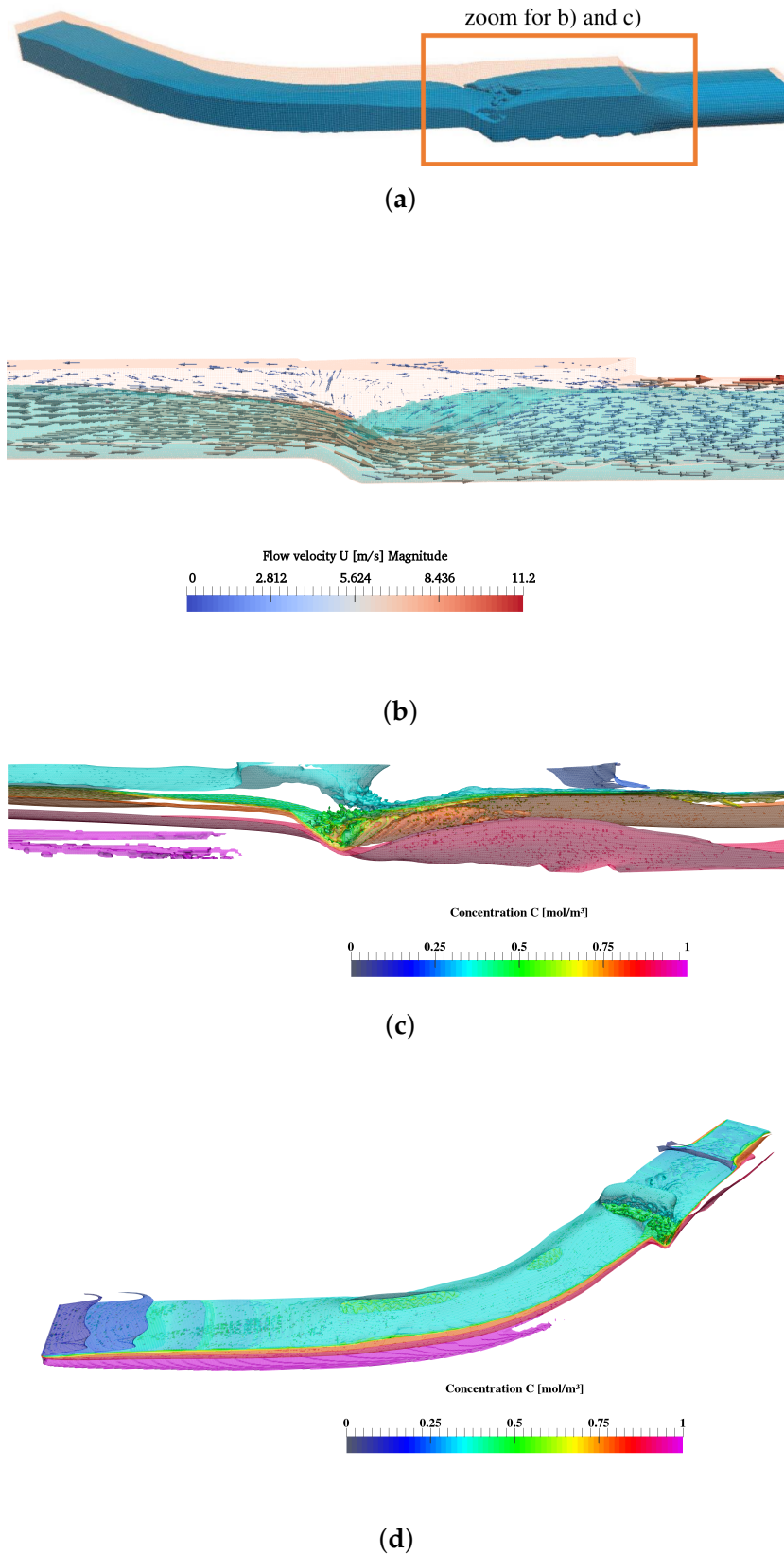


Figure 6.6: Mass transfer simulations in complex sewer geometry at  $t=10s$  (a) overview of the domain filled with water under steady-state conditions, b) flow velocities and water surface behaviour in hydraulic jump, c) tracer distribution in hydraulic jump, d) top view on tracer distribution).

## 6.5 Conclusions

H<sub>2</sub>S emissions and their consequences are an important topic when considering urban drainage and the design of sewer networks. In the past, different model approaches, from empirical to conceptual, have been developed in order to describe and predict H<sub>2</sub>S emissions and resulting odour. These models are horizontal one-dimensional approaches, therefore neglecting the occurrence of three-dimensional effects.

In this publication, a model approach has been introduced that can describe H<sub>2</sub>S emissions across the water surface using a mass transfer approach based on the Henry coefficient, which is implemented in the open source software OpenFOAM. Two-phase flow has been simulated using a VOF method. The solver has been extended by different key features that are crucial when describing H<sub>2</sub>S emissions. The temperature dependency of the Henry coefficient has been taken into account. Equilibrium conditions between HS<sup>-</sup> and H<sub>2</sub>S are described and enable the usage of the measured value for total dissolved sulphide and the pH value as input parameters. The solver also computes the partial pressure of H<sub>2</sub>S in the gas phase based on the simulated concentration of H<sub>2</sub>S<sub>g</sub>.

The new solver has been applied to different simple test cases and the results have been compared to analytical solutions. Furthermore, it has been applied to a highly complex three-dimensional test case to highlight the advantages of the new model approach. Compared to one-dimensional formulations, it can account for highly complex flow effects in a sewer stretch and describe mass transfer in such environments. The analysis of the results showed an increased mass transfer in the location of highest turbulence, which agrees with existing observations. The exact quantification of local mass transfer rates has been validated in Teuber et al. (in preparation) and has led to a good agreement with experimental results.

Overall, the new solver enables an analysis of mass transfer in complex three-dimensional test cases, the description of which has so far only been possible with major simplifications.

Future research will deal with further extensions of the solver to account for temperature effects in the fluids and reactive transport modelling.

## 6.6 Acknowledgements

The complex sewer geometry has been computed on the supercomputers of Norddeutscher Verbund für Hoch- und Höchstleistungsrechnen in Berlin.

The funding provided by the German Research Foundation (DFG) within the Research Training Group 'Urban Water Interfaces' (GRK 2032-1) is gratefully acknowledged.

We thank Prof. Arnau Bayón for providing the experimental data and the mesh for the complex sewer geometry.

## Chapter 7

# Mass transfer under turbulent conditions

This study will be submitted to Water Science and Technology (IWA Publishing) as:

---

Teuber, K., Broecker, T., Nützmann, G. & Hinkelmann, R.: CFD simulation of H<sub>2</sub>S mass transfer under turbulent conditions in a stirring tank, in preparation for submission to Water Science and Technology (IWA Publishing).

---

This is the preprint version of the article.

A detailed explanation of the solver extensions addressed in this paper is given in Appendix A. The setup of the stirring tank test case is listed in Appendix B.8.

### 7.1 Abstract

The present paper deals with a study of H<sub>2</sub>S emissions under turbulent conditions in a stirring tank. A new three-dimensional two-phase (water / air) solver which is able to describe H<sub>2</sub>S emissions across the water surface is connected to a dynamic meshing functionality and extended to compute the occurring mass transfer coefficient. H<sub>2</sub>S emissions are important to be investigated because of the possible health risk for sewer workers and high costs for sewer maintenance. The influence of turbulence on the mass transfer coefficient has been investigated in recent years but up to now there has not been any three-dimensional model to simulate the direct exchange of H<sub>2</sub>S between water and air phase. Being able to describe the mass transfer in a three-dimensional model can help to improve existing model concepts as well as to better examine hotspots of H<sub>2</sub>S emissions in order to give recommendations for design improvement.

### 7.2 Introduction

Cities in the modern world face problems caused by more and more centralized sewer systems. One of these problems is the occurrence of odour and corrosion due to hydrogen sulphide emissions across the wastewater-air interface, which cause a health risk for sewer workers as well as high costs for sewer maintenance.

In the past years, significant progress has been made in the field of understanding hydrogen sulphide (H<sub>2</sub>S) emissions in sewers. On the one hand, conceptual model approaches have been developed to describe the occurrence of odour and corrosion (Hvitved-Jacobsen

et al., 2013). On the other hand, numerous experiments have been conducted to better understand driving factors such as the influence of turbulence on  $H_2S$  mass transfer across the water surface (Carrera et al. (2017), Matias et al. (2017), Wu (1995)).

Being able to model and directly quantify these emissions cannot only improve existing model approaches by the possibility of investigating a wider range of cases but also to analyse details of sewer construction such as the design of  $H_2S$  hotspots and to find ways to improve the design.

State of the art modelling approaches to describe these in-sewer processes are one-dimensional approaches. However, previous research has shown that the flow processes occurring are three-dimensional, for example air phase velocities in the headspace of a circular sewer (Edwini-Bonsu and Steffler, 2006), raising the question of how much more accurate a three-dimensional Computational Fluid Dynamics (CFD) model could predict  $H_2S$  emissions. Furthermore, turbulent flow phenomena are ubiquitous in a sewer, starting in a gravity pipe due to the flow velocities present, but also higher levels of turbulence can be found in drop structures due to connections between pipe and manhole or due to obstacles. A correct quantification of the effects of turbulence, which are highly three-dimensional, on the  $H_2S$  mass transfer is therefore crucial for the development of reliable models.

One experimental setup to analyse mass transfer under turbulent conditions that has been investigated in previous publications are stirring tanks. A systematic sketch including measures which are relevant for this publication can be found in Figure 7.1.

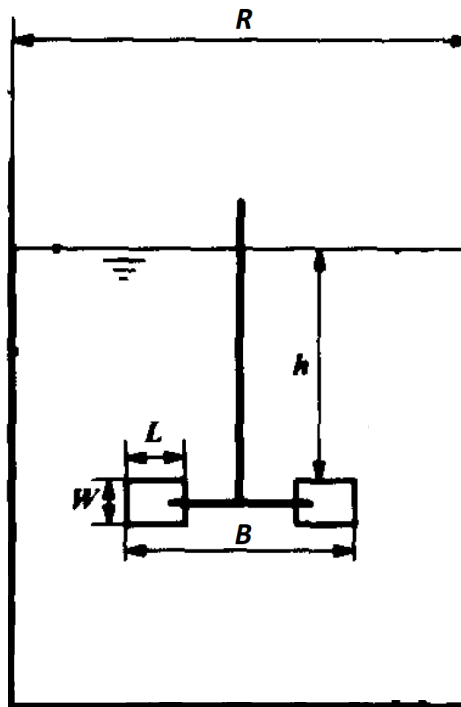


Figure 7.1: System sketch of stirring tank including relevant variables (Wu (1995), modified).

Wu (1995) analysed the influence of different factors such as the stirrer inundation ( $h/R$  – ratio between water level above stirrer  $h$  and stirrer diameter  $R$ ) and the stirring rate on  $O_2$

mass transfer. Carrera et al. (2017) investigated the influence of stirring rates on H<sub>2</sub>S mass transfer and used CFD results from FLUENT™ 1.4 to extract hydrodynamic parameters such as flow velocities. Being able to describe H<sub>2</sub>S emissions in a stirring tank with a CFD model cannot only enable us to investigate more complex phenomena on a larger scale but could also help avoiding lab experiments that come with a health risk and decrease the number of experiments necessary.

In Teuber et al. (2019b), a new three-dimensional two-phase solver for the prediction of H<sub>2</sub>S mass transfer called *interH2SFoam* has been introduced and tested on different application examples. In this publication, we will extend a dynamic meshing solver in OpenFOAM (*interDyMFoam*) by the functionalities of *interH2SFoam* as well as a functionality to compute the mass transfer coefficient. This new solver called *interDyMH2SFoam* enables us to analyse the effect of different stirring rates in a stirring tank on H<sub>2</sub>S mass transfer using a CFD model.

In this paper, first an overview over the materials and methods is given. Then, the results are evaluated and discussed. First, a graphic analysis is performed, then a sensitivity study on parameters such as the grid size, the influence of the turbulent diffusivity, the choice of turbulence model and the inundation of the stirrer is performed. In a quantitative analysis, the simulated results are then compared to experimental results by Carrera et al. (2017) and Wu (1995).

## 7.3 Methods

### 7.3.1 Geometry and mesh

In our model, the geometry analysed consists of a circular stirring tank. In the tank, a Rushton turbine is placed with a defined stirring rate. The mesh has been discretized using the OpenFOAM utility *snappyHexMesh*. The OpenFOAM solver *interDyMFoam*, which has been extended here, is capable of handling mesh motion using both a static and a rotating mesh domain. Therefore, the mesh motion has to be defined separately by specifying the rotation speed.

### 7.3.2 Numerical model

OpenFOAM version 2.4.0 has been used for the work presented in this paper. A new solver for two-phase simulations and mass transfer, which accounts for the temperature dependency of the Henry coefficient, has been introduced in Teuber et al. (2019b) and is applied to the turbulent case in this publication.

### Hydrodynamic simulations

Hydrodynamic simulations are based on the two-phase flow solver *interFoam* which uses a volume of fluid (VOF) approach that considers both phases as one fluid with changing fluid properties. One set of Navier-Stokes equations is solved. The volume fraction of a phase is stored as an additional variable and the phases are distinguished by an additional transport equation. The equations are defined as follows (Rusche, 2003):

Mass conservation equation:

$$\nabla \cdot \vec{U} = 0 \quad (7.1)$$

Momentum conservation equation:

$$\frac{\partial \rho \vec{U}}{\partial t} + \nabla \cdot (\rho \vec{U} \vec{U}) = -\nabla p_{rgh} + \nabla \cdot (\mu \Delta \vec{U}) + (\nabla \vec{U}) \nabla \mu - \vec{g} \cdot \vec{x} \nabla \rho \quad (7.2)$$

Where  $p_{rgh}$  is the static pressure minus hydrostatic pressure:

$$p_{rgh} = p - \rho \cdot \mathbf{g} \cdot \mathbf{h} \quad (7.3)$$

Volume of Fluid equation:

$$\frac{\partial \alpha}{\partial t} + \nabla \cdot (\alpha \vec{U}) + \nabla \cdot ((1 - \alpha) \vec{U}_{r\alpha}) = 0 \quad (7.4)$$

with the following parameters:

$$\rho = \alpha \rho_L + \rho_G (1 - \alpha) \quad (7.5)$$

$$\mu = \alpha \mu_L + \mu_G (1 - \alpha) \quad (7.6)$$

$$\mu = \mu_{phys} + \mu_{turb} \quad (7.7)$$

where  $\vec{U}$  is the velocity field [m/s];  $\rho$  is the density [kg/m<sup>3</sup>];  $t$  is time [s];  $p$  is the pressure [Pa];  $\mu$  is the dynamic viscosity [Ns/m<sup>2</sup>];  $\vec{g}$  is the acceleration vector due to gravity [m/s<sup>2</sup>];  $\vec{x}$  is a spatial position vector [m];  $\alpha$  is a volume fraction or indicator function [-];  $\vec{U}_f$  is the relative velocity between the phases [m/s]; the subscripts L and G denote the fluids water (L - liquid) and air (G - gas). For the dynamic viscosity  $\mu$ , the physical viscosity and the turbulent viscosity are considered (see Equation 7.7).

The indicator function  $\alpha$  is defined as:

$$\alpha = \begin{cases} 1 & \text{fluid L} \\ 0 < \alpha < 1 & \text{transitional region} \\ 0 & \text{fluid G} \end{cases} \quad (7.8)$$

The water surface is defined as the area where  $\alpha = 0.5$ .

The accuracy of the hydrodynamic simulations has been assessed in (Teuber et al., 2019a).

### Mass transfer simulations

Transport is considered by defining the H<sub>2</sub>S concentration as a passive tracer with an advection-diffusion equation (Equation 7.9). The physical diffusivity  $D_{phys}$  as well as the turbulent Schmidt number  $Sc_{turb}$ , which defines the turbulent diffusivity coefficient  $D_{turb}$ , are defined by the user (Equation 7.10).

$$\frac{\partial C}{\partial t} + \nabla \cdot (\vec{U} C) = \nabla \cdot (D_{phys} + D_{turb}) \nabla C \quad (7.9)$$

with

$$D_{turb} = \frac{\mu_{turb} / \rho}{Sc_{turb}} \quad (7.10)$$

Mass transfer at the wastewater-air interface is simulated using the approach defined by Haroun et al. (2010a,b) as it has been implemented by Nieves-Remacha et al. (2015) and

Severin (2017). The approach is based on the *interFoam* solver and considers one additional transport equation for both phases as outlined in Equations 7.9 and 7.10:

$$\frac{\partial C}{\partial t} + \nabla \cdot (\vec{U}C) = \nabla \cdot ((D_{phys} + D_{turb})\nabla C + \phi) \quad (7.11)$$

$$\phi = -(D_{phys} + D_{turb}) \left( \frac{C(1 - He)}{\alpha + He(1 - \alpha)} \right) \nabla \alpha \quad (7.12)$$

It contains a modification of the original solver in its consideration of diffusivity. The original approach by Haroun et al. (2010a) only considered molecular diffusivity  $D_{phys}$ , whereas in this publication  $D_{turb}$  is included into the formulation. The difference can be explained by the turbulence models used. Haroun et al. (2010a) performed simulations using Direct Numerical Simulation (DNS), which is able to describe small scale turbulence effect without any additional subgrid scale model, therefore no turbulent viscosity  $\mu_{turb}$  is calculated. A sensitivity study carried out in this paper will highlight the importance of including  $D_{turb}$  in the test cases analysed in this publication.

In order to distinguish the species transport between the two phases, the following conditions must be fulfilled at the interface:

$$He = \frac{C_L}{C_G} \quad (7.13)$$

$$(D_{phys,L} + D_{turb,L})\nabla C_L = (D_{phys,G} + D_{turb,G})\nabla C_G \quad (7.14)$$

Like density and viscosity, the concentrations and diffusion coefficients are considered as single-phase properties depending on the phase fraction value  $\alpha$ :

$$C = \alpha C_L + C_G(1 - \alpha) \quad (7.15)$$

The physical diffusivity  $D_{phys}$  is calculated by using a harmonic average:

$$D_{phys} = \left( \frac{D_{phys,L} \cdot D_{phys,G}}{\alpha D_{phys,L} + (1 - \alpha) D_{phys,G}} \right) \quad (7.16)$$

The diffusion coefficients for  $D_{phys,L}$  and  $D_{phys,G}$  are defined by the user. Note that the temperature dependency of these variables has to be accounted for.

The Henry coefficient depends on the temperature in the whole domain. Therefore, the temperature dependency has been added in a way that the solver takes one global temperature value as an input parameter.

The temperature dependent Henry coefficient is computed using the van't Hoff equation following Sander (2015):

$$He(T) = H^{cp} \exp \left( E \left( \frac{1}{T} - \frac{1}{T\Phi} \right) \right) \quad (7.17)$$

$$He(T) = 10^{-3} \frac{mols^2}{m^2kg} \exp \left( E \left( \frac{1}{T} - \frac{1}{T\Phi} \right) \right) \cdot 8.314 \frac{kgm^2}{s^2molK} \cdot 298.15K \quad (7.18)$$

Where  $He^{cp}$  is the Henry coefficient reported by Sander (2015) in the unit [mol/(m<sup>3</sup>Pa)],  $E$  is a temperature coefficient which is depending on the enthalpy of dissolution and defined as 2100 K (Sander, 2015),  $T^\Phi$  is the standard temperature 298.15 K corresponding to 25°C,  $R$  is the universal gas constant  $8.314 \frac{\text{kgm}^2}{\text{s}^2\text{molK}}$  and  $T$  is the temperature [K].

In order to combine dynamic meshing with mass transfer simulations, the respective functionalities for mass transfer had to be transferred or connected to the *interDyMFoam* solver, resulting in a new specialized solver *interDyMH2SFoam*.

### Calculation of mass transfer coefficient and volumetric mass transfer coefficient

In the literature, two important physical values can be found, when analysing the mass transfer coefficient. First of all, the mass transfer coefficient  $K_L$  and second the volumetric mass transfer coefficient  $K_L a$ , which is a multiplication of  $K_L a$  with  $a$  [m<sup>-1</sup>], the ratio between interfacial area and water volume. Many experiments report only  $K_L a$  because of the difficulty of measuring the exact interfacial area in an experiment. In this respect, CFD simulations offer the additional benefit of enabling the calculation of  $a$ .

The local mass transfer coefficient at the interface  $K_{L,local}$  [m/(sm<sup>2</sup>)] is calculated according to Haroun et al. (2010a) as

$$K_{L,local} = - \frac{((D_{phys} + D_{turb}) \nabla C + \phi) \cdot n_L}{\Delta C_{L,local}} \quad (7.19)$$

The mass transfer coefficient for the area of the interface,  $K_L$ , can then be computed by integrating  $K_{L,local}$  over the interfacial area:

$$K_L = \frac{1}{\lambda} \int_0^\lambda K_{L,local} d\zeta \quad (7.20)$$

where  $\lambda$  is the interface length and  $\zeta$  the curvilinear coordinate associated to the interface.

Furthermore, Carrera et al. (2017) propose a calculation of the mass transfer coefficient based on the degassing technique, which has been used in this publication to cross validate the simulated mass transfer coefficients. In the degassing technique, the measured decrease of the H<sub>2</sub>S concentration in the water phase has been fitted to Equation 7.21:

$$C_{L,H_2S} = C_{L,0} e^{-K_{L,H_2S} a (t-t_0)} \quad (7.21)$$

Where  $C_{L,0}$  is the initial concentration at  $t=t_0$ . In this publication, the bulk H<sub>2</sub>S concentration in the water phase as well as  $a$  have been calculated and  $K_{L,H_2S}$  was adjusted. To obtain the mass transfer coefficient, an automated curve fitting using the programming language Python has been carried out.

### 7.3.3 Turbulence

Turbulence and the impact of turbulence on flow can be simulated using different approaches. While DNS leads to most accurate results, the computational effort is highest since the turbulence is discretized by using small enough cell sizes and time steps to display all vortices (Maric et al., 2014), leading to a high computational effort, that is in most

cases still not practically applicable today.

Using Reynolds averaging, the mean velocity is divided into an average velocity component and a fluctuating velocity component resulting in a Reynolds stress tensor in the Navier-Stokes equations (RANS). This tensor describes an additional eddy viscosity and leads to new unknowns in the equations. These unknowns can be solved by using a two-equation model, that adds two coupled transport equations in order to describe convection and diffusion of turbulent energy. Depending on the model, these variables differ:  $k$  is the turbulent kinetic energy,  $\epsilon$  is the turbulent dissipation,  $\omega$  is the specific dissipation. For the  $k$ - $\epsilon$  turbulence models, three different formulations exist: the Standard (STD)  $k$ - $\epsilon$  model the Realizable (Shih et al., 1995) and the RNG  $k$ - $\epsilon$  model using Re-Normalisation Group (RNG) methods by Yakhot et al. (1992). RANS models used in this publication are the Standard  $k$ - $\epsilon$  (Launder and Sharma, 1974), the RNG  $k$ - $\epsilon$ , as well as the  $k$ - $\omega$  Shear Stress Transport (SST) (Menter, 1993, 1994).

In turbulent flows, the viscous sublayer of a boundary layer close to the wall gets very thin. In order to not discretize this sublayer by fine meshes, wall functions can be applied when RANS turbulence models are used. These wall functions account for the fact that the velocity profile normal to the wall follows a logarithmic profile, the log-law. The applicability of these wall functions can be described using the dimensionless wall distance  $y^+$ . It is defined as:

$$y^+ = \frac{y}{\nu v_\tau} \quad (7.22)$$

where  $y$  is the absolute distance from the wall,  $v_\tau$  denotes the friction velocity and  $\nu$  denotes the kinematic viscosity. Depending on the chosen RANS turbulence model and the respective wall function, different values of  $y^+$  and therefore different cell sizes in the nearfield of the wall are necessary (Maric et al., 2014). Due to the log-law, RANS turbulence models have smaller requirements in regard to cell size and time step than DNS and LES and are therefore prone to lead to the smallest computational effort.

Large Eddy Simulation (LES) stands between DNS and RANS models in terms of complexity. Large eddies are resolved spatially by choosing small enough cell sizes and small eddies are modelled using a subgrid scale model which leads to smaller necessary cell sizes than for RANS models (Maric et al., 2014).

### 7.3.4 Case study

The simulations are inspired by the experiments and simulations carried out by Carrera et al. (2017). The domain is discretized as a cylindrical tank. A Rushton turbine is placed above the bottom of the cylinder and two different levels of inundation are analysed. Fluid properties can be found in Table 7.1. A Schmidt number of 1 is defined. An initial concentration of  $0.073 \text{ mol/m}^3$ , based on results by Carrera et al. (2017), is imposed.

Table 7.1: Fluid properties as defined in the CFD simulations.

	Water phase	Air phase
Density $\rho$ [ $\text{kg/m}^3$ ]	1,000	1.20
Kinematic viscosity $\nu$ [ $\text{m}^2/\text{s}$ ]	$1.0 \cdot 10^{-6}$	$1.48 \cdot 10^{-5}$
Diffusion coefficient $D_{\text{phys}}$ [ $\text{m}^2/\text{s}$ ]	$1.8 \cdot 10^{-9}$	$1.74 \cdot 10^{-5}$

In order to validate the amount of  $H_2S$  emissions under steady state conditions for the respective stirring speed, the first 25s of the simulations are carried out without any  $H_2S$  concentration present in the domain and by only performing hydrodynamic simulations with the *interDyMFoam* solver. For this, an initial water level is defined depending on the desired inundation depth using the *setFields* function in OpenFOAM.

After 25s, the OpenFOAM extension *funkySetFields* is used in order to apply a certain  $H_2S$  concentration  $C$  in the areas where the fluid water is present (i.e.  $\alpha > 0.5$ ). After the  $H_2S$  has been applied in the computational domain, another 10s of simulations are being performed, this time by using the extended solver *interDyMH2SFoam*.

### 7.3.5 Initial and boundary conditions

The boundary conditions imposed to describe a stirring tank in the cylindrical geometry consist of cylinder walls at the sides and the bottom of the cylinder, an upper open air patch (top) as well as internal walls described by the shaft and stirrer. The usage of a dynamic meshing algorithm also requires the definition of an internal boundary surface between rotating and static mesh. The boundary surface between these regions is defined as Arbitrary Mesh Interface (AMI). The boundary regions are displayed in Figure 7.2.

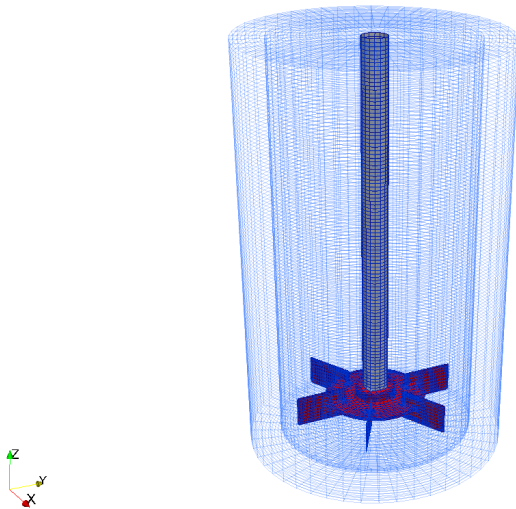


Figure 7.2: Computational grid used for the simulations including boundaries (red: stirrer, grey: shaft, blue (outer cylinder): cylinder walls, blue (inner cylinder): AMI, blue (upper plane): top).

At the walls, a no-slip condition is imposed. At the top, an atmospheric boundary condition is defined to allow fluids to enter and leave the domain. This is achieved by imposing a zero gradient (Neumann) condition to all variables except the pressure ( $p_{rgh}$ ) boundary condition, which is set to a fixed value of zero (Dirichlet) (atmospheric pressure). For the variables of the turbulence model, i.e.  $k$ ,  $\epsilon$  and  $\omega$ , an arbitrary low value is defined in the beginning of the simulations. During runtime, these values are corrected by the solver using calculated values.

## 7.4 Results and discussion

### 7.4.1 Graphic analysis

A visual analysis of the model results led to the conclusion that a plausible behaviour of the fluids in the stirring tank is reached. Figure 7.3 illustrates that the water surface forms different vortex shapes depending on the stirring velocity.

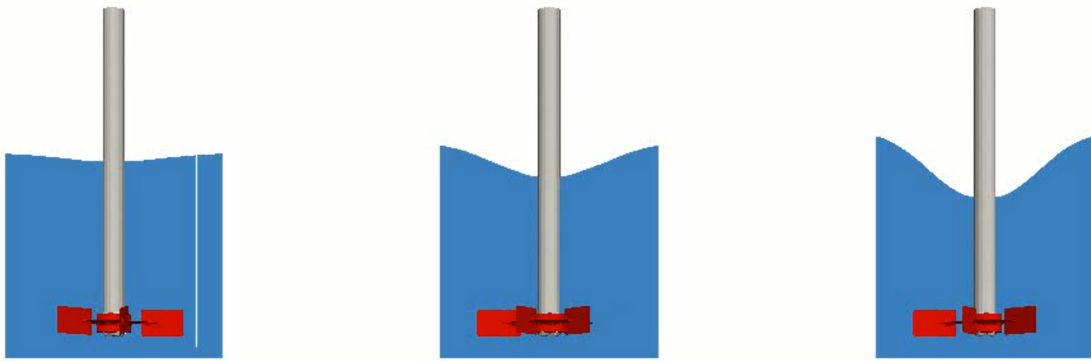


Figure 7.3: Vortex shapes for different stirring rates (left:  $N=0.8333$  1/s, middle:  $N=1.667$  1/s, right:  $N=2.333$  1/s).

### 7.4.2 Sensitivity analysis

A mesh and turbulence model sensitivity analysis has been conducted in order to determine the best combination to achieve accurate results.

Regarding the grid convergence, the simulations reached grid convergence at a grid size of 214,100 cells. The results of three different simulations performed on domains with 65,933, 214,100 and 374,127 cells were compared. The simulated  $U_x$ -velocities were compared in six different locations and the cumulated Root Mean Square Error (RMSE) has been calculated for each refinement step. The results yielded a  $RMSE=0.00306$  m/s between the coarse and medium sized mesh as well as an  $RMSE=0.00313$  m/s between medium and fine mesh, indicating a difference of 2.5% between the RMSE values of the different refinement steps. Adding further refinement to the mesh would lead to a decrease of the  $y^+$ -range out of the acceptable range between 30 and 300 for the application of wall functions, which is why the medium sized mesh has been chosen for further analysis. The final mesh is presented in Figure 7.2.

The different turbulence models significantly influence the calculated mass transfer coefficient. Figure 7.4 shows the influence of the choice of turbulence model on the resulting mass transfer coefficients. Both, RNG k- $\epsilon$  as well as the SST k- $\omega$  turbulence model show a significant increase of  $K_L$  as well as  $K_L a$ . A considerable difference can be found in the behaviour of the STD k- $\epsilon$  model. The slope of the  $K_L$  and  $K_L a$  curves show a decreasing trend for the observed stirring rates. The strong deviation can be explained by the differences in computed velocities and turbulent kinetic energy  $k$ , which influence the transport and transfer of H<sub>2</sub>S in the model.

In a second step, the importance of including the turbulent diffusivity into the mass transfer formulation has been analysed. Therefore, the simulation with a stirring rate of  $N = 2.33$  1/s and the RNG k- $\epsilon$  model has been performed with both, the *interDyMH2SFoam* solver as well as a variation that does not include  $D_{turb}$  into the solution. For the first case, the *interDyMH2SFoam* solver results in a mass transfer coefficient  $K_L = 0.0040$  m/s. Without consideration of  $D_{turb}$ , a resulting  $K_L = 0.0020$  m/s is achieved, which is close to the value computed for a stirring rate of  $N = 0.833$  m/s, which amounts to  $K_L = 0.0016$  m/s. When these two mass transfer coefficients are compared to the results and observations by Carrera et al. (2017) as well as Wu (1995), it becomes clear, that a significant increase of the mass transfer coefficient with increasing stirring rate is to be expected. All further discussion on the results and model validation is therefore exclusively conducted by including the turbulent diffusivity  $D_{turb}$  into the mass transfer approach and by using the results of the RNG k- $\epsilon$  model as well as the k- $\omega$  SST model. Both models show the most similar results in the computation of the mass transfer coefficient and coincide with the observations of Carrera et al. (2017) as well as Wu (1995) and will be compared in more detail in a later step. In both publications, at least a linear trend of increase has been observed with increasing stirring rates, depending on the inundation depth and test case, even an exponential trend was observed in some test cases.

Figure 7.5 shows the influence of inundation ratio  $h/R$  on the mass transfer coefficient as well as the volumetric mass transfer coefficient. It can be seen that the value of the mass transfer coefficient is not depending on the inundation ratio but the volumetric mass transfer coefficient is. This is reasonable due to its dependency on the area to volume ratio  $a$ , which changes due to the different volume, when a different water depth is being applied.

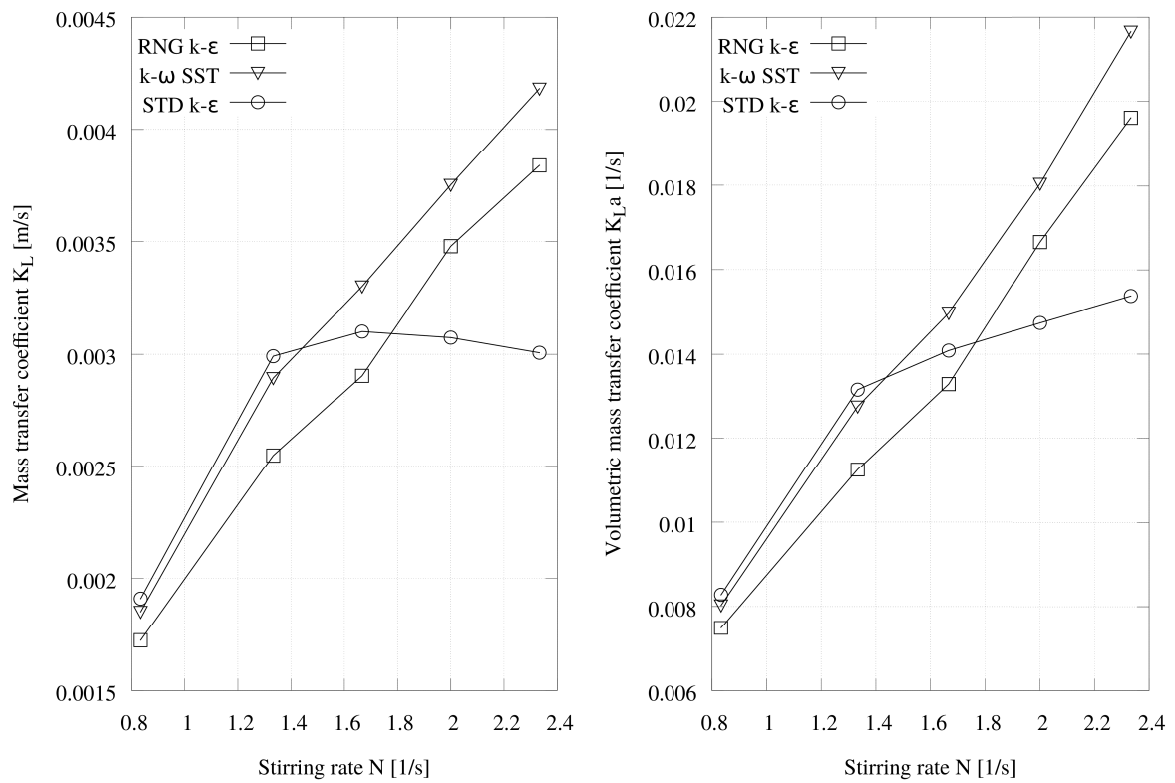


Figure 7.4: Influence of different turbulence models on the resulting mass transfer coefficient (inundation ratio of  $h/R = 0.7$ ).

The results furthermore agree with the observations by Wu (1995).

Overall, it has to be mentioned, that the sensitivity study is being complicated by the fact that no experimental values were available for the exact chosen setup. The choice of mesh and turbulence model are therefore made based on the experience of the authors and literature from comparable cases.

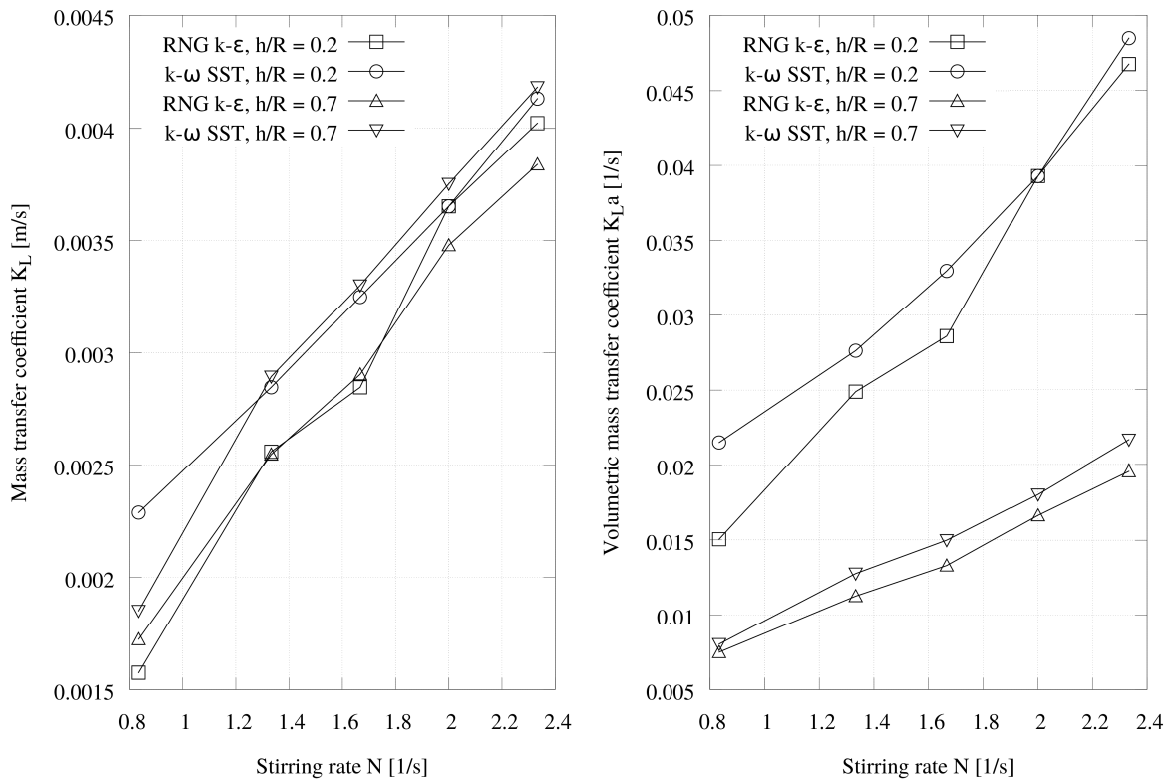


Figure 7.5: Influence of stirrer inundation on the mass transfer coefficient.

Table 7.2: Setup of stirring tank in CFD simulations and known metrics of experimental setup by Carrera et al. (2017) and Wu (1995).

	CFD simulations	Carrera et al. (2017)	Wu (1995)
Turbine	Rushton turbine (6 blades)	Rushton turbine	Rushton turbine (6 blades, 4 baffles)
Tank diameter T [m]	0.250	approximately 0.123 (estimated from Reynolds numbers, a and figures in publication)	0.202
Stirrer diameter B [m]	0.165	0.100 (calculated from Reynolds number)	0.101
Blade length L [m]	0.050	unknown	0.0253
Blade height W [m]	0.03	unknown	0.0202
Stirring rates N [1/s]	0.833, 1.333, 1.667, 2.000, 2.333	0.000, 0.833, 1.333, 1.667, 2.000, 2.333	0 - 900 (unknown intervals)
Area to volume ratio a [m <sup>-1</sup> ]	h/R = 0.2: 4.33 - 5.12 h/R = 0.7: 9.4 - 11.73	4.73 - 5.11	approximated h/R = 0.10: 50.00 h/R = 0.62: 7.07 (assuming no surface deformation due to stirring)
Reynolds number range [-]	22,687 - 63,525	8,333 - 23,333	0 - 153,015
Temperature [°C]	20	20	25

### 7.4.3 Quantitative analysis

The H<sub>2</sub>S emissions in the stirring tank have been analysed for six different stirring rates with two different inundation depths of the stirrer. The results were compared to experimental investigations by Carrera et al. (2017), who calculated the  $K_L a$  by using the degassing technique as outlined above, and to Wu (1995), who measured  $K_L a$  of O<sub>2</sub> with the steady-state sulphite feeding method in a stirring tank. The setups of the different domains are listed in Table 7.2. The resulting Reynolds numbers were computed by

$$Re = \frac{\rho_L N B^2}{\mu_L} \quad (7.23)$$

Where  $\rho_L$  is the density of the water phase [kg/m<sup>3</sup>],  $\mu_L$  is the dynamic viscosity of water [ $\frac{kg}{ms}$ ],  $B$  is the stirrer diameter [m] and  $N$  is the stirring rate [1/s].

Figure 7.6 and Figure 7.7 illustrate the published results (as extracted from the publications). Due to the different range of Reynolds numbers, the authors see difficulties in directly comparing the results to the observations by Carrera et al. (2017) and Wu (1995).

Therefore, the different results analysed are compared by plotting the Reynolds number in a range between 20,000 and 65,000 against the local mass transfer coefficient  $K_{L,local}$  in Figure 7.8. To do so, the range of the results of Carrera et al. (2017) have been divided by an estimated surface area derived from the given value for  $a$  and the figures shown in the publication. Furthermore, the range of the Reynolds numbers given in the publication has been used to derive the stirrer diameter which has been calculated to amount  $B=0.100$  m. The experimental results by Wu (1995) have been converted to  $K_{L,local}$  of H<sub>2</sub>S by applying the conversion factor  $\frac{K_{L,H_2S}}{K_{L,O_2}} = 0.64 + / - 0.24$  that has been observed by Carrera et al. (2017), resulting in the range of values displayed in Figure 7.8. Furthermore, the values have been divided by a constant surface area calculated using the given tank diameter.

The results displayed in Figure 7.8 allow only a limited comparison of the results because of multiple factors of uncertainty such as the unknown exact geometry analysed by Carrera et al. (2017) and the uncertainty when applying a conversion factor from O<sub>2</sub> to H<sub>2</sub>S

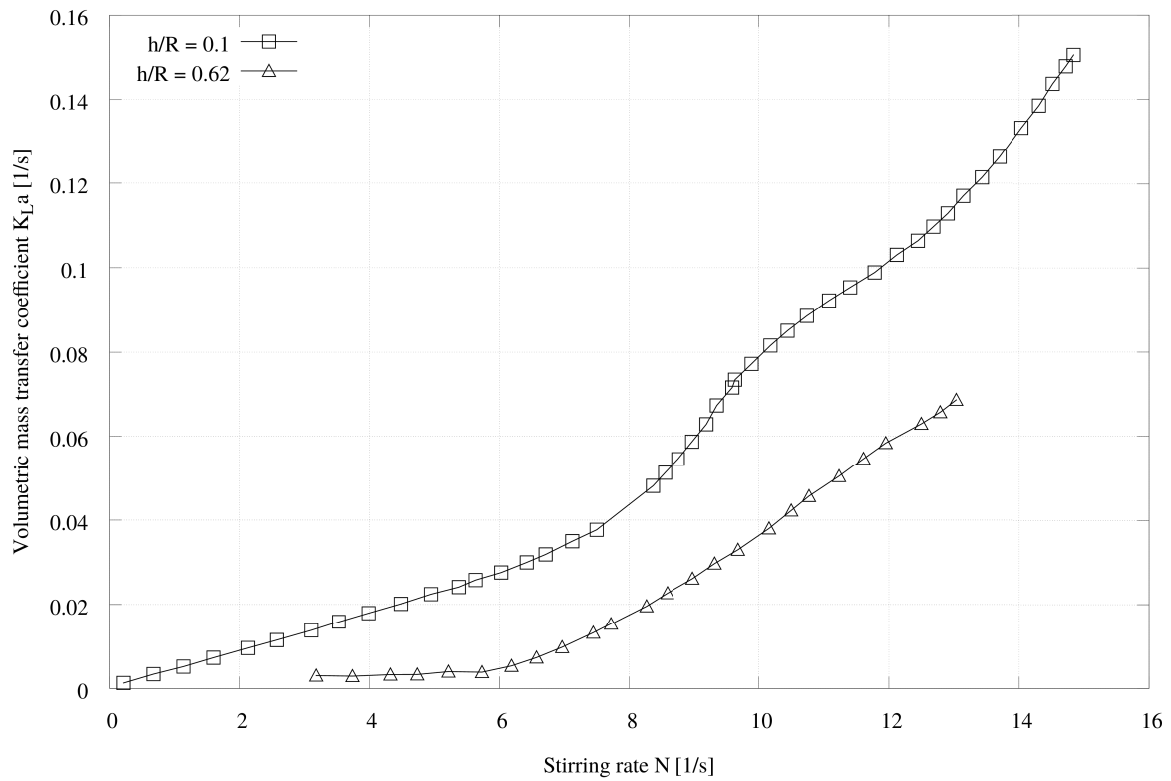


Figure 7.6: Influence of stirring rate and inundation ratio on mass transfer (Wu, 1995).

emissions for the results of Wu (1995) as well as the assumption of a constant water surface area for different stirring speeds.

From the results by Carrera et al. (2017), the two highest stirring rates result in Reynolds numbers in the area of interest ( $N=2$  1/s leading to  $Re=20,000$  and  $N=2.33$  1/s leading to  $Re=23,333$ ). In general, the  $k-\omega$  SST turbulence model computes slightly higher mass transfer rates than the RNG  $k-\epsilon$  turbulence model. But the simulated  $K_{L,local}$  values agree well with the results by Carrera et al. (2017) and Wu (1995).

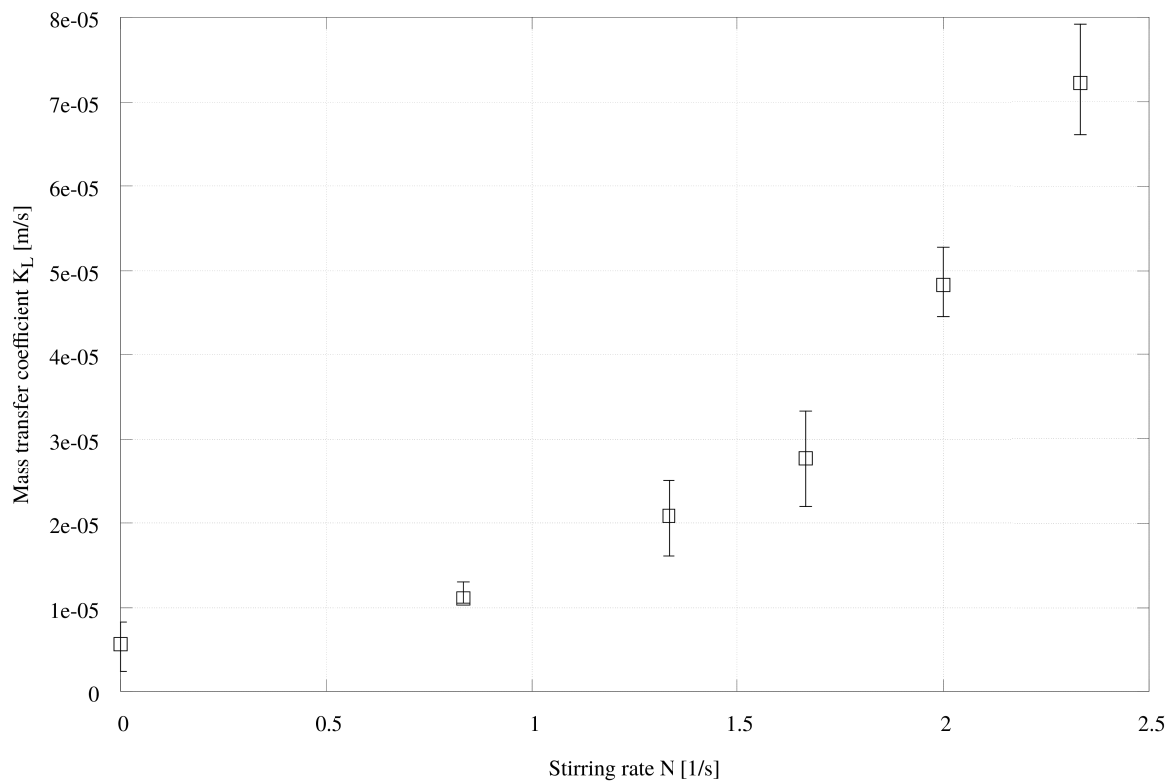


Figure 7.7: Influence of stirring rate on mass transfer (Carrera et al., 2017).

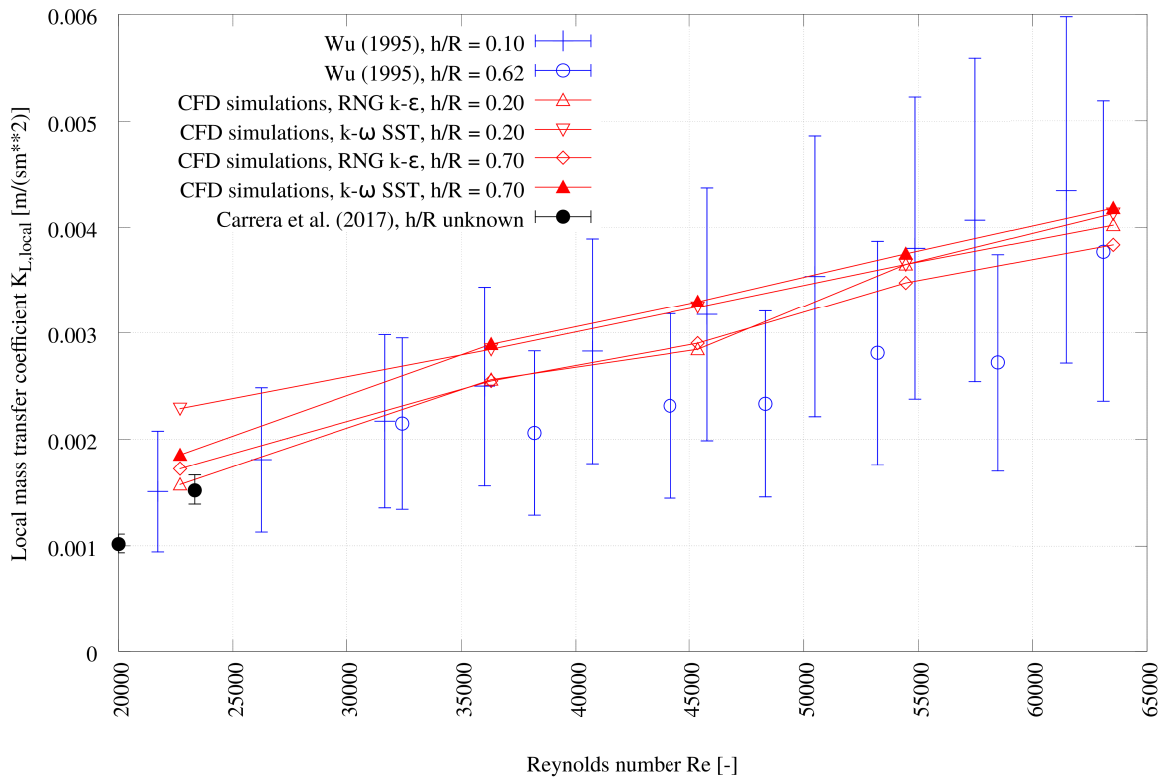


Figure 7.8: Comparison of relation between Reynolds number and volumetric mass transfer coefficient (Wu, 1995, Carrera et al., 2017).

## 7.5 Conclusions

The influence of turbulence on H<sub>2</sub>S mass transfer has been subject to intensive research in the past years. So far, a general understanding has been gained from experimental investigations but the influence has not been simulated using a numerical three-dimensional model.

In this publication, a CFD model has been developed to describe H<sub>2</sub>S mass transfer in a stirring tank using a dynamic meshing functionality in order to predict the mass transfer coefficient  $K_L$  as well as the volumetric mass transfer coefficient  $K_L a$  under turbulent conditions. After analysing the sensitivity of different parameters, namely, the choice of turbulence model, the turbulent diffusivity, the mesh size and the stirrer inundation, the resulting mass transfer coefficients in dependency of the Reynolds number were compared to experimental findings by Carrera et al. (2017) and (Wu, 1995). The  $k-\omega$  SST turbulence model generally calculated the highest mass transfer rates, whereas the RNG  $k-\epsilon$  model yielded comparable results. The STD  $k-\epsilon$  model was not able to account for the increase of mass transfer with increasing stirring rates. The mass transfer coefficient  $K_L$  was found to be independent of the stirrer inundation, while the volumetric mass transfer  $K_L a$  increased with decreasing stirrer inundation. Furthermore, the importance of including the turbulent diffusivity  $D_{turb}$  into the solver for this application has been shown.

A strong influence of the Reynolds number as well as the depth of stirrer inundation has been observed in alignment with existing publications. When the local mass transfer coefficient  $K_{L,local}$  of the simulated results is compared to the results from previous publications, a good agreement can be found.

For future work, the model is currently being further validated using experimental results from a stirring tank at TU Berlin and will be used afterwards to describe a turbulent H<sub>2</sub>S reactor. The simulation results will be used to gain a better understanding on the effect of the hydraulic design on the measured H<sub>2</sub>S concentrations.

Nevertheless, these results demonstrate that the new model for three-dimensional simulation of mass transfer in dynamic meshing environments is able to accurately describe the H<sub>2</sub>S mass transfer including its influencing parameters (stirrer inundation  $h/R$ , area to volume ratio  $a$ , Reynolds number  $Re$ ). This can help avoiding risky lab experiments for H<sub>2</sub>S emissions in the future and in a later step help to improve the design of H<sub>2</sub>S hotspots in sewer systems.

## Acknowledgements

The funding provided by the German Research Foundation (DFG) within the Research Training Group "Urban Water Interfaces" (GRK 2032-1) is gratefully acknowledged.

## Chapter 8

# Supplementary contributions

### 8.1 Advantages of three-dimensional flow simulations

This study was published as:

---

**Teuber, K.**, Broecker, T., Elsesser, W. & Hinkelmann, R.: Beyond shallow water flow: Navier-Stokes simulations with OpenFOAM, BIMoS Day: Shallow Water Flow Simulations, Berlin International Graduate School in Model and Simulation based Research, TU Berlin, Berlin, Germany, 2017.

---

This is the postprint version of the abstract submitted to the event.

#### Abstract

In the field of hydraulic engineering, shallow water flow models using the depth-averaged Navier-Stokes equations are often suitable to analyze flow phenomena. However, in certain application areas where a hydrostatic pressure distribution within the flow field is not given, these models reach their limits and alternatives have to be looked for. The model used to describe free surface flow is the interFoam solver as it is implemented in the open source software OpenFOAM. A collection of examples for these special applications using single and two-phase flow approaches will be presented in this talk. Beginning with a simple example of flow over a ground sill, the talk moves on to complex flow and transport simulations over ripples on a river bed. Apart from natural systems, the model can also be used to simulate flow in technical systems such as a sewer stretch containing different hydraulic structures such as weirs, flow transitions and quickly-varying shapes.

## 8.2 Possibilities extending the interH2SFoam solver to multicomponent reactive transport

This study was submitted as:

---

Dixit, A., Teuber, K., Barjenbruch, M., Stephan, D. & Hinkelmann, R.: Extension of a 3D two-phase flow model to multicomponent reactive transport for odour and corrosion control in sewer systems, Workshop on Applications of Multi-scale Approaches in Environmental Chemistry (AMARE), Rennes, France, 2019.

---

This is the preprint version of the abstract submitted to the conference.

### Abstract

Biological corrosion of sewers and sewage treatment plants constitutes a serious problem and its effects result in the loss of billions of dollars every year. Changing demography and more efficient use of water resources will lead to the reduction of the average volume of waste water and leads to higher residence times in the sewer canals. Due to climate change, i.e. warmer temperatures, the waste water in the canal will become more anaerobic. Therefore, sewer networks with a concrete construction are subjected to various mechanisms that subject it to rapid degradation. Due to the anaerobic conditions in sewage, sulfate present in the waste water can be reduced to sulfide by sulfate-reducing bacteria residing in the biofilms on the walls of the pipelines. For more than 70 years, researchers have been committed not only to study the processes for odour and corrosion but also creating empirical and conceptual models for explanations. However, within the last 20 years a deeper understanding has been gained thanks to the efforts of research groups in Denmark and Australia. Nearly all current models are confined to a one-dimensional approach which is very suitable but is unable to sufficiently capture the turbulent effects. However, for processes which are affected by the concentration profiles (e.g. H<sub>2</sub>S formation, mass transfer) and the air flow as well as for the surroundings of drops, steps and hydraulic jumps, a three-dimensional approach should be preferred accounting for water and gas phase. For this purpose, a high-resolution three-dimensional model in OpenFOAM for water and air flow, multi-component reactive transport and mass transfer between the water and air phase must be developed. Teuber et al. (2019b) have developed a 3D two-phase (water, air) flow and transport model that can account for temperature and pH dependency of the mass transfer of H<sub>2</sub>S. This poster concentrates on the conceptual and computational extension of the model of Teuber et al. (2019b) for reactive transport using and probably extending OpenFOAM libraries and the model validation.

### 8.3 Research on further multiphase CFD applications carried out at the Chair of Water Resources Management and Modeling of Hydrosystems, TU Berlin

This study was published as:

---

Broecker, T., Teuber, K., Elsesser, W. & Hinkelmann, R.: Multiphase Modeling of Hydrosystems Using OpenFOAM, in: Gourbesville P., Cunge J., Caignaert G. (eds) *Advances in Hydroinformatics*, Springer Water, 1013-1029, Springer, Singapore, 2018.

---

This is the abstract of the book chapter (postprint).

#### Abstract

This paper presents three computational fluid dynamics applications regarding multiphase modeling of hydro systems with the open source software OpenFOAM. The first model investigates flow processes of groundwater and surface water using an integral approach which solves the three-dimensional Navier–Stokes equations, extended by the consideration of porosities. For the validation, seepages through homogeneous dams with impervious foundations were compared with analytical and numerical solutions. A further application examines the water–air interface in sewer systems. The focus of the model lies on the description of in-sewer water–air flow and transformation processes, reaeration and hydrogen sulfide emission which highly depend on the three-dimensionality of the hydraulic behavior in the closed duct. A test case analyzing the hydraulic behavior in a sewer stretch showed a good agreement of the numerical results with measured water levels. In the third model, fluid–structure interaction is investigated applying FOAM Extend Project. Calculations of the fluid phase are linked with the solid phase via a coupling algorithm to achieve an equilibrium state. To describe the time-varying position of the fluid boundary, caused by the structural response, dynamic meshes are considered. A technical case, consisting of the air flow around a thin tower as well as a natural case, describing the water flow around aquatic vegetation and its response, were examined.

## 8.4 Application of free-surface flow and transport simulations to natural river beds

This study was published as:

---

Broecker, T., Elsesser, W., **Teuber, K.**, Özgen, I., Nützmann, G. & Hinkelmann, R.: High-resolution simulation of free-surface flow and tracer transport over streambeds with ripples, *Limnologica*, 68: 46-58, 2018.

---

This is the abstract of the article (postprint).

### **Abstract**

This study presents a novel high-resolution simulation of free-surface flow and tracer retention over a streambed with ripples based on varying ripple morphologies, surface hydraulics and the transport of a tracer pulse from surface water to surface dead zone. For the simulations, the computational fluid dynamics (CFD) model OpenFOAM was used to solve the three-dimensional Navier-Stokes equations in combination with an implemented transport equation. Pressure gradients at the streambed were used to account for hyporheic exchange, assuming water flow from high pressure zones to low pressure zones. Flow velocities, ripple sizes and spacing showed to significantly affect these pressure gradients, but also the transport of a passive tracer at the streambed, which was not investigated so far. Due to the velocity field, large parts of the tracer mass were transported alongside the main stream above the ripples. Tracer mass reaching the space between the ripples was temporarily retained due to low velocities and recirculations. It was shown that the retention is depending on the ripple size and space between the ripples as well as on the flow velocity. Decreasing ripple sizes and higher flow velocities lead to a smaller tracer retention. Furthermore we showed that the ripple length to height ratio controls the generation of recirculation zones which affect the residence time of the tracer significantly. Ripple spacing leads to temporarily higher tracer concentration at the streambed, but smaller tracer retention. We conclude that the impact of the streambed morphology on the hydraulics in combination with tracer retention should be addressed for a comprehensive understanding of compound movement, exchange and transformation within the hyporheic zone.

# Chapter 9

## Synthesis

This Chapter synthesizes the specific outcomes of Chapters 1 to 8.

### 9.1 Conclusions

Sewer networks are complex systems containing locations of highly complex turbulent multiphase flows and complex biochemical processes, for example the emission of  $H_2S$ . Existing model approaches tend to describe these processes in one-dimensional models, leading to simplified estimations of the overall emissions, which are valid for long sewer networks. They are not suitable for predicting the small-scale effects of certain geometrical features in the domain, especially in highly turbulent locations. A three-dimensional two-phase model can be used to investigate the local effects of the sewer geometry on a smaller scale. Including mass transfer into the model enables a detailed analysis of locations with high emissions.

The main outcome of this work are two OpenFOAM solvers that have been developed by extending existing solvers, namely the  $H_2S$  mass transfer solver for (waste)water-air simulations with static meshes (*interH2SFoam*) (Chapter 5), and the *interDyMH2SFoam* solver for dynamic meshes (Chapter 6). The two-phase simulation approach is based on the VOF method and mass transfer is described based on the work of Haroun et al. (2010a). After performing a thorough analysis and validation on the applicability of the hydrodynamic behaviour of the VOF method in closed conduits (Chapters 3 and 4), the first solver has been studied in several test cases based on the equilibrium conditions of concentrations in the two phases, ranging from benchmark tests with analytical solutions to a real world application of a complex sewer geometry. The second solver has been used to validate turbulent mass transfer in a laboratory scale experiment.

The simulation results are promising, the equilibrium conditions as well as the mass transfer rates could be reproduced by the solvers.

A short overview of supplementary work related to the research topic was given in Chapter 8.

#### 9.1.1 General outcomes

Before more specific conclusions of the different parts, hydrodynamics, transport and mass transfer are drawn, some general conclusions can be drawn:

- It is possible to describe water-air mass transfer in sewer systems or - more general, in closed conduits - by using a three-dimensional CFD model.
- The three-dimensional two-phase model is based on the VOF method and accounts for general mass transfer with an approach by Haroun et al. (2010a).
- Using a two-phase CFD model requires detailed knowledge about the geometry and flow conditions at the model boundaries in order to obtain stable simulations. It furthermore needs a high-quality and high-resolution three-dimensional computational mesh requiring more preprocessing than a one-dimensional model approach. Furthermore, the mesh quality significantly influences the quality of the results and grid convergence needs to be assessed. The choice of turbulence model is crucial for the model results and needs to be carefully evaluated for each test case.
- The three-dimensional simulations lead to a considerably higher computation time than one-dimensional approaches due to their high complexity, making the use of high performance computers necessary. The simulations offer the benefit of detailed insight into the local flow and mass transfer processes.
- Overall, the solvers yield accurate results for the flow properties, mass transfer rates and equilibrium conditions.
- Within the DFG Research Training Group UWI, different interfaces in sewer systems have been identified when analysing H<sub>2</sub>S emissions. These interfaces are namely the biofilm-(waste)water interface, the (waste)water-air interface as well as the air-(biofilm)-(concrete) wall interface. Three different projects focusing on different interfaces were established. Although the three projects focus on different interfaces, they can profit from each other's work in various ways. Within the work of this thesis, a major step towards the collaboration between the different projects has been made by solver customizations that can lead to a direct exchange of results between experiments and simulations. In Chapter 6, the solver `interH2SFoam` was customized to the direct demands of the experimental site. Therefore, the pH value and the total dissolved sulphide have been defined as input parameters for the model and the H<sub>2</sub>S concentration in the air phase has been calculated as partial pressure in the unit ppm to enable direct comparison with measurements. Furthermore, the single-phase transport of a tracer in the sewer pilot plant, as analysed in Chapter 5, led to valuable insights of concentration distributions between the concrete probes placed in the pilot plant. These insights can help interpret future results when corroded concrete probes are analysed and help design experiments.

### 9.1.2 Outcomes of hydrodynamic modelling

In Chapters 3 and 4, hydrodynamic three-dimensional two-phase simulations in closed conduits are performed using the VOF method as it is implemented in OpenFOAM's solver `interFoam`. The results are compared to experiments, analytical solutions and existing CFD models in order to assess the applicability of the solver for closed conduits and complex geometries as they can be found in sewer systems. The following conclusions are drawn for the hydrodynamic behaviour of the two-phase CFD simulations in closed conduits:

- Three different test cases were analysed. First, a two-dimensional single-phase flow of water has been analysed. The domain consisted of a two-dimensional channel bounded by an upper and a lower wall with a hill structure on its bottom. Results of

simulations with different RANS turbulence models were compared to experiments by Almeida et al. (1993). Overall, the Standard  $k-\epsilon$  turbulence model yielded best agreement and was chosen for the remaining simulations.

- For the free-surface flow over a ground sill, a comparison to analytical solutions using the continuity and Bernoulli equation led to a good agreement.
- The example of free-surface flow over a ground sill has been deeper analysed by varying the geometric shape of the sill and the flow conditions. Overall the simulations led to plausible results.
- A complex sewer geometry as it has been described by Bayón et al. (2015) has been simulated and compared to experiments from a 1:20 scale model as well as to results from an existing CFD model. The difference of this model to the existing CFD model is that the model yielded stable results although it has been simulated as a closed duct. The previous CFD model had to be simulated with an open atmospheric boundary because of stability problems.
- For the complex sewer geometry, the problem of instabilities for the setup of a closed duct had to be overcome. Therefore, the water level at the outlet boundary has not been defined by a boundary condition but by adding a weir structure in the close proximity of the outlet. Finding a way to describe complex flows in closed conduits has been a crucial part for this thesis due to the overall aim of investigating  $H_2S$  emissions in sewers. Being capable of describing such closed systems enables the future analysis of  $H_2S$  spreading in a sewer or in connecting points.

### 9.1.3 Outcomes of single-phase transport modelling

In Chapter 5, the outcomes of single-phase transport simulations are presented. Three different test cases are analysed. In a first test case, the limitations of adding a standard advection-diffusion equation to simulate single-phase transport phenomena in a two-phase system are shown. Then, two different ways of overcoming this problem are presented. The first solution is to describe the domain as a single-phase system and describing the interface as a boundary condition. The second approach uses the mass transfer approach developed by Haroun et al. (2010a) with a very low Henry coefficient. This approach enables a simulation of phase-constrained transport in a two-phase system. For the single-phase transport, the following conclusions are drawn:

- In a first step, a rectangular pipe with a length of 15m, a height of 1m and a width of 1m has been simulated as a free-surface flow with the `interFoam` solver and an additional standard advection-diffusion transport equation. The aim was to simulate tracer spreading in the water phase of the pipe. The simulation results showed a spreading of the tracer into the air phase when the tracer is placed in closed proximity to the water surface. This spreading can be considered unphysical when thinking of a dye tracer. Numerically it can be explained by the governing equations of the VOF method: Only one set of Navier-Stokes equations is solved and the phases are only accounted for by an additional transport equation. The solver is therefore not able to account for the change of phases accurately when an advection-diffusion transport equation is applied.
- As an alternative solution, the `interHarounFoam` solver which accounts for mass transfer by using a single-phase formulation and which depends on the Henry coefficient

has been applied to the same setup of a rectangular pipe. The Henry coefficient was specified with a very low value ( $10^{-6}$ ) and the tracer remained in the water phase.

- This solution has been furthermore applied to the complex sewer geometry. This setup has been chosen due to the high levels of turbulence present in the domain. The results were able to prove that the tracer travelled through locations of high turbulence without spreading into the air phase. Therefore, the conclusion can be drawn that applying the interHarounFoam solver to two-phase simulations with single-phase transport phenomena is one solution to retain the tracer in one phase.
- As an alternative solution, a single-phase simulation approach has been presented. This approach can be of interest when the behaviour of only one phase is of special interest. As an example, tracer spreading in the air phase of the pilot plant has been simulated by only considering the air phase. The water surface behaviour has been assumed to be stratified and the resulting air phase velocities at the interface and in the headspace were assumed to be following observations from existing publications. The velocities at the interface were described by applying a slip-condition.
- The results showed a tracer accumulation behind the concrete probes. This observation can be used for interpreting the results of concrete corrosion.
- The simulations furthermore showed that the single-phase approach is a way to describe transport in one phase in a computationally efficient way because in this case only one half of the pipe needs to be discretized. It comes with the limitation of being only applicable for uniform water levels.

#### 9.1.4 Outcomes of mass transfer modelling

In Chapters 6 and 7, the capabilities of the mass transfer solver introduced by Haroun et al. (2010a) are explored and novel extensions are presented. This is done by performing mass transfer simulations for equilibrium conditions and comparing the results to analytical solutions. The advantages of a three-dimensional formulation are shown by applying the solver to the complex sewer geometry. The functionalities of the extended solver are then applied to a dynamic meshing solver which is used to investigate the solver's capabilities of describing turbulent mass transfer. This is done by simulating  $H_2S$  mass transfer in a stirring tank and comparing the mass transfer rates to results of two laboratory scale experiments. The detailed conclusions are listed in the following:

##### Extension of interHarounFoam solver

- In a first step, several extensions to the interHarounFoam solver were developed in order to create a solver that is better suited to describe the specifics of  $H_2S$  mass transfer across the (waste)water-air interface.
- The temperature dependency of the Henry coefficient has been included by implementing the van't Hoff equation. The Henry coefficient then depends on a temperature for the whole computational domain which has to be defined by the user as a part of the preprocessing.

- The equilibrium between  $\text{H}_2\text{S}$  and  $\text{HS}^-$  in the wastewater has been implemented following Hvitved-Jacobsen et al. (2013). The model takes the values of the total dissolved sulphide and the pH and computed the resulting  $\text{H}_2\text{S}$  concentration in the water phase. This function is and has been integrated by using the OpenFOAM utility `swak4Foam`, the user can therefore decide whether the  $\text{H}_2\text{S}$  concentration should be computed or manually defined.
- Furthermore, the partial pressure of  $\text{H}_2\text{S}$  in the air phase is being computed by another extension. Because  $\text{H}_2\text{S}$  concentrations in the air phase are measured as a partial pressure and are then interpreted as odour intensity, this functionality offers the user the possibility of directly comparing simulation results to measured values. This extension therefore results in the description of odour in the air phase of a sewer.
- In a final step, the functionalities of the `interH2SFoam` solver have been connected to a dynamic mesh solver (`interDyMFoam`) in OpenFOAM in order to describe moving geometries resulting in a new solver `interH2SDyMFoam`, which has been used for the validation of turbulent mass transfer simulations.

### Validation and application of the `interH2SFoam` solver

- The solver was tested under equilibrium conditions in a tank partially filled with water. As transported pollutant,  $\text{H}_2\text{S}$  was chosen and the respective Henry coefficient as well as diffusivities were applied. The development of equilibrium conditions after a certain amount of time has been observed and the ratio between water phase and air phase concentration could be related to the Henry coefficient applied. The extensions regarding temperature dependency, equilibrium conditions and calculation of the partial pressure in the air phase were compared to analytical solutions by Hvitved-Jacobsen et al. (2013).
- The solver was then applied to a rectangular pipe with a length of 15 m and two different flow velocities. The resulting air flow velocities were compared to experimental results by Bentzen et al. (2016). The mass transfer simulations showed a minor importance of the mass transfer simulations in this case due to the strong advective transport in the domain.
- Therefore, the solver has been applied to the complex sewer geometry, which contains high levels of turbulence and three-dimensional flow velocities. Especially in the point of highest turbulence, the hydraulic jump, a higher mass transfer could be observed by analysing contour plots of the tracer distribution within the domain.
- The analysis in the rectangular pipe and the complex sewer geometry were able to show, that especially in complex geometries the application of the three-dimensional model approach can lead to valuable insights and could be used for the analysis of  $\text{H}_2\text{S}$  hotspots or for design optimizations.

### Validation under turbulent conditions

- The `interH2SDyMFoam` solver has been used to analyse turbulent mass transfer in a stirring tank and the results have been compared to the findings by Wu (1995) and Carrera et al. (2017).

- A circular tank with a Rushton turbine placed above the tank bottom has been simulated with different stirring rates and stirrer inundations, where the stirrer inundation is described by the ratio between water level above the Rushton turbine and stirrer diameter.
- A sensitivity analysis has been performed regarding the choice of turbulence model, the turbulent diffusivity and the stirrer inundation. The mass transfer coefficient  $K_L$  as well as the volumetric mass transfer coefficient  $K_{L,a}$  were compared. A sensitivity analysis of the turbulence models STD  $k-\epsilon$ , RNG  $k-\epsilon$  and  $k-\omega$  SST showed a good performance of the RNG  $k-\epsilon$  and  $k-\omega$  SST turbulence models. The stirrer inundation influenced the volumetric mass transfer coefficient  $K_{L,a}$ , whereby for smaller inundations a higher  $K_{L,a}$  has been observed. The results of the mass transfer coefficient  $K_L$  were independent of the stirrer inundation. This observation of the behaviour of  $K_L$  agreed with the observations by Wu (1995) and is reasonable when the fact is considered that by decreasing the stirrer inundation the water volume and therefore the interfacial area to volume ratio is increased.
- The simulated mass transfer rates were furthermore directly compared to the results by Wu (1995) and Carrera et al. (2017). A comparison on the basis of the Reynolds numbers showed a good agreement when the local mass transfer coefficient  $K_{L,local}$  is compared.  $K_{L,local}$  is independent of the interfacial area and the water volume in the domain. The Reynolds number in a stirring tank further accounts for the diameter of the stirrer of the turbine. These factors appear to be the most influencing factors for mass transfer in a stirring tank and therefore led to a good comparability of the different setups analysed.
- Overall, the work enabled a direct comparison between experimental and simulated results of turbulent mass transfer in a stirring tank. The simulated results agreed well with the experimental results and can therefore be considered as plausible, enabling a usage of the solver for more complex application cases.

### 9.1.5 Final notes

In general, two new CFD solvers for  $H_2S$  mass transfer in (waste)water-air systems have been developed and validated under turbulent conditions. The solvers are capable to describe transport and mass transfer of  $H_2S$  in sewers. By modifying the Henry coefficient and removing the functionalities for equilibrium conditions between  $H_2S$  and  $HS^-$  as well as the calculation of the partial pressure, it could be furthermore applied to different species such as oxygen or methane.

Additionally, the interFoam solver has been analysed regarding its ability to describe the hydrodynamics of water-air flow in closed conduits and the possibility to describe single-phase transport.

## 9.2 Outlook

A number of open issues are identified and could be addressed in future research in order to enhance the model's applicability to real-life conditions:

- Further validation is needed in order to test the approaches under field conditions: First, they can be validated using the setup of a stirring tank as presented in Chapter 7, which is currently being prepared at TU Berlin. The advantage is that in this case

the exact specifics of the geometry are known. Furthermore, a more advanced experimental setup using an H<sub>2</sub>S mass transfer reactor will be set up. The reactor uses real wastewater taking one step further into the direction of a model that can be applied under real life conditions. Furthermore, data from the BWB pilot plant will be used to validate the model.

- Regarding the temperature dependency, the model can be further extended to account for the temperature dependency of fluid properties such as the density, viscosity and H<sub>2</sub>S diffusivity which currently have to be defined by the user.
- When thinking about a network-wide application of the model in terms of a decision-support tool, the topics upscaling and parametrization should be addressed: Three-dimensional simulations lead to very high computation times compared to one-dimensional simulations. Looking at sewer systems that consist of networks of multiple kilometers of pipes and corrosion processes that take months to years, the simulations are not feasible. Extracting important parameters from the CFD model and feeding them into a one-dimensional approach, could improve the existing approaches. In the WATS model, this is partially already done by accounting for drop structures in the sewer network. It could be done for other points of high turbulence as well as, for example, hydraulic jumps in connection points between manholes and pipes.
- In order to include additional interfaces of the sewer, the biofilm can be integrated into the model: This can be done in a simple way by setting a boundary condition which is already possible with the current version of the model. A more complex consideration would demand the model to account for reactive transport in order to include the complex processes at the biofilm-(waste)water interface.
- Reactive transport modelling can furthermore help including the effect of countermeasures: The interHarounFoam solver implemented by Nieves-Remacha et al. (2015) offers the possibility of adding reactive transport by including the production term into the mass transport equation. This possibility should be first explored. If the approach is too simplified, OpenFOAM offers a solution for more complex reactions in the chemFoam solver. However, this solver is only designed for single cell, i.e. zero-dimensional, cases and a way to apply it to multi cell problems with multiple phases would be subject to future research.

The future work regarding further extension of the model is illustrated in Figure 9.1.

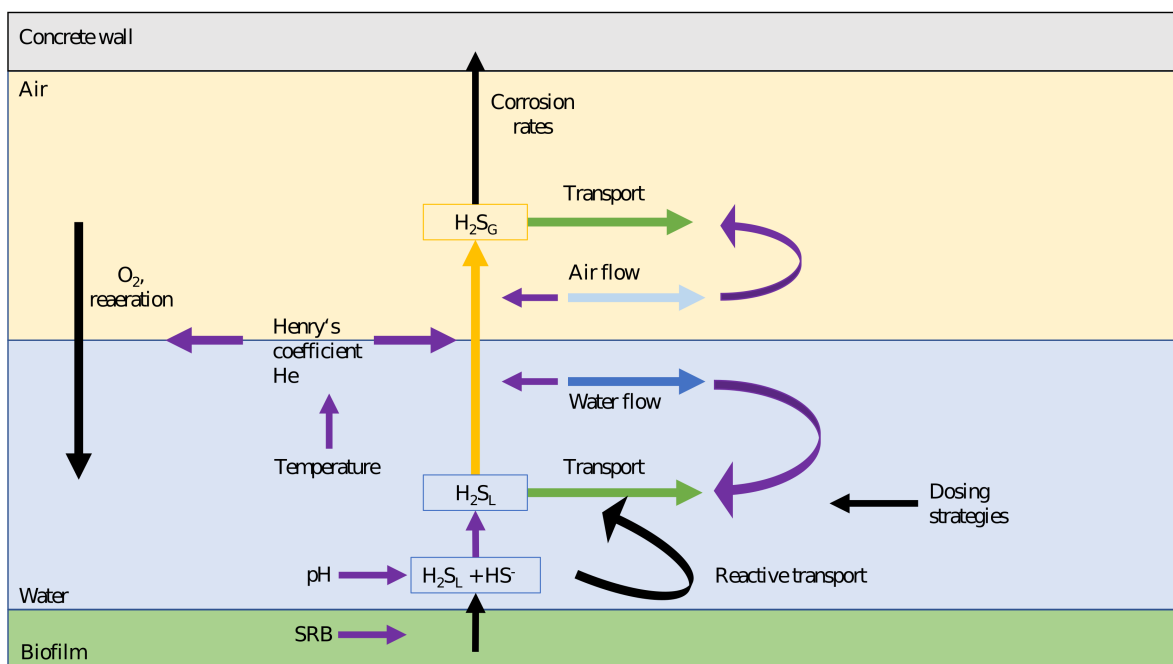


Figure 9.1: Sewer processes (following Hvitved-Jacobsen et al. (2013))

## **Appendix A**

# **Flow charts of solver extensions**

## A.1 Integration into the solution procedure

### A.1.1 interH2SFoam solver

Figure A.1 illustrates the solution procedure carried out within the interFoam solver.

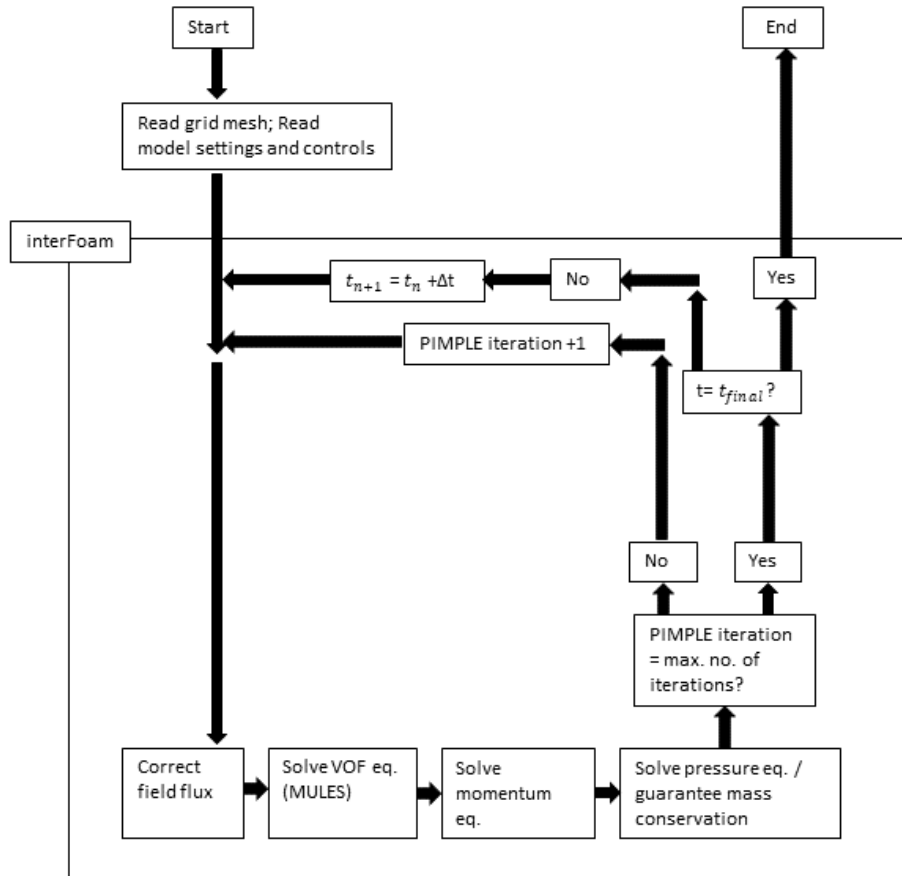


Figure A.1: Flow chart of interFoam solver (following Devolder et al. (2015), Lopes et al. (2017))

In Figure A.2, the solution procedure of the interH2SFoam solver is shown. The extensions made to the interFoam solver (see Figure A.1) are highlighted in green.

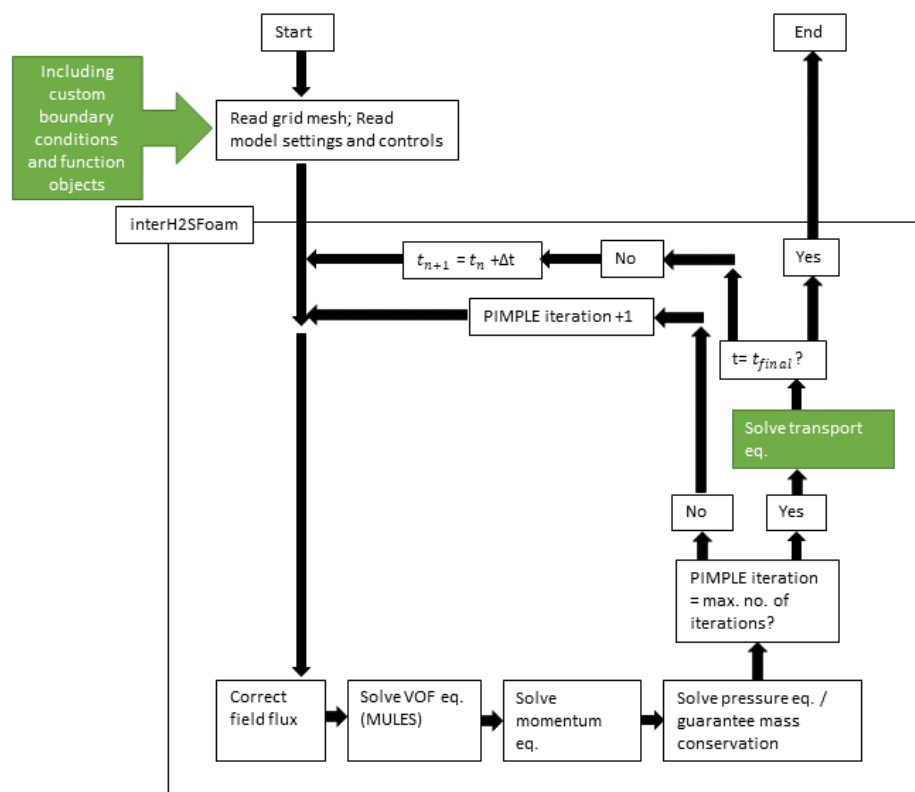


Figure A.2: Flow chart of interH2SFoam solver (following Devolder et al. (2015), Lopes et al. (2017)), solver extensions compared to interFoam solver in green

### A.1.2 interDyMH2SFoam solver

Figure A.3 illustrates the solution procedure carried out within the interDyMFoam solver, which is based on the interFoam (see Figure A.1) solver but includes a solution step for mesh motion.

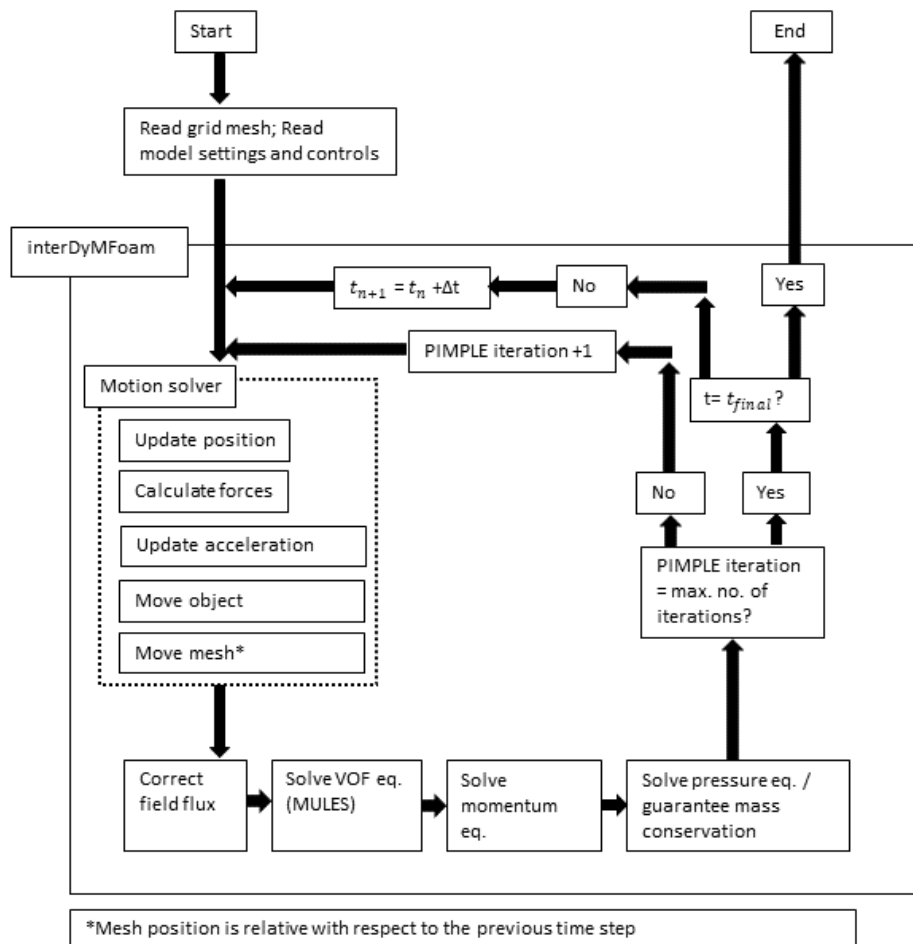


Figure A.3: Flow chart of interDyMFoam solver (following Devolder et al. (2015), Lopes et al. (2017))

In Figure A.4, the solution procedure of the interDyMH2SFoam solver is shown. The extensions made to the interDyMFoam solver (see Figure A.3) are highlighted in green.

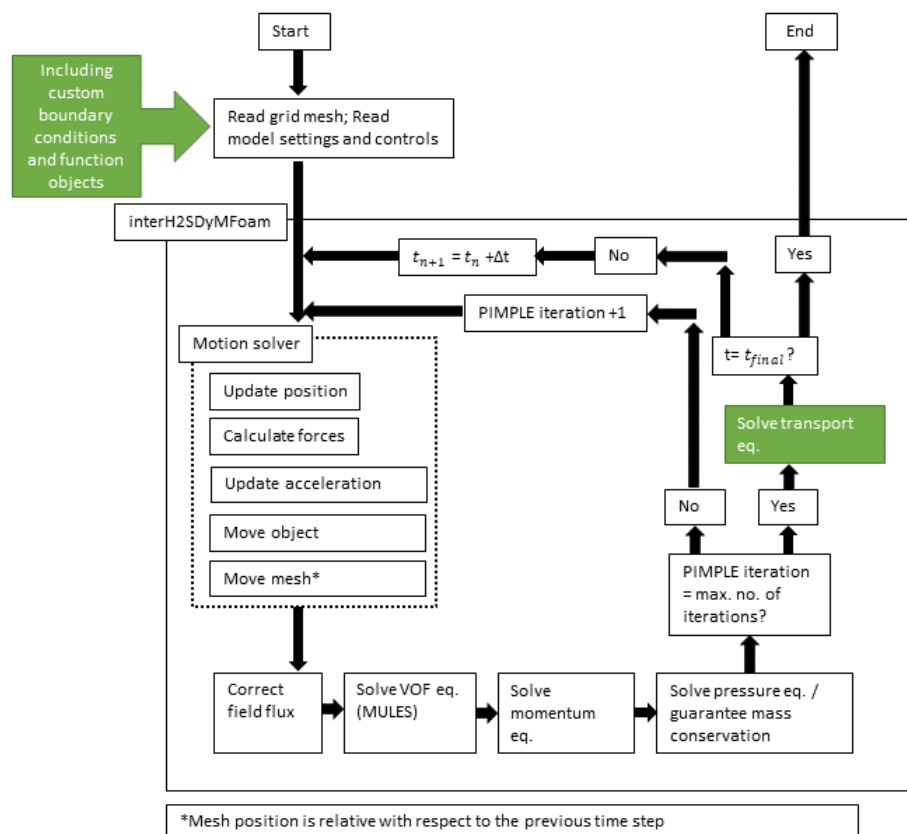


Figure A.4: Flow chart of interDyMH2SFoam solver (following Devolder et al. (2015), Lopes et al. (2017)), solver extensions compared to interFoam solver in green

## A.2 Code extensions and integration into the object-oriented framework

### A.2.1 File structure

In OpenFOAM, solver modifications should be stored in a specific user directory. In contrast to the official OpenFOAM solvers of the current release, which are stored in the directory `$WM_PROJECT_DIR` (full path of the directory illustrated in Figure A.5), custom solvers can be called via `$WM_PROJECT_USER_DIR` (full path of the directory illustrated in Figure A.6) (Nilsson, 2019).

In order to create the `interH2SFoam` solver, the folder containing the `interFoam` solver should be copied into a subdirectory of `$WM_PROJECT_USER_DIR` with the same file structure as the original `interFoam` solver (`/applications/solvers/multiphase`).

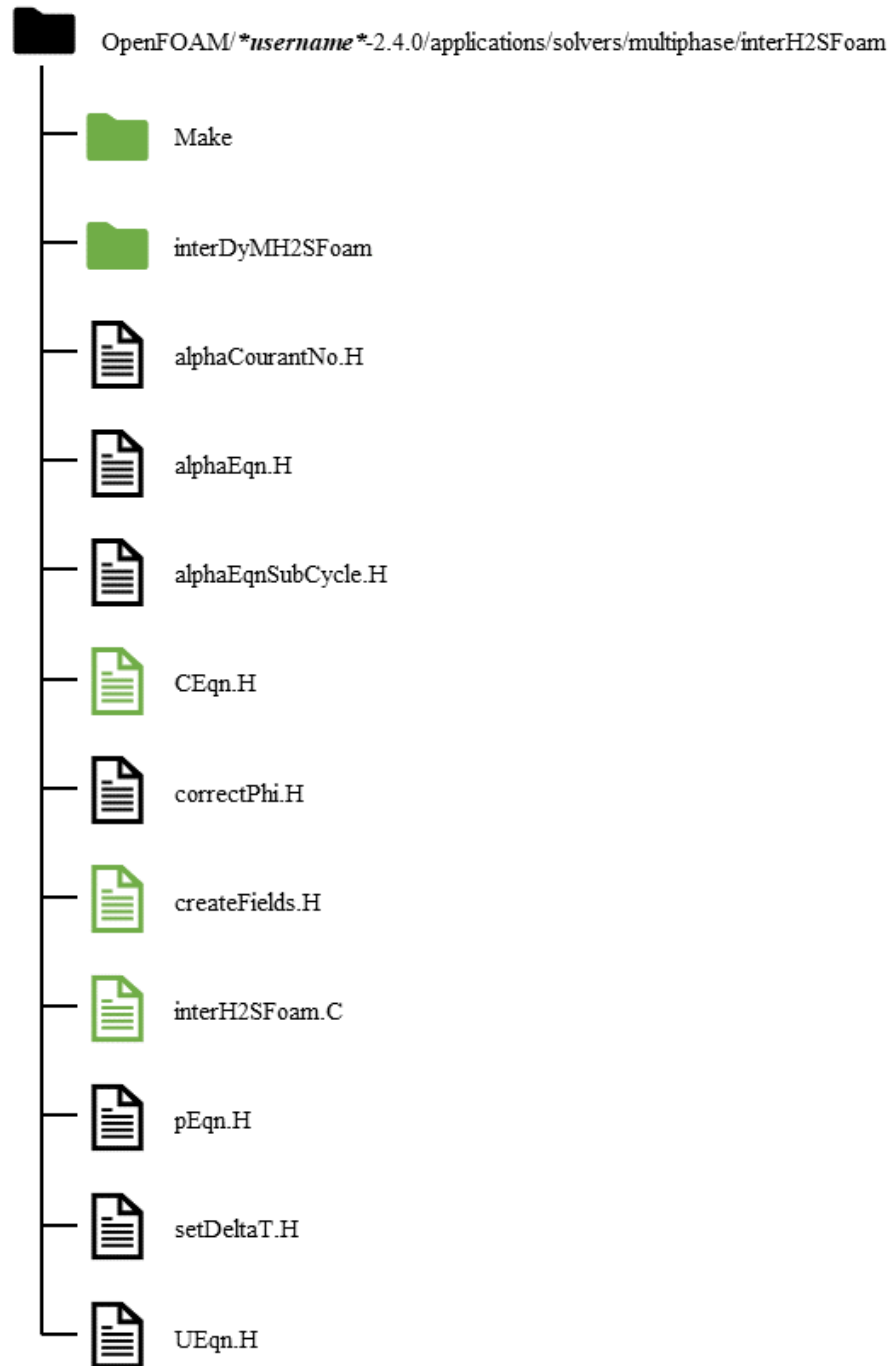
Then, modifications are to be made to files `createFields.H` and `interFoam.C`. The file `CEqn.H` will be newly created. In subfolders `Make` and `interDyMFoam`, further modifications will be made. The other subfolders of the original `interFoam` solver refer to other derived solvers and can be deleted. This refers to the folders `interMixingFoam`, `LTSInterFoam` and `porousInterFoam`. The remaining files are listed in Figure A.6. The files that need to be modified in a next step are highlighted in green. The file structure of the `interDyMH2SFoam` solver is illustrated in Figure A.7. As shown in Figures A.6 and A.7, the `interDyMH2SFoam` solver is placed as a subdirectory within the `interH2SFoam` solver directory.

In this thesis, transport simulations with an advection-diffusion transport equation were simulated using a modified `interFoam` solver called `passiveScalarInterFoam`. The file structure is comparable to the `interH2SFoam` solver and is illustrated in Figure A.8.

In the solver directory, the file `interFoam.C` is then renamed to `interH2SFoam.C` or `passiveScalarInterFoam.C`. The same applies for the `interDyMFoam` solver: The file `interDyMFoam.C` is renamed to `interDyMH2SFoam.C`. The modifications within the files will be outlined in the following Sections.



Figure A.5: File structure of interFoam solver

Figure A.6: File structure of `interH2SFoam` solver

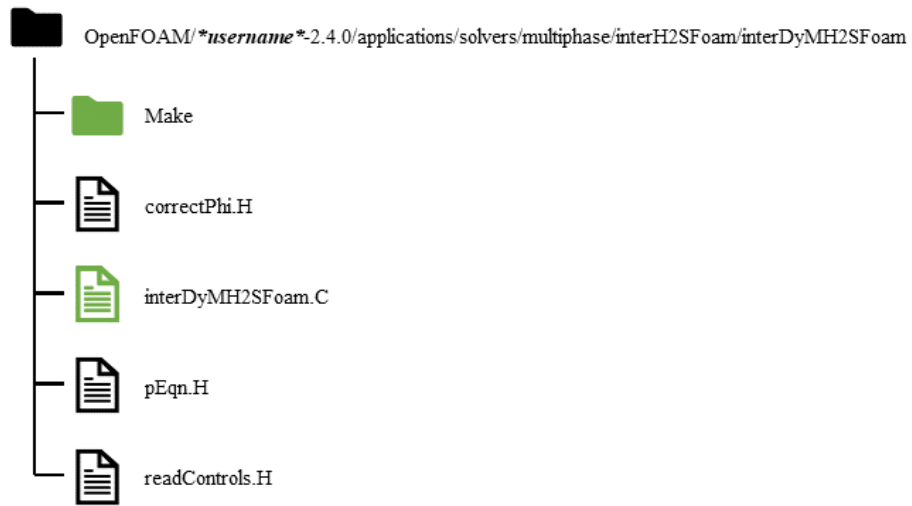


Figure A.7: File structure of interDyMH2SFoam solver

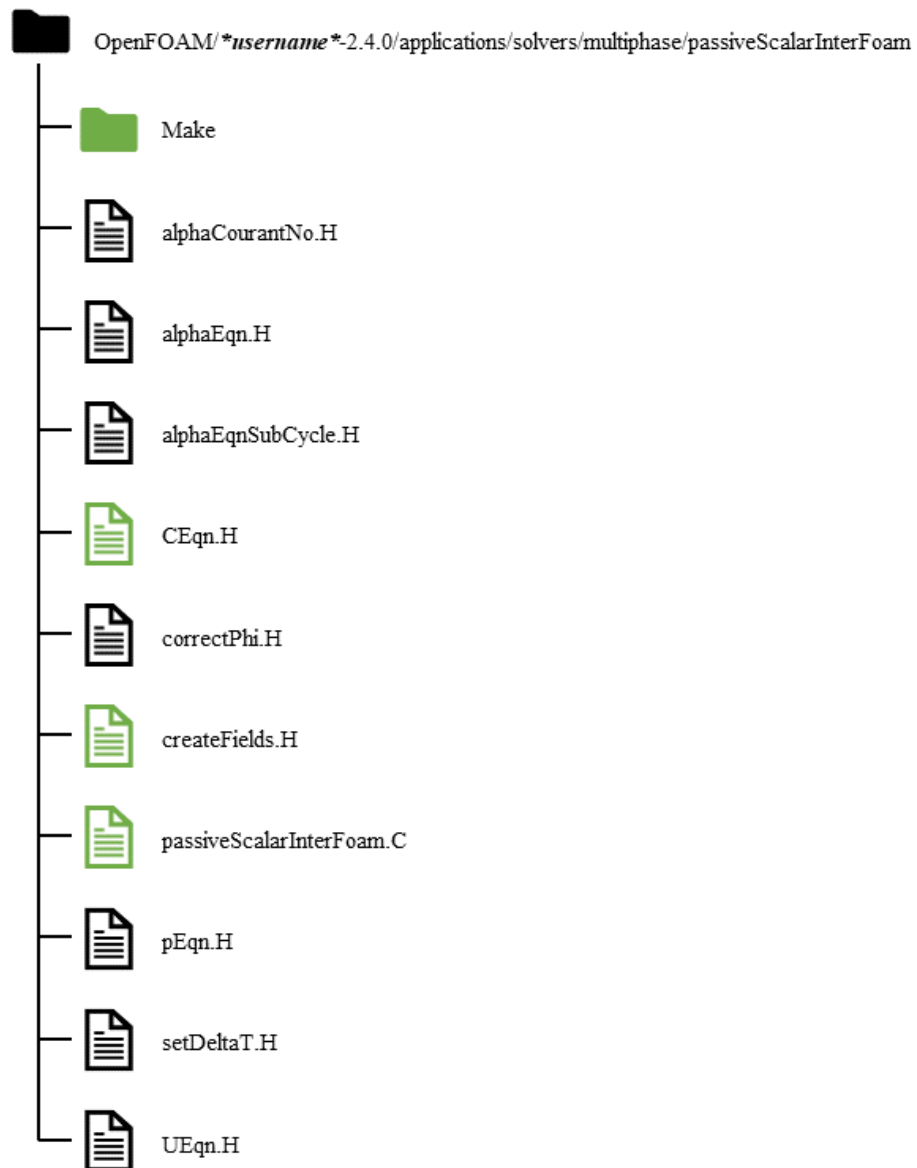


Figure A.8: File structure of `passiveScalarInterFoam` solver

### A.2.2 Make/files

The first step is to modify the files within the Make directory in order to ensure a correct initialization of the solver. In Listing A.1, the content of the file *files* in subfolder *Make* are illustrated for the *interH2SFoam* solver (Nilsson, 2019). For the *interDyMH2SFoam* and *passiveScalarInterFoam* solver, the modifications are made accordingly.

```
interH2SFoam.C  
EXE = $(FOAM_USER_APPBIN)/interH2SFoam
```

Listing A.1: Modified version of Make/files

### A.2.3 createFields.H

The relevant field variables and variables to extend the interFoam solver are defined within the file *createFields.H* (Listing A.2). In this file, the tracer is being defined as a volScalarField C. The temperature-dependent Henry coefficient is being computed by looking up the user-defined temperature from the case directory. Furthermore, the diffusivity is being read from the case directory.

```

Info << "Reading field C" << endl;
volScalarField C
(
    IObject
    (
        "C",
        runtime.timeName(),
        mesh,
        IObject::MUST_READ,
        IObject::AUTO_WRITE
    ),
    mesh
);
Info<< "Reading transportProperties\n" << endl;
IOdictionary transportProperties
(
    IObject
    (
        "transportProperties",
        runtime.constant(),
        mesh,
        IObject::MUST_READ_IF_MODIFIED,
        IObject::NO_WRITE
    )
);
// water phase (phase 1)
dimensionedScalar DT1
(
    transportProperties.lookup("DT1")
);
// air phase
dimensionedScalar DT2
(
    transportProperties.lookup("DT2")
);

dimensionedScalar Schmidtnumber
(
    transportProperties.lookup("Schmidtnumber")
);

volScalarField DT
(
    "DT",
    DT1 * DT2 / (alpha1 * DT1 + (1 - alpha1) * DT2)
);

```

```
);  
// Constant temperature in domain  
dimensionedScalar Temp  
(  
    transportProperties.lookup("Temp")  
);  
// Temperature dependent Henry coefficient for H2S, normal temperature of  
    25.15 degree  
dimensionedScalar He  
(  
    "He",  
    1/(0.001 * Foam::exp(2200.0*(1/Temp-1/298.15)) * 8.314 * Temp)  
);
```

Listing A.2: Initialization of relevant variables in createFields.H

## A.2.4 CEqn.H

Transport and mass transfer are described within the file *CEqn.H* which is displayed in Listing A.3.

```
{
  surfaceScalarField phiCi =
    (
      (
        fvc::interpolate((DT+(nut/Schmidtnumber))) *
        (1-He)
        / (fvc::interpolate(alpha1)+(1-fvc::interpolate(alpha1))*He)
      )
      * fvc::snGrad(alpha1)
    ) * mesh.magSf();

  solve
  (
    fvm::ddt(C)
    + fvm::div(phi, C, "div(phi,C)")
    - fvm::laplacian(fvc::interpolate(DT), C, "laplacian(C)")
    - fvm::laplacian((nut/Schmidtnumber), C, "laplacian(C)")
    + fvm::div(phiCi, C, "div(phi,C)")
    ,
    mesh.solver("C")
  );
}
```

Listing A.3: Mass transfer equation in CEqn.H

### A.2.5 interH2SFoam.C

For the mass transfer equation to be solved, it has to be included into the file *interH2SFoam.C*. This is done by calling the include command. Furthermore, the turbulent viscosity is being stored in a *volScalarField* so that it can be called when solving the mass transfer equation. In Listing A.4, the content of *interH2SFoam.C* is displayed and the changes highlighted in red.

```

/*
-----*|

=====
\\      /  F i e l d          /  OpenFOAM: The Open Source CFD Toolbox
\\      /  O p e r a t i o n    /
\\      /  A n d                /  Copyright (C) 2011-2015 OpenFOAM Foundation
  \\/      M a n i p u l a t i o n  /
-----

License
  This file is part of OpenFOAM.

  OpenFOAM is free software: you can redistribute it and/or modify it
  under the terms of the GNU General Public License as published by
  the Free Software Foundation, either version 3 of the License, or
  (at your option) any later version.

  OpenFOAM is distributed in the hope that it will be useful, but WITHOUT
  ANY WARRANTY; without even the implied warranty of MERCHANTABILITY or
  FITNESS FOR A PARTICULAR PURPOSE. See the GNU General Public License
  for more details.

  You should have received a copy of the GNU General Public License
  along with OpenFOAM. If not, see <http://www.gnu.org/licenses/>.

Application
  interFoam

Description
  Solver for 2 incompressible, isothermal immiscible fluids using a VOF
  (volume of fluid) phase-fraction based interface capturing approach.

  The momentum and other fluid properties are of the "mixture" and a single
  momentum equation is solved.

  Turbulence modelling is generic, i.e. laminar, RAS or LES may be selected.

  For a two-fluid approach see twoPhaseEulerFoam.

\*-----
*/

#include "fvCFD.H"
#include "CMULES.H"

```

```

#include "EulerDdtScheme.H"
#include "localEulerDdtScheme.H"
#include "CrankNicolsonDdtScheme.H"
#include "subCycle.H"
#include "immiscibleIncompressibleTwoPhaseMixture.H"
#include "turbulenceModel.H"
#include "pimpleControl.H"
#include "fvIOoptionList.H"
#include "fixedFluxPressureFvPatchScalarField.H"

#include "convectionScheme.H"

// * * * * *
//

int main(int argc, char *argv[])
{
    #include "setRootCase.H"
    #include "createTime.H"
    #include "createMesh.H"

    pimpleControl pimple(mesh);

    #include "initContinuityErrs.H"
    #include "createFields.H"
    #include "readTimeControls.H"
    #include "createPrghCorrTypes.H"
    #include "correctPhi.H"
    #include "CourantNo.H"
    #include "setInitialDeltaT.H"

    // * * * * *
    //

    Info<< "\nStarting time loop\n" << endl;

    while (runTime.run())
    {
        #include "readTimeControls.H"
        #include "CourantNo.H"
        #include "alphaCourantNo.H"
        #include "setDeltaT.H"

        runTime++;

        Info<< "Time = " << runTime.timeName() << nl << endl;

        // --- Pressure-velocity PIMPLE corrector loop
        while (pimple.loop())
        {
            #include "alphaControls.H"
            #include "alphaEqnSubCycle.H"

```

```

mixture.correct();

#include "UEqn.H"

// --- Pressure corrector loop
while (pimple.correct())
{
    #include "pEqn.H"
}

if (pimple.turbCorr())
{
    turbulence->correct();
}
}

// interH2SFoam: read nut for mass transfer equation and solve mass
// transfer equation by including "CEqn.H"
volScalarField nut("nut", turbulence->nut());
#include "CEqn.H"

runTime.write();

Info<< "ExecutionTime = " << runTime.elapsedCpuTime() << " s"
    << "   ClockTime = " << runTime.elapsedClockTime() << " s"
    << nl << endl;
}

Info<< "End\n" << endl;

return 0;
}

// *****
//

```

Listing A.4: Extension of interFoam.C to interH2SFoam.C, see highlighted in red

### A.2.6 Integration of `interDyMH2SFoam`

Similarly to the above mentioned steps, the `interDyMFoam` folder has to be modified to account for mass transfer and be renamed to `interDyMH2SFoam`. As for the modification of the `interFoam` solver, the directory has to be renamed from `interDyMFoam` to `interDyMH2SFoam`. After resetting the solver using `wclean`, the file *Makefiles* has to be modified similarly to Listing A.1 but with the new solver name `interDyMH2SFoam`. Then, the *interDyMFoam.C* has to be renamed to *interH2SDyMFoam.C* and Listing A.5 has to be written into *interH2SDyMFoam.C*. Finally, the solver has to be recompiled using `wmake` to account for the changes within the code.

```
volScalarField nut("nut", turbulence->nut());
#include "CEqn.H"
```

Listing A.5: Extension of `interDyMH2SFoam.C`

### A.2.7 Passive scalar transport

For the `passiveScalarInterFoam` solver, the file `CEqn.H` contains a standard advection-diffusion equation as displayed in Listing A.6. The other changes within the file structure are to be made in a similar way as for the `interH2SFoam` solver.

```
fvScalarMatrix CEqn
(
    fvm::ddt(C)
  + fvm::div(phi, C)
  - fvm::laplacian(D, C)
  - fvm::laplacian((nut/Schmidtnumber), C)
);
CEqn.solve();
```

Listing A.6: `CEqn.H` for `passiveScalarInterFoam`

## A.3 Function objects and boundary conditions

### A.3.1 Equilibrium conditions

Equilibrium conditions between  $H_2S$  and  $HS^-$  are computed using a custom boundary condition. The boundary condition is implemented using the OpenFOAM extension `swak4Foam` and is displayed in Listing A.7. It is defined as a boundary condition for the tracer concentration in the file `C` within the subfolder `0` of the case directory.

```
bottom
{
    type                groovyBC;
    variables            "pH=7.5;CHS=1.0;pKa=7.0;";
    valueExpression     "(CHS*pow(10,pKa-pH)/(1+pow(10,pKa-pH)))/32";
    // placeholder
    value                0.001;
}
```

Listing A.7: Boundary conditions for equilibrium conditions

### A.3.2 Calculation of partial pressure in ppm

The extension is added to the model by adding a function object using the OpenFOAM extension `swak4Foam`. The code is added to the `controlDict` file in the `system` folder of the case directory. The relevant libraries have to be imported and the function object has to be defined. The code displayed in Listing A.8 needs to be added to the bottom of the `controlDict` file.

```
libs (
  "libOpenFOAM.so"
  "libswakFunctionObjects.so"
  "libsimpleFunctionObjects.so"
);
functions
{
  conc_ppm
  {
    type expressionField;
    fieldName ppm;
    valueType internalField;
    aliases {
      alphawater alpha.water;
    }
    expression "(1 - alphawater) * 1e6 * C/1000 * 27 * 0.008206";
    autowrite true;
    verbose true;
  }
}
```

Listing A.8: Function object for calculation of partial pressure in ppm in `controlDict`

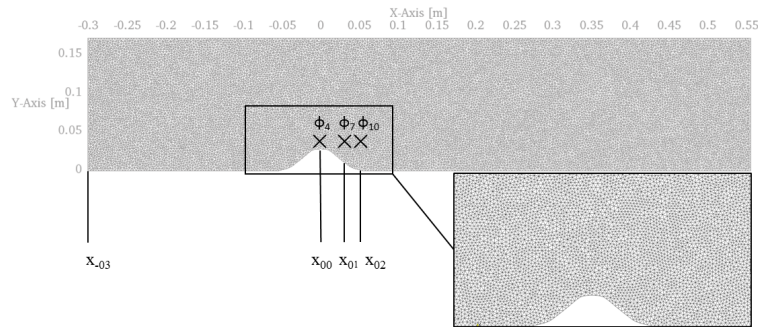
## **Appendix B**

### **Test case overview**

## B.1 Single-phase flow over a ground sill

Table B.1: Model setup of ERCOFTAC test case

**Title: Single-phase flow over a ground sill**



<b>General</b>	
Referred to in chapters	2.4.2, 3.3.1, 4.3
References	Almeida et al. (1993), Davroux et al. (1995)
Published in	Teuber et al. (2017), Teuber et al. (2016), Teuber et al. (2019a)
<b>Domain discretization</b>	
Dimensions	two-dimensional (length: 0.85m, height (max): 0.17m)
Mesh generator	GMSH
Number of cells	31,102
Turbulence models	Standard $k-\epsilon$ , Standard $k-\omega$ , $k-\omega$ SST, LES
<b>Hydrodynamic simulations</b>	
Solver	interFoam
Time step	variable, converged against 0.005 s RANS simulations and against 0.001 s for LES
Simulation time	10s
<b>Single-phase transport simulations</b>	
<i>None performed</i>	
<b>Mass transfer simulations</b>	
<i>None performed</i>	

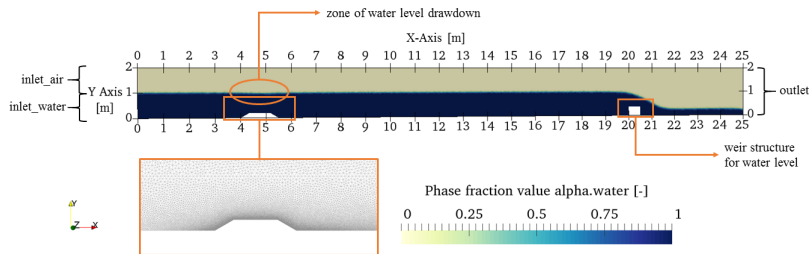
Table B.2: Boundary conditions for hydrodynamic simulations of single-phase flow over a ground sill (Turbulence properties calculated using <https://www.cfd-online.com/Tools/turbulence.php>)

	alpha.water [-]	prgh [ $\frac{kg}{m \cdot s^2}$ ]	U [m/s]	k [ $\frac{m^2}{s^2}$ ]	$\epsilon$ [ $\frac{m^2}{s^3}$ ] / $\omega$ [ $\frac{1}{s}$ ]
inlet	inletOutlet inletValue: uniform 1 value: uniform 1	zeroGradient	fixedValue value: parabolic function following experimental results, applied using funkySetBoundary	turbulentIntensity- KineticEnergyInlet intensity: 0.03 value: uniform 0.00622	$\epsilon$ : turbulentMixingLength- DissipationRateInlet mixingLength: 0.0119 value: uniform 0.00371 $\omega$ : fixedValue value: \$internalField zeroGradient
outlet	zeroGradient	fixedValue	zeroGradient	zeroGradient	zeroGradient
upper and lower wall	zeroGradient	fixedValue value: uniform 1667.7	fixedValue value: uniform (0 0 0)	kqRWallFunction value: uniform 0	$\epsilon$ : epsilonWallFunction value: uniform 0 $\omega$ : omegaWallFunction value: \$internalField
sidewalls initial condi- tions	empty uniform 1	empty uniform 0	empty uniform (0 0 0)	empty uniform 0.00622	empty $\epsilon$ : uniform 0.00371 $\omega$ : uniform 6.62906

## B.2 Two-phase flow over a two-dimensional hill

Table B.3: Model setup, two-phase flow over a two-dimensional hill

Title: Two-phase flow over a two-dimensional hill



<b>General</b>	
Referred to in chapters	2.4.2, 3.3.2, 4.4
References	-
Published in	Teuber et al. (2017), Teuber et al. (2016), Teuber et al. (2019a)
<b>Domain discretization</b>	
Dimensions	two-dimensional: cases 1,2: length: 25m, height (max): 2m case 3: length: 35m, height (max): 6m three-dimensional: extension of case 1: length: 25m, height (max): 2m, width: 1m
Mesh generator	GMSH
Number of cells	68,542 (cases 1 and 2, comparable cell numbers for ground sill variations referred to in chapter 4.4), 175,762 (case 3), 685,420 (3D case based on case 1)
Turbulence models	Standard k- $\epsilon$
<b>Hydrodynamic simulations</b>	
Solver	interFoam
Time step	variable, converged against 0.001 s
Simulation time	100s
<b>Single-phase transport simulations</b>	
<i>None performed</i>	
<b>Mass transfer simulations</b>	
<i>None performed</i>	

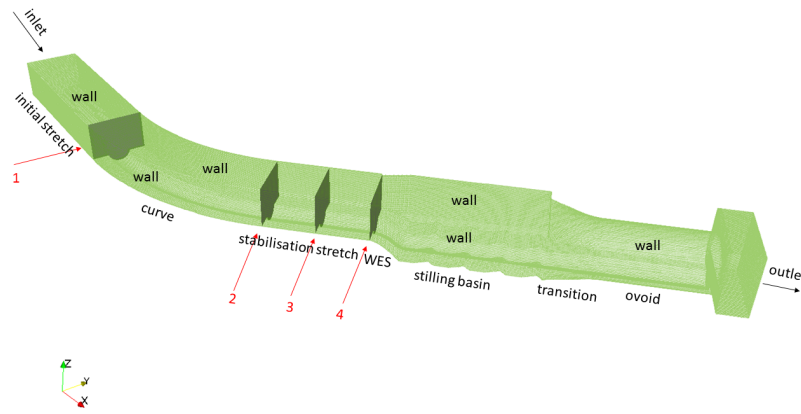
Table B.4: Boundary conditions for hydrodynamic simulations of two-phase flow over a hill (case 1, 2D setup, turbulence properties were calculated using <https://www.cfd-online.com/Tools/turbulence.php>)

	alpha.water [-]	prgh [ $\frac{kg}{m \cdot s^2}$ ]	U [m/s]	k [ $\frac{m^2}{s^2}$ ]	$\epsilon$ [ $\frac{m^2}{s^3}$ ]
inlet_air	inletOutlet inletValue: uniform 0 value: uniform 0	totalPressure p0: uniform 0 U: U phi: phi rho: rho psi: none gamma: 1 value: uniform 0 zeroGradient	zeroGradient	fixedValue value: \$internalField	fixedValue value: \$internalField
inlet_water	inletOutlet inletValue: uniform 1 value: uniform 1	zeroGradient	fixedValue value: uniform (1 0 0) (for other cases respective velocities)	fixedValue value: \$internalField	fixedValue value: \$internalField
outlet	zeroGradient	fixedValue value: uniform 0	inletOutlet	zeroGradient	zeroGradient
upper and lower wall sidewalls initial condi- tions	zeroGradient empty uniform 0 define initial water level of 1m using setFields (volScalarFieldValue alpha.water 1)	zeroGradient empty uniform 0	inletValue: uniform (0 0 0) value: uniform (0 0 0) fixedValue value: uniform (0 0 0) empty uniform (0 0 0) define initial flow velocity of 1 using setFields (volVectorFieldValue U (1 0 0))	zeroGradient zeroGradient empty uniform 0.00375	zeroGradient zeroGradient empty uniform 0.00054

### B.3 Complex sewer geometry

Table B.5: Model setup of complex sewer geometry

Title: Complex sewer geometry



<b>General</b>	
Referred to in chapters	hydrodynamic simulations: 2.4.2, 3.3.3 single-phase transport: 5.3.2 mass transfer: 6.3.4, 6.4.3
References	Bayón et al. (2015)
Published in	hydrodynamic simulations: Teuber et al. (2017), Teuber et al. (2016), Teuber et al. (2019a) single-phase transport: Teuber et al. (2019c) mass transfer: Teuber et al. (2019b)
<b>Domain discretization</b>	
Dimensions	three-dimensional (length: approx. 95 m, height (max): 7.50m)
Mesh generator	snappyHexMesh
Number of cells	3,029,223
Turbulence models	Standard k-ε
<b>Hydrodynamic simulations</b>	
Solver	interFoam
Time step	variable, converged against 0.00019 s
Simulation time	200s
<b>Single-phase transport simulations</b>	
Solvers	interH2SFoam with modified Henry coefficient
Simulation time	10s, starting from quasi steady-state reached by hydrodynamic simulations
Tracer diffusivity	water: $10^{-5} m^2/s$ air: $10^{-5} m^2/s$
Schmidt number	1.0
Henry coefficient	$10^{-6}$
<b>Mass transfer simulations</b>	
Solver	interH2SFoam
Simulation time	10s, starting from quasi steady-state reached by hydrodynamic simulations
Tracer diffusivity	water: $10^{-3} m^2/s$ air: $10^{-3} m^2/s$
Schmidt number	1.0
Temperature	298 K

Table B.6: Boundary conditions for simulations of complex sewer geometry (turbulence properties were calculated using <https://www.cfd-online.com/Tools/turbulence.php>)

	alpha.water [-]	prgh [ $\frac{kg}{m \cdot s^2}$ ]	U [m/s]	k [ $\frac{m^2}{s^2}$ ]	$\epsilon$ [ $\frac{m^2}{s^3}$ ]	C [ $\frac{mol}{m^3}$ ] (only applies to single-phase transport and mass transfer cases)
inlet_air	inletOutlet inletValue: uniform 0 value: uniform 0	totalPressure p0: uniform 0 U: U phi: phi rho: rho psi: none gamma: 1 value: uniform 0 fixedFluxPressure	pressureInletOutlet- Velocity phi: phi tangentialVelocity: uniform (0 0 0) value: uniform (0 0 0)	zeroGradient	zeroGradient	zeroGradient
inlet_water	inletOutlet inletValue: uniform 1 value: uniform 1 zeroGradient	flowRateInletVelocity volumetricFlowRate: 100 inletOutlet inletValue: uniform (0 0 0) value: uniform (0 0 0) fixedValue value: uniform 0	flowRateInletVelocity volumetricFlowRate: 100 inletOutlet inletValue: uniform (0 0 0) value: uniform (0 0 0) fixedValue value: uniform 0	fixedValue value: \$internalField	turbulentMixingLength- DissipationRateInlet mixingLength: 0.005 value: uniform 0.0375 inletOutlet inletValue: \$internalField	zeroGradient
outlet	zeroGradient	fixedValue value: uniform 0	inletOutlet inletValue: uniform (0 0 0) value: uniform (0 0 0) fixedValue value: uniform (0 0 0)	inletOutlet inletValue: \$internalField value: \$internalField kqWallFunction value: uniform 0.063;	inletOutlet inletValue: \$internalField value: \$internalField epsilonWallFunction value: uniform 0.0375	zeroGradient
bottom	zeroGradient	fixedFluxPressure	fixedValue value: uniform (0 0 0)	kqWallFunction value: uniform 0.063 uniform 0.063	epsilonWallFunction value: uniform 0.0375 uniform 0.0375	single-phase transport: zeroGradient mass transfer: fixedValue value: 1 zeroGradient
top wall and side walls	zeroGradient	fixedFluxPressure	fixedValue value: uniform (0 0 0) uniform (0 0 0)	kqWallFunction value: uniform 0.063 uniform 0.063	epsilonWallFunction value: uniform 0.0375 uniform 0.0375	zeroGradient
initial condi- tions	uniform 0	uniform 0	uniform (0 0 0)	uniform 0.063	uniform 0.0375	uniform 0, and for - single-phase transport: use setFields to define box where C = 1 - mass transfer: use expression in funkySet- Fields to define C = 1 where <i>alpha.water</i> > 0.5

## B.4 Single-phase transport in rectangular pipe

Table B.7: Model setup of single-phase transport in rectangular pipe test case

<b>Title: Single-phase transport in rectangular pipe</b>	
<b>General</b>	
Case description	Tracer transport along rectangular channel case 1: interFoam extended by standard advection-diffusion equation case 2: interH2SFoam with modified Henry coefficient
Referred to in chapters	5.1, 5.3.2
References	-
Published in	Teuber et al. (2019c)
<b>Domain discretization</b>	
Dimensions	three-dimensional (length: 15m, height (max): 1m, depth: 1m)
Mesh generator	blockMesh
Number of cells	45,000
Turbulence model	Standard k- $\epsilon$
<b>Hydrodynamic simulations</b>	
<i>None performed</i>	
<b>Single-phase transport simulations</b>	
Solvers	case 1: interFoam extended by advection-diffusion equation case 2: interH2SFoam with modified Henry coefficient
Simulation time	150s
Tracer diffusivity	water: $10^{-3}m^2/s$ air: $10^{-3}m^2/s$ (high diffusivity in order to force fast spreading during transport along the channel)
Schmidt number	1.0
<b>Mass transfer simulations</b>	
<i>None performed</i>	

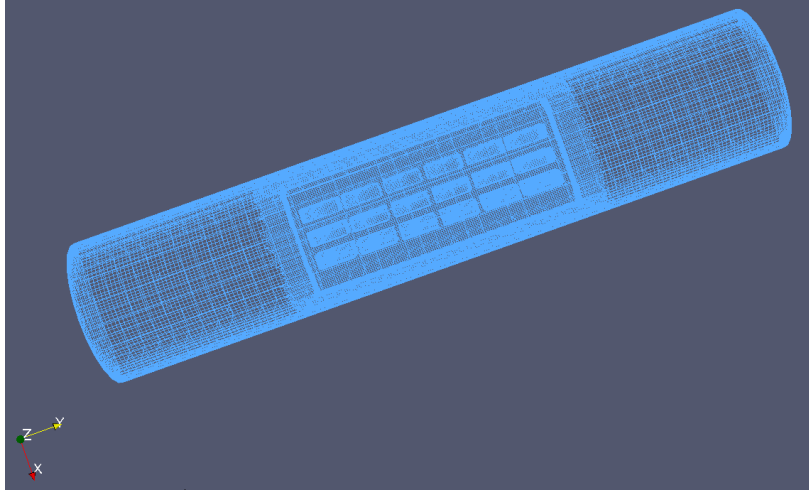
Table B.8: Boundary conditions for simulations of single-phase transport in rectangular pipe (turbulence properties were calculated using <https://www.cfd-online.com/Tools/turbulence.php>)

	alpha.water [-]	prgh [ $\frac{kg}{m \cdot s^2}$ ]	U [m/s]	k [ $\frac{m^2}{s^2}$ ]	$\epsilon$ [ $\frac{m^2}{s^3}$ ]	C [ $\frac{mol}{m^3}$ ]
inlet_air	inletOutlet inletValue: uniform 0 value: uniform 0	totalPressure p0: uniform 0 U: U phi: phi rho: rho psi: none gamma: 1 value: uniform 0 fixedFluxPressure	zeroGradient	zeroGradient	zeroGradient	zeroGradient
inlet_water	inletOutlet inletValue: uniform 1 value: uniform 1	fixedFluxPressure	flowRateInletVelocity volumetricFlowRate: 0.05	turbulentIntensity- KineticEnergyInlet intensity: 0.05 value: uniform 0.00004 zeroGradient	turbulentMixing- LengthDissipation- RateInlet mixingLength: 0.038 value: uniform 5e-7 inletOutlet inletValue: \$internalField value: \$internalField	zeroGradient
outlet	zeroGradient	zeroGradient	outletPhaseMean- Velocity Umean: 0.1 alpha: alpha.water value: uniform (0.1 0 0) fixedValue value: uniform (0 0 0)	zeroGradient	inletOutlet inletValue: \$internalField value: \$internalField	zeroGradient
bottom	zeroGradient	fixedFluxPressure	fixedValue value: uniform (0 0 0)	kqWallFunction value: uniform 0.00004;	epsilonWallFunction value: uniform 5e-7	zeroGradient
top wall and side walls	zeroGradient	fixedFluxPressure	fixedValue value: uniform (0 0 0)	kqWallFunction value: uniform 0.00004;	epsilonWallFunction value: uniform 5e-7	zeroGradient
initial condi- tions	uniform 0 use setFields to define water phase ( <i>alpha.water</i> = 1) within bounding box between (0 0 -1) and (15 0.5 2)	uniform 0	uniform (0.1 0 0)	uniform 0.00004	uniform 5e-7	uniform 0 use setFields to de- fine initial tracer con- centration (C = 1) within bounding box between (10.1 0.4) (1.5 0.4 0.6)

## B.5 Concrete probes in sewer pilot plant

Table B.9: Concrete probes in sewer pilot plant

Title: Concrete probes in sewer pilot plant



<b>General</b>	
Case description	Single-phase tracer transport around concrete probes in sewer pilot plant
Referred to in chapters	5.3.1
References	-
Published in	Teuber et al. (2019c)
<b>Domain discretization</b>	
Dimensions	three-dimensional (length: 2m, height (max): 0.3m, depth: 0.5m)
Mesh generator	SnappyHexMesh
Number of cells	1,041,772
Turbulence model	laminar
<b>Hydrodynamic simulations</b>	
Solver	interFoam
Simulation time	50s
Time step	variable, converged against 0.024 s
<b>Single-phase transport simulations</b>	
Solvers	interFoam extended by advection-diffusion equation
Simulation time	65s, starting from quasi steady-state reached by hydrodynamic simulations
Tracer diffusivity	air: $10^{-9} m^2/s$
Schmidt number	1.0
<b>Mass transfer simulations</b>	
<i>None performed</i>	

Table B.10: Boundary conditions for transport simulations around concrete probes (turbulence properties were calculated using <https://www.cfd-online.com/Tools/turbulence.php>)

	alpha.water [-]	prgh [ $\frac{kg}{m \cdot s^2}$ ]	U [m/s]	C [ $\frac{m^0}{m^3}$ ]
inlet	inletOutlet inletValue: uniform 0 value: uniform 0	totalPressure p0: uniform 0 U: U phi: phi rho: rho psi: none gamma: 1 value: uniform 0	pressureInlet- OutletVelocity phi: phi tangentialVelocity: uniform (0 0 0) value: uniform (0 0 0)	zeroGradient
outlet	zeroGradient	fixedValue value: uniform -0.02	inletOutlet inletValue: uniform (0 0 0)	zeroGradient
watersurface	zeroGradient	fixedFluxPressure	value: uniform (0 0 0) fixedValue value: uniform (0 0.5 0)	zeroGradient
pipe	zeroGradient	fixedFluxPressure	fixedValue	zeroGradient
concrete	zeroGradient	fixedFluxPressure	value: uniform (0 0 0) fixedValue	zeroGradient
probes	uniform 0	uniform 0	value: uniform (0 0 0) uniform (0 0 0)	uniform 0
initial conditions				use setFields to define initial tracer concentration (C = 1) within bounding box between (0 1.379 0) (100 2.12 100)

## B.6 Quasi one-dimensional cubic tank

Table B.11: Model setup of quasi one-dimensional cubic tank

<b>Title: Quasi one-dimensional cubic tank</b>	
<b>General</b>	
Case description	Validation of mass transfer solver extensions using a cubic tank setup and analysing the equilibrium conditions at steady state case 1: analysis of concentration profile at normal temperature (298.15 K) case 2: analysis of concentration profile at different temperature (293.15 K) case 3: analysis of computed equilibrium conditions between $HS^-$ and $H_2S$ using new boundary condition and analysis of calculated partial pressure of $H_2S$ in air phase
Referred to in chapters	6.3.4, 6.4.1
References	-
Published in	Teuber et al. (2019b)
<b>Domain discretization</b>	
Dimensions	quasi one-dimensional (height: 1m, width: 1m, depth: 1m)
Mesh generator	blockMesh
Number of cells	10,000
Turbulence models	laminar
<b>Hydrodynamic simulations</b>	
<i>None performed (no fluid flow in domain)</i>	
<b>Single-phase transport simulations</b>	
<i>None performed</i>	
<b>Mass transfer simulations</b>	
Solver	interH2SFoam
Simulation time	1000s
Time step	0.1 s
Tracer diffusivity	water: $10^{-2}m^2/s$ air: $10^{-2}m^2/s$ (a high diffusivity was chosen because only the equilibrium conditions established were of interest)
Temperature	298.15 K and 293.15 K

Table B.12: Boundary conditions for simulations of quasi one-dimensional cubic tank

	alpha.water [-]	prgh [ $\frac{kg}{m \cdot s^2}$ ]	U [m/s]	C [ $\frac{mol}{m^3}$ ]
bottom	zeroGradient	zeroGradient	fixedValue value: uniform (0 0 0)	- cases 1 and 2: fixedValue value: uniform 1 - case 3: groovyBC according to Listing A.7
top wall and side walls	zeroGradient	zeroGradient	fixedValue	zeroGradient
initial conditions	use setFields to define a water level of 0.5 m ( <i>alpha.water</i> = 1 for $h < 0.5m$ , <i>alpha.water</i> = 0 elsewhere)	uniform 0	value: uniform (0 0 0) uniform (0 0 0)	use setFields to define initial concentration in water phase ( $C = 1$ for $h < 0.5m$ , $C = 0$ elsewhere)

## B.7 Mass transfer in rectangular duct

Table B.13: Model setup of mass transfer in rectangular duct

<b>Title: Mass transfer in rectangular duct</b>	
<b>General</b>	
Case description	Mass transfer simulations according to test cases 7 (here: case 1) and 21 (here: case 2) as carried out by Bentzen et al. (2016). Hydrodynamic simulations were carried out until a quasi steady-state has been reached, then the mass transfer simulations have been performed.
Referred to in chapters	6.3.4, 6.4.2
References	Bentzen et al. (2016)
Published in	Teuber et al. (2019b)
<b>Domain discretization</b>	
Dimensions	three-dimensional (length: 15m, height: 0.26m, width: 0.3m)
Mesh generator	GMSH
Number of cells	307,970
Turbulence model	laminar
<b>Hydrodynamic simulations</b>	
Solver	interFoam
Time step	variable, converged against 0.007 s (case 1), 0.019 (case 2)
Simulation time	200s
<b>Single-phase transport simulations</b>	
<i>None performed</i>	
<b>Mass transfer simulations</b>	
Solver	interH2SFoam
Simulation time	50s, starting from quasi steady-state reached by hydrodynamic simulations
Tracer diffusivity	water: $2.2 \cdot 10^{-9} m^2/s$ air: $1.74 \cdot 10^{-5} m^2/s$
Schmidt number	1.0
Temperature	298 K

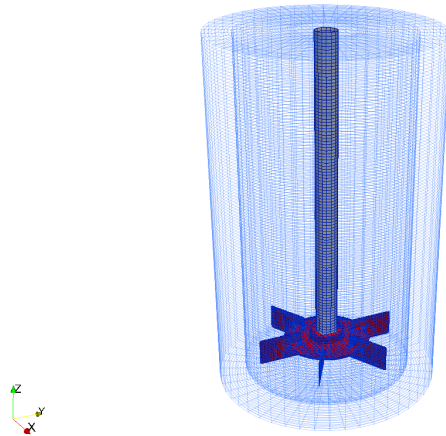
Table B.14: Boundary conditions for mass transfer in rectangular duct

	alpha.water [-]	prgh [ $\frac{kg}{m \cdot s^2}$ ]	U [m/s]	C [ $\frac{mol}{m^3}$ ] (only applies to mass transfer cases)
inlet_air	inletOutlet inletValue: uniform 0 value: uniform 0	totalPressure p0: uniform 0 U: U phi: phi rho: rho psi: none gamma: 1 value: uniform 0	pressureInletOutletVelocity phi: phi tangentialVelocity: uniform (0 0 0) value: uniform (0 0 0)	zeroGradient
inlet_water	inletOutlet inletValue: uniform 1 value: uniform 1	fixedFluxPressure	flowRateInletVelocity volumetricFlowRate: 0.0072 (case 1, 0.0164 for case 2)	fixedValue value: uniform 1
outlet	zeroGradient	fixedValue value: uniform -0.025	inletOutlet inletValue: uniform (0 0 0)	inletOutlet inletValue: uniform (0 0 0)
bottom	zeroGradient	fixedFluxPressure	fixedValue	value: uniform (0 0 0) zeroGradient
top wall and side walls	zeroGradient	fixedFluxPressure	fixedValue	zeroGradient
initial conditions	uniform 0	uniform 0	value: uniform (0 0 0) uniform (0 0 0)	uniform 0, use expression in funkySetFields to define C = 1 where <i>alpha.water</i> > 0.5

## B.8 Stirring tank

Table B.15: Model setup of stirring tank

Title: Mass transfer in stirring tank



### General

Case description	Mass transfer simulations according to experiments as carried out by Carrera et al. (2017). Hydrodynamic simulations were carried out with different stirring rates (case 1: 50 rpm, case 2: 80 rpm, case 3: 100 rpm, case 4: 120 rpm, case 5: 140 rpm) until a quasi steady-state has been reached, then the mass transfer simulations have been performed.
Referred to in chapter	7
References	Carrera et al. (2017)
Published in	Teuber et al. (in preparation)
<b>Domain discretization</b>	
Dimensions	three-dimensional (tank diameter: 0.25m, blade length: 0.05m, blade height: 0.03m)
Mesh generator	SnappyHexMesh
Number of cells	214,100
Turbulence model	RNG k- $\epsilon$
<b>Hydrodynamic simulations</b>	
Solver	interFoam
Time step	variable, converged against 0.007 s (case 1), 0.019 (case 2)
Simulation time	25s
<b>Single-phase transport simulations</b>	
<i>None performed</i>	
<b>Mass transfer simulations</b>	
Solver	interH2SFoam
Simulation time	10s, starting from quasi steady-state reached by hydrodynamic simulations
Tracer diffusivity	water: $1.4 \cdot 10^{-9} m^2/s$ air: $1.5 \cdot 10^{-5} m^2/s$
Schmidt number	1.0
Temperature	298 K

Table B.16: Boundary conditions for stirring tank

	alpha.water [-]	prgh [ $\frac{kg}{m^3s^2}$ ]	U [m/s]	k [ $\frac{m^2}{s^2}$ ]	$\epsilon$ [ $\frac{m^2}{s^3}$ ]	C [ $\frac{mol}{m^3}$ ] (only applies to mass transfer cases)
top	inletOutlet inletValue: uniform 0 value: uniform 0	totalPressure p0: uniform 0 U: U phi: phi rho: rho psi: none gamma: 1 value: uniform 0	pressureInletOutletVelocity phi: phi tangentialVelocity: uniform (0 0 0) value: uniform (0 0 0)	inletOutlet inletValue: 1e-5 value: uniform 1e-5	inletOutlet inletValue: \$internalField value: \$internalField	inletOutlet inletValue: 0 value: 0
static walls	zeroGradient	fixedFluxPressure value: uniform 0	fixedValue	kqWallFunction	epsilonWallFunction	zeroGradient
rotating wall elements	zeroGradient	fixedFluxPressure	value: uniform (0 0 0) movingWallVelocity value: \$internalField; cyclicAMI	value: uniform 1e-5 kqWallFunction value: uniform 1e-5	value: uniform 1e-5 epsilonWallFunction value: uniform 1e-5	zeroGradient
AMI	cyclicAMI	cyclicAMI	cyclicAMI	cyclicAMI	cyclicAMI	cyclicAMI
initial conditions	use setFields to define a water level of 0.5 m ( <i>alpha.water</i> = 1 for $h < 0.5m$ , <i>alpha.water</i> = 0 elsewhere)	uniform 0	uniform (0 0 0)	uniform 1e-5	uniform 1e-5	uniform 0, use expression in funkySetFields to define C = 0.073 where <i>alpha.water</i> > 0.5

# Bibliography

- Almeida, G., Durao, D., and Heitor, M.: Wake flows behind two-dimensional model hills, *Experimental Thermal and Fluid Science*, 7(1), 87–101, 1993.
- Ashley, R.: *Solids in Sewers: Characteristics, Effects and Control of Sewer Solids and Associated Pollutants* (Scientific and Technical Report), IWA Publishing, 2004.
- Auguet, O., Pijuan, M., Guasch-Balcells, H., Borrego, C., and Gutierrez, O.: Implications of downstream nitrate dosage in anaerobic sewers to control sulfide and methane emissions, *Water research*, 68, 522–532, 2015.
- Barjenbruch, M.: Prevention of odour emergence in sewage networks, *Water science and technology*, 47(7-8), 357–363, 2003.
- Barjenbruch, M., Hinkelmann, R., Huhnt, W., Krämer, T., Nehrig, M., and Rühmland, S.: *An Online-Monitoring and Operating System to Prevent Odour and Corrosion in Sewer Networks, Feasibility Study*, 2008.
- Barlag, C., Hinkelmann, R., Helmig, R., and Zielke, W.: Adaptive methods for modelling transport processes in fractured subsurface systems, in: *3rd International Conference on Hydrosience and Engineering*, Cottbus, Center of Computational Hydrosience and Engineering, The University of Mississippi, vol. 284, 1998.
- Bates, P., Lane, S., and Ferguson, R.: *Computational Fluid Dynamics: Applications in Environmental Hydraulics*, John Wiley & Sons, Ltd., Chichester, UK, 2005.
- Bayón, A. and Lopez-Jimenez, P.: Numerical analysis of hydraulic jumps using OpenFOAM, *Journal of Hydroinformatics*, 17(4), 662–678, 2015.
- Bayón, A., Vallés-Morán, F., and López-Jiménez, P.: Numerical analysis and validation of South Valencia sewage collection system diversion, in: *36th IAHR World Congress*, The Hague, The Netherlands, 2015.
- Bentzen, T., Østertoft, K., Vollertsen, J., Fuglsang, E., and Nielsen, A.: Airflow in Gravity Sewers—Determination of Wastewater Drag Coefficient, *Water Environment Research*, 88(3), 239–256, 2016.
- Berberović, E., van Hinsberg, N., Jakirlić, S., Roisman, I., and Tropea, C.: Drop impact onto a liquid layer of finite thickness: Dynamics of the cavity evolution, *Physical Review E*, 79(3), 036 306, 2009.
- Bjerre, H. L., Hvitved-Jacobsen, T., Teichgräber, B., and Schlegel, S.: Modeling of aerobic wastewater transformations under sewer conditions in the Emscher River, Germany, *Water Environment Research*, 70(6), 1151–1160, 1998.

- Boon, A. and Lister, A.: Formation of sulphide in rising main sewers and its prevention by injection of oxygen, *Prog. Wat. Tech.*, 1975.
- Caretto, L., Gosman, A., Patankar, S., and Spalding, D.: Two calculation procedures for steady, three-dimensional flows with recirculation, in: *Proceedings of the third international conference on numerical methods in fluid mechanics*, pp. 60–68, Springer, 1973.
- Carrera, L., Springer, F., Lipeme-Kouyi, G., and Buffiere, P.: A review of sulfide emissions in sewer networks: overall approach and systemic modelling, *Water Science and Technology*, 73(6), 1231–1242, 2016.
- Carrera, L., Springer, F., Lipeme-Kouyi, G., and Buffiere, P.: Sulfide emissions in sewer networks: focus on liquid to gas mass transfer coefficient, *Water Science and Technology*, 75(8), 1899–1908, 2017.
- Celik, I., Ghia, U., and Roache, P.: Procedure for estimation and reporting of uncertainty due to discretization in CFD applications, *Journal of Fluids*, 130(7), 078 001, 2008.
- Cifani, P., Michalek, W., Priems, G., Kuerten, J. G., van der Geld, C., and Geurts, B. J.: A comparison between the surface compression method and an interface reconstruction method for the VOF approach, *Computers & Fluids*, 136, 421–435, 2016.
- Damián, S.: Description and utilization of interFoam multiphase solver, URL: <http://infotech.unl.edu.ar/upload/3be0e16065026527477b4b948c4caa7523c8ea52.pdf>, 2012.
- Damián, S.: An extended mixture model for the simultaneous treatment of short and long scale interfaces, Ph.D. thesis, Universidad Nacional Del Litoral, Argentina, 2013.
- Davroux, A., Hoa, C., and Laurence, D.: Flow over a 2D hill—reference solutions for k–and second moment closure turbulence models, in: *ERCOFTAC Workshop*, Karlsruhe, 1995.
- De Belie, N., Monteny, J., and Taerwe, L.: Apparatus for accelerated degradation testing of concrete specimens, *Materials and Structures*, 35(7), 427–433, 2002.
- Devolder, B., Schmitt, P., Rauwoens, P., Elsässer, B., and Troch, P.: A Review of the Implicit Motion Solver Algorithm in OpenFOAM to Simulate a Heaving Buoy, 2015.
- DIN 1045-2:2008-08: Tragwerke aus Beton, Stahlbeton und Spannbeton–Teil 2: Beton–Festlegung, Eigenschaften, Herstellung und Konformität–Anwendungsregeln zu DIN EN 206-1, Beuth Verlag Berlin, 2008.
- DIN E 197-1: 2011-11: Zement – Teil 1: Zusammensetzung, Anforderungen und Konformitätskriterien von Normalzement; Deutsche Fassung EN 197-1:2011., Beuth Verlag Berlin, 2011.
- DIN EN 196-1:2005-05: Prüfverfahren für Zement – Teil 1: Bestimmung der Festigkeit; Deutsche Fassung EN 196-1:2005, Beuth Verlag Berlin, 2005.
- E DIN 19573:2013-06: Mörtel für Neubau und Sanierung von Entwässerungssystemen außerhalb von Gebäuden, Beuth Verlag Berlin, 2013.
- Edwini-Bonsu, S. and Steffler, P.: Air flow in sanitary sewer conduits due to wastewater drag: a computational fluid dynamics approach, *Journal of Environmental Engineering and Science*, 3(5), 331–342, 2004.

- Edwini-Bonsu, S. and Steffler, P.: Dynamics of air flow in sewer conduit headspace, *Journal of Hydraulic Engineering*, 132(8), 791–799, 2006.
- Fourie, C. and Alexander, M.: A dynamic hydrochloric acid test for evaluating acid resistance of sewer pipe concrete, in: *Workshop on Performance of Cement-based Materials in Aggressive Aqueous Environments-Characterisation, Modelling, Test Methods and Engineering Aspects*, pp. 104–113, RILEM Publications SARL, 2008.
- Freudenthal, K., Koglatis, J., Otterpohl, R., and Behrendt, J.: Prediction of sulfide formation in sewer pressure mains based on the IWA Anaerobic Digestion Model No. 1 (ADM1), *Water Science and Technology*, 52(10-11), 13–22, 2005.
- Ganigué, R., Jiang, G., Sharma, K., Chen, J., Vuong, L., and Yuan, Z.: Online Control of magnesium hydroxide dosing for sulfide mitigation in sewers: algorithm development, simulation analysis, and field validation, *Journal of Environmental Engineering*, 142(12), 04016069, 2016.
- Gessner, M., Hinkelmann, R., Nützmann, G., Jekel, M., Singer, G., Lewandowski, J., Nehls, T., and Barjenbruch, M.: Urban water interfaces, *Journal of Hydrology*, 514, 226–232, 2014.
- Gilchrist, F.: Microbiological studies of the corrosion of concrete sewers by sulphuric acid producing bacteria, *South African Industrial Chemist*, 7, 214–215, 1953.
- Greenshields, C. J.: OpenFOAM user guide, OpenFOAM Foundation Ltd, version 2.4.0, 3(1), 47, 2015.
- Grengg, C., Mittermayr, F., Baldermann, A., Böttcher, M., Leis, A., Koraimann, G., Grunert, P., and Dietzel, M.: Microbiologically induced concrete corrosion: A case study from a combined sewer network, *Cement and Concrete Research*, 77, 16–25, 2015.
- Haroun, Y., Legendre, D., and Raynal, L.: Volume of fluid method for interfacial reactive mass transfer: application to stable liquid film, *Chemical Engineering Science*, 65(10), 2896–2909, 2010a.
- Haroun, Y., Legendre, D., and Raynal, L.: Direct numerical simulation of reactive absorption in gas–liquid flow on structured packing using interface capturing method, *Chemical Engineering Science*, 65(1), 351–356, 2010b.
- Higuera, P., Lara, J., and Losada, I.: Simulating coastal engineering processes with OpenFOAM®, *Coastal Engineering*, 71, 119–134, 2013.
- Hinkelmann, R.: *Efficient Numerical Methods and Information-Processing Techniques for Modeling Hydro- and Environmental Systems*, Lecture Notes in Applied and Computational Mechanics, Springer Berlin Heidelberg, 2005.
- Hoang, D., van Steijn, V., Portela, L., Kreutzer, M., and Kleijn, C.: Benchmark numerical simulations of segmented two-phase flows in microchannels using the Volume of Fluid method, *Computers & Fluids*, 86, 28–36, 2013.
- Hüttl, R.: Flugaschebetone mit hohem Säurewiderstand im Kühlturm-und Wasserbau–Historie, Stand der Technik und Bewertungskriterien, *VGB Power-Tech*, 4, 2008.
- HV-Consult: Description of the WATS model, URL <http://hvcon.com/Download/Description%20of%20the%20WATS%20model.pdf>, 2019.

- Hvitved-Jacobsen, T., Jütte, B., Nielsen, P., and Jensen, N.: Hydrogen sulphide control in municipal sewers, in: Pretreatment in chemical water and wastewater treatment, pp. 239–247, Springer Berlin Heidelberg, 1988.
- Hvitved-Jacobsen, T., Raunkjær, K., and Nielsen, P. H.: Volatile fatty acids and sulfide in pressure mains, *Water Science and Technology*, 31(7), 169–179, 1995.
- Hvitved-Jacobsen, T., Vollertsen, J., and Nielsen, A.: Sewer processes: microbial and chemical process engineering of sewer networks, CRC press, Boca Raton, USA, 2013.
- Issa, R.: Solution of the implicitly discretised fluid flow equations by operator-splitting, *Journal of computational physics*, 62(1), 40–65, 1986.
- Jasak, H.: Error analysis and estimation for the finite volume method with applications to fluid flows., Ph.D. thesis, Imperial College London (University of London), 1996.
- Ji, Z.: Water Quality and Eutrophication. Hydrodynamic and Water Quality: Modeling Rivers, Lakes, and Estuaries, John Wiley & Sons, Inc., Hoboken, New Jersey, 2008.
- Jiang, G., Sun, J., Sharma, K., and Yuan, Z.: Corrosion and odor management in sewer systems, *Current Opinion in Biotechnology*, 33, 192–197, 2015.
- Kaempfer, W. and Berndt, M.: Estimation of service life of concrete pipes in sewer networks, *Durability of Building Materials and Components*, 8, 36–45, 1999.
- Keough, S.: Optimising the Parallelisation of OpenFOAM Simulations, Tech. rep., Defence Science and Technology Organisation Fishermans Bend Australia Maritime Div., 2014.
- Kinyua, M., Zhang, J., Camacho-Céspedes, F., Tejada-Martinez, A., and Ergas, S.: Use of physical and biological process models to understand the performance of tubular anaerobic digesters, *Biochemical Engineering Journal*, pp. 35–44, 2016.
- Kortelainen, J.: Meshing tools for open source CFD-a practical point of view, VTT, Espoo, Finland, Tech. Rep, 2009.
- Launder, B. and Sharma, B.: Application of the energy-dissipation model of turbulence to the calculation of flow near a spinning disc, *Letters in Heat and Mass Transfer*, 1(2), 131–137, 1974.
- Leigh, N. G. and Lee, H.: Sustainable and Resilient Urban Water Systems: The Role of Decentralization and Planning, *Sustainability*, 11(3), 918, 2019.
- Lopes, P., Leandro, J., and Carvalho, R. F.: Self-Aeration Modelling Using a Sub-Grid Volume-Of-Fluid Model, *International Journal of Nonlinear Sciences and Numerical Simulation*, 18, 559–574, 2017.
- Maric, T., Hopken, J., and Mooney, K.: The OpenFOAM technology primer, Sourceflux, 2014.
- Matias, N., Nielsen, A., Vollertsen, J., Ferreira, F., and Matos, J.: Reaeration and hydrogen sulfide release at drop structures, in: 8th International Conference on Sewer Processes and Networks, Rotterdam, The Netherlands, 2016.
- Matias, N., Nielsen, A., Vollertsen, J., Ferreira, F., and Matos, J.: Erratum: Water Science and Technology 75 (10), 2257–2267: Liquid-gas mass transfer at drop structures, Natércia Matias, Asbjørn Haaning Nielsen, Jes Vollertsen, Filipa Ferreira and José Saldanha Matos, *Water Science and Technology*, 76(6), 1584–1594, 2017.

- Matsché, N., Saracevic, E., Bertrán de Lis, F., and Brooks, L.: Korrosions-und Geruchsprobleme in Abwasserdruckleitungen, Institut für Wassergüte, Ressourcenmanagement und Abfallwirtschaft der Technischen Universität Wien, 2005.
- Matta, E.: Multi-dimensional flow and transport modeling of a surface water body in a semi-arid area, Ph.D. thesis, Technische Universität Berlin, Germany, 2018.
- Menter, F.: Zonal two equation  $k$ - $\omega$  turbulence models for aerodynamic flows, in: 23rd Fluid Dynamics, Plasmadynamics, and Lasers Conference, p. 2906, 1993.
- Menter, F.: Two-equation eddy-viscosity turbulence models for engineering applications, *AIAA Journal*, 32(8), 1598–1605, 1994.
- Morgan, G.: Application of the interFoam VOF code to coastal wave/structure interaction, Ph.D. thesis, University of Bath, 2013.
- Nielsen, P., Raunkjær, K., and Hvitved-Jacobsen, T.: Sulfide production and wastewater quality in pressure mains, *Water Science and Technology*, 37(1), 97–104, 1998.
- Nieves-Remacha, M., Yang, L., and Jensen, K.: OpenFOAM computational fluid dynamic simulations of two-phase flow and mass transfer in an advanced-flow reactor, *Industrial & Engineering Chemistry Research*, 54(26), 6649–6659, 2015.
- Nilsson, H.: How to implement your own application, URL [http://www.tfd.chalmers.se/~hani/kurser/OS\\_CFD\\_2011/ImplementApplication.pdf](http://www.tfd.chalmers.se/~hani/kurser/OS_CFD_2011/ImplementApplication.pdf), 2019.
- ÖNORM B 4710-1: Beton–Teil 1: Festlegung, Herstellung, Verwendung und Konformitätssachweis (Regeln zur Umsetzung der ÖNORM EN 206-1 für Normal-und Schwerbeton), Wien: Österreichisches Normungsinstitut, 2007.
- Parker, C.: The corrosion of concrete: 1. The isolation of a species of bacterium associated with the corrosion of concrete exposed to atmospheres containing hydrogen sulphide., *Australian Journal of Experimental Biology and Medical Science*, 23(2), 14–17, 1945.
- Patankar, S. and Spalding, D.: A calculation procedure for heat, mass and momentum transfer in three-dimensional parabolic flows, in: *Numerical Prediction of Flow, Heat Transfer, Turbulence and Combustion*, pp. 54–73, Elsevier, 1983.
- Petersen, L. and Lohaus, L.: Entwicklung eines Prüfstandes für Parameterstudien zur Säurebeständigkeit von Hochleistungsbetonen, *Proceedings of 16th International Baustofftagung (Ibausil)*, pp. 0637–0644, 2006.
- Pomeroy, R. and Parkhurst, J.: The forecasting of sulfide build-up rates in sewers, in: *Eighth International Conference on Water Pollution Research*, pp. 621–628, Elsevier, 1978.
- Rootsey, R. and Yuan, Z.: New insights into sewer odour and corrosion, in: *6th International Conference on Sewer Processes and Networks*, Queensland, Australia, 2010.
- Rootsey, R., Melchers, R., Stuetz, R., Keller, J., and Yuan, Z.: Taking control of odours and corrosion in sewers, in: *Proceedings of Australia's National Water Conference and Exhibition (OzWater 2012)*, Sydney, Australia, pp. 8–10, Citeseer, 2012.
- Rusche, H.: Computational fluid dynamics of dispersed two-phase flows at high phase fractions, Ph.D. thesis, Imperial College London (University of London), 2003.

- Rutz, M.: Laboratory investigation of physical disintegration of gross solids in the sewer, MSc. Thesis. ETH Zürich, 2016.
- Sander, R.: Compilation of Henry's law constants (version 4.0) for water as solvent., *Atmospheric Chemistry & Physics*, 15(8), 2015.
- Schankat, M.: *DiaTrans: A Multi-component Model for Density-driven Flow, Transport and Biogeochemical Reaction Processes in the Subsurface*, Citeseer, 2010.
- Schulze, L. and Thorenz, C.: The multiphase capabilities of the CFD toolbox OpenFOAM for hydraulic engineering applications, in: *ICHE 2014. Proceedings of the 11th International Conference on Hydroscience & Engineering*, pp. 1007–1016, 2014.
- Schulze, L. and Thorenz, C.: Mehrphasenmodellierung im Wasserbau, in: *Wasserbauwerke - Vom hydraulischen Entwurf bis zum Betrieb*, pp. 53–58, Bundesanstalt für Wasserbau, 2015.
- Severin, T.: *Computational Fluid Dynamics Assisted Design of Thin-Layer Cascade Photobioreactor Components*, Ph.D. thesis, Technische Universität München, 2017.
- Sharma, K., De Haas, D., Corrie, S., O'Halloran, K., Keller, J., and Yuan, Z.: Predicting hydrogen sulfide formation in sewers: a new model, *Journal of the Australian Water Association*, 35(2), 132–137, 2008a.
- Sharma, K., Yuan, Z., de Haas, D., Hamilton, G., Corrie, S., and Keller, J.: Dynamics and dynamic modelling of H<sub>2</sub>S production in sewer systems, *Water Research*, 42(10-11), 2527–2538, 2008b.
- Shih, T., Liou, W. W., Shabbir, A., Yang, Z., and Zhu, J.: A new k- $\epsilon$  eddy viscosity model for high reynolds number turbulent flows, *Computers & Fluids*, 24(3), 227–238, 1995.
- Shuard, A., Mahmud, H., and King, A.: Comparison of two-phase pipe flow in OpenFOAM with a mechanistic model, *IOP Conference Series: Materials Science and Engineering*, 121(1), 2016.
- Smagorinsky, J.: General circulation experiments with the primitive equations: I. The basic experiment, *Monthly Weather Review*, 91(3), 99–164, 1963.
- Teuber, K., Broecker, T., Barjenbruch, M., and Hinkelmann, R.: High-Resolution Numerical Analysis of Flow Over a Ground Sill Using OpenFOAM, in: *Proceedings of the 12th International Conference on Hydroscience & Engineering (ICHE)*, Tainan, Taiwan, 2016.
- Teuber, K., Sielaff, M., Despot, D., Stephan, D., Barjenbruch, M., and Hinkelmann, R.: Modeling and Measuring of Interfaces in Sewer Systems, in: *Proceedings of the 37th IAHR (International Association for Hydro-Environment Engineering and Research) World Congress*, Kuala Lumpur, Malaysia, 2017.
- Teuber, K., Broecker, T., Bayón, A., Nützmänn, G., and Hinkelmann, R.: CFD-modelling of free-surface flows in closed conduits, *Progress in Computational Fluid Dynamics*, 19(6), 2019a.
- Teuber, K., Broecker, T., Bentzen, T., Nützmänn, G., and Hinkelmann, R.: Using computational fluid dynamics to describe H<sub>2</sub>S mass transfer across the water-air interface in sewers, *Water Science and Technology*, 79(10), 1934–1946, 2019b.

- Teuber, K., Broecker, T., Jaydev, S. D., Goitom, G. M., Sielaff, M., Despot, D., Stephan, D., Barjenbruch, M., and Hinkelmann, R.: Multiphase CFD-Simulation of Transport Phenomena in Sewer Systems, in: In: Mannina G. (eds) *New Trends in Urban Drainage Modelling. UDM 2018. Green Energy and Technology.*, Springer Cham., 2019c.
- Teuber, K., Broecker, T., Nützmänn, G., and Hinkelmann, R.: CFD simulation of H<sub>2</sub>S mass transfer under turbulent conditions in a stirring tank, *Water Science and Technology*, in preparation.
- Thaker, J. and Banerjee, J.: CFD simulation of two-phase flow phenomena in horizontal pipelines using openfoam, in: *Proceedings of the 40th National Conference on Fluid Mechanics & Fluid Power*, 2013.
- Thistlethwayte, D.: *Control of sulphides in sewerage systems*, Ann Arbor Science, 1972.
- Thorenz, C. and Strybny, J.: On the numerical modelling of filling-emptying systems for locks, in: *10th International Conference on Hydroinformatics*, 2012.
- Ubbink, O.: *Numerical prediction of two fluid systems with sharp interfaces*, Ph.D. thesis, University of London London, UK, 1997.
- Vollertsen, J., Nielsen, A., Yang, W., and Hvitved-Jacobsen, T.: Effects of in-sewer processes: a stochastic model approach, *Water science and technology*, 52(3), 171–180, 2005.
- Vollertsen, J., Nielsen, A., Jensen, H., Wium-Andersen, T., and Hvitved-Jacobsen, T.: Corrosion of concrete sewers—the kinetics of hydrogen sulfide oxidation, *Science of the total environment*, 394(1), 162–170, 2008.
- Wang, C., Xu, Z., Lai, C., and Sun, X.: Beyond the standard two-film theory: Computational fluid dynamics simulations for carbon dioxide capture in a wetted wall column, *Chemical Engineering Science*, 184, 103–110, 2018.
- Ward, M., Hamer, G., McDonald, A., Witherspoon, J., Loh, E., and Parker, W.: A sewer ventilation model applying conservation of momentum, *Water Science and Technology*, 64(6), 1374–1382, 2011.
- Wilcox, D.: Reassessment of the scale-determining equation for advanced turbulence models, *AIAA Journal*, 26(11), 1299–1310, 1988.
- Wu, H.: An issue on applications of a disk turbine for gas-liquid mass transfer, *Chemical Engineering Science*, 50(17), 2801–2811, 1995.
- Yakhot, V., Orszag, S., Thangam, S., Gatski, T., and Speziale, C.: Development of turbulence models for shear flows by a double expansion technique, *Physics of Fluids A: Fluid Dynamics*, 4(7), 1510–1520, 1992.
- Yang, L., Nieves-Remacha, M. J., and Jensen, K. F.: Simulations and analysis of multiphase transport and reaction in segmented flow microreactors, *Chemical Engineering Science*, 169, 106–116, 2017.
- Yongsiri, C., Vollertsen, J., Rasmussen, M., and Hvitved-Jacobsen, T.: Air–water transfer of hydrogen sulfide: an approach for application in sewer networks, *Water Environment Research*, 76(1), 81–88, 2004.